UNIVERSIDADE FEDERAL DO CEARÁ

CENTRO DE CIÊNCIAS

PROGRAMA DE PÓS-GRADUAÇÃO EM QUÍMICA

EDINILTON MUNIZ CARVALHO

METALLO-DRUGS AS NITRIC OXIDE ($NO^{\bullet}$) AND/OR NITROXYL (HNO) DONORS: DEVELOPMENT OF NEW AGENTS AND INVESTIGATION OF ANTICANCER, ANTIHYPERTENSIVE AND ANTITUBERCULOSIS ACTIVITIES

FORTALEZA

2020

EDINILTON MUNIZ CARVALHO

METALLO-DRUGS AS NITRIC OXIDE (NO•) AND/OR NITROXYL (HNO) DONORS: DEVELOPMENT OF NEW AGENTS AND INVESTIGATION OF ANTICANCER, ANTIHYPERTENSIVE AND ANTITUBERCULOSIS ACTIVITIES

Tese apresentada ao Programa de Pós-Graduação em Química, da Universidade Federal do Ceará, como requisito parcial para obtenção do Título de Doutor em Química. Área de Concentração: Química Inorgânica.

Orientador: Prof. Dr. Luiz Gonzaga de França Lopes.
Orientadora: Profa. Dra. Vania Bernardes-Génisson.
Coorientador: Prof. Dr. Eduardo Henrique Silva de Sousa.
Coorientador: Prof. Dr. Remi Chauvin.

FORTALEZA
2020

Dados Internacionais de Catalogação na Publicação
Universidade Federal do Ceará
Biblioteca Universitária
Gerada automaticamente pelo módulo Catalog, mediante os dados fornecidos pelo(a) autor(a)

C322m Carvalho, Edinilton Muniz.
Metallo-drugs as nitric oxide (NO•) and/or nitroxyl (HNO) donors: development of new agents and investigation of anticancer, antihypertensive and antituberculosis activities / Edinilton Muniz Carvalho. – 2021.
229 f. : il. color.

Tese (doutorado) – Universidade Federal do Ceará, Centro de Ciências, Programa de Pós-Graduação em Química, Fortaleza, 2021.
Orientação: Prof. Dr. Luiz Gonzaga de França Lopes.
Coorientação: Profa. Dra. Vania Bernardes-Génisson.

1. Iron complexes. 2. Nitric oxide. 3. Nitroxyl. 4. Antiangiogenesis. 5. Vasodilation. I. Título.
CDD 540

EDINILTON MUNIZ CARVALHO

METALLO-DRUGS AS NITRIC OXIDE (NO•) AND/OR NITROXYL (HNO) DONORS: DEVELOPMENT OF NEW AGENTS AND INVESTIGATION OF ANTICANCER, ANTIHYPERTENSIVE AND ANTITUBERCULOSIS ACTIVITIES

Tese apresentada ao Programa de Pós-Graduação em Química, da Universidade Federal do Ceará, como requisito parcial para obtenção do Título de Doutor em Química. Área de Concentração: Química Inorgânica.

Aprovado em: 24/11/2020.

BANCA EXAMINADORA

_____

Prof. Dr. Luiz Gonzaga de França Lopes (Orientador, Brasil)
Universidade Federal do Ceará (UFC)

_____

Profa. Dra. Vania Bernardes-Génisson (Orientadora, França)
Université Toulouse III - Paul Sabatier (UPS)

_____

Prof. Dr. Eduardo Henrique Silva de Sousa (Coorientador, Brasil)
Universidade Federal do Ceará (UFC)

_____

Prof. Dr. Remi Chauvin (Coorientador, França)
Université Toulouse III - Paul Sabatier (UPS)

_____

Prof. Dr. Gilles Gasser
Université Chimie ParisTech

_____

Prof. Dr. Pablo Machado
Pontifícia Universidade Católica do Rio Grande do Sul (PUC-RS)

_____

Profa. Dra. Maria Conceição Ferreira de Oliveira
Universidade Federal do Ceará (UFC)

_____

Prof. Dr. Eric Benoist
Université Toulouse III - Paul Sabatier (UPS)

ACKNOWLEDGMENT

After an intensive work, my PhD is nearing its end. In that time, my knowledge at Chemistry as well as my experimental and research skills have been significantly improved. At this moment, I take this opportunity to thank all the people who directly or indirectly helped me to finish one of the most important stages of my life.

First of all, I would like to express my most sincere and immeasurable gratitude to my supervisors, Prof. Vania Bernardes-Génisson, Prof. Luiz Gonzaga de França Lopes, Prof. Eduardo Henrique Silva de Sousa, and Prof. Remi Chauvin, for their support, encouragement, companionship, and helpfulness. Whenever I needed, they were always available to help me, both in academic and personal life.

My first steps in academic life were guided and assisted by Prof. Eduardo Sousa. Without a doubt, he is one of my greatest references. Thank you very much for choosing me and helping me evolve. Without his help, it would not have been possible for me to complete my PhD. His contribution to this thesis is notorious.

After my graduation, I had (and still have) the honor of starting and finishing the Master's degree with Prof. Luiz Lopes, who is also my Brazilian PhD supervisor. His knowledge, enthusiasm and encouragement helped me to get firm until this moment. I am also extremely grateful for accepting me as a student and for helping me write this thesis.

Prof. Vania Bernardes-Génisson was one of the most important and significant professionals that I have had the privilege of knowing as a student. I have no words to express how grateful I am for welcoming me as a student (not to mention as a son) during my doctoral studies in France. Always concerned and attentive to whether the research was going well, but her care was not limited to academic life. On several occasions she supported me especially in the most difficult and troubled moments of my stay in France. I cannot fail to mention the dedication and professionalism in writing this thesis, it is not possible to briefly explain how much of your love and time were invested in this work. Thank you so much for everything.

Prof. Remi Chauvin, one of the greatest chemists in the world, sometimes I find myself without believing that I had the time to work and share a phase of my life with you. Your creativity and enthusiasm are contagious. Doing science by your side was an incredible experience. Thank you very much for the discussions and for helping me to evolve as a chemist and person. In addition, I could not fail to mention the good atmosphere at the lab. Thank you very much for opening the doors of your laboratory for me and for guiding me

throughout this stage. From my arrival in France to writing this thesis, your contributions were and are extremely important to me. I sincerely feel honored to have been your doctoral student.

In addition, I would like to thank the members of my thesis committee: Prof. Maria Conceição F. de Oliveira ("Universidade Federal do Ceará", Brazil), Prof. Gilles Gasser ("Université Chimie Paris Tech", France), Prof. Pablo Machado ("Pontifícia Universidade Católica do Rio Grande do Sul", Brazil), and Prof. Eric Benoist ("Université de Toulouse III", France), for having accepted the invitation to participate in this defense, contributing in an insightful and significant way in improving this work.

I would like to thank all members of the "Bioinorgânica" group at the "Universidade Federal do Ceará": the professors Alda Karine, Francisco Audísio, Izaura Diógenes, Idalina Carvalho, Jackson Rodrigues, Tércio Paulo and Elisane Longhinotti, your contributions were essential in my academic life.

I have to thank all my friends from the lab. "Bioinorgânica": Aurideia, Florêncio, Gilmara, Josi, Maiara, Monilson, Ricardo, Walysson, Lucas, Patty, Alan, Giam, Iury, Leonardo, Manigat, Wellison, Karol, Dieric, Juliana, Geângela, Vitória, Carlos Daniel, Vivânia, Mikael and André Florêncio. Directly or indirectly, all of you contributed to this moment.

I would like to thank Prof. Tércio Paulo for his help in several experiments both in Brazil and in France, as well as his wife, Mari. The moments we shared in France were extremely important for me, especially when it comes to a situation where you are far from your family and friends. Finally, we became good friends.

I would like to say thanks to the friends that France gave me: Cécile, Marwa, Chongwei, Dmytro, Abdelhak, Sameh, Amal, Sarah and Hend. You have helped me a lot to endure the difficulties of distance from home. In particular, I would like to extend my most sincere thanks to my "sisters" Cécile and Marwa, and my "brother" Abdelhak. I consider you as part of my family. I also have to say thanks Valerie for always being available to help me inside and outside the lab.

I also have to thank my friend Jéssica de Lima for helping, supporting and crying with me in the moments that I most needed. You are very important to me.

I would like to thank the "Universidade Federal do Ceará - UFC" for all the support it has offered me during these more than 10 years. It was literally a second home for me. I also would like to thank "Laboratoire de Chimie de Coordination – LCC" and "Centre

National de la Recherche Scientifique – CNRS" for providing a safe and comfortable workplace, and "Université Paul Sabatier III - UPS" for offering us various interesting and useful courses and training.

I am also indebted to Dr. Alix Sournia Saquet and Dr. Lionel Rechignat, their involvement and contributions in the electrochemistry and EPR experiments, respectively were essential.

I would like to thank Prof. David A. Wink and his team for the antiangiogenic activity experiments, Prof. Nilberto Robson Falcão do Nascimento and his team for vasodilation tests, Professors Cristiano V. Bizarro and Pr. Luiz A. Basso for anti-TB tests, and Mrs Sandra Bourgeade-Delmas and Prof. Nicolas Fabre for cytotoxicity, anti-leishmaniasis and anti-malaria tests.

I would like to say thanks to my family, especially my mother Maria Veraleide da Masceno Muniz, for always accompanying me and being present at all times. She is one of the main reasons, for which I want to become a PhD. Thank you!

This study was financed in part by the Coordenação de Aperfeiçoamento de Pessoal de Nível Superior - Brasil (CAPES) - Finance Code 001.

Finally, I have to thank the CAPES-COFECUB project for their financial support.

RESUMO

Câncer, doenças cardiovasculares e tuberculose (TB) são os principais desafios terapêuticos, para os quais várias estratégias medicamentosas têm sido desenvolvidas, incluindo o uso de agentes inorgânicos como metalofármacos e NO• (óxido nítrico) / HNO (nitroxila). Dentro desta perspectiva, esta tese aborda o desenho, síntese, estudos físico-químicos e avaliação biológica de fármacos a base de metal capazes de liberar NO• e/ou HNO. Dois tipos de plataformas orgânicas são, portanto, considerados como ligantes em complexos de $Fe^{II/III}$ concebidos como fontes potenciais de NO•/HNO: o ligante cyclam (1,4,8,11-tetraazaciclotetradecano) e três ligantes de ácido hidroxâmico (ArC(O)NHOH). O primeiro capítulo trata da reatividade química do complexo *trans*-[Fe (cyclam)(NO)Cl]Cl_2, que se decompõe ao liberar NO• sob condições fisiológicas de pH e temperatura, sendo o processo significativamente acelerado após a irradiação de luz em 365 nm. Em contraste, experimentos *in vitro* na presença de glutationa revelaram que o mesmo complexo produz HNO. Estudos de angiogênese mostraram que o complexo é capaz de inibir significativamente o fator induzível por hipóxia (HIF-1α) induzido por hipóxia ou na presença de um doador de NO• (Spermine NONOate) em células de câncer de mama: este resultado é consistente com uma liberação de HNO via nitrosil complexo de ferro. Por outro lado, os ensaios de vasodilatação, usando anéis aórticos de rato pré-contraídos, revelaram que o complexo exibe um relaxamento com IC_{50} de 910 nM, contra um IC_{50} de 24 nM para o medicamento de referência, nitroprussiato de sódio. Os próximos capítulos tratam da liberação de HNO por ácidos hidroxâmicos aromáticos promovida por oxidação. O Capítulo 2 enfoca o mecanismo de oxidação dos ácidos hidroxâmicos isonicotinóico, nicotinóico e pirazinóico, mediado por ferricianeto de potássio ($K_3[Fe^{III}(CN)_6]$) em condições de pH fisiológico. Foi mostrado que a ativação oxidativa dos ácidos hidroxâmicos estudados, mediada por complexo de Fe^{III}, envolve a produção do intermediário *N,O*-di(di)azinoilhidroxilamina com liberação concomitante de HNO, ao invés da espécie acil nitroso. Os ácidos hidroxâmicos livres também foram avaliados frente a diferentes atividades biológicas e usados como controles comparativos dos complexos de ferro descritos no capítulo 3. Esses complexos de pentacianoferrato(II), $Na_3Fe^{II}(CN)_5$(ArCONHOH), inicialmente concebidos como potenciais híbridos de isoniazida (INH, pró-droga anti-TB de primeira linha, para o qual o radical isonicotinoil é o metabólito ativo) e delamanid (anti-TB de terceira linha, para a qual HNO é o metabólito ativo), foram sintetizados e caracterizados por técnicas espectroscópicas, voltametria cíclica, e cálculos DFT. Usando espectroscopia EPR e RMN de ^1H, a oxidação desses complexos de Fe^{II} através

de H_2O_2 resultou na liberação de HNO e formação dos ácidos carboxílicos correspondentes, através de uma provável transferência de elétrons intramolecular. Em contraste do que foi observado com o complexo INH ($Na_3[Fe^{II}(CN)_5(INH)]$), nenhum "azinoyl radical" foi evidenciado como produto de oxidação dos complexos de ácido hidroxâmico. Em vez disso, os ácidos carboxílicos correspondentes foram formados, em particular, a formação do ácido pirazinóico, que é o metabólito ativo da pirazinamida, outro pró-fármaco antitubercular, se mostra relevante para o tratamento da tuberculose resistente à pirazinamida, uma vez que a ativação poderia ocorrer sem assistência da enzima pirazinamidase do *Mycobacterium tuberculosis* (*Mtb*). Os ácidos hidroxâmicos livres e os complexos correspondentes não mostraram qualquer ação antibiótica contra cepa de *Mtb* em crescimento ativo/não resistente. No entanto, os complexos mostraram uma forte atividade vasodilatadora dose-dependente e reversível, próxima à do nitroprussiato (64-250 nM *vs* 13 nM). Os ácidos hidroxâmicos livres se mostraram 19 a 76 vezes menos ativos do que os complexos correspondentes. Com base em experimentos *in vivo*, o $Na_4[Fe^{II}(CN)_5(PyCONHO^-)]$ também mostrou um perfil de atividade cardiovascular promissora, indicando tal complexo como um interessante agente antihipertensivo.

Palavras-chave: Antiangiogênese. Cyclam. Ácidos hidroxâmicos. Complexos de ferro. Óxido nítrico. Nitroxila. Mecanismos de ativação oxidativa. Tuberculose. Vasodilatação.

ABSTRACT

Cancer, cardiovascular diseases and tuberculosis (TB) are major therapeutic challenges, for which various drug strategies have been developed, including the use of inorganic agents such as metallo-drugs and NO• (nitric oxide) / HNO (nitroxyl). Within this prospect, the thesis objective addresses the design, synthesis, physical-chemical studies and biological evaluation of metal-based drugs capable of releasing NO• and/or HNO with pharmacological effects. Two types of organic platforms are thus envisaged as ligands in $Fe^{II/III}$ complexes devised as potential sources of NO•/HNO: the spectator cyclam ligand (1,4,8,11-tetraazacyclotetradecane) and three reactive azine hydroxamic acid ligands (ArC(O)NHOH). The first chapter deals with the chemical reactivity of a *trans*-[Fe(cyclam)(NO)Cl]Cl_2 complex, which is shown to decompose by releasing NO• under physiological pH and temperature conditions, the process being significantly accelerated upon light irradiation at 365 nm. In contrast, *in vitro* experiments in the presence of glutathione revealed that the same complex produces HNO. Angiogenesis studies showed that the complex is able to significantly inhibit the hypoxia-inducible factor (HIF-1α) induced by hypoxia or addition of a NO• donor (Spermine NONOate) in breast cancer cells: this result is consistent with a release of HNO by the nitrosyl complex. On the other hand, vasodilation assays using precontracted rat aortic rings revealed that the complex exhibits a relaxation IC_{50} of 910 nM, *vs* 24 nM for the reference drug, nitroprusside. The next chapters deal with the oxidation-promoted release of HNO from aromatic hydroxamic acids. Chapter 2 focuses on the oxidation mechanism of isonicotinoic, nicotinoic and pyrazinoic hydroxamic acids, mediated by potassium ferricyanide ($K_3[Fe^{III}(CN)_6]$) in physiological pH conditions. It is shown that oxidative activation of aryl hydroxamic acids, mediated by Fe^{III}, involves the production of the *N,O*-di(di)azinoylhydroxylamine intermediate with concomitant release of HNO, instead of the putative acyl nitroso species. The free hydroxamic acids were also evaluated for different biological activities and used as controls to be compared with iron complexes described in chapter 3. These pentacyanoferrate(II) complexes, $Na_3Fe^{II}(CN)_5$(ArCONHOH), initially devised as potential hybrid of isoniazid (INH, first-line anti-TB prodrug, for which the isonicotinoyl radical is the active metabolite) and delamanid (third-line anti-TB, for which HNO is the active metabolite), were synthesized and characterized by spectroscopic techniques, cyclic voltammetry, and DFT calculations. Using EPR and ^1H NMR spectroscopy, oxidation of these Fe^{II} complexes with H_2O_2 was shown to result in the release of HNO and corresponding azinoic acids, through a likely intramolecular electron transfer. In

contrast to what was observed from the INH complex ($Na_3[Fe^{II}(CN)_5(INH)]$), no azinoyl radical species was evidenced to be produced from the corresponding hydroxamic acid complexes. Instead, the corresponding carboxylic acids were found to be formed, in particular pyrazinoic acid which is the active metabolite of pyrazinamide, another antitubercular pro-drug: this result would be relevant for the treatment of pyrazinamide-resistant tuberculosis, as the activation could thus occur without assistance of the pyrazinamidase enzyme of *Mycobacterium tuberculosis* (*Mtb*). The free hydroxamic acids and corresponding complexes did not show any antibiotic action against an actively growing/non-resistant *Mtb* strain. However, the complexes showed a strong dose-dependent and reversible vasodilation activity, close to that of nitroprusside (64-250 nM *vs* 13 nM). The free hydroxamic acids were found ca. 19- to 76-fold less active than the corresponding complexes. On the basis of *in vivo* experiments, $Na_4[Fe^{II}(CN)_5(PyCONHO^-)]$ also showed a promising cardiovascular activity profile for the development of a new antihypertensive agent.

Keywords: Antiangiogenesis. Cyclam. Hydroxamic acids. Iron complexes. Nitric oxide. Nitroxyl. Oxidative activation mechanisms. Tuberculosis. Vasodilation.

RÉSUMÉ

Le cancer, les maladies cardiovasculaires et la tuberculose (TB) sont des défis de santé majeurs pour lesquels diverses stratégies médicamenteuses ont été développées, y compris l'utilisation d'agents inorganiques tels que des complexes métalliques et l'oxyde nitrique ($NO^{\bullet}$) ou le nitroxyle (HNO). L'objectif de la thèse porte sur la conception, la synthèse, les études physico-chimiques et l'évaluation biologique de molécules à base de métaux capables de libérer $NO^{\bullet}$ et/ou HNO avec des effets pharmacologiques. Deux types de plates-formes organiques sont envisagés comme ligands des complexes de fer, conçus comme sources potentielles de $NO^{\bullet}$/HNO : le ligand spectateur cyclam (1,4,8,11-tétraazacyclotétradécane) et les ligands réactifs du type azine acide hydroxamique (ArC(O)NHOH). Le premier chapitre traite de la réactivité du complexe *trans*-$[Fe(cyclam)(NO)Cl]Cl_2$, qui se décompose en libérant $NO^{\bullet}$ à pH physiologique, le processus est accéléré par irradiation lumineuse à 365 nm. En revanche, des expériences *in vitro* en présence de glutathion ont révélé que le même complexe produit HNO. Des études d'angiogenèse ont montré que le complexe est capable d'inhiber le "facteur inductible par hypoxie" (HIF-1α) induit par hypoxie ou ajout d'un donneur de $NO^{\bullet}$ (Spermine NONOate) dans les cellules cancéreuses du sein, résultat cohérent avec une libération de HNO. Des tests de vasodilatation, des anneaux aortiques de rat précontractés, ont révélé que le complexe présente une CI_{50} de relaxation de 910 nM, contre 24 nM pour le médicament de référence nitroprussiate. Les chapitres suivants traitent de la libération de HNO par oxydation d'acides hydroxamiques aromatiques. Le chapitre 2 se concentre sur le mécanisme d'oxydation des acides hydroxamiques isonicotinoïque, nicotinoïque et pyrazinoïque par le ferricyanure de potassium à pH physiologique. Il est montré que l'activation oxydante des acides hydroxamiques par des ions Fe^{III} implique la production de l'intermédiaire *N,O*-di(di)azinoylhydroxylamine avec libération concomitante de HNO, au lieu de l'espèce hypothétique acyl nitroso. Les acides hydroxamiques ont été évalués pour différentes activités biologiques et utilisés comme témoins pour être comparés aux complexes de fer décrits au chapitre 3. Les complexes de type $Na_3Fe^{II}(CN)_5(ArCONHOH)$, initialement conçus comme modèles de médicaments hybride d'isoniazide (INH, anti-TB, dont le radical isonicotinoyle est le métabolite actif) et du délamanide (anti-TB, dont HNO est le métabolite actif), ont été synthétisés et caractérisés par des techniques spectroscopiques, voltammétrie cyclique, et calculs DFT. En utilisant la spectroscopie RPE et RMN ^1H, l'oxydation de ces complexes de Fe^{II} avec H_2O_2 s'est avérée entraîner la libération de HNO et des acides azinoïques correspondants, via un probable

transfert d'électrons intramoléculaire. Contrairement à ce qui a été observé pour le complexe $Na_3[Fe^{II}(CN)_5(INH)]$, aucun radical azinoyle n'a été produit à partir des complexes d'acide hydroxamiques. Les acides carboxyliques correspondants ont par contre été observés, en particulier l'acide pyrazinoïque, métabolite actif du pyrazinamide, un autre promédicament anti-TB: ce résultat est *a priori* pertinent pour le traitement de la TB résistante au pyrazinamide, car l'activation pourrait ainsi se produire sans l'aide de l'enzyme pyrazinamidase de *Mycobacterium tuberculosis* (*Mtb*). Les acides hydroxamiques libres ou complexés n'ont montré aucune action antibiotique contre une souche de *Mtb* non résistante en croissance active. Cependant, les complexes ont montré une forte activité de vasodilatation dose-dépendante et réversible, proche de celle du nitroprussiate (64-250 nM *vs* 13 nM). Les acides hydroxamiques libres ont été 19 à 76 fois moins actifs que les complexes correspondants. Sur la base d'expériences *in vivo*, $Na_4[Fe^{II}(CN)_5(PyCONHO^-)]$ a aussi montré un profil d'activité cardiovasculaire prometteur pour le développement d'un nouveau médicament antihypertenseur.

Mots clés : Antiangiogenèse. Cyclam. Acides hydroxamiques. Complexes de fer. Oxyde nitrique. Nitroxyle. Mécanismes d'activation oxydante. Tuberculose. Vasodilatation.

SUMMARY OF FIGURES

SUMMARY OF SCHEMES

LIST OF TABLES

ABBREVIATIONS

cPTIO	2-(4-carboxyphenyl)-4,4,5,5-tetramethylimidazoline-1-oxyl-3-oxide Potassium Salt
CVDs	Cardiovascular Diseases
Cyclam	1,4,8,11-tetraazacyclotetradecane
DFT	Density Functional Theory
EPR	Electron Paramagnetic Resonance
FDA	Food and Drug Administration
GSH	Glutathione
GTN	Glyceryl Trinitrate
HIFs	Hypoxia-inducible Factors
IC	Inhibitory Concentration
ILCT	Intraligand Charge Transfer
INH	Isoniazid
IPA/NO	Sodium 1-(isopropylamino)diazen-1ium-1,2-diolate
IQG607	$Na_3[Fe(CN)_5(INH)]$
LLCT	Ligand-to-ligand Charge Transfer
MDR-TB	Multidrug-resistant Tuberculosis
MLCT	Metal-to-ligand Charge Transfer
Mtb	*Mycobacterium tuberculosis*
NO	Nitric Oxide
NOS	Nitric Oxide Synthases
PZA	Pyrazinamide
sGC	Soluble Guanylate Cyclase
SNP	Sodium Nitroprusside
TB	Tuberculosis
TD-DFT	Time-dependent DFT
WHO	World Health Organization

TABLE OF CONTENTS

1 INTRODUCTION

Cancer, cardiovascular disorders, and tuberculosis are diseases that significantly affect the world population. Among the therapeutic strategies used to treat these diseases, administration of medicines is one of the most important, allowing the control of health problems, and improving the quality of patients' life. Such strategy has been increasingly adopted however, spite of the benefits brought by the use of medicines, in many cases, mainly in situations of prolonged use as for cardiovascular therapy, several side effects are observed. For cancer, the discovery for miraculous molecules allowing the cure of the disease is still anxiously waited. Moreover, the emergence of infectious diseases promoted by pathogenic strains resistant to conventional antibiotics (e.g., *Mycobacterium tuberculosis* towards isoniazid and rifampicin) is also a worldwide health problem urgently needing for new agents that could exhibit better efficacy and lesser side-effects.

While chemical organic drugs are largely employed to treat these affections and others, inorganic compounds have been much less developed. However, a few inorganic drugs containing metal atoms can also play a crucial role in therapeutic (e.g., $LiCO_3$, cisplatin, sodium nitroprusside, etc.) and diagnostic (e.g., Magnevist® and Cardiolite®, etc.) arsenals. Among the inorganic compounds involving metals, metallo-drug is a class of molecules that exhibits a series of chemical characteristics (e.g., charge variation and metal-ligand interaction) and properties (e.g., redox activity and Lewis acid properties) that make it excellent scaffold for the development of new medicinal chemistry strategies. Additionally, another family of inorganic compounds that draw our attention is the nitric oxide ($NO^{\bullet}$) and nitroxyl (HNO) molecules, which are both widely studied due to their relevant biological properties. As these molecules are very unstable and cannot be planned as direct drugs, pro-drugs able to release these reactive species *in vivo* are also of our interest. All these advances prompted us to propose new anticancer, antihypertensive and antituberculosis drug-development strategies based on the release of $NO^{\bullet}$/HNO mediated by transition-metal. In this context, this thesis focuses on the design, synthesis, physico-chemical and biological studies of new metal complexes able to release $NO^{\bullet}$/HNO in physiological conditions as a way to assist in the treatment of cancer, hypertension disorders, and tuberculosis.

The overview presented in the introduction is devoted in the first part to highlight the place of metal complexes in therapeutics and in a second part, to point out the significant biological aspects of NO• and HNO, their pharmacological importance in the context of cancer, cardiovascular disease and tuberculosis, and finally, to report their organic and inorganic donors. The results obtained under this thesis are presented in the form of scientific papers. The first part of this thesis (Chapter 1) describes the study of the reactivity of the Fe^{II} complex, *trans*-[Fe(cyclam)(NO)Cl]Cl_2, with regard to the release of NO• through a photochemical process and the release of HNO via the activation of the complex by biological reducing agents. The vasodilation properties of this nitrosyl complex were also examined.

The second part of this thesis is divided in two chapters (chapters 2 and 3). In the chapter 2, a mechanistic study of the oxidative activation of three (di)azine hydroxamic acids (isonicotino-, nicotino-, and pyrazino- hydroxamic acids) was described. These results led us to propose a new mechanism for the activation of these (di)azine hydroxamic acids in aqueous medium. These compounds were also evaluated for different biological activities and they were used as control molecules to be compared to the metal-drugs prepared in the chapter 3. In the third chapter, three new pentacyanoferrate(II) complexes derived from the aromatic hydroxamic acids mentioned above, originally conceived as a potential hybrid of isoniazid (front-line antitubercular, for which radical isonicotinoyl is the active metabolite) and delamanid (third-line anti-TB, for which HNO is the active metabolite), were synthesized, characterized and their ability to release dual active metabolites (NO•/HNO and aroyl radical) in the presence of H_2O_2, as well as their biological effects as antitubercular and cardiovascular agents were investigated.

1.1 Metallo-drugs in medicine - Brief historical account (overview)

Metallo-drugs constitute a class of pharmaceutical substances that contains a metal as an active ingredient. Several substances in this class have been used in therapeutic and diagnostic medicine throughout history.[1] In terms of modern chemotherapy, the first metallo-drug used was salvarsan (Figure 1), an arsenic(III)-based antimicrobial agent developed by the German physician Paul Ehrlich in 1910. It was used in the treatment of syphilis, before being replaced by penicillin after World War II.[1,2] Several other treatments based on metallo-drugs have emerged, such as gold

compounds (e.g., gold cyanide ($K[Au(CN)_2]$) and sodium aurothiomalate) for the treatment of tuberculosis during the years of 1925-1935 (described as the "Gold Decade").[3] Despite the ineffectiveness of such complex ions in the treatment of tuberculosis in animals, the same compounds proved to be effective in the treatment of rheumatoid arthritis, culminating with the oral use of the drug auranofin (Figure 1) in 1985,[4] for the treatment of this pathology.

Figure 1 - Examples of three first prescribed metallo-drugs.

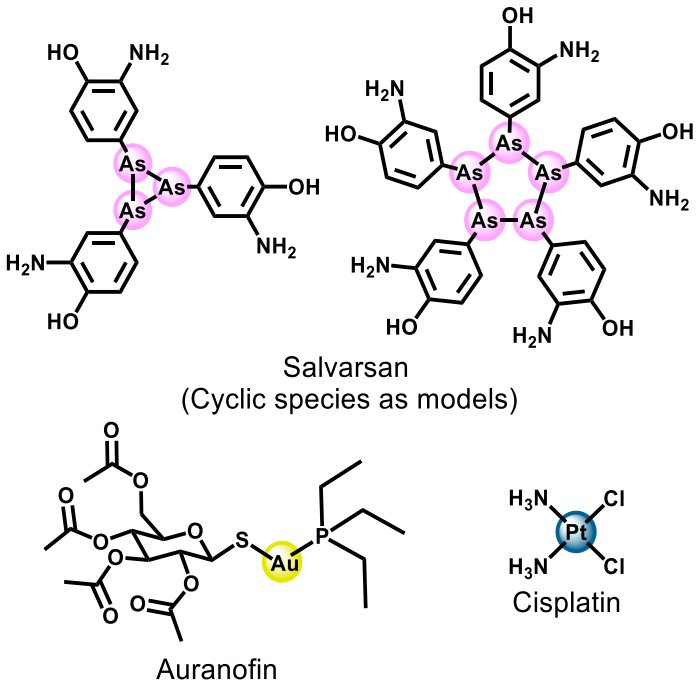

Reference: Elaborated by the author.

Another milestone of modern medicine involves the metal-complex *cis*-diamminedichloroplatinum(II) (cisplatin or platinol) (Figure 1), first synthesized in 1845 by the Italian chemist Michele Peyrone.[5] However, it was the chemists Barnett Rosenberg and Loretta VanCamp who, in 1965, while studying the effect of electric current on *Escherichia coli*, reported biological actions of cisplatin. Rosenberg's work culminated with the discovery of cisplatin as one of the most well-known antitumor agent of all times, leading to development of a series of analogues, which have been used in ca. 50% of all cancer treatments.[5,6]

1.2 Relevant properties of metal complexes within the therapeutic context

Metal complexes provide highly versatile platforms for drug design. In addition to the variations in the metal nature and oxidation state, metal ions adopt diverse geometries and coordination numbers, allowing the adjustment of chemical reactivity in terms of kinetics (bond exchange rates) and thermodynamics (metal-ligand bond strengths, redox potential, etc.).[7] Not only the metal, but also the ligands are anticipated to play important roles in the biological activity, such as recognition of the outer sphere by a target, or biological action resulting from the release of the ligand.[7] According to a brief summary cited by Haas and Franz,[8] the properties that make a platform of metallic complexes useful and versatile in biology are:

i. *Charge Variation* – "Metal ions are positively charged in aqueous solution, but that charge can be manipulated depending on the coordination environment so that a metal complexed by ligands can be cationic, anionic, or neutral."
ii. *Metal-Ligand Interaction* – "Metal ions bind to ligands via interactions that are often strong and selective. The ligands impart their own functionality and can tune properties of the overall complex that are unique from those of the individual ligand or metal. The thermodynamic and kinetic properties of metal−ligand interactions influence ligand exchange reactions."
iii. *Structure and Bonding* – "Metal−ligand complexes span a range of coordination geometries that give them unique shapes compared with organic molecules. The bond lengths, bond angles, and number of coordination sites can vary depending on the metal and its oxidation state."
iv. *Lewis Acid Properties* – "Metal ions with high electron affinity can significantly polarize groups that are coordinated to them, facilitating hydrolysis reactions."
v. *Partially Filled d-shell* – "For the transition metals, the variable number of electrons in the d-shell orbitals (or f-shell for lanthanides) imparts interesting electronic and magnetic properties to transition metal complexes."

vi. *Redox Activity* – "Coupled with the variability of electrons in the d-shell is the ability for many transition metals to undergo one-electron oxidation and reduction reactions."

Despite these advantages, the current diversity of metal complexes with medical therapeutic application is still limited. However, metallo-drugs are more widely represented in the category of diagnostic compounds (gadolinium, technetium, indium compounds among others).[1,9-11] As part of this thesis, the next section will focus on therapeutic metal complexes with cardiovascular, cancer and tuberculosis interests.

1.3 Anticancer metallo-drugs

Cisplatin, *cis*-$(NH_3)_2PtCl_2$, was the first metal-based drug used clinically against cancer (Figures 1 and 2).[1] Currently, it is believed that its mode of cytotoxic action is mainly due to its ability to interact with DNA by forming stable adducts. Replacement of anionic Cl^- ligands by neutral H_2O ligands, mediated by the variation in chloride concentration inside of the cells, has been identified as the main route of activation. The globally cationic hydrolyzed complex $[(NH_3)_2PtCl_{2-x}(H_3O)_x]^{x+}$, is a potent electrophile agent able to react with any nucleophile, including sulfhydryl groups on proteins and nitrogen donor atoms on nucleic acids. Cisplatin therapy including combination with other drugs has been considered as a standard protocol against many types of cancer.[12] Nevertheless, new platinum drugs were investigated due to serious side effects of cisplatin, in addition to the aim of prolonging the use inducing drug resistance. Other platinum(II)-containing anticancer drugs such as carboplatin, approved in 1989 by the Food and Drug Administration (FDA), and oxaliplatin, approved in 2002 by FDA, have thus been also used (Figure 2).[1,12]

Figure 2 - Anticancer platinum metallo-drugs clinically used or in current clinical trials.

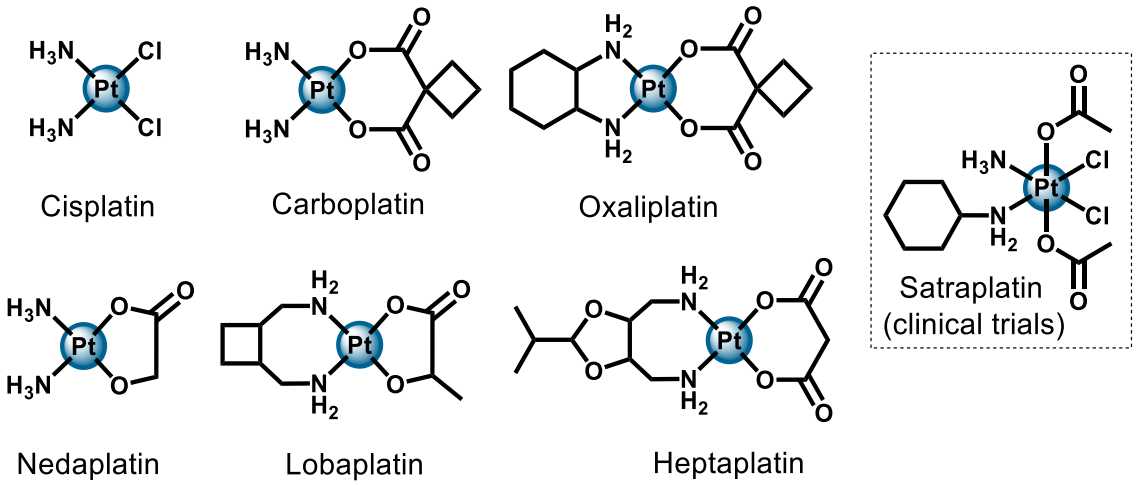

Reference: Elaborated by the author.

New Pt^{II} complexes, nedaplatin, lobaplatin, and heptaplatin (Figure 2), were prepared and clinically used in Japan, China, and South Korea, respectively.[13] Beside this, low spin $5d^6$ Pt^{IV} octahedral complexes have also been explored as potential anticancer agents, such as satraplatin (JM216) (Figure 2), the first orally administered platinum analogue, which is currently in advanced Phase III clinical trials.[14]

Like platinum (Pt), substances containing arsenic (As) are also examples of approved drugs and in clinical studies for the treatment of cancer (Figure 3). Arsenic trioxide (trisenox) was approved by the FDA in 2000 particularly for the treatment of promyelocytic leukemia, but its toxicity, as well as the substantially reduced antitumor effects, limit its use in the treatment of other non-APL (Acute Promyelocytic Leukemia) cancers.[15] Liu and co-workers,[16] recently indicated that the main target of trisenox, responsible for its cytotoxic action, is the promyelocytic leukemia protein (PML). Therefore, new therapeutic agents based on As have been developed, such as *S*-dimethylarsino-glutathione (Darinaparsin®, ZIO-101) (Figure 3), a new chemotherapy agent in Phases I/II of clinical trial, which has shown more potent anticancer properties against various types of solid tumors and hematologic malignancies, both *in vitro* and *in vivo*.[15] Its molecular mechanism of action remains unclear; recently, however, Sun and collaborators[15] showed that darinaparsin (Figure 3), when interacts with nucleosome, destabilizes this latter, leading to cellular apoptosis.

Figure 3 - Arsenic anticancer metallo-drugs: trisenox (clinically used) and darinaparsin (in clinical trials).

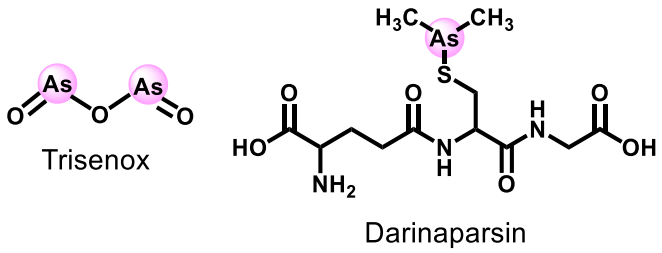

Reference: Elaborated by the author.

Problems related to platinum metallo-drugs in the treatment of cancer have also stimulated the search for anticancer drugs containing ruthenium. Ruthenium complexes have emerged as a promising alternative to platinum-based chemotherapy. Imidazolium(imidazole)(dimethylsulfoxide)tetrachlororuthenate(III) (NAMI-A) (Figure 4) was the first ruthenium complex to achieve clinical investigations in humans. It was synthesized for the first time by Mestroni and collaborators in Italy.[17] In preclinical studies, NAMI-A showed promising antimetastatic activity. It was well successful in Phase I clinical trial, but in studies of Phase II it showed limited efficacy, resulting in a halt in clinical development. Indazolium *trans*-tetrachlorobis(1*H*-indazole)ruthenate(III)] (KP1019) (Figure 4) was another ruthenium derivative that entered in Phase I clinical trial, however its low solubility limited its progress in the later stages. Nevertheless, its sodium salt derivative, KP1339 (Figure 4), has advanced in clinical tests.[18] Finally, [Ru(II)(4,4′-dimethyl-2,2′-bipyridine(dmb))$_2$(2-(2′,2″:5″,2‴-terthiophene)-imidazo[4,5-*f*][1,10]phe-nanthroline)]Cl_2 (TLD1433) (Figure 4) is the first metal-based photosensitizer, not containing a tetrapyrrolic fragment, to enter in clinical trials for non-muscle invasive bladder cancer treatment via photodynamic therapy (PDT). It is currently in Phase I/II clinical trials.[18,19]

Figure 4 - Structures of ruthenium compounds in clinical trials.

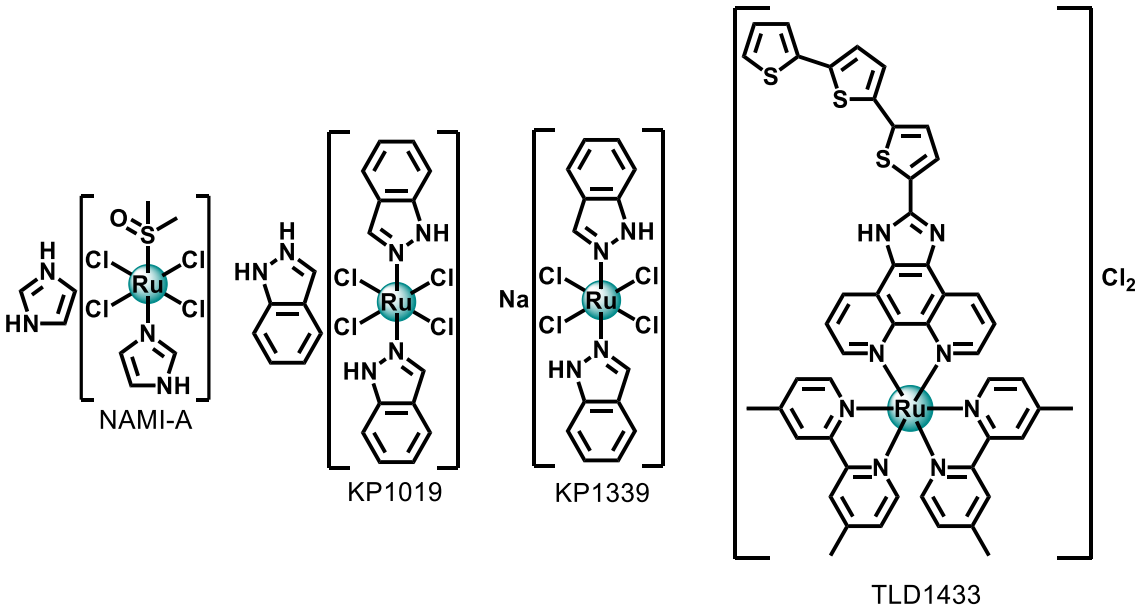

Reference: Elaborated by the author.

Gallium (Ga) and molybdenum (Mo) compounds (Figure 5) are also included in the list of chemotherapeutic agents in clinical testing phases. Some examples are: gallium nitrate ($Ga(NO_3)_3$) (Figure 5), that displayed antineoplastic activity against non-Hodgkin's lymphoma and bladder cancers in Phase I/II clinical trials,[20] and two hexacoordinate complexes: gallium(III) *tris*(maltolate) (Figure 5), which is in Phases I/II of clinical tests in patients with prostatic neoplasms, multiple myeloma, bladder neoplasms and lymphoma, (ClinicalTrials.gov Identifier: NCT00050687)[21] and *tris*(8-quinolato)gallium(III) (KP46) (Figure 5) successfully tested in a Phase I clinical trial against kidney cancer.[22] It is believed that the antiproliferative activity of these two complexes is related to the inhibition of ribonucleotide reductase, the iron-dependent enzyme essential for DNA synthesis, triggering apoptosis.[7] *Bis*-Choline tetrathiomolybdate (ATN-224) (Figure 5), is a molybdenum(VI) metallo-drug derivative, currently in Phases I/II of clinical tests, with patients affected by various forms of cancer (melanoma, breast, colon, kidney, and relapsed prostate cancer). These studies indicate that the possible chemotherapeutic action of ATN-224 may be related to its ability to chelate and inhibit copper-transporting ATPases.[23]

Figure 5 - Chemotherapeutic agents based on gallium(III) and molybdenum(VI) metals assayed in clinical trials.

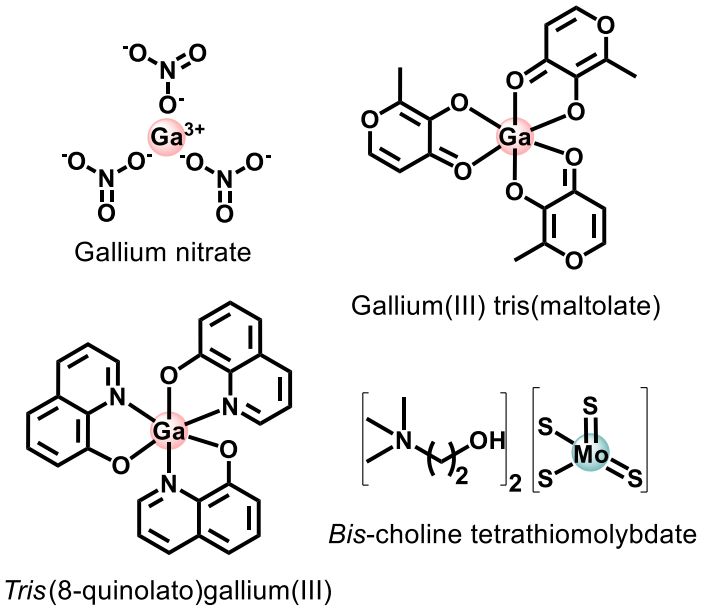

Reference: Elaborated by the author.

1.4 Cardiovascular metallo-drugs

The number of metallo-drugs used for the treatment of cardiovascular disorders in clinical trials is much lower than the number of complexes developed for the treatment of cancer. Currently, the only metallic drug used for cardiovascular therapeutic purposes is sodium nitroprusside (SNP, $Na_2[Fe(CN)_5NO]$) (Figure 6), an Fe^{II} complex used in cardiac surgery, hypertensive crises, heart failure, vascular surgery, pediatric surgery, and other acute applications.[24] SNP is the first metal complex used in cardiovascular therapy, discovered by Playfair in 1849. The effectiveness of this metallo-drug, as a hypertensive agent, was only established in 1955.[24,25] The pharmacological action of SNP is based on its ability to release $NO^{\bullet}$. However, the rapid release of $NO^{\bullet}$, and the emergence of the cyanide toxicity, has been suggested as the main causes of the side effects observed for this prodrug.[24] Several other metal complexes have been developed and tested as less toxic and more efficient agents than SNP, however none of the representatives have yet participated in clinical trials yet. Some of these complexes will be described in the section 2.6.

Figure 6 - Cardiovascular metallo-drugs in clinical use (SNP) and clinical trials Phases I/II (Oxacom® and M40403 (clinical phases suspended)).

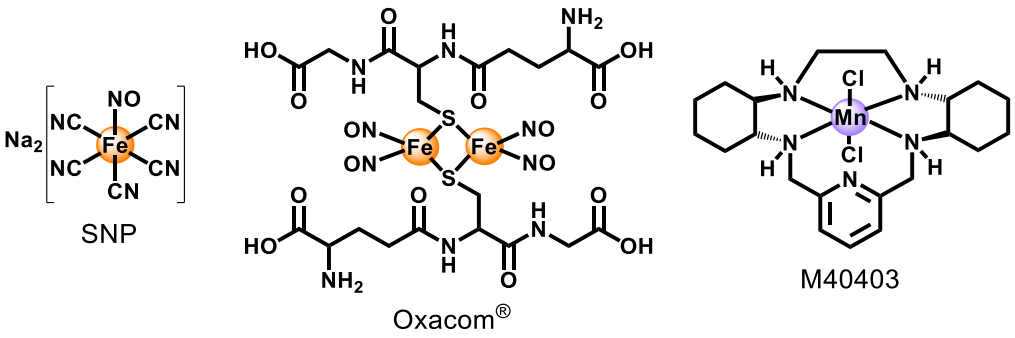

Reference: Elaborated by the author.

Oxacom®, the dinitrosyl iron complex (DNIC) (Figure 6), is a promising candidate for the development of a cardiovascular metallo-drug as it has proven to be an effective hypotensive drug, with no adverse effects reported so far. It is currently in Phase I/II clinical trials.[26] The endogenous effects of Oxacom® are related to its ability to delivery $NO^{\bullet}$, with sGC (soluble guanylate cyclase) as its main target, similar to SNP. The process of sGC activation via $NO^{\bullet}$ and the consequent vasorelaxation activity will be detailed in the section 2.3.2 paragraph 6. M40403, the SOD mimicking manganese(II) (pentaaza)macrocycle (Figure 6), is another example of a hypotensive metallo-drug in clinical trials (Phase I/II clinical trials currently suspended). It is indicated that its action is related to its ability to mimic the activity of superoxide dismutase, eliminating superoxide radicals and exerting beneficial effects on models of intestinal ischemia-reperfusion, and on acute inflammation.[27]

1.5 Antituberculosis metallo-drugs

During the years of 1925 − 1935, also known as the “Gold Decade”, gold cyanide, sodium aurothiomalate, and sodium aurothiosulfate Au^{I} compounds were used for the treatment of pulmonary tuberculosis. Although auranofin is in clinical trials (Phase II) as a possible agent in host directed therapy for tuberculosis in combination with rifabutin,[28] the majority of gold-based metallo-drugs available today are classified as antirheumatic drugs.[1,29] At the date of this thesis, there is no metallo-drug clinically approved for use in tuberculosis. Although there are a significant number of metal

complexes with a potential antitubercular activity proven,[30,31] few or none are in pre-clinical or clinical phases of study and, in most cases, their mechanisms of action have rarely been explored. Some examples of these complexes are illustrated in Figure 7, their respective minimum inhibitory concentration (MIC) values against *Mtb* H37Rv cells are also presented.[30-36]

Figure 7 - Promising metal-complex antitubercular compounds and their minimum inhibitory concentration (MIC) against *Mtb* $H_{37}Rv$ cells.

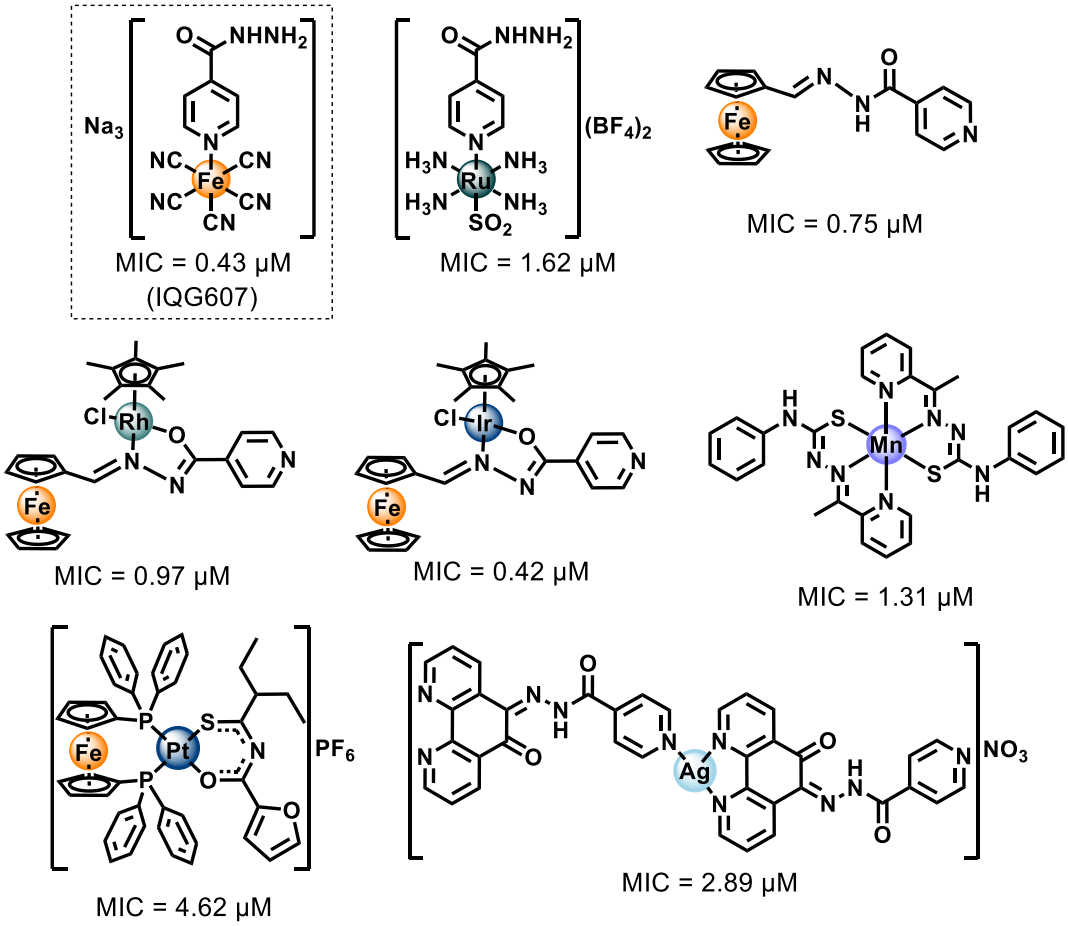

Reference: Adapted from 30-36.

Nonetheless, Sousa e co-workers,[31] synthesized an isoniazid metal complex with pentacyanoferrate(II) moiety, called IQG607 ($Na_3[Fe(CN)_5(INH)]$, INH = isoniazid) (Figure 7). This compound showed significantly promising inhibitory activity against *Mtb* $H_{37}Rv$ cells (MIC = 0.43 μM), in addition to the *in vitro* inhibition of the enoyl-ACP reductase enzyme (InhA), even without using catalase-peroxidase KatG enzyme.[31] The mechanistic studies carried out by Sousa and collaborators indicated that the action of this complex may be related to its ability to be oxidized by biologically relevant agents (e.g H_2O_2, O_2^-).[37] Once oxidized, IQG607 is converted to its active

isonicotinoyl radical form (INH active species), responsible, after reaction with NADH, for inhibition of an InhA of *Mtb*. Inhibition of this enzyme involves interruption of mycolic acid bio-synthesis, an essential constituent of the bacterial cell wall. Unlike INH, IQG607 could be a potential anti-TB metallo-drug targeting InhA without depending on catalase-peroxidase KatG enzyme. Although this mechanistic route may not occur *in vivo*,[38] IQG607 has exhibited exciting toxicological and pharmacological profiles, indicating also a potential to reduce the lengthy treatment once in combination with other first-line drugs.[39] These promising biological activities of IQG607 have stimulated the advances in pre-clinical studies.[39-43]

1.6 Nitric oxide (NO•) and nitroxyl (HNO) in medicine and their donors as therapeutic platforms

1.6.1 Nitric oxide (NO•)

The role of nitric oxide (NO•) in biology was elucidated in the early 1980s, when researchers understood that NO• was the endothelium-derived relaxing factor (EDRF), which is involved in the stimulation of the soluble guanylate cyclase protein (sGC) via interaction with the heme group.[44,45] These discoveries led Robert F. Furchgott, Louis J. Ignarro and Ferid Murad to be awarded the Nobel Prize in Medicine or Physiology in 1998.

1.6.1.1 Biological production of nitric oxide

This small molecule is produced endogenously via the oxidation of L-arginine to L-citrulline, catalyzed by three types of isoenzymes called nitric oxide synthases (NOS) (Figure 8A and B).[46,47] The main isoforms are known as: neuronal (nNOS or NOS1),[48] inducible (iNOS or NOS2),[49] and endothelial enzymes (eNOS or NOS3),[47,50] but there are others.[51] Most of the known effects of NO• are directly related to the stimulation of sGC (Figure 8C).[45,52] This stimulus occurs through the NO• bond to the heme-iron unity of the beta subunit of sGC causing conformational changes that accelerate the conversion of guanosine-5'-triphosphate (GTP) into cyclic guanosine-3′,5′-monophosphate (cGMP) and pyrophosphate (PPi).[53,54] The important secondary messenger cGMP is responsible to trigger a series of downstream processes in the body.[55-59]

Figure 8 - Endogenous production of nitric oxide. Panel A shows the two-step formation of NO• from arginine to citrulline, through the intermediate *N*-omega-hydroxy-L-arginine formation. This reaction is catalyzed by nitric oxide synthase (NOS) with participation of O_2, NADPH and the cofactor tetrahydrobiopterin (H_4B) (Panel B). Panel C shows NO• diffusion from its production site (e.g., endothelial cells) into another cell reaching soluble guanylate cyclase (sGC), whose enzymatic activity is strongly stimulated with conversion of GTP to cGMP.

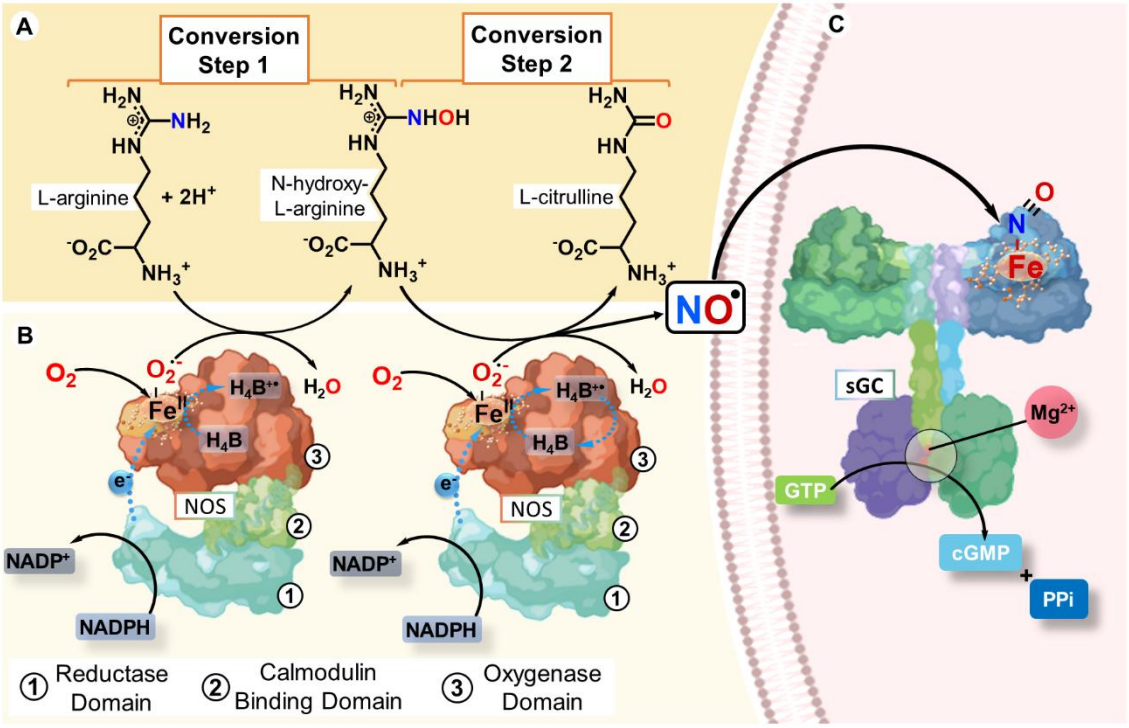

Reference: Elaborated by the author.

A one-electron reduced form of nitric oxide, called nitroxyl (HNO),[60] has also brought considerable attention due to some distinct biological and/or pharmacological properties. This molecule exhibits protective effects against reperfusion damage for the treatment of myocardial infarction,[61] ability to improve myocardial contractility in the treatment of heart failure,[62] aldehyde dehydrogenase inhibitory activity in the treatment of alcoholism,[63] and tumor growth inhibitory property and antiangiogenic effect in cancer treatment.[64,65]

1.6.2 Nitroxyl (HNO)

Nitroxyl (HNO), a small molecule whose pKa is ca. 11.4,[66,67] was first mentioned by the Italian scientist Angelo Angeli, who obtained experimental evidence for the release of HNO and nitrate from sodium trioxodinitrate salt ($N_2Na_2O_3$).[68,69] The currently known Angeli's salt (AS) was placed in evidence as the first HNO donor with

unique pharmacological properties, even before the discovery of the biological roles of $NO^{\bullet}$.[68] Endogenous HNO production in human is still speculative, requiring further studies, which have motivated the scientific community.[66,70-74] One of the main issues contributing to this scenario is the fast reactivity of HNO, which decomposes reacting with itself to generate N_2O (k = (8 ± 3) x 10^6 M^{-1} s^{-1}),[75] with $NO^{\bullet}$ (k = (5.8 ± 0.4) x 10^6 M^{-1} s^{-1})[75] or O_2 ((1.8 ± 0.3) x 10^4 M^{-1} s^{-1})[76] (Scheme 1).

Scheme 1 - HNO decomposition reactions followed by their respective constants.

$$HNO + HNO \longrightarrow N_2O + H_2O \qquad k = 8\ (\pm 3) \times 10^6\ M^{-1}\ s^{-1}$$

$$HNO + NO^{\bullet} \longrightarrow N_2O_2^{-} + H^{+} \qquad k = 5.8\ (\pm 0.4) \times 10^6\ M^{-1}\ s^{-1}$$

$$HNO + O_2 \longrightarrow ONOOH \qquad k = 1.8\ (\pm 0.3) \times 10^4\ M^{-1}\ s^{-1}$$

Reference: Adapted from 75 and 76.

During the last decades, several pathways for HNO endogenous production have been proposed.[74,77] The first one is associated to the absence of the cofactor tetrahydrobiopterin (H_4B) during endogenous production of $NO^{\bullet}$ as a way to generate HNO.[78] This cofactor works in different ways during the synthesis of $NO^{\bullet}$, such as by stabilizing a dimeric structure of NOS (nitric oxide synthases),[79-81] accelerating the decomposition of the complex dioxygen-ferrous heme (NOS-$Fe^{II}(O_2)$),[78,82] and increasing the rate of consumption of NADPH (Figure 8B).[83,84] In addition, this cofactor is essential for the biosynthesis of $NO^{\bullet}$ rather than for that of HNO.[51,85] So, it is possible that under these conditions of low concentrations or in absence of H_4B, the production of HNO is favored. Based on that, mechanistic studies suggested NOS-$Fe^{II}(O_2^{\bullet-})$ would react with *N*-omega-hydroxy-L-arginine (NOHA), converting this hydroxamic intermediate into L-citrulline, water, ferric enzyme NOS-Fe^{III} and HNO.[51,78] Other possible pathways for HNO biosynthesis are the decomposition of nitrosothiols,[86,87] through nitrosothiol enzymatic reduction,[88-90] and oxidation of hydroxylamine (NH_2OH) by hemeproteins,[74,77] which will be discussed below.

1.6.2.1 HNO endogenous synthesis by NOS

While there is a consensus on the mechanism of $NO^{\bullet}$ biosynthesis, HNO endogenous production is still poorly understood. This is likely due to the high instability of HNO and the lack of effective detection methods.[72,91] Nonetheless, there

are some proposed routes for HNO production in cells. As mentioned before, one of the first proposals was based on the conventional NO• biosynthesis pathways in conditions of low H_4B concentration.[51,78,80,82-84] In the endogenous NO• synthesis, the absence of H_4B increases the probability of HNO release rather than NO•. According to Stuehr and co-workers,[78] the NOHA intermediate can be produced by NOS and L-arginine in the absence of H_4B, requiring only the participation of the NADPH cofactor. This can lead to the formation of a nitroso intermediate, which can ensue with production of HNO. This nitroso intermediate can react with the heme group to produce NOS-Fe^{II}(NO), which might release HNO without any oxidative species. Scheme 2 shows the proposed mechanism of HNO production from L-arginine/NOS/NADPH system without H_4B cofactor.

Scheme 2 - The biological synthesis of NO• and likely production of HNO by NOS, references.

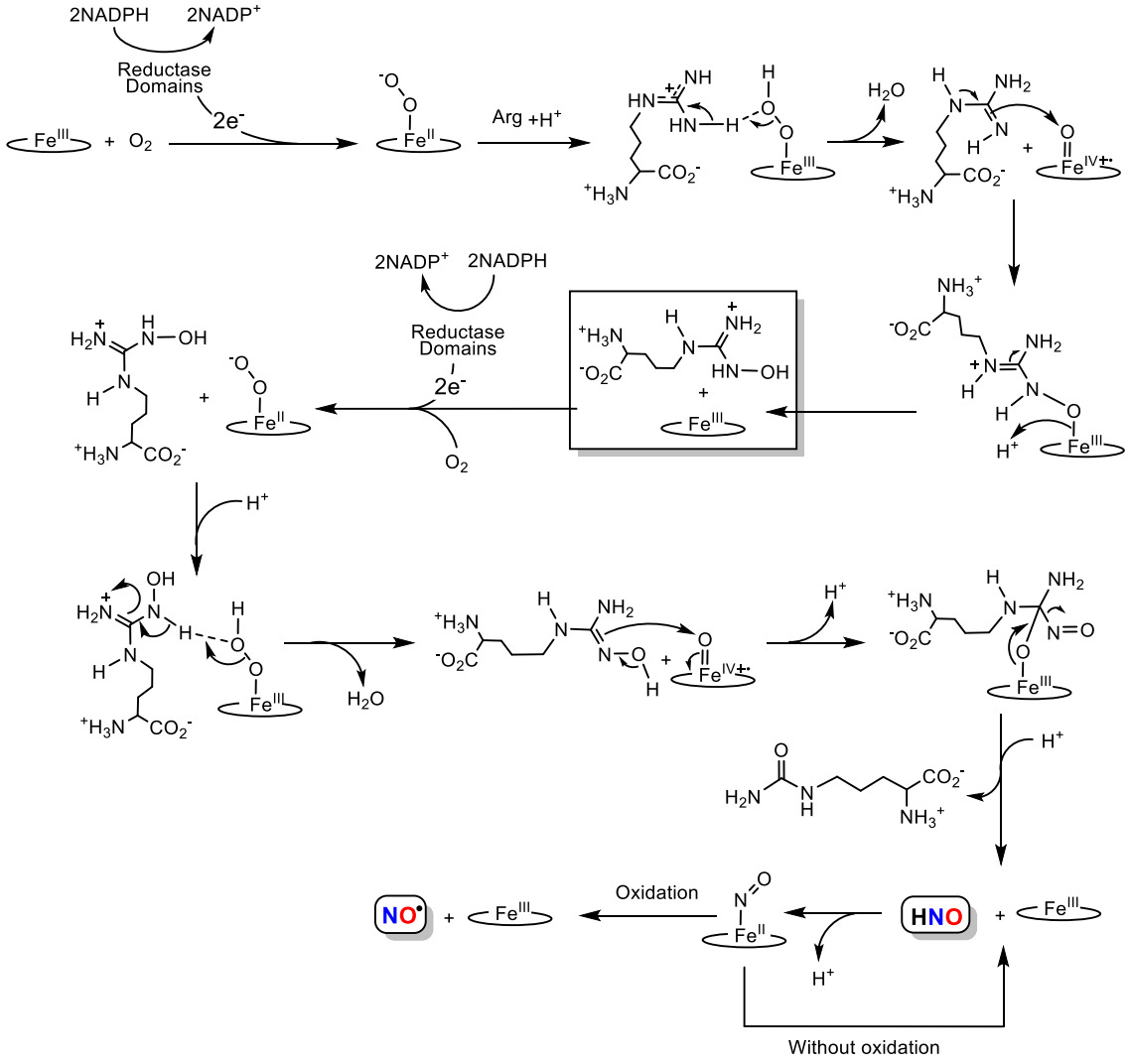

Reference: Adapted from 51, 78, 80, 83, and 84.

1.6.2.2 HNO endogenous production mediated by nitrosothiols decomposition

Another possible endogenous route for the production of HNO arises from the decomposition of nitrosothiols (RSNO), which is considered the most physiologically relevant pathway.[86,87,92] RSNO are products of the reaction between nitric oxide and thiols (RSH). Thiols are biomolecules that play important biological roles and can be found in abundance as large (cysteine rich proteins) or small molecules.[93,94] The homocysteine (Hcy), cysteine (Cys), cysteinylglycine (CysGly), and glutathione (GSH) are examples of thiols performing vital functions in physiological processes. These molecules can be found in cells in different concentration ranges (from 5-15 μM for Hcy to 0.5-10 mM for GSH).[95-97] RSNO is produced by the reaction of $NO^{\bullet}$ with thiols under aerobic conditions, where nitrogen oxides play a critical role (Scheme 3).[98]

Scheme 3 - Nitrosothiol (RSNO) production under aerobic conditions.

$$2NO^{\bullet} + O_2 \longrightarrow 2NO_2$$
$$NO_2 + NO^{\bullet} \longrightarrow N_2O_3$$
$$N_2O_3 + RSH \longrightarrow H^+ + NO_2^- + RSNO$$

Reference: Adapted from 98.

Some authors also reported the production of RSNO through a reaction of the nitrosonium cation (NO^+) with thiolate anion (RS^-).[99-101] However, free NO^+ is stable only at low pH (~ 2.0),[102] while thiolate formation, dependent on the nature of the molecule and pH medium, is more abundant at pH > 7.[103-107] Due to these properties, this route is likely less relevant in biology.

1.6.2.3 HNO production by enzymatic reduction

Enzymatic reduction of $NO^{\bullet}$ mediated by superoxide dismutase (SOD) or xanthine oxidase (XO) under anaerobic conditions has been described as a potential route for HNO production. SOD can directly reduce $NO^{\bullet}$ to HNO in the absence of O_2 through a reversible process.[88,89] In another reductive process, XO catalyzes an expected irreversible process where hypoxanthine is used as an electron donor to reduce $NO^{\bullet}$ to HNO, in the absence of oxygen.[90] However, these routes of production of HNO are still under debate, particularly considering the methodology employed for HNO detection, which is susceptible to bring significant mistakes.[108,109]

Another protein earlier claimed to produce HNO was the cytochrome c via a direct reduction of NO• to HNO, under anaerobic conditions,[110] however, major doubts were raised due to the probe used during those studies. Later, the same team has concluded HNO was indeed not produced discarding this route as a biological option.[111]

1.6.2.4 HNO production by hydroxylamine oxidation

Another possible pathway for the biosynthesis of HNO is the oxidation of hydroxylamine (NH_2OH) to HNO mediated by heme proteins using H_2O_2.[74,112-114] Wink and coworkers found that heme proteins containing proximal histidine ligand (e.g., horseradish peroxidase, lactoperoxidase, myeloperoxidase, myoglobin, and hemoglobin) could catalyze the conversion of NH_2OH to HNO, in the presence of hydrogen peroxide (H_2O_2).[112] Recently, Álvarez and coworkers confirmed this hypothesis, reporting that myoglobin catalyzes HNO production via peroxidation of NH_2OH.[74]

Hydroxylamine is a cellular metabolic product commonly found in physiological environments,[113,115,116] its oxidation into HNO is caused by the intermediate heme $Fe^{IV•}$=O formed by the reaction of heme Fe^{III} with H_2O_2 found in the cellular medium.[117,118] This reaction involves the heme $Fe^{IV•}$=O, which oxidizes NH_2OH that decomposes into HNO and H_2O, restoring heme Fe^{III} as described in Scheme 4.[112,119,120]

Scheme 4 - HNO synthesis via oxidation of hydroxylamine (NH_2OH) mediated by heme proteins and H_2O_2.

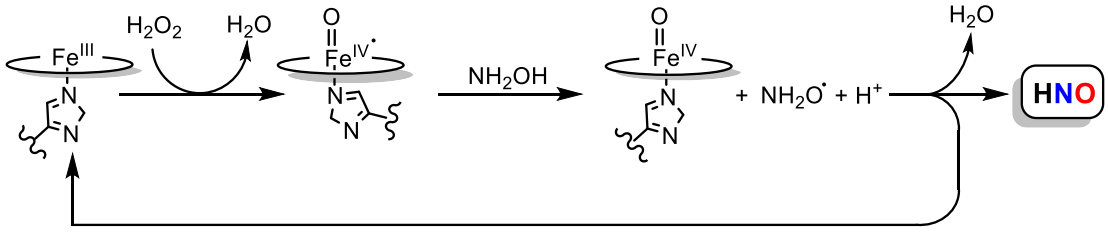

Reference: Adapted from 112 and 117-120.

1.7 The pharmacological importance of NO• and HNO in cancer, cardiovascular and tuberculosis diseases

We have already mentioned that NO• and HNO play key roles in various physiological processes.[121-123] In the context of this thesis, only the implication of

NO•/HNO in cancer, cardiovascular and tuberculosis affections will be considered. A summary of each pathology will be addressed below mainly in order to explain how HNO can be considered as pertinent therapeutic agent.

1.7.1 Cancer

Cancer (neoplasia or malignant tumor) is the name for a set of diseases that have in common the uncontrollable cell growth.[124] Cells that grow out of control, also called cancer cells or tumor cells, are the result of genetic mutations that lead to growth, unrestricted cell division, and resistance to apoptosis.[125] As cancer cells increase, the process of cellular angiogenesis is stimulated, which in turn induces blood vessels formation as a way of obtaining nutrients and oxygen.[126,127] In the course of these processes, eventually, tumor cells can invade adjacent tissues spreading to other parts of the body, this process is called metastasis.[128]

i. Global panorama

The International Classification of Diseases lists more than 600 types of cancer. According to the World Health Organization (WHO), cancer is one of the main causes of death in the world, having registered 9.6 million deaths in 2018, with an estimated 29.4 million cases in 2040.[124] In 2018, the most diagnosed cancer type was lung (11.6% of all cases), followed by female breast (11.6%) and colorectal cancer (10.2%).[124] From a geographical point of view, the incidence of cancer is influenced by sex and type of cancer. In 2018 the highest rates of lung cancer in men were reported in Micronesia/Polynesia (52.2 cases per 100,000 inhabitants), while in women it was in Northern America (30.7 cases per 100,000 inhabitants), while the highest rates of breast and prostate cancers occurred in Australia/New Zealand (breast = 106.8 cases per 100,000 inhabitants, and prostate = 96.6 per 100,000 inhabitants).[129]

ii. Prevention and treatment

Cancer is within non-communicable diseases (NCDs, or chronic diseases), configuring as non-transmissible, presenting long treatment, and can result from a combination of genetic, physiological, socioenvironmental, economic and behavioral factors.[130,131] The main factors that can influence the onset of cancer are: smoking (the agent that most contributes to cancer mortality), infections (e.g., *Helicobacter pylori* - stomach cancer, human papillomavirus (HPV) - cervical cancer, hepatitis B and C

viruses - liver cancer), diet, overweight, physical inactivity, alcohol use, occupational exposures (e.g., workers exposed to chemicals), pollution, food contaminants, medical drugs, ultraviolet and ionizing radiation, immunosuppressive drugs, and genetic susceptibility.[124,132,133]

Cancer is generally the most complex disease in terms of treatment among NCDs. Treatment can occur through surgery (procedure in which a surgeon removes cancer from your body), immunotherapy (treatment that helps your immune system fight cancer), hormone therapy (treatment that blocks the body's natural production of hormones), radiotherapy (treatment that uses high doses of radiation to kill cancer cells and shrink tumors), chemotherapy (use of drugs to kill cancer cells) and targeted therapy (treatment that targets proteins that control how cancer cells grow, divide, and spread).[124,134-139] Targeted therapy can work via different mechanisms: i) helping the immune system to destroy can cells,[140] ii) starving cancer cell from hormones that they need to growth,[141] iii) helping cancer cells to go through dying process,[142] iv) delivering cell-killing substances to cancer cell,[143] and v) stopping signals that favor blood vessels formation, blocking the neo-angiogenesis of the tumor.[127] This last approach is a known way how $NO^{\bullet}$/HNO exert their anticancer action.

Cancer treatment can occur through one or more combined treatment modalities/techniques. The combination of chemotherapy and targeted therapy, for example antiangiogenic drugs, have increased the progression-free survival (PFS, time period during and after treatment, in which a patient lives with the disease, but it does not get worse) of patients with metastatic cancer (pancreatic, colorectal, and breast), compared to treatment using chemotherapy alone.[126,127,144,145] These results helped to validate the concept of antiangiogenic agents in the treatment of cancer. Several antiangiogenic molecules have been approved by the Food and Drug Administration (FDA) for use as anticancer agents in combination with chemotherapy.[127] Figure 9 illustrates some examples of approved antiangiogenic drugs with their respective therapeutic indications.

Figure 9 - FDA approved antiangiogenic drugs and their targets in parentheses.

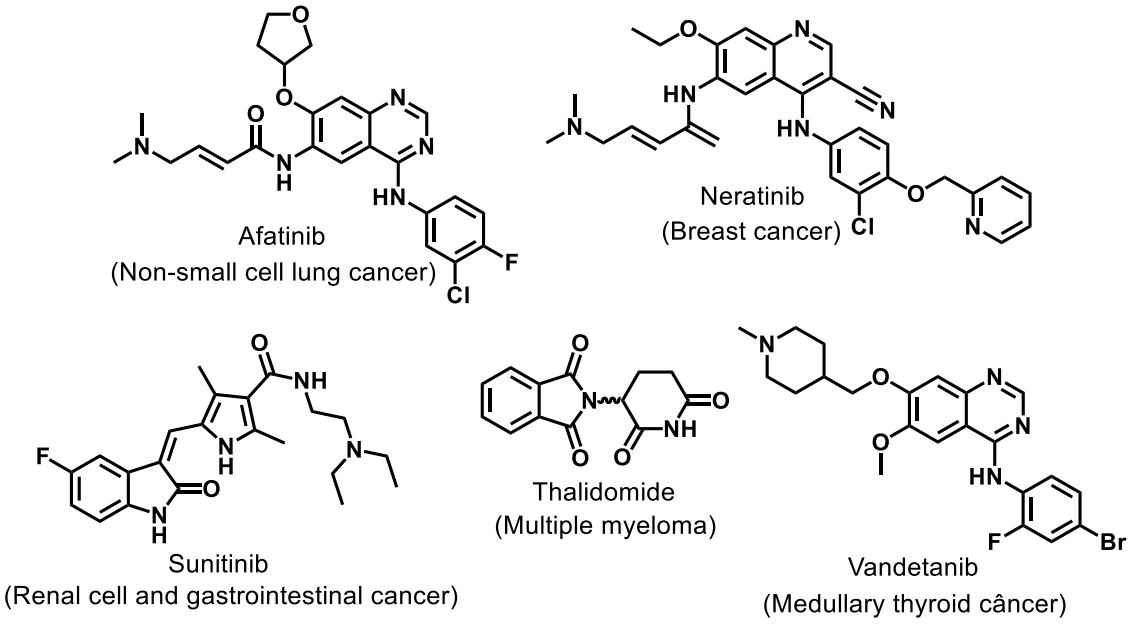

Reference: Elaborated by the author.

NO• can have beneficial and harmful roles on cancer disease tightly dependent on its biological levels. At low concentrations (100-300 nM), NO• can promote cancer growth through cell stimulation and enhancement of angiogenesis and metastasis. On the other hand, at high concentrations of NO• (>400 nM), it can disrupt cancer cell growth via apoptosis induction, tumor sensitization to chemo-, radio-, or immuno-therapy treatments, and may also function by reversing resistance to chemotherapy and by inhibiting the angiogenic and metastatic cascades.[146,147]

Angiogenesis is a normal and complex process controlled by certain biomolecules produced in the body, and consists of the growth of new blood vessels from existing ones.[148] These new blood vessels will serve to take up the oxygen necessary to the growth of the cancer cell.[126]

In cancer cells, the production of pro-angiogenic factors is induced in hypoxia conditions (caused by abnormal accelerated metabolism), which leads to the rapid and chaotic formation of blood vessels. Adaptation to different levels of oxygen in the cell (normal and cancer cells) is mediated by a family of transcriptional regulators, called hypoxia-inducible factors (HIFs).[127] HIFs are heterodimers consisting of an oxygen-independent β-subunit (HIF-β) and an oxygen-dependent α-subunit (HIF-α), which has three isoforms (HIF-1α, HIF-2α and HIF-3α).[127]

Under normoxia, transcriptional activity of HIF is specifically suppressed through the degradation of the HIF-1α subunits, via a hydroxylation process mediated by an asparaginyl hydroxylase factor. Low oxygen conditions induce the stabilization of HIF-1α, promoting the upregulation of several pro-angiogenic genes including VEGF (vascular endothelial growth factor), FGF (fibroblast growth factor), and PDGF (platelet derived growth factor).[127,149] The latters are responsible for inducing the formation of endothelial cells composing the blood vessels.[148] Thus, these different pro-angiogenic factors have been considered as promising targets for anticancer therapy.[126,127,145]

NO• and HNO have played a key role in the regulation of HIF-1α in tumor cells. While NO• has been indicated as a stabilizing agent for HIF-1α in normoxic conditions, HNO has been shown to act in the opposite way, blocking HIF-1α stabilization, induced by both hypoxia and NO• in normal air conditions, and hence inducing antiangiogenesis and cell death by apoptosis.[65,150-152] These properties open doors for the use of HNO donor agents as new and promising anticancer platforms. In the section 2.5, several HNO donor agents with potential antiangiogenesis and anticancer action are reported. One of such examples is object of this thesis and is described in chapter 1.

1.7.2 Cardiovascular diseases

Cardiovascular diseases (CVDs), or heart disease, are a group of disorders of the heart and blood vessels (cardiovascular system), including coronary heart disease, cerebrovascular disease, angina pectoris, myocardial infarction (heart attack), rheumatic heart disease, hypertensive heart disease, stroke, heart failure, cardiomyopathy, cardiac arrhythmias, among others.[153-155]

i. Global panorama

According to WHO, CVDs are the number 1 cause of death globally, with about 17.9 million deaths per year (31% of all deaths worldwide).[153] Roth and co-workers reported that in 2015 the countries with the highest CVD rates were those in Western and Eastern sub-Saharan Africa with 9,475 and 8,444 cases per 100,000 inhabitants, respectively.[156]

ii. Prevention and treatment

CVDs also belong to NCDs, therefore they are not transmissible, they tend to have a long duration, and the resulting factors for these diseases can be genetic, physiological, environmental and behavioral.[130,131] Several factors can contribute to the

development of CVDs: tobacco use, physical inactivity, unhealthy diet (rich in salt, fat, and calories), harmful use of alcohol, high blood pressure (hypertension), high blood sugar (diabetes), high blood lipids (e.g., cholesterol), overweight and obesity, poverty and low educational status, advancing age, male gender, genetic disposition and psychological factors (e.g., stress, depression).[154] Currently, it is also known that Coronavirus Disease 2019 (COVID-19) pneumonia has significantly influenced the increase in clinical complications in patients with CVDs.[157-160]

The choice for healthier lifestyle habits, good social habits avoiding stress, panic, among others, has proved to be an extremely strong ally in the prevention and treatment of CDVs.[161] Many heart problems are also amenable to treatment via surgical procedure and medication.[154,162,163] Cardiovascular drugs have been the most prescribed drugs in the world. The purpose of these medications is to prevent and treat morbid conditions that affect the cardiovascular system.[163]

Generally, the use of cardiovascular drugs is directed towards disease-related pathophysiological mechanisms, that is, cardiovascular drugs include compounds that directly regulate the function of the heart and blood vessels, through interaction with certain biological targets, resulting in a therapeutic response.[164] For example, in cases of hypertension, the treatment can occur by different types of drugs with different actions: diuretics, β-blockers, calcium (Ca^{2+}) channel blockers, ACE (angiotensin converting enzyme) inhibitors, α-adrenergic receptor, and direct vasodilators.[155,165,166] Some examples of classic antihypertensive drugs used in cardiovascular treatment are listed in Figure 10, their classification within the group of antihypertensive drugs is also indicated.[165,166]

Figure 10 - Some examples of cardiovascular drugs, followed in the parentheses by their pharmacological class.

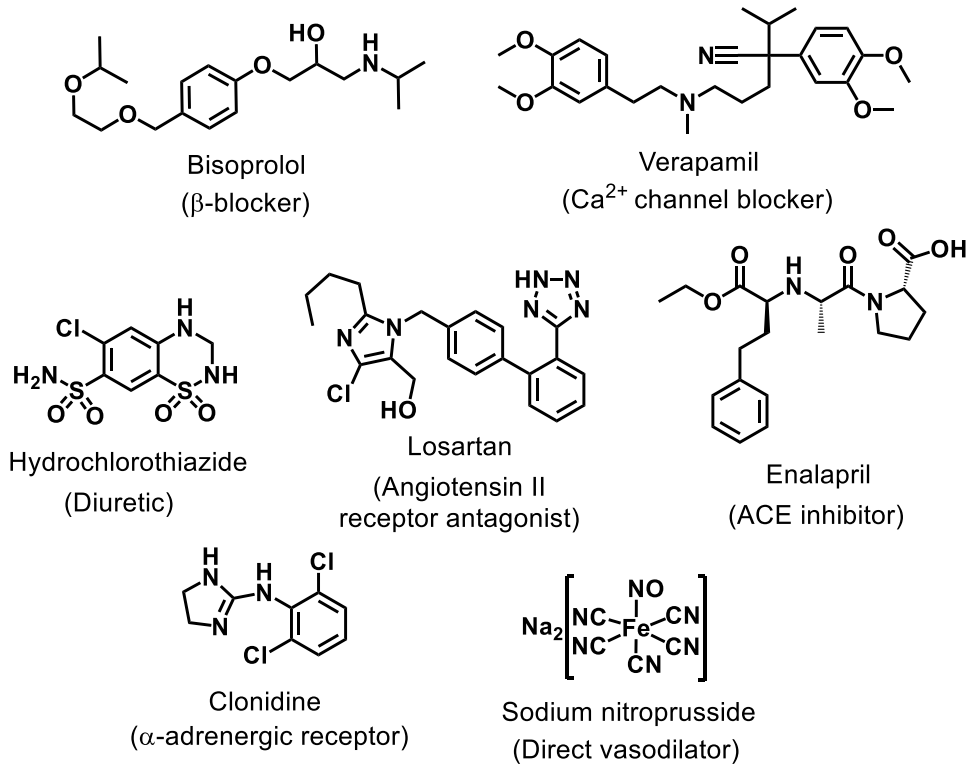

Reference: Elaborated by the author.

Vasodilation is one of the main therapeutic strategies to obtain an antihypertensive effect. In this thesis, we are particularly interested on the antihypertensive effects of NO•/HNO. From a mechanistic point of view, after the production of NO• in the body, either endogenously or through donor drugs, NO• readily diffuses through cell membranes, until it reaches its main target, soluble guanylate cyclase (sGC) protein (Figure 11).[54] sGC is a heterodimeric protein made up of two subunits α and β. The β subunit has the prosthetic group (heme), which has a strong affinity for NO•. When NO• binds to Fe^{II}-heme of sGC, it disrupts the bond between Fe^{II} and the histidine residue (105) of the protein, a phenomenon also called *trans*-labilizing effect of NO•. As a result of the previous step, a significant conformational change in sGC is initiated in order to activate the catalytic site of the enzyme. This activation promotes an increase in Mg^{2+} dependent catalytic activity, resulting in the conversion of GTP into PPi and cGMP.[54] The latter regulates the effect of several biological systems such as cGMP-dependent protein kinases, ion channels, and phosphodiesterases, responsible for mediating several physiological processes including vasodilation.[167]

HNO also acts as a potent vasodilator, however, despite numerous mechanisms for HNO mediated vasodilation have been proposed, including NO•-like activity on sGC, the mechanisms of HNO in the cardiovascular system remain controversial.[168,169]

Figure 11 - Activation mechanism of soluble guanylate cyclase by NO•.

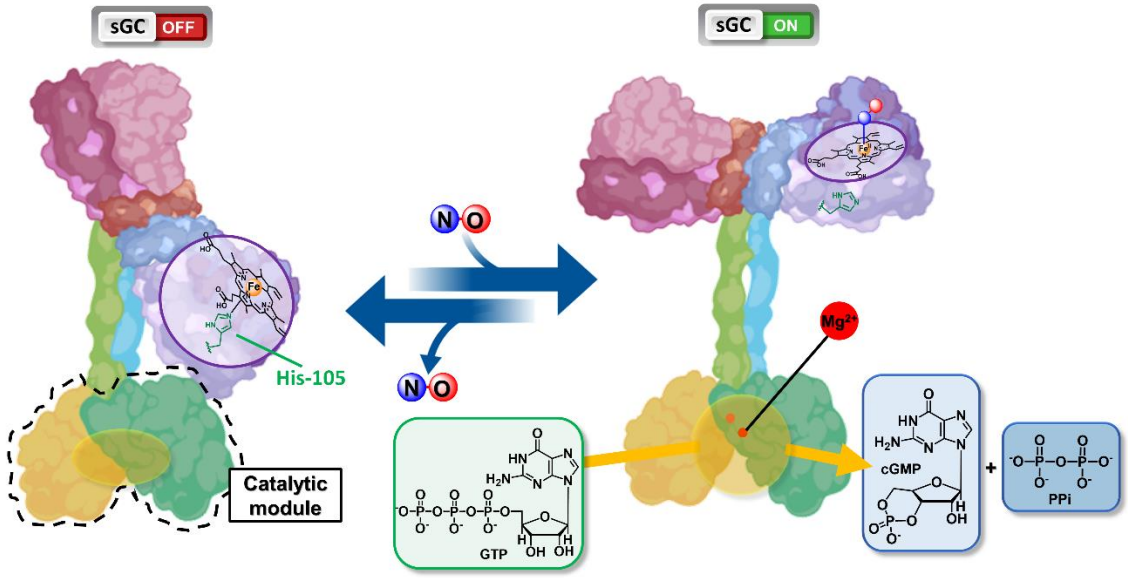

Reference: Adapted from 170.

1.7.3 Tuberculosis

Tuberculosis (TB) is an infectious disease caused by the *Mycobacterium tuberculosis* (*Mtb*) bacillus. It mainly affects the lungs (pulmonary TB) but can also affect other organs (extrapulmonary TB).[171]

i. Global panorama

WHO indicates TB as one of the main infectious diseases present in the world. In 2018, it was estimated that 10 million people were contaminated by TB, and 1.5 million had died from it.[171] More than one third of the current world's population (1.7 billion) has latent tuberculosis, which means that these people are asymptomatically infected with *Mtb*.[172] From a geographical perspective, tuberculosis is widespread worldwide, however, in 2018, the majority of the cases, estimated by WHO, were concentrated in South-East Asia Region (44%), African Region (24%) and Western Pacific Region (18%), with the most affected countries being India (2,690 cases per 100,000 inhabitants), Indonesia (845 cases per 100,000 inhabitants) and China (866 cases per 100,000 inhabitants).[171]

ii. Transmission of disease

In general, transmission occurs when an infected person coughs, sneezes or speaks, releasing pathogens into the air through micro-droplets of mucus, so a simple inhalation is enough to become infected.[173] In cases of primary infection, tuberculosis is usually cured spontaneously by the action of the host's immune system.[174] The bacilli ingested by macrophages multiply and trigger a chemotactic reaction, in which other macrophages and other defensive cells are attracted to the infected area. This agglomerate of cells, forms a granuloma (or tuber), in which *Mtb* develops poorly due to lack of oxygen and can therefore remain inactive. The disease remains in the latent phase and the lesions calcify. However, although tuberculosis bacilli are phagocyted by immune cells (e.g., macrophages, neutrophils, dendritic cells), they do have virulence factors that allow them to survive within these phagocytic cells.[175]

In 90% of cases of primary infection, the tubercular *bacillus* remains inactive. In this case, the infection is latent (latent TB infection (LTBI)), and asymptomatic, in addition, the host is not at risk of contagion.[173,175] Nevertheless, in conditions of low immunity (HIV-1 serostatus, diabetes, undernutrition, immunosuppressive),[171] *Mtb* tubers can be reactivated causing local inflammation and impairing the functioning of the lungs. Eventually a deficient immune response results in necrosis and rupture of granulomas, dispersing more infectious bacilli in the airways.[176,177] This pathological condition is called pulmonary tuberculosis (pulmonary TB). If adequate treatment does not occur, the spread of tuberculosis bacilli throughout the host's body can lead to extrapulmonary tuberculosis (extrapulmonary TB), in addition to eventual death.[178]

iii. Treatment

The cell wall of *Mycobacterium* is the main characteristic of this genus. It is rich in fatty acids and lipids, making this microorganism one of the most pathogenic species to humans. *Mtb* has an extremely complex and impermeable mycobacterial wall, this protection consists of peptidoglycan, arabinogalactan, mycolic acids, and external lipids.[179] This protective structure contributes significantly to high virulence and resistance to classic antibiotic treatments.[180]

The treatment of TB consists of the use of vaccine and antibiotics. In the case of treatment through vaccination, *Bacillus* Calmette – Guérin (BCG) is the only one specifically used to prevent severe forms of tuberculosis (TB meningitis and miliary TB) in children.[181] Another alternative is the use of antibiotics that are divided into

first–, second- and third-line drugs. The treatment modalities depend on the bacteria's sensitivity to the antibiotics used. Details are presented below.

iv. First-line antitubercular drugs

Treatment regimen for all new cases of all forms of pulmonary and extrapulmonary tuberculosis (except meningoencephalitis), as well as for all cases of relapse and return after default, consists of 6 months. In the first 2 months, there is a daily intake of the four first-line drugs rifampicin, isoniazid (INH), pyrazinamide (PZA) and ethambutol (Figure 12), followed by another 4 months, using only rifampicin and INH, in order to ensure the complete extermination of *Mtb* from the host body.[182]

Figure 12 - First-line antitubercular drugs.

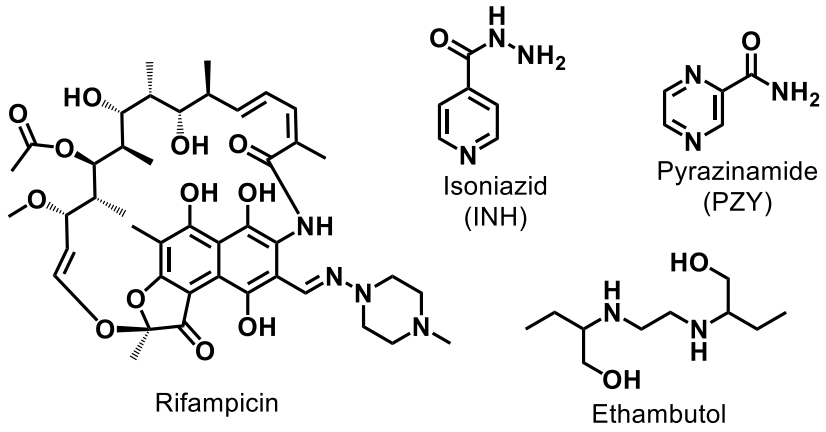

Reference: Elaborated by the author.

v. Second-line antitubercular drugs

The emergence of treatment-resistant bacteria using first-line antitubercular drugs has resulted in the employment of other medicines called second-line antitubercular drugs. The main second-line antitubercular drugs are: *p*-aminosalicylic acid, thioamides (ethionamide and prothionamide), cycloserine derivatives (cycloserine and terizidone), aminoglycosides (amikacin e streptomycin) and fluoroquinolones (levofloxacin and moxifloxacin) (Figure 13). Nevertheless, these compounds are generally less potent, more toxic, and more expensive. In addition, drug-resistant TB treatment is long, ranging from 9-12 months (shorter regimen) and 18-20 months (longer regimen).[183]

Figure 13 - Some examples of antitubercular second-line drugs.

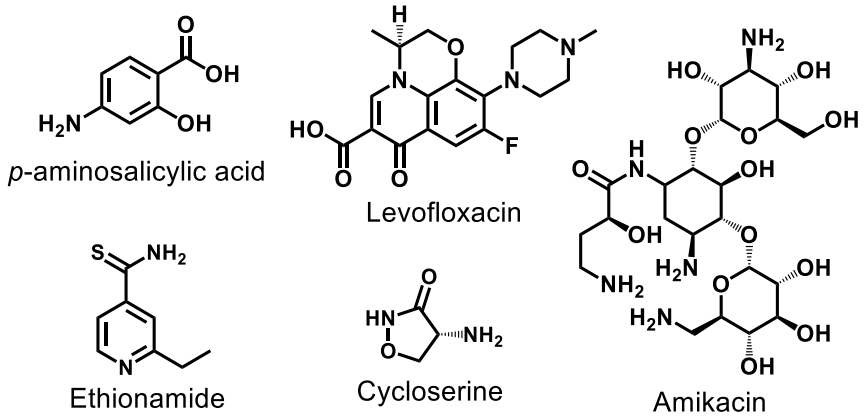

Reference: Elaborated by the author.

vi. Third-line antitubercular drugs

Although the development of second-line drugs provides a cure for many multidrug-resistant tuberculosis (MDR-TB) patients, in some cases, the treatment is not effective beyond the high toxicity of these drugs.[184] As a way to overcome these treatment failures, new drugs with MDR-TB action, called antitubercular third-line drugs, have been developed. Three examples of third-line antitubercular drugs are bedaquiline, delamanid, and pretomanid. These drugs were the last antitubercular molecules approved for clinical use, bedaquiline in 2012 (by FDA), delamanid in 2014 (by European Medicines Agency (EMA)), and pretomanid in 2019 (by FDA) (Figure 14).[184,185] WHO recently included bedaquiline and delamanid in the group of medicines recommended for use in longer MDR-TB regimens.[186]

Figure 14 - Structures of bedaquiline, delamanid, and pretomanid.

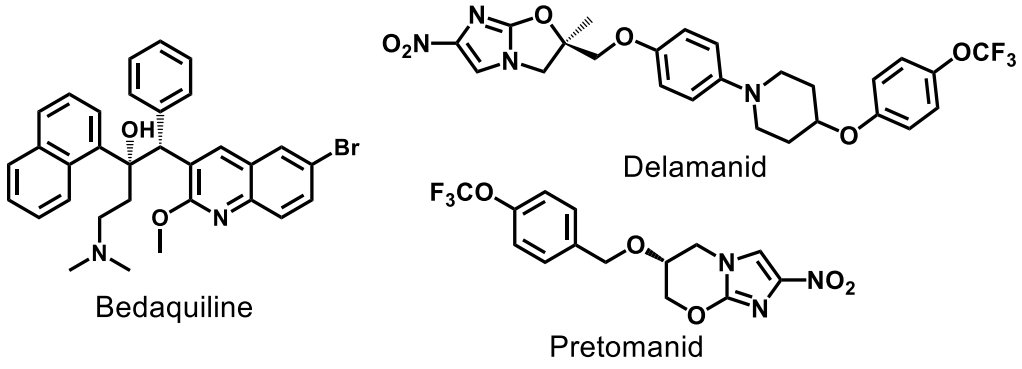

Reference: Elaborated by the author.

Within the context of this thesis, delamanid stands out because it is reported as a HNO donor prodrug with anti-TB action. Despite delamanid is known to inhibit methoxy mycolic and keto-mycolic acids biosynthetic pathways, its mode of action at molecular level remains uncertain.[187] It has been shown that to exert its anti-TB activity, an intracellular bioreductive activation via mycobacterial nitroreductase enzyme (Ddn) is required, consequently producing HNO/NO• as potential active metabolites (scheme 5).[188] In fact, it has been proposed that HNO and NO• have anti-TB action, however the way, in which these molecules act against *Mtb* is still not well elucidated.[189,190]

Scheme 5 - Proposed mechanism for the activation reaction of delamanid by the Ddn enzyme, reference.

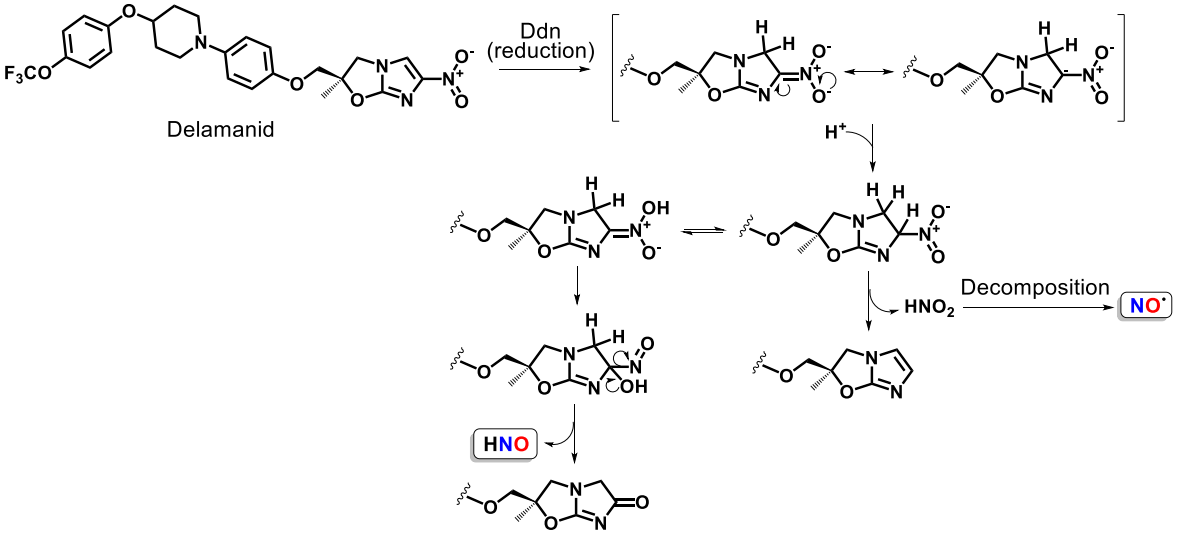

Reference: Adapted from 187.

The pharmacological properties of NO•/HNO, discussed above, offer new medical perspectives for the use of NO•/HNO as a promising new anticancer, antihypertensive and anti-TB agent. As NO•/HNO are molecules highly unstable with no ideal chemical and pharmacokinetic properties to justify its use alone, the development of a new chemical family, able to act as pro-dugs and deliver NO•/HNO *in vivo*, is an exciting research topic, in which several researchers are working on it. In the next paragraph, an overview of NO• and HNO donors will be discussed.

1.8 Nitric oxide (NO•) donors

Nitric oxide must reach certain biological levels to establish its effects, which can vary from signaling regulation of blood pressure to cellular apoptosis of

cancer cells. This illustrates well how critical are the strategies to delivery this molecule in a controlled and selective way to guarantee proper targeting and dosing of NO•.[191] Aiming at different targets, several strategies have been used in the design NO• donors, particularly taking advantages of specific stimulus promoted by the body (e.g., pH, and enzymatic reaction) or even externally (e.g., light). Throughout the text, we will discuss the chemistry and biological properties of some NO• donors.

1.8.1 Organic Nitrates

Organic nitrite molecules are the oldest class of NO• donors.[192] Structurally they are nitric acid esters, generally represented by the formula $RONO_2$. The glyceryl trinitrate (GTN), pentaerythrityl tetranitrate (PETN), and isosorbide dinitrate (ISDN), are examples of molecules that integrate this group (Figure 15). GTN is one of the most commonly known nitric acid esters, originally used in the industry of explosives, then recognized as a drug in the treatment and prevention of angina pectoris pain.[193] Curiously, the famous Alfred Nobel who made a fortune developing explosive formulations including GTN, was indeed treated with this same compound due to his angina pectoris medical problem. Today, GTN is also used in hypertensive crises and erectile dysfunction.[194,195] Several other organic nitrates have been used in the treatment of cardiovascular diseases,[196] angina pectoris, pre-eclampsia, pulmonary hypertension, and chronic heart failure in combination with hydralazine.[197-199]

Figure 15 - Classic organic nitrates.

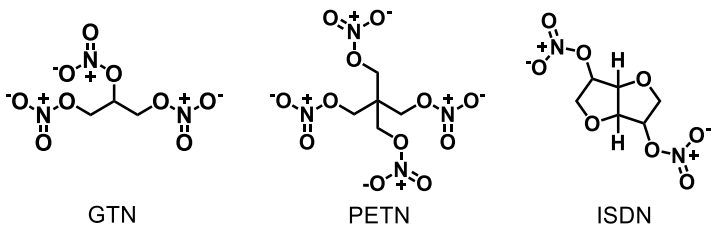

Reference: Elaborated by the author.

However, due to the side effects of some organic nitrates,[196,200-206] the scientific community moved to explored its use in hybrid compounds of known drugs, expecting to generate dual pharmacological activities. The nicorandil (antianginal drug),[207] 2-acetoxy-benzoate-2-(2-nitroxymethyl)-phenyl ester (NCX4016, colorectal cancer prevention in clinical trials Phase I),[208] HCT 3012 (analgesic and anti-inflammatory drug in clinical trials Phase III),[209] and NCX 701 (analgesic and anti-

inflammatory drug in clinical trials Phase I),[209] are examples of hybrid molecules developed with promising application in different biological segments: antianginal, analgesic, anticancer, and anti-inflammatory. Figure 16 illustrates various nitrate hybrid drugs and describes the parent organic drug and the reasons for incorporating the nitrate group.

Figure 16 - New nitrate hybrids and the goals for their development.

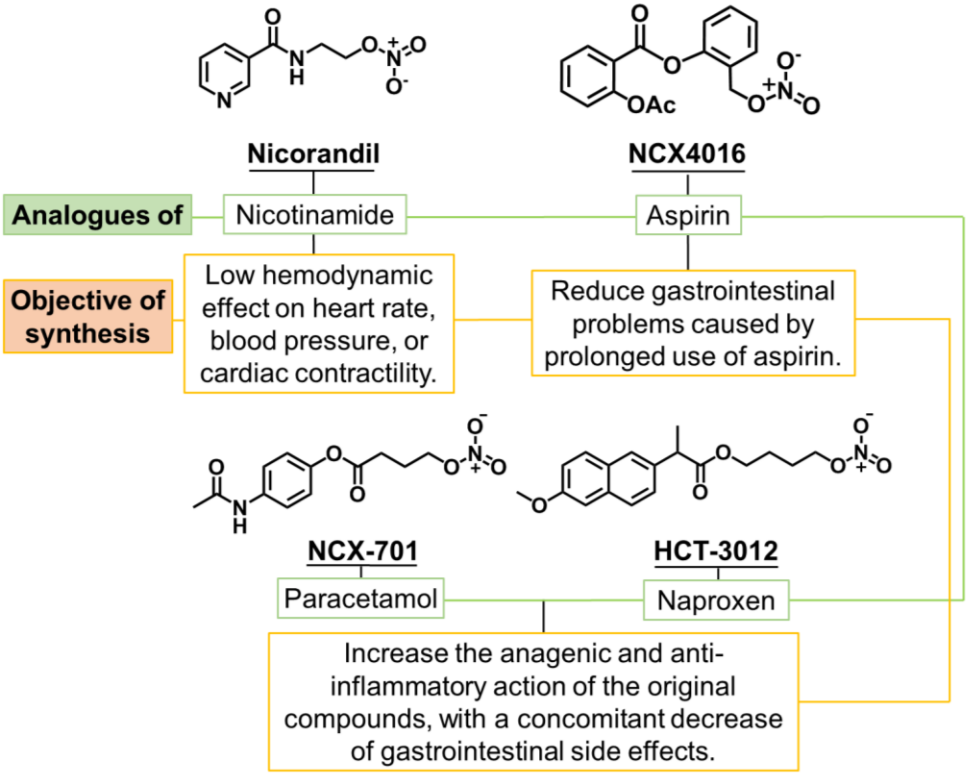

Reference: Elaborated by the author.

Most of the biological effects of organic nitrates are attributed to their ability to release NO•. In general, organic nitrates are able to release NO• after reaction with enzymatic systems (e.g., cytochrome P450, xanthine oxidoreductase, glutathione-*S*-transferase, and aldehyde dehydrogenase 2), ferrous-heme proteins (deoxyhemoglobin and deoxymyoglobin), or thiols.[192,196,210] Glutathione is an exception because its reaction with organic nitrates must be catalyzed by glutathione-S-transferase.[192]

The mechanism of NO• release through organic nitrates in physiological medium requires reduction reactions involving three electrons.[211] In reductions catalyzed by enzymatic systems and ferrous-heme proteins, the first step produces hydrated nitrate ester, which decomposes into nitrite ester releasing water. Hydrolysis of

nitrite ester yields the respective alcohol and nitrous acid (HNO_2). In the final step, HNO_2 can be reduced producing $NO^{\bullet}$ and H_2O (Scheme 6A).[211] In the case of enzymatic reduction involving thiol, the reaction occurs by a nucleophilic attack in the nitrogen of nitrate group. This reaction yields an alcohol and an unstable intermediate thionitrate. This latter can further react (nonenzymic) with another thiol molecule producing HNO_2 and disulfides,[212] or decompose into $NO^{\bullet}$ and sulfenyl product (Scheme 6B).[213]

Scheme 6 - Mechanism of nitrate organic reduction by enzymatic systems (without thiol participation) and ferrous-heme proteins (A) or enzymatic reduction involving thiols (B).

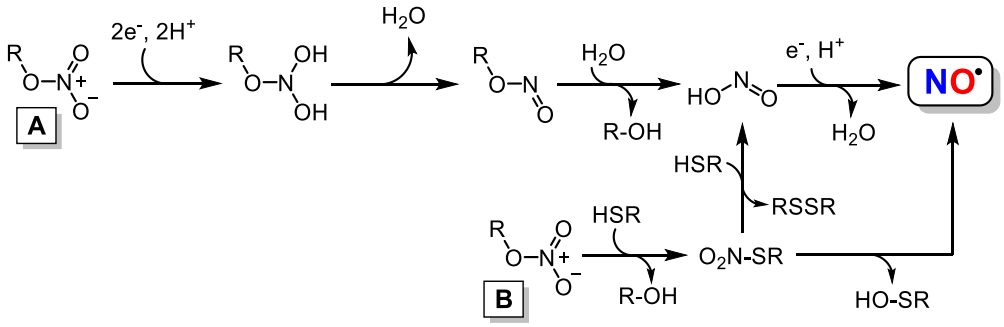

Reference: Adapted from 211-213.

1.8.2 Secondary amines-based diazeniumdiolates (NONOates)

The diazeniumdiolates or NONOates compounds have a $^{-}O\text{-}N{=}N\text{-}O^{-}$ (NONO) moiety connected to a primary or secondary amine. This type of molecule, in special the secondary amines, is considered standard $NO^{\bullet}$ donors and is thus used in several experimental models. DEA NONOate, DETA NONOate, PROLI NONOate, SPER NONOate, and MAHMA NONOate are some examples of these donors (Figure 17).[214,215] A series of studies have shown the ability of NONOates derivatives to release $NO^{\bullet}$, where these molecules were investigated for biological activities such as vasodilation,[216,217] platelet aggregation inhibition,[218] and modulation of angiogenesis.[214]

Figure 17 - Structures of some NONOates derivatives molecules.

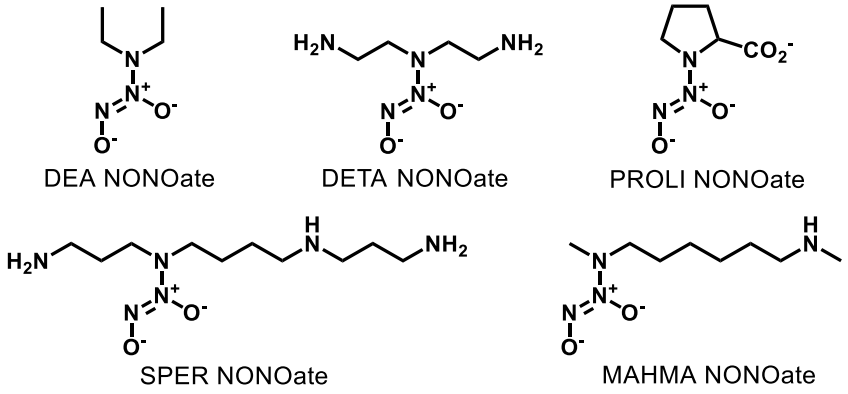

Reference: Elaborated by the author.

Diazeniumdiolate compounds are unstable under physiological conditions and can decompose directly generating up to 2 equivalents of NO• per NONO moiety. However, the rate of NO• release is dependent on the temperature, pH and structure of the parent compound.[219,220] In general, the decomposition of NONOates is acid-dependent, such a decomposition mechanism can follow two different pathways potentially leading to the same final products as depicted in Scheme 7.[221]

Scheme 7 - Mechanism of diazeniumdiolates decomposition.

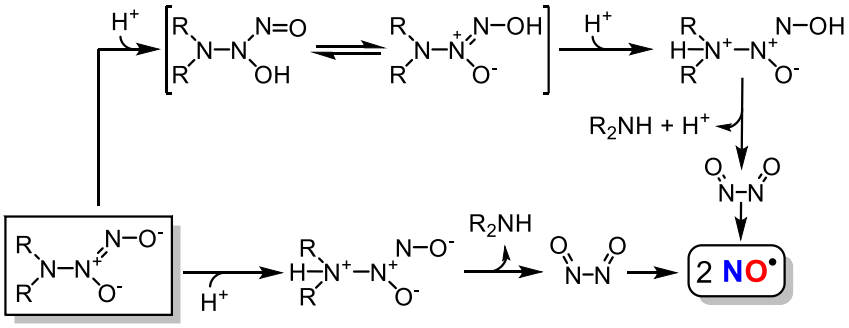

Reference: Adapted from 221.

In order to fine-tune the release of NO• by these NONOates, several new pro-drugs containing this functional group have also been developed in analogy to what was previously shown for DEA and PROLI NONOate. For example V-PYRRO/NO (1-[(ethenyloxy)-NNO-azoxy]-pyrrolidine), a pro-drug with hepatoprotective properties against a variety of toxins, and JS-K (O^2-(2,4-dinitrophenyl) 1-[(4-ethoxycarbonyl)piperazin-1-yl]diazen-1-ium-1,2-diolate), a promising anticancer pro-

drug (Figure 18).[222] Basically, all these proposal compounds are activated through the diazeniumdiolate moiety with the production of NO• under physiological conditions. Until now, NONOates are not yet approved for clinical use.[223] Up to our knowledge only a single study using NONOate derivative MK-8150 (Figure 18) in hypertension treatment (clinical trials Phase I) exist.[224] However, the control of the NO• release as well as its targeted delivery through structural modulation, make NONOates potential candidates for therapeutic use.

Figure 18 - Structure of some promising NONOates derivatives.

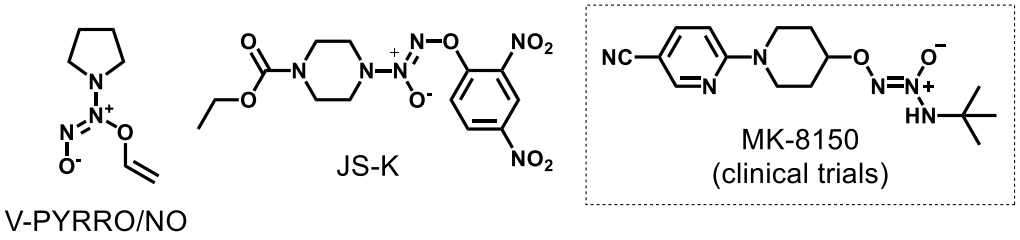

Reference: Elaborated by the author.

1.8.3 S-Nitrosothiols (RSNOs)

S-nitrosothiols (RS-NO) are considered one of the most common NO• releasers. Some well-known *S*-nitrosothiols derivatives are *S*-nitroso-glutathione (GSNO), *S*-nitroso-cysteine (SNO-Cys), *S*-nitroso-*N*-acetylpenicillamine (SNAP), and 1-nitroso-thiogalactose tetraacetate (SNAG),[192] which are illustrated in Figure 19.

Figure 19 - Structure of some *S*-Nitrosothiols (RSNOs).

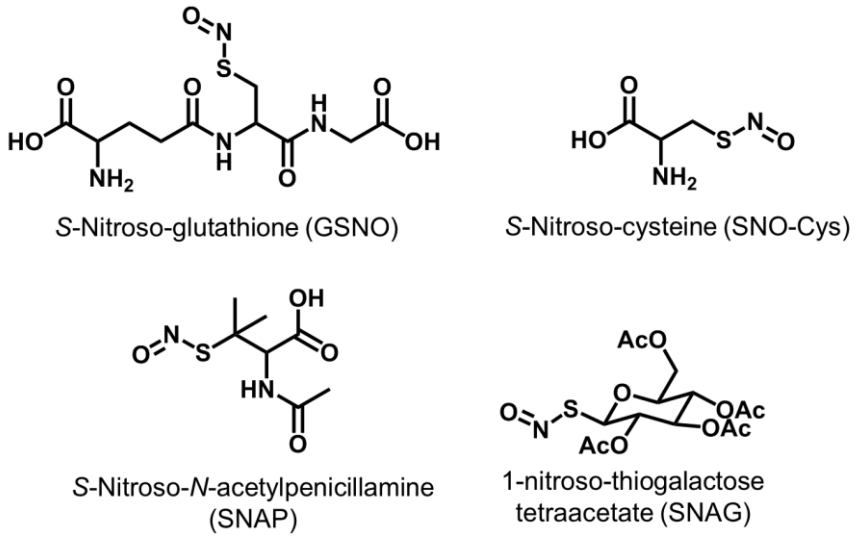

Reference: Elaborated by the author.

S-Nitrosothiols accomplish several functions in the body such as vasodilation, wound healing, anti-infectious action, and analgesic action against inflammatory pain.[225] In general, the properties of *S*-nitrosothiols are directly associated with their decomposition and the release of NO•. This process can be induced by certain metal ions,[226,227] superoxide reductases (CuZn-SOD),[228] heat,[229,230] and light.[231] The mechanisms for all of these induced-decomposition processes are depicted in Scheme 8.[227,228,232]

Scheme 8 - Mechanism of RSNOs decomposition induced by Cu^{+} ions (A), enzymes (CuZn-SOD) (B), other metal ions (Hg^{2+} and Ag^{+}) (C), heat and light (D).

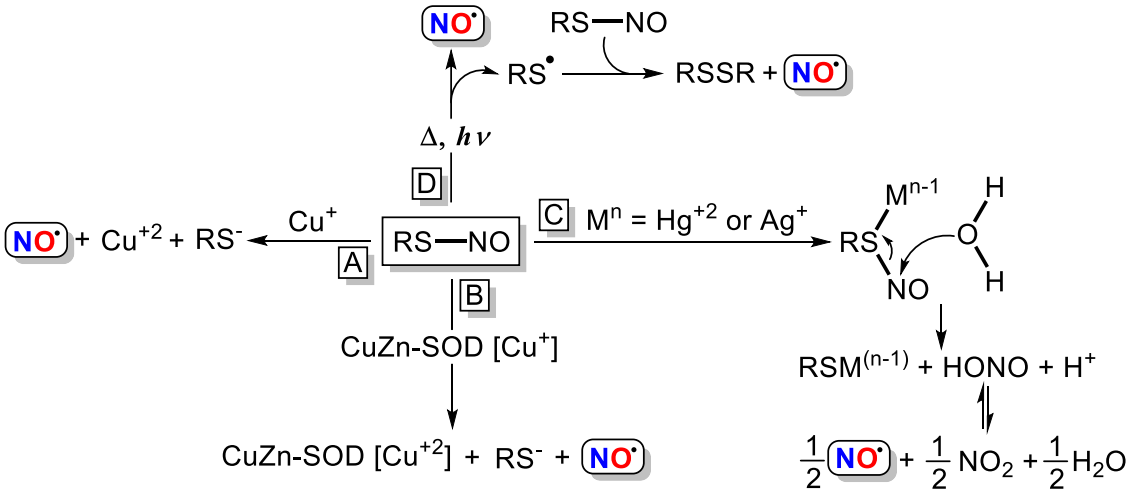

Reference: Adapted from 226-232.

Currently, no *S*-nitrosothiols are available to clinical use, but there are a large number of clinical studies mainly to the GSNO, demonstrating their advantageous features, especially in the cardiovascular disorders.[233,234] In addition, its potential use in the treatment of asthma has also been evaluated (in clinical trials Phase I, ClinicalTrials.gov Identifier: NCT03926741).[235]

1.8.4 Furoxans

Furoxans are molecules containing an 1,2,5-oxadiazole-2-oxides heterocycle as part of their structures. Currently furoxans have no clinical application, however, these molecules have many pharmacological activities including anti-inflammatory,[236] antituberculosis, antimalarial,[237,238] antiplatelet, antithrombotic,[239] and anticancer,[240] which have drew the attention of the scientific community. Additionally, many of the new reported furoxans have been designed by modifying known drug

structures, enabling the potentiation of pharmacological action and reduction of possible side effects (Figure 20).[236-239,241-243]

Figure 20 - Structure of some promising furoxan hybrid-based agents.

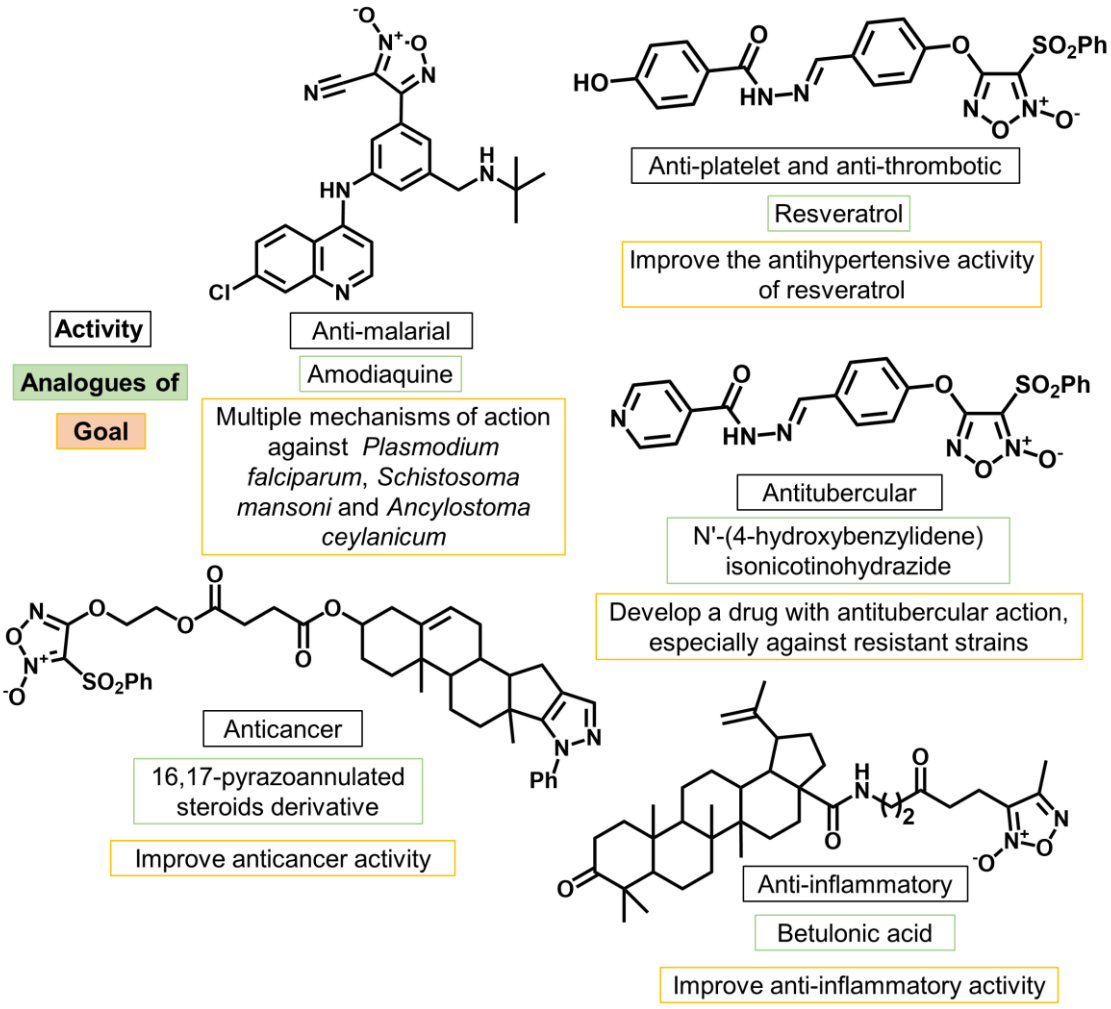

Reference: Elaborated by the author.

In general, these molecules release NO• in physiological medium through reaction with thiols.[218,244,245] The mechanistic proposal for this process is based on the nucleophilic attack of thiolate ions to the 4 or 3 positions of the furoxan ring, followed by the opening of a heterocyclic ring with formation of a nitroso intermediate. The latter can decompose releasing HNO, which, in turn, may react either with molecular oxygen, or other oxidative species yielding NO•. The formation of nitrosothiol is also a possible pathway to explain NO• formation (Scheme 9).[246] Interestingly, despite the supposed generation of HNO in this class of molecules, the literature ignore that the observed

pharmacological actions of these derivatives may also be related to HNO. A detailed analysis of the mechanism of the NO• or HNO release by this class of pro-drugs is thus necessary.

Scheme 9 - Mechanism of furoxan-based molecules in releasing NO• by reaction with thiol.

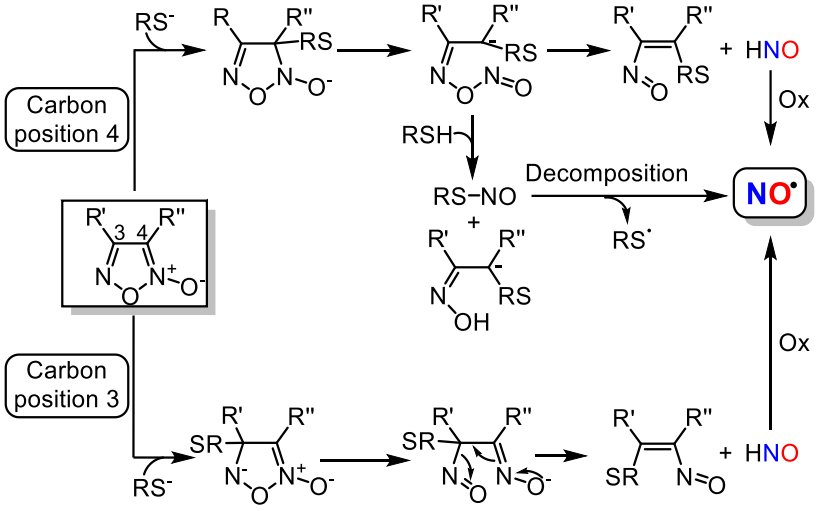

Reference: Adapted from 246.

Besides that, other authors indicated that the decomposition of certain furoxan-based molecules can also occur through simultaneous nucleophilic attack in both 3 and 4 positions.[247] This proposal indicates decomposition of these molecules to release NO• is tightly dependent on their structure-reactivity. Beyond the reaction with thiol, photoisomerization has been suggested as a way to induce NO• release.[248,249]

1.8.5 Sydnonimines

The sydnonimines are a class of direct NO• donors, which have in their structure the mesoionic heterocyclic functional group oxadiazole, as shown in Figure 21. These compounds have also shown many pharmacological activities such as antihypertension,[250] anti-ischemic,[251] prevention of reperfusion damage,[252] and others,[253] associated to the release of NO• under physiological conditions. Molsidomine is the most well studied compound of this class. It is currently used as antianginal pro-drug in several countries in Europe.[244,254] Sydnocarb® is another example of sydnomine used clinically, however it is only used in Russia as a psychostimulant.[255] In order to improve the action of sydnonimines pro-drugs, new sydnonimine derivatives has been developed, especially through the hybridization of the sydnonimine moiety with

chemical carriers (Figure 21). Cai, Nortcliffe and collaborators developed new sydnonimines linked to carbohydrates and amino acids through carbamate-linked, enabling the recognition and internalization of these molecules by cells.[256,257] These strategies are highly interesting considering the importance of providing local and temporal dose of NO• to achieve greater efficacy and minimal side effects.

Figure 21 - Structures of some sydnonimine-based compounds.

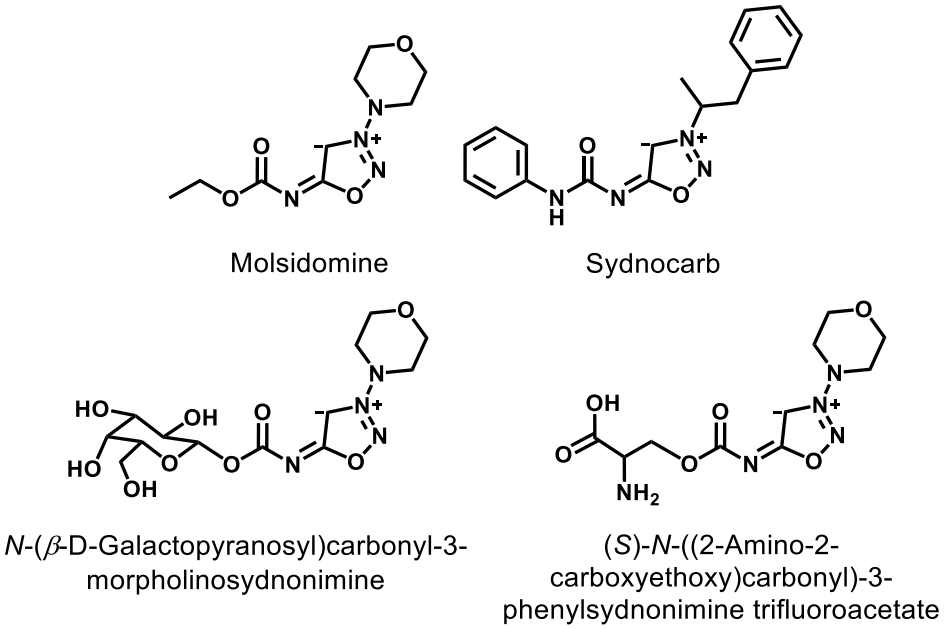

Reference: Elaborated by the author.

In general, for these sydnonimine-based compounds, the release of NO• depends on the pH, and their reactivities are associated to their chemical structures. Besides that, enzymatic reactions (e.g., esterase or glycosidases)[253,256] or reactions with thiols[257,258] can increase the rate of the NO• release *in vivo*. In physiological medium, O_2 plays a key role in the release of NO•, after an enzymatic conversion of oxadiazole compound to the ring-open form intermediate, this lasted is oxidized by O_2, enabling the production of NO•.[259] As example, mechanism for the release of NO• by molsidomine is illustrated in Scheme 10.

Scheme 10 - Mechanism proposed by Janczuk and co-workers for the release of NO• by molsidomine.

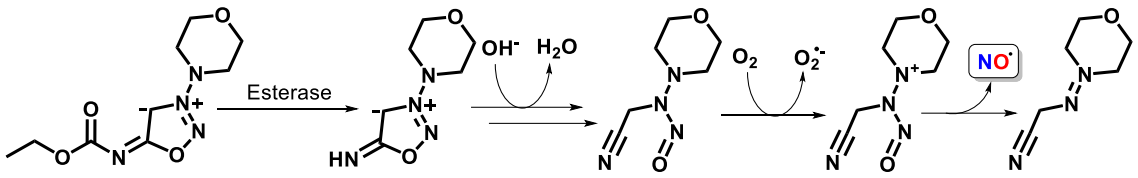

Reference: Adapted from 192.

1.9 Nitroxyl (HNO) donors

Despite relatively recent reports on the biochemical, pharmacological and physiological properties of HNO, this molecule is extremely unstable, dimerizing easily into N_2O (8×10^6 M^{-1} s^{-1}, pH 7.4, 22 °C). This process hinders the direct use of HNO and still raises debates about possible routes for the biosynthesis. Thus, the use of HNO donors has been essential for a better understanding of its biological role and for the appropriate use of this molecule. In addition, in analogy with NO• donors, different HNO releasing molecules have been developed and studied in order to generate new therapeutic agents, given the pharmacological potential of HNO. Differently from the NO• donor class, there are no HNO donors currently in clinical use.

1.9.1 Angeli's salt and primary amine diazeniumdiolate-based donors

Sodium trioxodinitrate or Angeli's salt (AS, $Na_2N_2O_3$), is an inorganic salt synthesized by Angelo Angeli more than 120 years ago (Scheme 11A).[68] This inorganic compound is currently one of the most commonly used HNO donor, especially in pharmacological studies.[77] AS releases HNO through spontaneous decomposition from pH 4 to 8.[260] Among the *in vivo* pharmacological effects observed for AS, one can mention: anti-inflammatory, vasodilator and anticancer.[65,261-263] Nevertheless, under physiological conditions, AS has a short half-life time ($t_{1/2}$ = 2.3 min) requiring relatively high concentrations to achieve physiological responses, which has limited its therapeutic applications.[216] Thus, new HNO donors have been developed and biologically investigated. O^2-alkylated primary amine-based diazeniumdiolates are a class of HNO donors structurally similar to AS, but with a longer half-life time under physiological conditions and, in addition, with a possibility to undergo an enzymatic activation (esterase or β-galactosidase -mediated hydrolysis).[264-265]

Scheme 11 - Angeli's salt (A), AcOM-IPA/NO (B), and Gal-IPA/NO (C) decomposition.

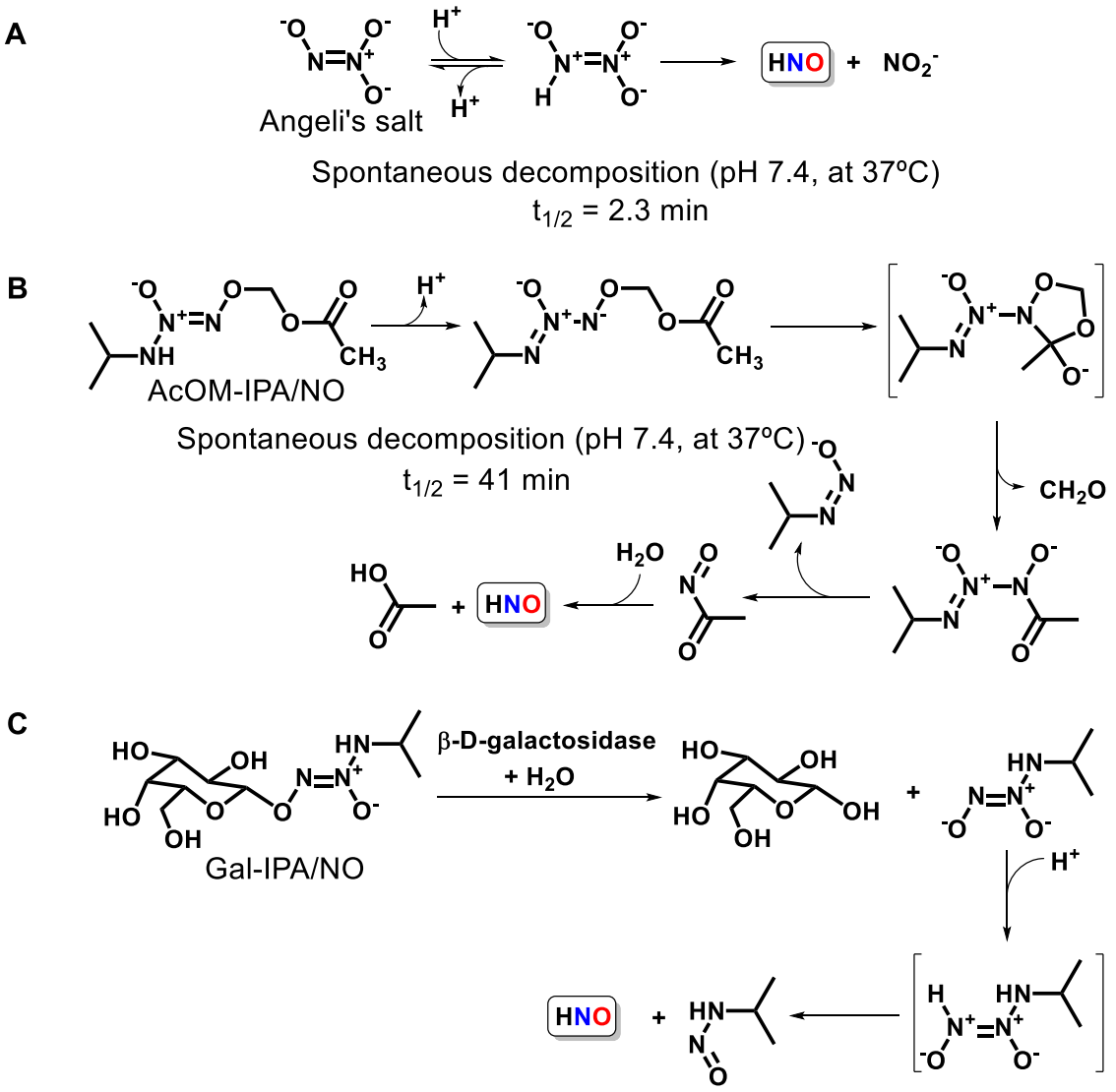

Reference: Adapted from 260, 264 and 265.

Primary amine-based donors generally have short HNO release rates, besides the ability to release NO• based on pH, making them chemically similar to AS.[216,260,266] However, through O^2-alkylation of the diazeniumdiolate group, the rate of decomposition can be fine tuned, which can also be achieved by other strategies (e.g., enzymatic activation). Keefer and collaborators,[264] developed an O^2-alkylated primary amine-based diazeniumdiolates pro-drug called AcOM-IPA/NO. This molecule showed capacity to release HNO spontaneously under physiological conditions, like AS, but with a release rate ($t_{1/2}$ = 41 min) significantly longer than AS (Scheme 11B). Furthermore, AcOM-IPA/NO mostly releases HNO without traces of NO•, which makes

an important agent in the study of the chemical and pharmacological properties of HNO. Regarding to O^2-alkylated primary amine-based diazeniumdiolates enzyme-activated, Holland and co-workers synthesized a hybrid of α-D-galactose and IPA/NO (sodium 1-(isopropylamino)diazen-1-ium-1,2-diolate), named Gal-IPA/NO, which releases HNO with half-life time of 140 min upon catalysis with β-galactosidase (Scheme 11C).[265] This result showed, besides the slow HNO release rate, that such modification generates a promising tool that can allow modulation of the HNO releasing.

1.9.2 Hydroxylamine-based donors

N-Hydroxybenzenesulfonamid or Piloty's acid (PA) (Figure 22) is a well-known HNO donor like AS. In spite of being an old compound, whose synthesis was reported in 1896, PA has not been much used in biological studies involving HNO. This is likely due to a decomposition process that, in basic solutions (pH 8), occurs with a relatively long half-life time of 561 min.[267] PA has a hydroxylamine group linked to a sulfonyl group, which if deprotonated can produce an anionic intermediate that decomposes releasing HNO (Scheme 12). In order to improve its application in a physiological environment, Toscano and collaborators modified the structure of PA by introducing a bromine group at position 2 of the benzene ring, resulting in a derivative called 2-bromo-Piloty's acid with efficient HNO releasing action in physiological medium (pH 7.4 at 24 °C).[268] Thus, several derivatives have been synthesized, including CXL-1020, which is in Phase I/II of clinical studies (Figure 22).[267,269,270] Other structural modification approaches have also been explored. Nakagawa and co-workers,[271] in order to develop new PA derivatives capable of releasing HNO via light stimulation, modified the hydroxamic group of the 2-nitro-Piloty's acid by incorporating a photolabile protecting group (7-diethylaminocoumarin-4-yl)methyl. They obtained a Piloty's acid derivative (*N*-((7-(diethylamino)-2-oxo-2H-chromen-4-yl)methoxy)-2-nitrobenzenesulfonamide) that upon light irradiation (from 400-430 nm) promoted the release of the precursor PA in an anionic form, which then decomposes releasing HNO. Other classes of molecules containing hydroxylamine group have been explored as potential HNO donors in physiological environments. Toscano and collaborators developed new compounds such as (hydroxylamino)barbituric acid (HABA) and (hydroxylamino)pyrazolone (HAPY), which under physiological conditions exhibit half-life times of 0.7 to 107 min at pH 7.4 and 37 °C (Figure 22).[272-274]

Figure 22 - Examples of some hydroxylamine-based donors.

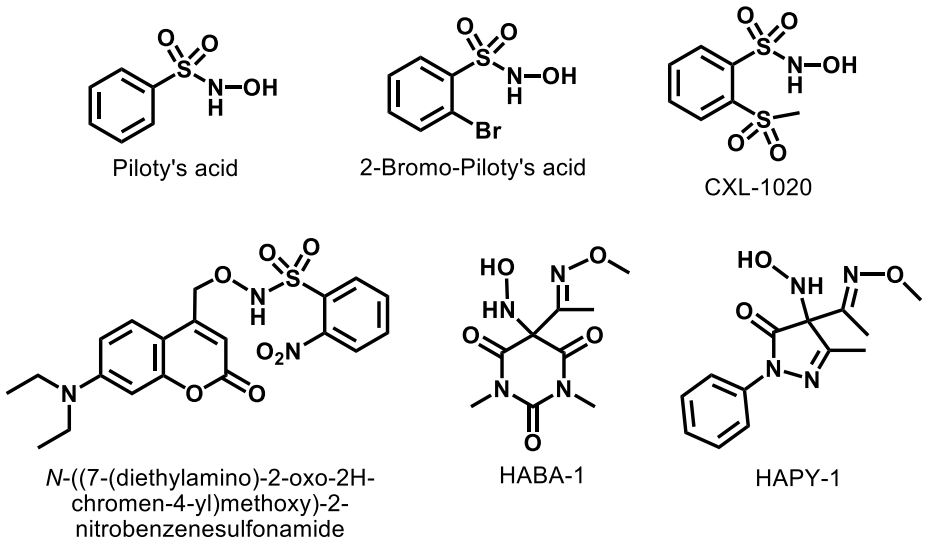

Reference: Elaborated by the author.

Scheme 12 - General mechanism of HNO release.

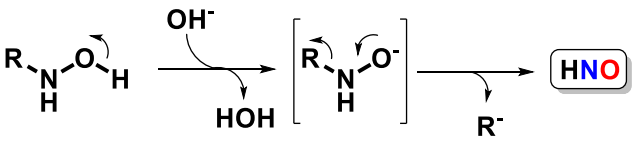

Reference: Adapted from 267.

1.9.3 Nitroso-based donors

Nitroso compounds constitute a class of HNO donors through reactions with nucleophiles in aqueous medium.[275-277] Unlike derivatives of AS and PA, it has been shown that nitroso compounds, under physiological conditions, behave mainly as HNO donors. However, these species are extremely reactive, being in most cases produced *in situ* as intermediates via oxidative, photochemical and thermal reactions.[278,279] King and collaborators synthesized a series of nitroso acyloxy compounds (the most known of them is 1-nitrosocyclohexyl acetate (NCA)) (Scheme 13),[275,276] which under physiological conditions releases HNO after hydrolysis. In addition to them, they also prepared nitroso acyl derivatives 9,10-dimethylanthracene cycloadducts, which upon a thermal retro-Diels-Alder decomposition (40 ºC) releases acyl nitroso compounds being a source of HNO (Scheme 13).[277] These latter derivatives can also donate HNO through photoinduced retro-Diels-Alder reaction, as demonstrated by Miyata and co-

workers.[280,281] The ability of these molecules to act as HNO donor pro-drugs have encouraged biological studies with promising cardiovascular properties.[282-284]

Scheme 13 - Mechanism of the decomposition of nitroso derivatives in HNO, promoted by nucleophilic attack (OH^-) or thermal/photoinduction retro-Diels-Alder reaction.

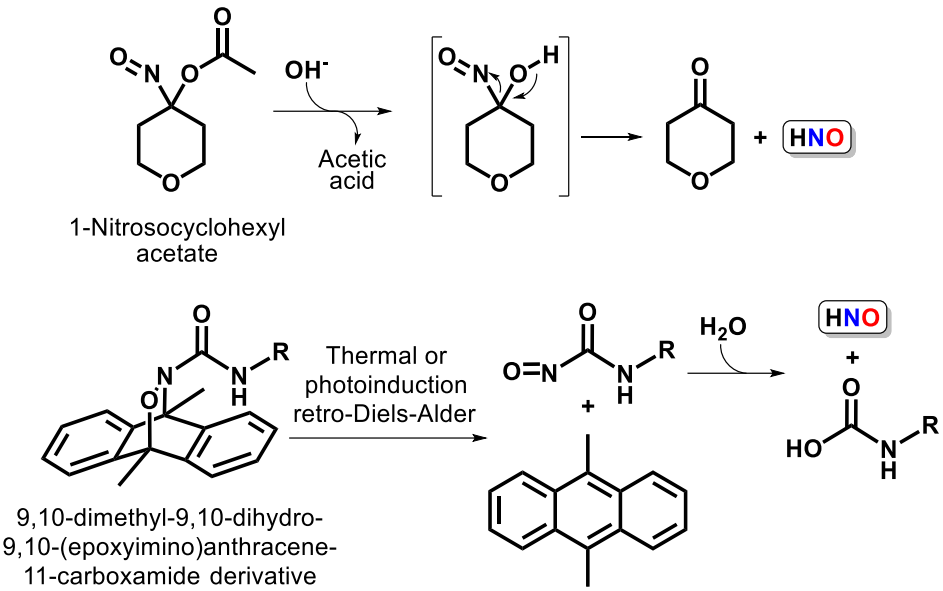

Reference: Adapted from 275-277.

1.9.4 Hydroxamic acid-based donors

The first report on hydroxamic acids was dated back to 1869, when H. Lossen synthesized the oxalohydroxamic acid molecules,[279] and until today these compounds continue to be studied with new synthetic approaches and possible applications in organic and inorganic chemistry,[285-289] as well as in pharmacology.[285,286,290,291] These hydroxamic acid-base donors are illustrated by the following drugs: vorinostat (SAHA, approved by FDA in 2006 to treat the cutaneous T-cell lymphoma),[292] belinostat (PXD101, approved by FDA in 2014 to treat the relapsed or refractory peripheral T-cell lymphoma),[293] panobinostat (LBH-589, approved by FDA in 2015 to treat multiple myeloma),[294] and hydroxyurea used in the treatment of sickle cell disease (Figure 23).[295]

Figure 23 - Hydroxamic acid donors.

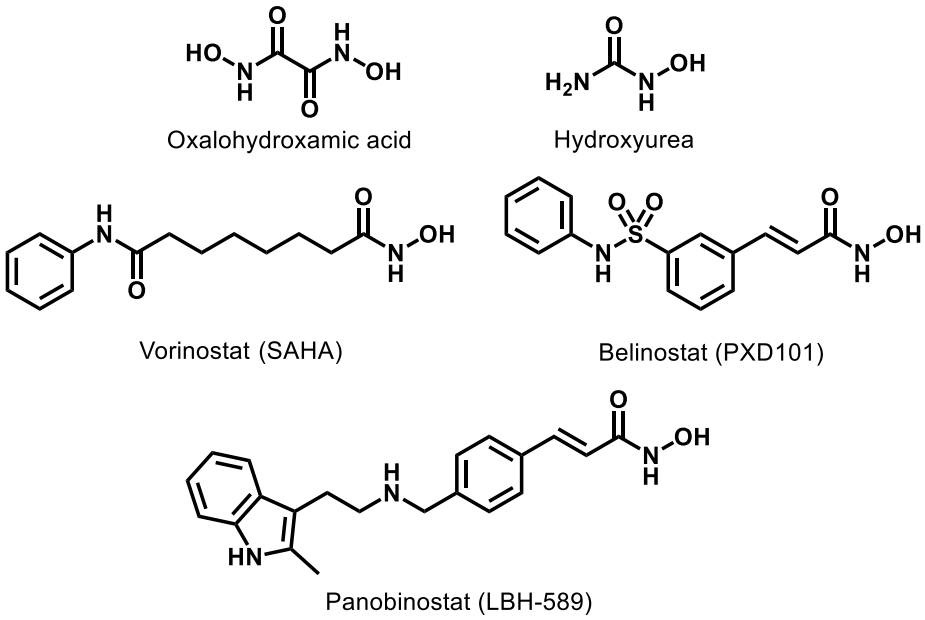

Reference: Elaborated by the author.

Hydroxamic acids are within the class of nitrosocarbonyl precursor. In fact, hydroxamic acids have been reported as HNO donors through oxidation of the -NH-OH group to an acyl nitroso intermediate, which reacts with nucleophiles to release HNO.[278,296] The oxidative activation of hydroxamic acids has been studied in a physiological context aiming to explain the possible mechanisms of pharmacological action of these molecules.[297,298] Goldstein and collaborators have shown that SAHA can be oxidized under hypoxic conditions by $MbFe^{III}/H_2O_2$ system in physiological medium, causing enhanced radiological response of tumors by multiple mechanisms, supposedly attributed to the production of HNO and $NO^{\bullet}$.[297]

1.10 $NO^{\bullet}$/HNO metal-based donors

Several metal-based compounds have been developed showing potential pharmacological action.[17,299] Despite that and the knowledge of the important biological roles played by metallo-proteins,[47,54,300,301] supporting the therapeutic potential of metal complexes, there are still not many metallo-drugs in clinical use, particularly if compared to organic-based drugs.[17,299] Related to the clinical use of $NO^{\bullet}$ donor metallo-compounds, there is only one case, sodium nitroprusside (SNP, $Na_2[Fe(CN)_5NO]$). First prepared in 1849 by Playfair, SNP, a cyanoferrate complex, has been used in cardiac surgery with hypertensive crisis conditions and other acute hemodynamic emergency

applications.[24] Nonetheless, some harmful side effects are related to its administration, due to the rapid release of NO• and cyanide. This latter can be managed by the co-administration of sodium thiosulfate and hydroxocobalamin.[24] Recently, a material containing SNP anchored in silica-based nanoparticles was prepared, where vasorelaxation activity similar to that of isolated SNP was noticed along with a significant reduction in cytotoxicity, proving an alternative for the safer and broader use of SNP in medicine.[302]

In addition to strategies based on nanomaterials, several NO• metal donors have been developed in order to provide more efficient cardiovascular activities with lower undesired side effect to the patient. Oxacom®, a dinitrosyl iron complex (DNIC) containing glutathione as a ligand (Figures 6 and 24), is undergoing clinical trials in Phases I/II. This compound represents an exciting example of a new hypotensive drug with no adverse effects reported to date.[26,303]

Polypyridine ruthenium-nitrosyl complexes (Figure 24) have been considered as another large class of NO• donors widely studied by several laboratories. Many of these compounds have also shown moderate antihypertensive activities (e.g., EC_{50} from 200 to 690 nM) compared to SNP.[304-306] These activities suggest that they may have opportunities to be used as models for antihypertensive drugs. Metal-compounds carrying NO• have also been investigated as NO• photoreleaser agents, opening further opportunities.[304,305,307,308]

Figure 24 - Structures and *in vitro* vasodilation action of nitrosyl iron and ruthenium complexes (4-bzpy = 4-benzoylpyridine, ImN = imidazole, and tu = thiourea).

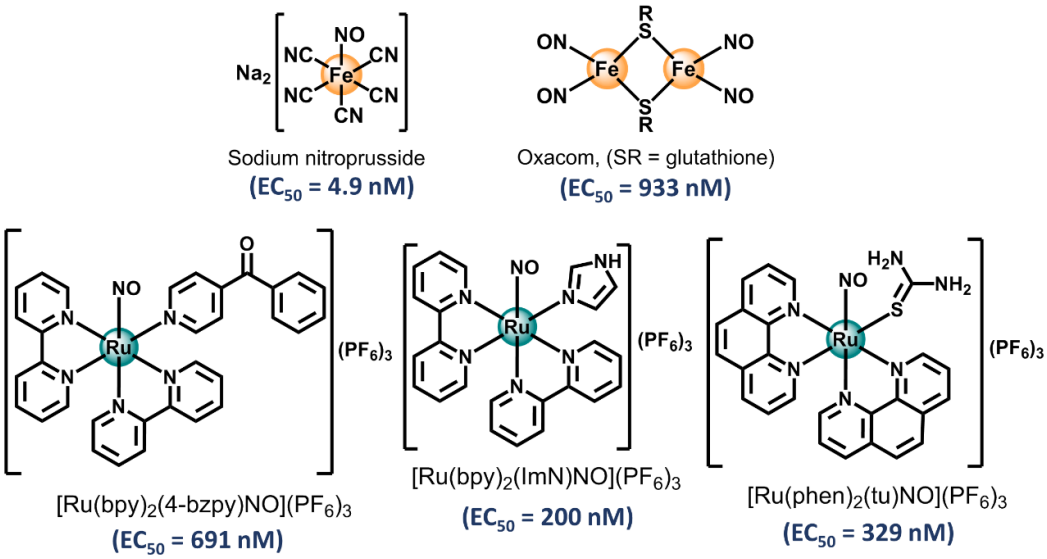

Reference: Adapted from 304-306.

1.10.1 Photorelease of NO• by nitrosyl complexes

Phototherapy has emerged as an alternative way to minimize the toxicity of many treatments thanks to the possibility of performing more efficient temporal and local dosing of the drug.[309] Several metal complexes have been investigated as NO• releasing phototherapeutic agents.[304,305,307,308] Metal complexes are versatile in terms of design and reactivity modulation, which have raised interest in their use as model photosensitizers.[19,310-312] The incidence of irradiation (UV-Vis) in a metallo-nitrosyl compound induces formations of an excited state, in which π* anti-bonding orbitals of the nitrosyl ligand are electronically populate, leading to a decrease in the bond order between the metallic center and NO•, promoting the release of the ligand.[304,305,308]

The $[Ru(bpy)_2(SO_3)NO](PF_6)$ complex is an interesting example on the modulation of reactivity based on the substitution of ancillary monodentate ligand. Once sulfite, bound through S atom, is used as ligand, there was a significant change in the overall electronic density of NO• moiety if compared to that of a complex with an N-based ligand instead (e.g., isonicotinamide). This can dramatically alter the acid-base equilibrium of nitrosyl/nitrite found for these systems (Scheme 14). Depending on the equilibrium constant for this process we can have in physiological pH mainly nitrite or nitrosyl bound species, which can modulate NO• release and reactivity. NO• photorelease may occur more efficiently if the nitrosyl bound is the main species.

Scheme 14 - Generic acid-base nitrosyl/nitrite equilibrium for polypyridine ruthenium-nitrosyl complexes.

$$[M(L)_x(NO)]^n{}_{(aq)} + 2\ OH^- \rightleftharpoons [M(L)_x(NO_2)]^{(n-2)}{}_{(aq)} + H_2O_{(aq)}$$

Reference: Adapted from 313.

By replacing isonicotinamide (isn) ligand for sulfite ion (SO_3^{2-}) in the $[Ru(bpy)_2(L)NO]^{n+}$ system, there is a remarkable increased in the pH values for the conversion of nitrosyl into nitrite ligand, from 1.45 to 10.32 (Figure 25).[313] This major change upon binding sulfite allowed the nitrosyl species to become the main species under physiological conditions and might be a reason for many promising biological properties found for this compound. Photorelease (463 nm) of NO• from the $[Ru(bpy)_2(SO_3)NO]^+$ complex was validated using the selective NO• trap cPTIO (2-(4-carboxyphenyl)-4,4,5,5-tetramethylimidazoline-1-oxyl-3-oxide potassium salt).[152] In

contrast, in the presence of thiols (e.g., glutathione), the $[Ru(bpy)_2(SO_3)NO]^+$ complex released HNO. Other polypyridine ruthenium compounds have also showed a pH of nitrosyl/nitrite (1:1) conversion close to or higher than the physiological pH (6.4-8.0) (Figure 25). Interestingly, all these metallo-nitrosyl derivatives show indeed an ancillary ligand bound to ruthenium through sulfur atom, indicating that such ligands can positively influence the acid-base nitrosyl/nitrite equilibrium. Those results showed the use of sulfur-based ligands as a relevant strategy in the development of new therapeutic platforms for NO•/HNO release.[152,305,313,314]

Figure 25 - Structures of some metallo-nitrosyl compounds and pH of nitrosyl/nitrite conversion (isn = isonicotinamide, tu = thiourea and tbz = thiobenzamide).

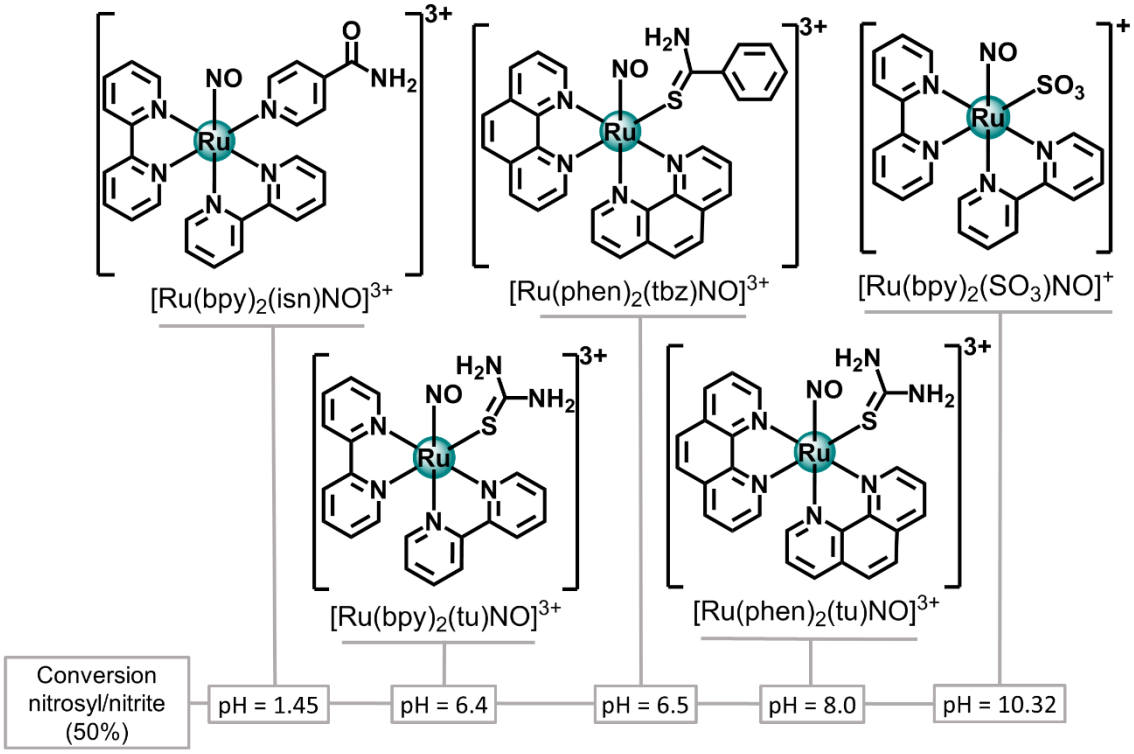

Reference: Adapted from 152, 305, 313, and 314.

Recently, two interesting new strategies involving photoactivation of metal complexes were published. The first one was based on the indirect route for NO• photorelease. Cardoso and co-workers developed a new Ru(II) nitrosylsulphito complex (*trans*-$[Ru(NH_3)_4(isn)(N(O)SO_3)]^+$) (Figure 26), where upon photoactivation (355-410 nm) there is a release of $ONSO_3^-$ species, which further decomposes into NO• and $SO_3^{\bullet -}$.[315] It is interesting to note that there are only a few metallic systems with *N*-

bonded nitrosylsulphite ($N(O)SO_3$) ligand isolated and characterized, indicating this strategy has room for many further investigations as demonstrated by Cardoso.

Figure 26 - Structures of nitrosyl Fe^{II} $[Fe(NO)(^{TMS}PS_2)(^{TMS}PS_2H)]$ and ruthenium(II) nitrosylsulphito *trans*-$[Ru(NH_3)_4(isn)(N(O)SO_3)](PF_6)$ (isn = isonicotinamide) complex.

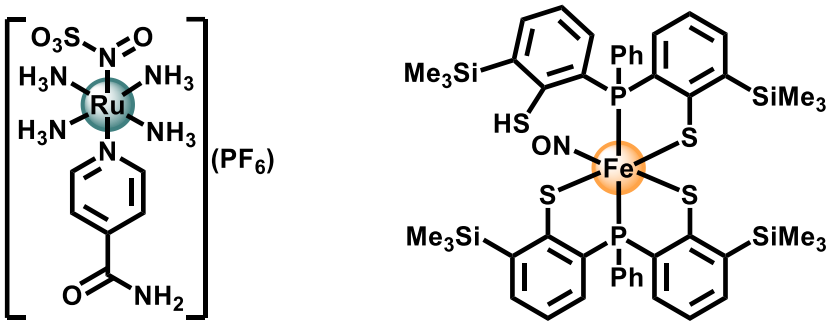

trans-$[Ru(NH_3)_4(isn)(N(O)SO_3)](PF_6)$
(Indirect NO photoreleaser)

$[Fe(NO)(^{TMS}PS_2)(^{TMS}PS_2H)]$
(HNO photoreleaser)

Reference: Elaborated by the author.

Another exciting case is based on the photorelease of HNO. Lee and collaborators developed an nitrosyl iron complex based on the 2,2′-dimercapto-3,3′-bis(trimethylsilyl)diphenyl)phenylphosphine ($^{TMS}PS2H_2$) ligand.[316] This compound upon light irradiation (> 400 nm) showed formation of $NO^{\bullet}$ that was reduced to HNO by a thiol group (-SH) already present in the structure (Figure 26). This photorelease of HNO features as a rare case via an iron complex nitrosyl, considering that in many cases $NO^{\bullet}$ is found as NO^+ and requires two-electrons for HNO production.

One key issue for nitrosyl complexes as a photoreleaser species is the wavelength capable to promote this stimulus, which, unfortunately, in most of the cases requires highly energetic light. Despite that, any suitable phototherapy requires stable compounds with efficient activation using light from 650 to 900 nm, called therapeutic window, where light has maximum penetration in the skin with minimum issue on other biomolecules.[317] Several authors have developed strategies for the delivery of $NO^{\bullet}$ to biological targets, mainly aiming at application within the therapeutic window, systems such as Roussin's Red Salt ester, Ru(salen)(Cl)NO, $Cr(cyclam)(ONO)_2^+$, $[Mn(PaPy_2Q)(NO)]^+$, in addition to nano-structured materials, are part of these therapeutic proposals as described elsewhere.[307,308,318]

2 OBJECTIVE

Taking into account that NO•/HNO can exhibit a large spectrum of interesting therapeutic actions and metal complexes can be useful in medicinal chemistry, the objective of this thesis is the development of new design strategies involving the synthesis and physicochemical and biological studies of metal complexes able to carry and delivery the biological active agent, NO•/HNO.

The first chapter aims to i) study the reactivity of the nitrosyl complex *trans*-[Fe(cyclam)(NO)Cl]Cl_2, ii) investigate the stability of this complex under physiological conditions (pH 7.4 at 37º C) in order to assess the influence of any possible spontaneous decomposition, as well as the identification of possible products generated, iii) ascertain the influence of light (365 nm) on the possible release of NO•, and iv) verify the biological potential of the *trans*-[Fe(cyclam)(NO)Cl]Cl_2 as an antiangiogenic agent with potential anticancer property. Besides that, another important objective is to investigate the vasodilation profile of the nitrosyl complex. All results from this work are already published and presented in chapter 1.[319]

In order to advance in the search for new NO•/HNO donor platforms for therapeutic purposes, we explored the ability of aromatic hydroxamic acid derivatives to release NO•/HNO after oxidative reaction steps. This platform could be of particular interest due to the possible mechanism of activation of this type of molecule, in addition to NO•/HNO release (metabolite active of the anti-TB drug delamanid and vasodilatator agent), an aroyl radical intermediate or an aromatic carboxylic acid might also be formed, which can be seen, respectively, as the corresponding active metabolites of isoniazid and pyrazinamide, two major antitubercular drugs. Thus, the second part of this thesis describes two chapters. The aim of the first one (chapter 2) is the investigation of the intermolecular oxidative activation mechanism of the isonicotino-, nicotino-, and pyrazino- hydroxamic acids, respective analogues of isoniazid (anti-TB), nicotinamide (vitamin B3), and pyrazinamide (anti-TB), by reaction with potassium ferricyanide ($K_3[Fe^{III}(CN)_6]$) in pH physiological conditions. This work could assist in the design of new drugs. This study has also been published in a scientific peer-reviewed journal and presented in chapter 2.[285] Then, the third project (chapter 3) is relative to the synthesis of new Fe^{II} complexes formulated with isonicotino-, nicotino- and pyrazino- hydroxamic acid ligands bound to the $[-Fe(CN)_5]^{n-}$ moiety, as well as the study of the mechanism of the oxidative activation of these metal complexes by H_2O_2 and structural characterization of the species formed. This synthetic approach is applied aiming at

development of new antituberculosis and cardiovascular agents. This latest study was equally published in a peer-reviewed journal and is presented in chapter 3.[320]

OBJECTIF

Compte tenu du fait que le NO•/HNO peut présenter un grand spectre d'actions thérapeutiques intéressantes et que les complexes métalliques peuvent être un outil intéressant en chimie inorganique médicinale, l'objectif de cette thèse est le développement de nouvelles stratégies de conception de médicaments impliquant la synthèse et l'étude physicochimique et biologique de complexes métalliques capables de porter et de délivrer l'agent actif biologique, NO•/HNO.

Le premier chapitre vise à i) étudier la réactivité du complexe nitrosyl *trans*-[Fe(cyclam)(NO)Cl]Cl_2, ii) étudier la stabilité de ce complexe dans des conditions physiologiques (pH 7,4 à 37 ºC) afin d'évaluer l'influence de toute décomposition spontanée possible, ainsi que l'identification des produits possibles générés, iii) déterminer l'influence de la lumière (365 nm) sur la libération possible de NO• , et iv) vérifier le potentiel biologique du *trans*-[Fe(cyclam)(NO)Cl]Cl_2 en tant qu'agent antiangiogénique avec une propriété anticancéreuse potentielle. De plus, l'investigation du profil vasodilatateur du complexe nitrosyle est également un des objectifs de cette thèse. Les résultats de ces travaux ont déjà été publiés et sont présentés au chapitre 1.[319]

Afin d'avancer dans la recherche de nouveaux châssis moléculaires capables de relarguer NO•/HNO et d'avoir des intérêts thérapeutiques, nous explorons l'habilité des dérivés aromatiques azotés de l'acide hydroxamique à libérer NO•/HNO après une étape de réaction oxydative. Cette forme de châssis moléculaire pourrait avoir un intérêt tout particulier parce qu'en fonction du mécanisme d'activation de ce type de molécule, outre la libération de NO•/HNO (métabolite actif du délamanide -médicament anti-TB- et agent vasodilatateur), un intermédiaire de type radical aroyle ou un acide carboxylique aromatique pourrait également être formé, ce qui pourrait être considéré, respectivement, comme le métabolite actif de l'isoniazide ou du pyrazinamide, deux pro-drogues antituberculeuses majeurs. Ainsi, la deuxième partie de cette thèse est divisée en deux projets. Le but du premier (chapitre 2) est l'étude d'un mécanisme intermoléculaire de l'activation oxydative des acides hydroxamiques dérivés des acides isonicotinoique, nicotinoique et pyrazinoique, analogues respectifs de l'isoniazide (anti-TB), du nicotinamide (vitamine B3) et du pyrazinamide (antituberculeux), par le ferricyanure de potassium ($K_3[Fe^{II}(CN)_6]$) dans des conditions physiologiques de pH. Ceci afin d'aider à la conception de nouveaux médicaments.

Cette étude a également été publiée dans une revue scientifique et est ici présentée dans le chapitre 2.[285] Ensuite, le troisième projet (chapitre 3) est relatif à la synthèse de nouveaux complexes de Fe^{II} associant les ligands d'acide hydroxamique isonicotinique, nicotinique et pyrazinique au fragment $[\text{-}Fe(CN)_5]^{n-}$, ainsi qu'à l'étude d'un mécanisme intramoléculaire d'activation oxydative de ces complexes (oxydation via H_2O_2) suivi d'une caractérisation structurale des espèces formées. Cette approche de synthèse a été appliquée dans le but de développer de nouveaux agents antituberculaires et cardiovasculaires. Cette dernière étude est présentée dans le chapitre 3.[320]

3 PART 1 - NITROSYL IRON COMPLEX: CYCLAM AS THERAPEUTIC PLATFORM

The increase number of cases of cardiovascular diseases and cancer has led the scientific community to seek new treatment strategies that are more efficient and less harmful to patients. The part 1 of this manuscript presents the chemical and biological studies of a known nitrosyl Fe^{II} complex, which has never been further investigated from a pharmacological perspective. In the context of this thesis a special emphasis on the release of NO•/HNO and on potential antiangiogenic and cardiovascular action was placed.

3.1 Introduction

Among the drugs used to treat cardiovascular diseases, the SNP is the only metal complex available.[24] As we mentioned in the introduction of this thesis, in addition to the release of CN^-, another factor that limits the widespread use of this drug, is its powerful vasodilating action, due to fast release of NO• in the body.[24] In order to obtain more moderate NO• donor agents, with lower toxicity compared to SNP, several other metal complexes have been explored, for example, the DNIC 2,2'-bipyridine- $Fe(NO)_2$,[321] SNP analogs ($K_n[M(CN)_5NO]$ (M = V, Cr, Mn and Co with n = 3, or M = Mo with n = 4)),[322] and polypyridine ruthenium derivatives such as $[Ru(bpy)_2(ImN)NO](PF_6)_3$ (bpy = 2,2'-bipyridine, ImN = imidazol) and $[Ru(phen)_2(tu)NO](PF_6)_3$ (phen = phenanthroline, tu = thiourea).[305,306]

In addition to the development of new nitrosyl complexes with therapeutic potential related to the NO• release, the discussion about the ability of these complexes to release HNO has also emerged, since the latter shows also biological relevance. Sousa and collaborators,[152] motivated to identify the possible production of HNO by $[Ru(bpy)_2(SO_3)NO]^+$, have studied the reaction of this ionic complex with glutathione (GSH). This study have shown, through the use of a selective trap to distinguish NO/HNO and cellular angiogenesis assays, the potential ability of this complex to release HNO under physiological conditions. Thus, HNO production in a physiological context has also been an important part of the reactivity studies involving nitrosyl complexes.

Holanda and his collaborators developed in 2007 a new nitrosyl iron(II) complex using 1,4,8,11-tetraazacyclotetradecane (Cyclam) as ligand, called *trans*-$[Fe(cyclam)(NO)Cl]Cl_2$.[323] This complex has been studied from a chemical point of view, being indicated as a promising photoreleaser of NO•. However, such results lacked data

showing NO• can be directly produced from the complex. Additionally, no results proving HNO release as well as relevant biological tests were available. Thus, the *trans*-[Fe(cyclam)(NO)Cl]Cl_2 complex is an interesting system to be explored mainly from a biological point of view.

In view of that, the following article presents details of the reactivity study of the well-known nitrosyl complex, *trans*-[Fe(cyclam)(NO)Cl]Cl_2, with emphasis on examining the differential release capacity of NO• and HNO, either through photochemical stimulation or reaction with GSH. By using a selective probe cPTIO (2-(4-carboxyphenyl)-4,4,5,5-tetramethylimidazoline-1-oxyl-3-oxide potassium) for UV-Vis and EPR techniques, or through other experimental (Griess reagent) and theoretical studies (density functional theory (DFT) and time-dependent DFT (TD-DFT)), we were able to confirm the NO• production from the complex via light stimulus (365 nm). On the other hand, the reaction of *trans*-[Fe(cyclam)(NO)Cl]Cl_2 complex with GSH indicated the HNO production, as well as the formation of an intermediate adduct between the nitrosyl complex and GSH (*trans*-[Fe(cyclam)(Cl)N(*O*)SG]$^+$).[152] The hypothesis that this complex can release HNO in the presence of thiols has been reinforced by a cell angiogenesis assay based on the HIF-1α degradation. Additionally, the vasorelaxation capacity of the metal complex ion was assessed, in comparison to the SNP, and a more moderate vasodilation activity was noticed. These results, in addition to the evidences of its low cytotoxicity,[319] made the *trans*-[Fe(cyclam)(NO)Cl]Cl_2 complex a potential therapeutic model for cardiovascular diseases.

3.2 Chapter 1 - Nitrosyl trans-[Fe(cyclam)(NO)Cl]Cl2 complex - new approach in anticancer and antihypertensive treatments

3.2.1 Article 1 : Journal of Inorganic Biochemistry, 2020, 210, 111133 - Résumé de l'article en français

A divergent mode of activation of a nitrosyl iron complex with unusual antiangiogenic activity

Edinilton Muniz Carvalho, Lisa A. Ridnour, Florêncio Sousa Gouveia Júnior, Pedro Henrique Bezerra Cabral, Nilberto Robson Falcão do Nascimento, David A.Wink, Douglas W. Franco, Mayara Jane Campos de Medeiros, Daniel de Lima Pontes, Elisane Longhinotti, Tércio de Freitas Paulo, Vania Bernardes-Génisson, Remi Chauvin, Eduardo Henrique Silva Sousa, Luiz Gonzaga de França Lopes.

*Journal of Inorganic Biochemistry, **2020**, 210, 111133*

Les complexes métalliques libérant oxyde nitrique (NO•) et/ou nitroxyle (HNO), ont fait l'objet d'études dans une perspective thérapeutique. L'exemple le plus connu est le complexe de fer appelé nitroprussiate de sodium (SNP, $Na_2[Fe(CN)_5NO]$). Ce puissant agent capable de libérer NO• est utilisé dans les cas cliniques d'hypertension artérielle. Cependant, son administration prolongée peut provoquer plusieurs effets secondaires dus à une libération trop rapide de NO• et de l'ion cyanure. Ces limitations ont conduit à la recherche de nouveaux agents alternatifs à base de métaux, en espérant avoir une libération plus lente de NO• et des effets secondaires moindres. De nombreux laboratoires se sont concentrés sur la synthèse et la caractérisation de complexes nitrosylés libérant du NO• en réponse à des stimuli lumineux ou après une réduction chimique.

Dans le cadre de cette thèse, nous avons étudié dans un premier temps la réactivité chimique et la stabilité du complexe de fer, *trans*-$[Fe(cyclam)(NO)Cl]^{2+}$ (cyclam = 1,4,8,11-tétraazacyclotétradécane) (**1**) (Figure 27). L'étude de stabilité thermique du composé **1** dans des conditions physiologiques (pH 7,4, 37 ºC), a été réalisée en utilisant des techniques spectroscopiques : infrarouge, ($N{\equiv}O^+$ at 1894 cm^{-1}), et UV-Vis, (λ = 235 nm (transitions de transfert de charge de type intra-ligand (TCIL) et métal-ligand (TCML)) et 360 nm (transition de type transfert de charge ligand-ligand)), et chronoampérométriques (électrode NO• sélective). Ces études ont révélé que le complexe nitrosyle se décompose en solution, au

moyen d'un processus d'oxydoréduction intramoléculaire spontané dans lequel le ligand NO^+ est réduit par oxydation du centre métallique, provoquant sa libération sous forme de NO^0 et la production du complex *trans*-$[Fe(cyclam)(H_2O)_2]^{3+}$ complex.

Figure 27 - Structure des complexes *trans*-$[Fe(cyclam)(NO)Cl]Cl_2$ (**1**) et *trans*-$[Fe(cyclam)Cl_2]Cl$ (**3**).

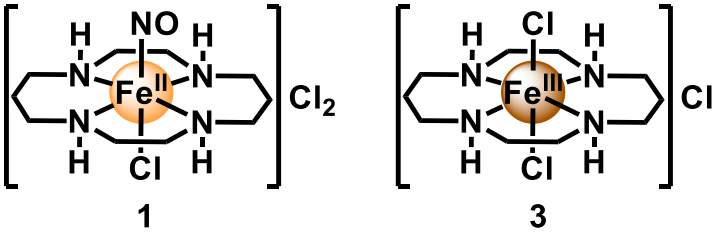

Référence : Élaboré par l'auteur.

La capacité de la lumière à induire la libération de NO• ou de HNO à travers le complexe **1** a également été évaluée. À l'instar de l'étude précédente, ces expériences ont également été menées dans des conditions aqueuses tamponées (pH 7,4, 37 ºC) et suivies à l'aide de techniques spectroscopiques (UV-Vis et résonance paramagnétique électronique (RPE)). L'utilisation du piège sélectif cPTIO (2-(4-carboxyphényl)-4,4,5,5-tétraméthylimidazoline-1-oxyl-3-oxyde de potassium) a permis l'identification et la distinction des espèces NO•/HNO, car les réponses spectroscopiques générées sont différentes. L'irradiation (365 nm) du composé **1** en présence de cPTIO, a conduit à la production de l'espèce cPTI (Schème 15), montrant une réaction directe du cPTIO et du NO•.[324] La photo-libération de NO• par le complexe **1** a également été renforcée par le test de Griess et des études théoriques (théorie fonctionnelle de la densité (DFT) et DFT en fonction du temps (TD-DFT)).

Schème 15 - Produits de réaction du cPTIO avec NO• ou HNO.

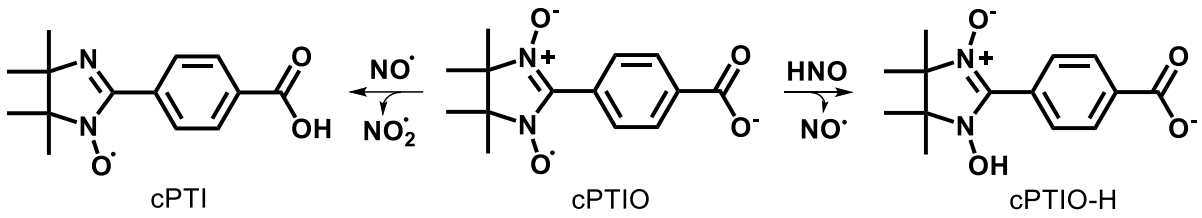

Référence : Élaboré par l'auteur.

La réaction du complexe nitrosylé avec le glutathion (GSH) a été suivie par l'infrarouge, UV-Vis, Stopped-Flow et RPE. Les résultats ont indiqué que la présence de GSH provoque des changements significatifs dans le profil spectroscopique du complexe. Dans l'infrarouge, la bande caractéristique de l'étirement de la liaison N=O du groupe NO^+ (1894 cm^{-1}) a été complètement supprimée après 5 minutes de réaction, indiquant que le ligand nitrosyle est directement affecté dans le processus. Cette même réaction a également été suivie par RPE en utilisant la sonde cPTIO, où la disparition du signal caractéristique de la forme cPTIO était presque complète après 15 minutes de réaction, indiquant que le produit cPTIO-H (Schème 15) non radicalaire était généré. Ce dernier, à son tour, est une preuve solide de la réaction du précurseur cPTIO avec HNO.[324] Ainsi, ce résultat corrobore l'hypothèse que l'un des principaux composés produits lors de la réduction du complexe *trans*-$[Fe(cyclam)(NO)Cl]^{2+}$ par le GSH est HNO. Afin d'étudier le mécanisme d'activation réductrice du complexe nitrosyle par le GSH, l'utilisation des techniques « Stopped-Flow » et d'UV-Vis ont également été mises à profit. Il a été possible d'observer que le GSH provoque des changements significatifs dans le spectre électronique du complexe nitrosylé. Au cours de la réaction, une bande d'absorption maximale à 541 nm a été observée. Dans la littérature il a été rapporté que la réaction du SNP avec H_2S, est responsable de la formation du complexe intermédiaire $[Fe(CN)_5N(O)SH]^{3-}$; cette espèce étant responsable de l'apparition d'une bande d'absorption électronique avec un maximum à 535 nm à pH 7,4.[325] Un comportement similaire a été observé pour la réaction de la cystéine avec d'autres complexes nitrosylés.[326,327] Ainsi, l'apparition de la bande à 541 nm dans la réaction étudiée dans le cadre de cette thèse, est une forte indication de la formation d'intermédiaires réactifs entre le complexe de fer *trans*-$[Fe(cyclam)(NO)Cl]^{2+}$ et le GSH. Cet intermédiaire est appelé *trans*-$[Fe(cyclam)(Cl)N(O)SG]^+$. Au fur et à mesure que la réaction progresse, la bande de 541 nm finit par diminuer presque totalement. Comme l'expérience suivie par RPE indiquait la formation de HNO, nous avons proposé que la désintégration de la bande à 541 nm est liée à une seconde réduction par une autre molécule de GSH, conduisant à la production de HNO, ainsi qu'à la dégradation de l'adduit.

Dans les cellules cancéreuses, la production de facteurs pro-angiogéniques est induite dans des conditions d'hypoxie (provoquée par un métabolisme accéléré anormal). L'adaptation à différents niveaux d'oxygène dans la cellule est médiée par une famille de régulateurs transcriptionnels appelés facteurs inductibles par l'hypoxie (HIF).[127] Sous normoxie, l'activité transcriptionnelle de HIF est spécifiquement supprimée par la dégradation de sa sous-unité α dépendante de l'oxygène (HIF-α). Des conditions de faible teneur en

oxygène induisent la stabilisation de HIF-1α, favorisant l'angiogenèse cellulaire.[148] Ainsi, la protéine HIF-1α a été considérée comme une cible prometteuse pour la thérapie anticancéreuse.[127]

NO• et HNO joue un rôle clé dans la régulation de HIF-1α dans les cellules tumorales. Alors que NO• a été indiqué comme agent stabilisant pour HIF-1α dans des conditions normoxiques, HNO s'est avéré agir dans le sens inverse, bloquant la stabilisation de HIF-1α, à la fois dans des conditions induites par l'hypoxie ou par NO•, ce dernier dans des conditions normales d'air.[65,150] Basé sur ces informations, la capacité antiangiogénique du complexe *trans*-$[Fe(cyclam)(NO)Cl]^{2+}$ a été évaluée en utilisant le test de stabilité HIF-1α. Cette expérience, réalisée en collaboration avec l'équipe du Pr. David A. Wink où « National Cancer Institute, Cancer and Inflammation Program, Frederick – USA », a montré une diminution significative de l'accumulation de HIF-1α causée par le composé étudié. Parallèlement, le complexe **1** a également démontré une action antiangiogénique potentielle, via le test de formation du tube endothélial. Le test de formation du tube endothélial des cellules HUVEC (cellules endothéliales humaines de veine ombilicale) a démontré qu'en présence du composé **1**, le nombre de vaisseaux était significativement réduit par rapport au composé précurseur sans NO^+ (composé **3**, *trans*-$[Fe(cyclam)Cl_2]^+$, Figure 27). Cette partie du travail a également été réalisée avec la collaboration du Pr. David A. Wink.

Les propriétés vasodilatatrices du composé **1** ont également été explorées, celui a présenté une CI_{50} = 910 nM (valeur correspondant à la concentration minimale nécessaire du composé pour provoquer une vasodilatation à 50%), tandis que celle de molécule de référence SNP est de 24 nM. Cette partie du travail a été réalisée avec la collaboration du Pr. Nilberto R. F. do Nascimento. Cette activité modérée, attribuée à libération de NO• ou HNO, ajoutée à la faible cytotoxicité du complexe (mesurée à travers les lignées cellulaires cancéreuses B16-F10 et HUH-7),[319] fait du composé **1** une plateforme thérapeutique prometteuse pour des molécules à propriétés antihypertensive avec des avantages par rapport au SNP. En effet, l'activité du complexe **1** peut être indicative d'une libération plus contrôlée de NO•, évitant les problèmes d'hypotension causés par la libération trop rapide de NO• associée au SNP. De plus, ce complexe n'est pas concerné par le relargage des ions cyanures toxiques. En résumé, ce composé prometteur mérite des études biologiques complémentaires afin de découvrir tout son potentiel thérapeutique, car il représente l'un des premiers composés de type nitrosyle de Fe^{II} à présenter touts les avantages pharmacologiques mentionnées ici.

3.3 Article 1: Journal of Inorganic Biochemistry, 2020, 210, 111133 - Printed

Journal of Inorganic Biochemistry 210 (2020) 111133

Contents lists available at ScienceDirect

Journal of Inorganic Biochemistry

journal homepage: www.elsevier.com/locate/jinorgbio

A divergent mode of activation of a nitrosyl iron complex with unusual antiangiogenic activity

Edinilton Muniz Carvalho[a,g,h], Lisa A. Ridnour[b], Florêncio Sousa Gouveia Júnior[a], Pedro Henrique Bezerra Cabral[c], Nilberto Robson Falcão do Nascimento[c], David A. Wink[b], Douglas W. Franco[d,1], Mayara Jane Campos de Medeiros[e], Daniel de Lima Pontes[e], Elisane Longhinotti[f], Tércio de Freitas Paulo[a], Vania Bernardes-Génisson[g,h], Remi Chauvin[g,h], Eduardo Henrique Silva Sousa[a,*], Luiz Gonzaga de França Lopes[a,*]

[a] Departamento de Química Orgânica e Inorgânica, Grupo de Bioinorgânica, Universidade Federal do Ceará–UFC, P.O Box 6021, Fortaleza, CE CEP 60440-900, Brazil
[b] National Cancer Institute, Cancer and Inflammation Program, Frederick, MD 21702, United States
[c] Instituto Superior de Ciências Biomédicas, Universidade Estadual do Ceará–UECE, Paranjana Av, 1700, Fortaleza, Ceará 60740-00, Brazil
[d] Instituto de Química de São Carlos, Universidade de São Paulo – USP, P.O. Box 780, São Carlos, SP CEP 13566-590, Brazil
[e] Laboratório de Química de Coordenação e Polímeros (LQCPol), Instituto de Química, Universidade Federal do Rio Grande do Norte (UFRN), Natal CEP 59078-970, Brazil
[f] Departamento de Química Analítica e Físico-Química, Universidade Federal do Ceará–UFC, P.O Box 6021, Fortaleza, CE CEP 60440-900, Brazil
[g] CNRS, LCC (Laboratoire de Chimie de Coordination), 205, route de Narbonne, BP 44099, F-31077 Toulouse, Cedex 4, France
[h] Université de Toulouse, UPS, INPT, F-31077 Toulouse, Cedex 4, France

ARTICLE INFO

Keywords:
Nitric oxide
Nitroxyl
Iron complex
Vasodilation
Anti-angiogenesis

ABSTRACT

Nitric oxide (NO) and nitroxyl (HNO) have gained broad attention due to their roles in several physiological and pathophysiological processes. Remarkably, these sibling species can exhibit opposing effects including the promotion of angiogenic activity by NO compared to HNO, which blocks neovascularization. While many NO donors have been developed over the years, interest in HNO has led to the recent emergence of new donors. However, in both cases there is an expressive lack of iron-based compounds. Herein, we explored the novel chemical reactivity and stability of the *trans*-[Fe(cyclam)(NO)Cl]Cl_2 (cyclam = 1,4,8,11-tetra-azacyclotetradecane) complex. Interestingly, the half-life ($t_{1/2}$) for NO release was 1.8 min upon light irradiation, *vs* 5.4 h upon thermal activation at 37 °C. Importantly, spectroscopic evidence supported the generation of HNO rather than NO induced by glutathione. Moreover, we observed significant inhibition of NO donor- or hypoxia-induced HIF-1α (hypoxia-inducible factor 1α) accumulation in breast cancer cells, as well as reduced vascular tube formation by endothelial cells pretreated with the *trans*-[Fe(cyclam)(NO)Cl]Cl_2 complex. Together, these studies provide the first example of an iron-nitrosyl complex with anti-angiogenic activity as well as the potential dual activity of this compound as a NO/HNO releasing agent, which warrants further pharmacological investigation.

1. Introduction

Nitric oxide (NO) is a key biological mediator of several important physiological and pathophysiological processes, including relaxation of smooth muscle cells, control of platelet aggregation, and memory, to name a few [1–4]. The nitroxyl molecule (HNO), a monoelectronic reduction product of NO, has also emerged potential biological mediator due to its exciting pharmacological properties, including some divergent activities when compared to NO [5]. In this regard, HNO enhances myocardial contractility along with coronary relaxation during heart failure [6], inhibits aldehyde dehydrogenase (ALDH) in alcoholism treatment [7], and inhibits tumor growth and angiogenesis of breast cancer cells, through its ability to limit the accumulation of hypoxia-inducible factor-1 (HIF-1α). The latter is overexpressed in tumor cells favoring their proliferation [8]. These observations have prompted a growing interest in the design and synthesis of novel NO

* Corresponding authors.
E-mail addresses: eduardohss@dqoi.ufc.br (E.H.S. Sousa), lopeslu@dqoi.ufc.br (L.G.d.F. Lopes).
[1] In memoria.

https://doi.org/10.1016/j.jinorgbio.2020.111133
Received 11 March 2020; Received in revised form 3 June 2020; Accepted 7 June 2020
Available online 20 June 2020
0162-0134/

[9,10] and HNO donors [11,12] as biological tools and/or pharmacological agents.

Although new HNO donors with promising pharmacological profiles have emerged, their number are few when compared to a wider variety of available NO releasing agents [13,14]. The majority of HNO-delivering compounds are organic-based species including Piloty's acid (benzenesulphonydroxamic acid), as well as a few basic inorganic representatives such as the Angeli's salt (AS, $Na_2N_2O_3$) and cyanamide (NH_2CN) [13,15]. Only a few metal-based HNO-carrier compounds have been synthesized, with limited characterization of biological activities [16–20].

The reduction of NO to form HNO by reaction with hydrogen sulfide [21], reducing alcohols (*e.g.* ascorbic acid, tyrosine) [22], or thiols (*e.g.* 1-hexanethiol, cysteine) has been shown [23]. Interestingly, the biological activity of HNO seems to rely, at least in part, on its reactivity with thiols, usually producing sulfinamides, disulfides or sulfenic acid [24,25]. The mechanism of HNO-mediated inhibition on aldehyde dehydrogenase [26], phospholamban [27] and glyceraldehyde-3-phosphate dehydrogenase [28] is centered on its reaction with cysteine. Another important target of HNO is the hypoxia-inducible factor 1 alpha (HIF-1α) [29], which mediates several signaling cascade processes involved in cancer progression [30]. As a matter of fact, HNO has an opposing regulatory activity on HIF-1α compared to NO. While NO prevents HIF-1α degradation, HNO has the opposite effect, making it an interesting candidate for use in cancer therapy [8,29].

The potential use of metal complexes in medicine, particularly iron-based complexes, has greatly expanded [31–38]. One example of a metal-based NO donor employed in the clinical is sodium nitroprusside (SNP, $Na_2[Fe(CN)_5NO]$), an iron cyanide complex [39], which can quickly release NO. This complex has been used in cardiac surgery with hypertensive crisis conditions, heart failure, vascular surgery, and other acute hemodynamic emergency applications. However, it is known to cause harmful side effects due to the fast release of NO as well as cyanide, the latter of which can be reduced by co-administration of thiosulfate [40]. Nevertheless, these limitations have prompted the search for alternative new metal-based agents, with a slower release of NO and lower side effects.

Many laboratories including ours have focused on the synthesis and characterization of metal nitrosyl compounds for scientific and clinical use. Our nitrosyl complexes release NO in response to light stimulus or chemical reduction [41–56]. Toward this end, we have developed a series of nitrosyl complexes with promising biological activities such as vasodilation [43,45,57], neuroprotection (ischemia and reperfusion cases) [58], pain relief from gout arthritis [59], anti-parasitic (*Leishmania* (*Viannia*) *braziliensis* [60], *Trypanosoma cruzi* [61]), gastric protection [62], anti-analgesic [63], and anti-paracoccidioidomycosis activities [64]. We have also demonstrated that HNO is produced by the reaction of $[Ru(bpy)_2(SO_3)(NO)]^+$ (bpy = 2,2′-bipyridine) **(2)** (Fig. 1) with thiols [65], a reactivity that may also be responsible for some of the biological activities reported for this compound [58,61,63,64]. Importantly, the physiological responses promoted by NO or HNO release from these and other metal complexes are initially related to the efficiency of the reduction process $NO^+ + e^- \rightarrow NO^0$. This process can be modulated by the type of auxiliary ligand (σ-donor, π-acceptor) employed in the coordination sphere, which modulates the electrochemical potential and bonding strength of the NO^+ ligand [66].

Here, we investigated the chemical reactivity and stability of the nitrosyl iron-based compound, *trans*-$[Fe(cyclam)(NO)Cl]^{2+}$ (cyclam = 1,4,8,11-tetraazacyclotetradecane) **(1)** (Fig. 1). A previous study showed that this complex has two redox potentials at +605 mV and −465 mV (*vs* NHE) assigned to reduction processes centered on the nitrosyl moiety [67]. In addition to that, HNO has also been proposed a key product of the reaction of biological thiols with ruthenium nitrosyl complexes, *e.g.* **2** (Fig. 1), which has prompted the investigation of other similar complexes [65]. This reactivity may be of particular clinical relevance considering that some aggressive tumors have shown an increase in glutathione levels, which may be used as a selective trigger for NO and HNO release during treatment of these tumors [68]. This work reports the investigation of the chemical route of HNO generation by reaction of the complex **1** with glutathione, and NO generation by a photochemical process. To accomplish these tasks, we took advantage of a series of probes, validating NO and HNO production, along with biological studies to support its potential pharmacological application.

2. Experimental

2.1. Chemicals

All reagents were of analytical grade and used without any prior purification. Griess reagent, glutathione (GSH), iron chloride (II) ($FeCl_2{\cdot}xH_2O$), 1,4,8,11-tetraazacyclotetradecane (cyclam), deferoxamine (*N*-[5-[[4-[5-[acetyl(hydroxy)amino]pentylamino]-4-oxobutanoyl]-hydroxyamino]pentyl]-*N′*-(5-aminopentyl)-*N′*-hydroxybutanediamide, ammonium hexafluorophosphate (NH_4PF_6), horse skeletal myoglobin, monobasic and dibasic potassium phosphate salts (KH_2PO_4, K_2HPO_4) were purchased from Sigma-Aldrich. The spin trap 2-(4-carboxyphenyl)-4,4,5,5-tetramethylimidazoline-1-oxyl-3-oxide potassium salt (cPTIO), diethylenetriaminepentaacetic acid (DTPA), N-[4-[1-(3-aminopropyl)-2-hydroxy-2-nitrosohydrazino]butyl]-1,3-propanediamine (SPER/NO, Spermine NONOate), and Angeli's salt (AS, $Na_2N_2O_3$) were obtained from Santa Cruz Biotechnology.

The complexes *trans*-$[Fe(cyclam)Cl_2](PF_6)$ **(3)**, *cis*-$[Fe(cyclam)Cl_2]Cl$ **(4)** and **1** were prepared as described in the literature [67,69].

2.2. Computational studies

The geometry of the complex ion **1** was optimized at the density functional theory (DFT) level [70]. All calculations were performed by the Gaussian 09 program package (Gaussian Inc., Wallingford, CT) [71] using the B3LYP [72] functional. The LANL2DZ relativistic effective core potential basis set [73] was used for the Fe atom and the 6-31G(d) basis set [70,74] was employed for other atoms. The absence of any imaginary frequency in vibrational analysis calculations supports that optimized geometry is at a minimum of the potential energy.

The time-dependent DFT (TD-DFT) approach was applied to calculate the vertical excitation energies of the **1**. Particularly, in the case of the vertical excitation energies, the polarizable continuum model was used to take into account the solvent effect, where the dielectric constant of water was considered [75]. The molecular orbitals composition, FTIR, UV–Vis spectra, and assignment of the transitions were extracted from output files using Multiwfn [76] and GaussSum 3.0 software [77].

2.3. Instruments, sample handling and preparations

The absorption spectra in the UV–Vis range were obtained using the following spectrophotometers: Cary model 5000 UV/VIS–NIR (Varian/Agilent), Diode-Array Hewlett-Packard model 8453, Perkin-Elmer UV/Vis/NIR Spectrometer – Lambda 35, and Stopped-flow model SX 20 Applied Photophysics, where fast kinetics were obtained in the latter. The temperature of all reactions was controlled using a thermostatic water bath coupled to the spectrophotometer holder cell. A quartz cuvette with an optical pathlength of 1.0 cm was employed. The vibrational spectra in the infrared range were obtained in an ABB-Bomen FTLA 2000-102 spectrometer with spectral window 400–4000 cm^{-1} using attenuated total reflectance (ATR). Light irradiation at 365 nm was carried out using Vilber Lourmat light VL-6.LC, wavelength 365/254 nm, filter size 145 × 48 mm and 6 W of power, with a distance between lamp and sample solution of 20 cm, and temperature controlled at 25 °C. The electronic paramagnetic resonance spectra (EPR) were recorded with a Bruker spectrometer, model Elexsys E500 coupled

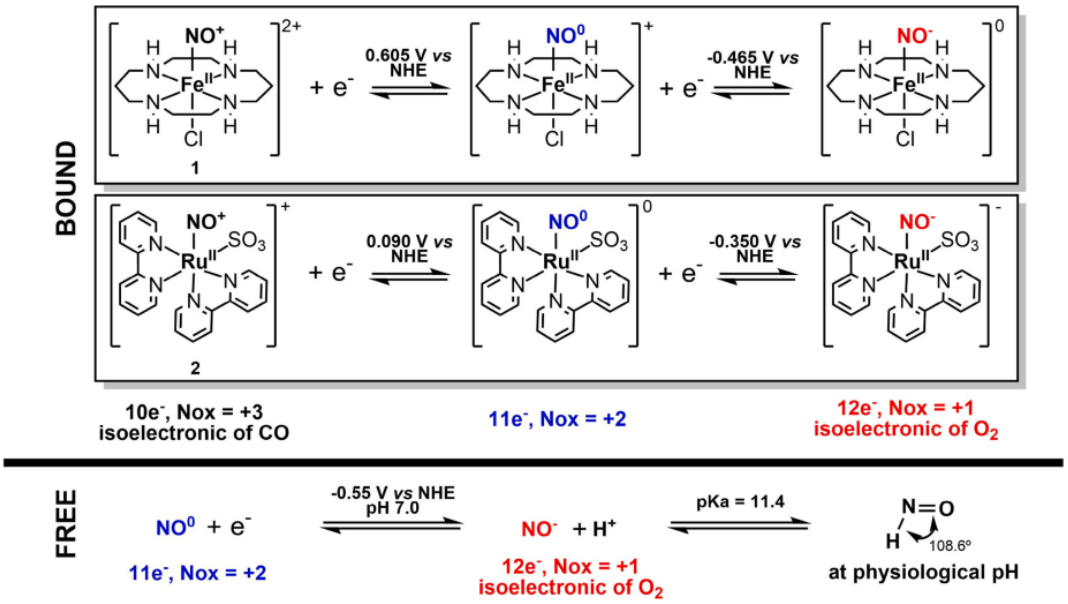

Fig. 1. Structures of the *trans*-[Fe(cyclam)(NO)Cl]$^{2+}$ (**1**) and *cis*-[Ru(bpy)$_2$(SO$_3$)(NO)]$^+$ (**2**) ions, along with their electrochemical processes associated with the bound nitrosyl moiety, and comparison with free NO in solution.

to a rectangular cavity operating in X-band (9.81GHz), using modulation amplitude = 0.2 G, quality factors of a cavity (Q) = 1500, microwave power = 10.23 mW, attenuation of 13 dB with repeated number of 2 scans.

The water used in all procedures was obtained from a water ultrapurification system with > 18 MΩ·cm (Direct Q® 3UV, Millipore). The stock solution of Angeli's salt was prepared in 10 mM NaOH solution, and its concentration determined using its molar extinction coefficient at 248 nm (ε = 8.2 × 10^3 M^{-1} cm^{-1}) [15]. The solutions of cPTIO, met-myoglobin (Mb-Fe^{3+}) and GSH were freshly prepared using 0.1 M phosphate buffer, pH 7.4 solution. Stock solution of NO was prepared by bubbling NO gas through an anaerobic 0.1 M phosphate buffer solution, pH 7.4 solution, for 30 min, admitting a saturation concentration reported in the literature [78]. The solution of Mb-Fe^{3+} was prepared under anaerobic conditions, and its concentration was determined using its molar extinction coefficient at 408 nm (ε = 1.88 × 10^5 M^{-1} cm^{-1}) [79]. All solutions of the complex were prepared in 0.1 M phosphate buffer, pH 7.4 solution.

Nitric oxide release was measured by electrochemical method using an ISO-NOP electrode (World Precision Instruments, Inc., Sarasota, FL, USA). The NO meter was connected to a TBR 4100 – Free Radical Analyzer data acquisition system (World Precision Instruments, Inc., Sarasota, FL, USA) and to a computer through a Lab-Trax-4/16 Bridge (World Precision Instruments, Inc., Sarasota, FL, USA). Before measurements, it was properly calibrated following manufacturer instructions.

2.4. NO/HNO thermal release

The thermal stability of the complex was monitored by UV–Vis spectroscopy using 100 μM of compound **1** dissolved in 0.1 M phosphate buffer pH 7.4 solution, under aerobic conditions. This study was also performed with the *trans*-[Fe(cyclam)Cl$_2$]$^+$ complex ion (**3**), under the same conditions, for comparative purposes. The solutions of these complexes were prepared and monitored for *ca.* 22.5 h at 37 °C.

The stability of the nitrosyl complex was also studied by FTIR/ATR using a 10 mM solution of the complex ion in 0.1 M phosphate buffer pH 7.4 solution at 37 °C. The complex stability was monitored based upon the presence of a band at 1894 cm^{-1}, assigned to the ν(NO$^+$), measured under aerobic conditions at time 0 and 24 h.

To validate thermal release of NO/HNO, the NO selective electrode and three other probes, cPTIO, Griess reagent and Mb-Fe^{3+}, were employed. Two solutions of the nitrosyl complex were prepared in 0.1 M phosphate buffer pH 7.4 solution, monitored by UV–Vis spectroscopy while under aerobic conditions for 24 h at 37 °C. The first solution contained 200 μM of the NO complex, 100 μM of cPTIO and 200 μM of DTPA, and the second solution contained 134 μM of the NO complex, 6.7 μM of Mb-Fe^{3+} and 134 μM of DTPA under anaerobic conditions. The chelating agent DTPA was used to avoid possible interference caused by free metal ions and did not promote any change in the nitrosyl complex structure. For comparative purposes, positive controls in the absence of the complex were used.

The amperometric detection of NO with selective electrode was carried out using a 100 μM solution of the complex prepared in 0.1 M phosphate buffer pH 7.4 solution, under aerobic conditions. The sample was monitored through 24 h at 37 °C, under slow magnetic stirring and in the absence of light. Data were recorded with the Labscribe 3 software (World Precision Instruments, Inc., Sarasota, FL, USA). Nitrite levels were measured over a period of 24 h at 37 °C using UV–Vis spectroscopy in aerobic solutions containing 50 mM of Griess reagent and 2 mM of *trans*-[Fe(cyclam)(NO)Cl]$^{2+}$. A solution containing the *trans*-[Fe(cyclam)Cl$_2$]$^+$ complex and Griess reagent served as control.

2.5. NO/HNO photorelease

Studies of NO photorelease were carried out using light irradiation at 365 nm, and monitored by absorption spectroscopy and EPR. Similar to the thermal release studies, cPTIO and Griess reagent were used as NO probes. The solutions containing cPTIO and the metal complex were prepared in 0.1 M phosphate buffer pH 7.4 and monitored for 15–20 min at 23 °C. UV–Vis measurements were performed in solutions containing 200 μM of *trans*-[Fe(cyclam)(NO)Cl]$^{2+}$, 100 μM of cPTIO and 200 μM of DTPA, while EPR measurements were conducted in solutions containing 400 μM of *trans*-[Fe(cyclam)(NO)Cl]$^{2+}$ and

200 μM cPTIO. Positive controls for HNO included Angeli's salt (HNO donor) and a saturated solution of NO with the cPTIO probe. In addition, a light irradiated (30–60 min) solution containing the cPTIO probe in the absence of complex served as a negative control. The measurements with Griess reagent were performed in water; the UV–Vis spectrum of a solution containing 50 mM of Griess reagent and 2 mM of *trans*-[Fe(cyclam)(NO)Cl]$^{2+}$ was measured at 23 °C at time 0 and 15 min after stimulation with light irradiation. A control without the metal complex was also performed.

2.6. Reaction of the trans-[Fe(cyclam)(NO)Cl]$^{2+}$ with glutathione

The reaction of the *trans*-[Fe(cyclam)(NO)Cl]$^{2+}$ complex ion with glutathione (GSH) was monitored using ATR infrared, EPR, UV–Vis spectroscopies and stopped-flow technique. In the experiment monitored by ATR infrared, the reaction was carried out in solutions containing 10 mM of *trans*-[Fe(cyclam)(NO)Cl]$^{2+}$ and 100 mM of GSH in 0.5 M phosphate buffer pH 7.4 solution. The EPR study was done in a solution of 200 μM of cPTIO, 400 μM of *trans*-[Fe(cyclam)(NO)Cl]$^{2+}$, 4 mM of GSH and 400 μM of DTPA, in 0.1 M phosphate buffer, pH 7.4. This reaction was monitored for 18 min and spectra recorded every 10 s.

Fast kinetics measurements were performed in solutions containing 5 mM *trans*-[Fe(cyclam)(NO)Cl]$^{2+}$ and 150 mM GSH, prepared upon fast mixing using stopped-flow technique in 0.5 M phosphate buffer pH 7.4 solution at 37 °C, maintaining conditions of pseudo-first-order reaction.

2.7. HIF-1α inhibition assay

MCF-7 or MB-231 cancer cells (2×10^6 cells) were plated into 60 mm cell culture dishes in RPMI complete medium supplemented with 10% FBS (Heat-Inactivated Fetal Bovine Serum) and penicillin-streptomycin and incubated overnight. The next day, the cells were pretreated with *trans*-[Fe(cyclam)(NO)Cl]$^{2+}$ for 30 min in serum-free medium, then treated with a 100 μM spermine NONOate solution (SPER/NO) for 4 h or incubated in a hypoxia chamber at 1.1% of O_2. The cells were then rinsed with cold phosphate-buffered saline, scrape harvested, centrifuged, and the pellet was resuspended and sonicated in lysis buffer [1% Nonidet P-40 0.5% sodium deoxycholate 0.1% SDS and protease inhibitor mixture (Calbiochem)]. After a 10 min of incubation on ice, the samples were centrifuged at 10,000 ×*g*, and the supernatant protein concentration was determined using the BCA Protein Assay Kit (Pierce). HIF-1α signals were normalized to (divided by) their respective alpha-tubulin densitometry measurements.

2.8. Automated capillary Western blot (WES)

Western blots were performed using WES, an automated capillary-based size sorting system (ProteinSimple, San Jose CA). All procedures were performed with the manufacturer's reagents according to their user manual. In this assay, 8 μL of diluted protein lysate was mixed with 2 μL of 5× fluorescent master mix and heated at 95 °C for 5 min. The samples (1 μg), blocking reagent, wash buffer, primary antibodies, secondary antibodies, and chemiluminescent substrate were dispensed into designated wells in a manufacturer-provided microplate. The plate was loaded into the instrument and protein was drawn into individual capillaries on a 25 capillary cassette provided by the manufacturer. Protein separation and immune-detection were performed automatically on the individual capillaries using default settings. The data were analyzed using the Compass software (ProteinSimple, San Jose CA). While some differences between α-tubulin loading controls were observed, HIF-1 signals were normalized to (divided by) their respective α-tubulin densitometry measurements. These numbers were then normalized to SPER/NO (or hypoxia) control to give %Control, which provided an accurate change in expression following treatment. Results obtained from WES are consistent with those using PAGE. Data are representative of $n = 3$ individual experiments.

2.9. In vitro angiogenesis assay

Anti-angiogenic effects were examined using an *in vitro* angiogenesis assay kit (ECM625, EMD Millipore, Billerica MA) according to the manufacturer's recommendations. In this assay, on-ice ECMatrix was mixed with 10× diluent buffer and 50 μL aliquotted per well into a cold 96-well plate. The plate was briefly centrifuged at 4 °C, then incubated at 37 °C to allow the matrix to solidify. HUVEC cells (15,000) at passage 3 were prepared in the presence and absence of drug and gently layered on top of the matrix. The cells were incubated at 37 °C for 5 h and endothelial cell tube formation was monitored and quantified by the number of tube formations.

2.10. Vasodilation assay

For this assay, rats were sacrificed by an overdose of sodium thiopental (150 mg/kg), and thoracic aorta was carefully removed and cut into rings of about 5 mm in length. The aortic rings were mounted in a 5 mL organ bath containing Krebs-Henseleit medium with the following composition: 120 mM NaCl, 4.7 mM KCl, 1.8 mM $CaCl_2$, 1.43 mM $MgCl_2$, 25 mM $NaHCO_3$, 1.17 mM KH_2PO_4, glucose and maintained at 37 °C. After equilibration, the rings were pre-contracted with 1 μM phenylephrine, and after stabilization of the system, cumulative concentration-response curves were constructed using the complex *trans*-[Fe(cyclam)(NO)Cl]$^{2+}$ in a concentration range of 1 nM to 10 μM. Sodium nitroprusside was used as control. This assay was performed using 7 independent measurements prepared with different animals for statistical analysis. All procedures were performed according to the ethics committee of State University of Ceará number 2897836/15.

2.11. Cell viability assays

The cytotoxicity of the *trans*-[Fe(cyclam)(NO)Cl]$^{2+}$ complex was evaluated in two different cell lines, B16–F10 (ATCC CRL-6475) and HUH-7 (JCRB-0403) cancer cells, using the 3-(4,5-dimethylthiazol-2-yl)-2,5-diphenyltetrazoliumbromide (MTT) protocol. The cells were seeded into 96-well plates at a density of 5×10^3 cells per well (100 μL) and allowed to attach overnight in 100 μL medium incubated at 37 °C, 5% CO_2: the cells were allowed to adhere for 12 h. Then, the medium was replaced by 100 mL of fresh medium without fetal calf serum (FCS). Growth arrested cells were released from the G0 phase by addition of 10% FCS in the medium in the absence (control) or in the presence of different concentrations of the iron complex (0.01 to 500 μM) dissolved in the cell culture medium for 24 h at 37 °C and 5% CO_2. The medium was removed and MTT (1 mg mL^{-1}) in DMEM (Dulbecco's Modified Eagle Medium) was added. After 4 h, the medium was aspirated and the formazan crystals were dissolved in ethanol 96%. Absorbance was read in a microplate reader (Epoch Biotek Instruments) at 570 nm. Three independent experiments were performed and two replicate cultures were used for each complex concentration in each independent experiment. The number of viable cells was expressed as a percentage relative to untreated controls, and the concentrations required for 50% inhibition of cell viability (IC_{50}) were calculated from dose–response curves.

3. Results and discussion

3.1. Thermal stability and NO release

Investigation of the thermal stability of nitrosyl complex **1** thermal stability was accomplished by monitoring UV–Vis spectroscopic changes in 0.1 μM phosphate buffer pH 7.4 solution, for *ca.* 22.5 h at 37 °C (Fig. 2A). Spectroscopic changes were defined by the

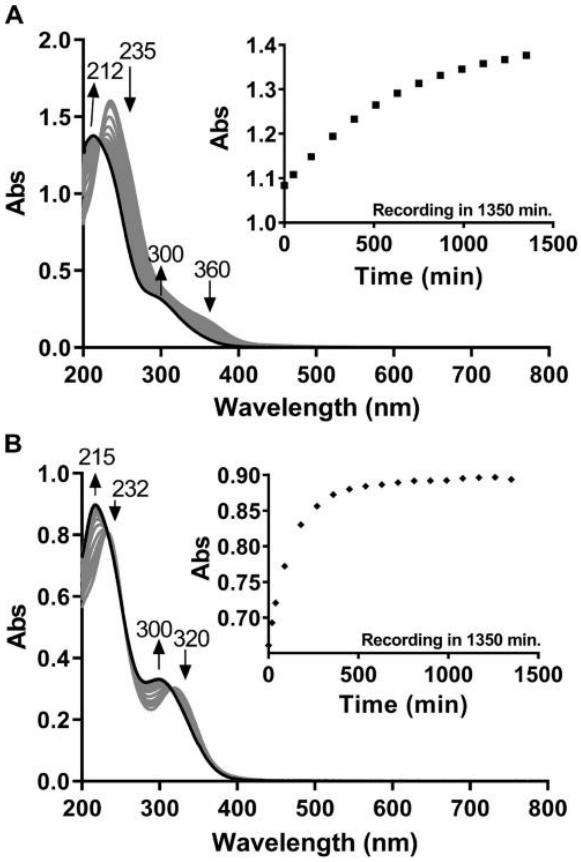

Fig. 2. Thermal stability of the iron complexes under aerobic conditions. A. Spectroscopic changes for **1** (100 μM), inset shows the kinetic curve based on changes at 212 nm. B. Spectroscopic changes for **3** (*trans*-$[Fe(cyclam)Cl_2]^+$, 100 μM), inset shows the kinetic curve at 215 nm. The spectra were monitored by electronic spectroscopy for *ca.* 22.5 h in 0.1 M phosphate buffer pH 7.4 solutions at 37 °C. Final spectrum in black.

disappearance of bands at 235 and 360 nm, followed by the appearance of sharper bands at 212 and 300 nm including an apparent isosbestic point at 224 nm.

During thermal incubation, a remarkable resemblance was observed between the final spectra obtained for **1** and **3**, under the same experimental conditions (Fig. 2). Previously, it was reported that the complex **3** shows rapid chloride exchange in water [80]. This result suggested that **1** might indeed be a slow NO- and Cl^--releasing complex, whose integrity of the iron-cyclam moiety is still maintained after 24 h, yielding a *trans*-$[Fe(cyclam)(H_2O)_2]^{3+}$ **(5)** final species. Additionally, this thermal process was also investigated using FTIR-ATR as shown in Fig. 3A. The intensity of the band at 1894 cm^{-1}, which is attributed to NO^+ stretching, was reduced by more than 50% after 24 h at 37 °C. This result further supported a slow thermal release of NO.

Griess reagent was used to indirectly validate thermal NO production, which was noticed as shown in Fig. 3B. After 24 h, the absorbance at 550 nm increased due to the reaction of Griess reagent with nitrite, where the latter may derive from a one-electron oxidation of nitric oxide under aerobic conditions [81]. This type of indirect measurement has been widely used in the literature concerning metallonitrosyl [82,83]. The control reaction using Griess reagent and the precursor **3** did not show any changes (Supporting information Fig. S5). In addition to this, thermal release of NO was measured directly by using a

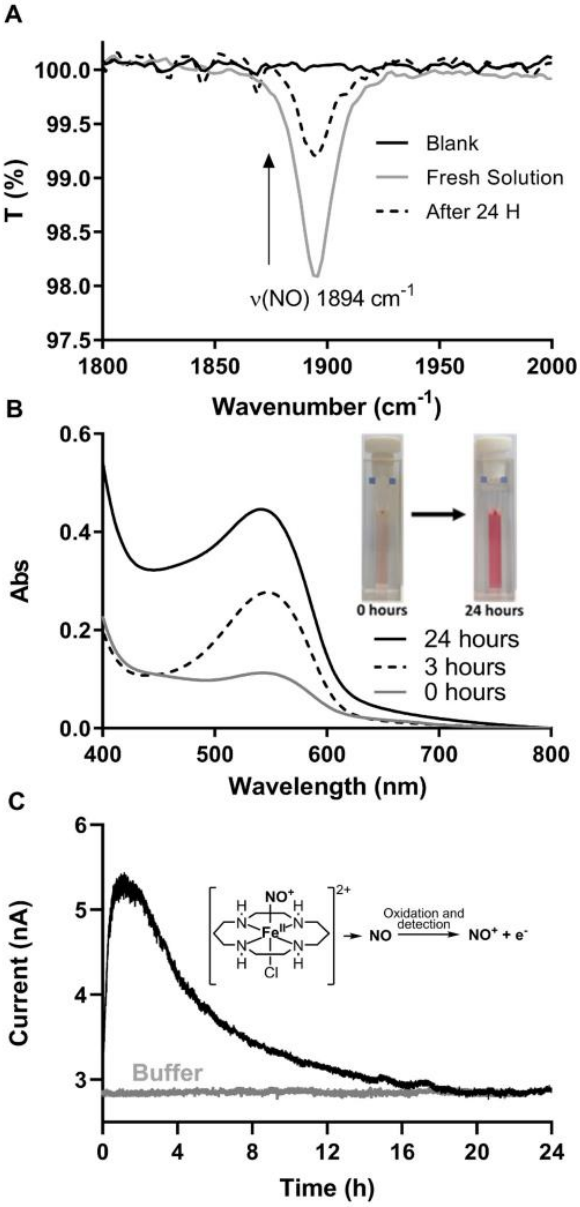

Fig. 3. Thermal release of NO. A. Monitoring of **1** (10 mM) in 0.1 M phosphate buffer pH 7.4 solution at 37 °C by FTIR-ATR. B. Electronic spectra of Griess reagent (50 mM) and **1** (2 mM) in aqueous solution for 24 h at 37 °C. C. Chronoamperogram of NO release by **1** (100 μM) (black line) in 0.1 M phosphate buffer pH 7.4 solution for 24 h at 37 °C. The signal measured for buffer (gray line) was also shown, monitored for 24 h at 37 °C.

selective NO sensor. An increase in current over time was observed, followed by a decrease and stabilization of the current, which strongly supports thermal release of NO. These results supported the fact that *trans*-$[Fe(cyclam)(NO)Cl]^{2+}$ decomposes in solution by means of a spontaneous intramolecular redox process, where the NO^+ ligand is reduced by oxidation of the metal center, causing its release in the form of NO^0 and the production of the aqua ferric complex (Scheme 1A).

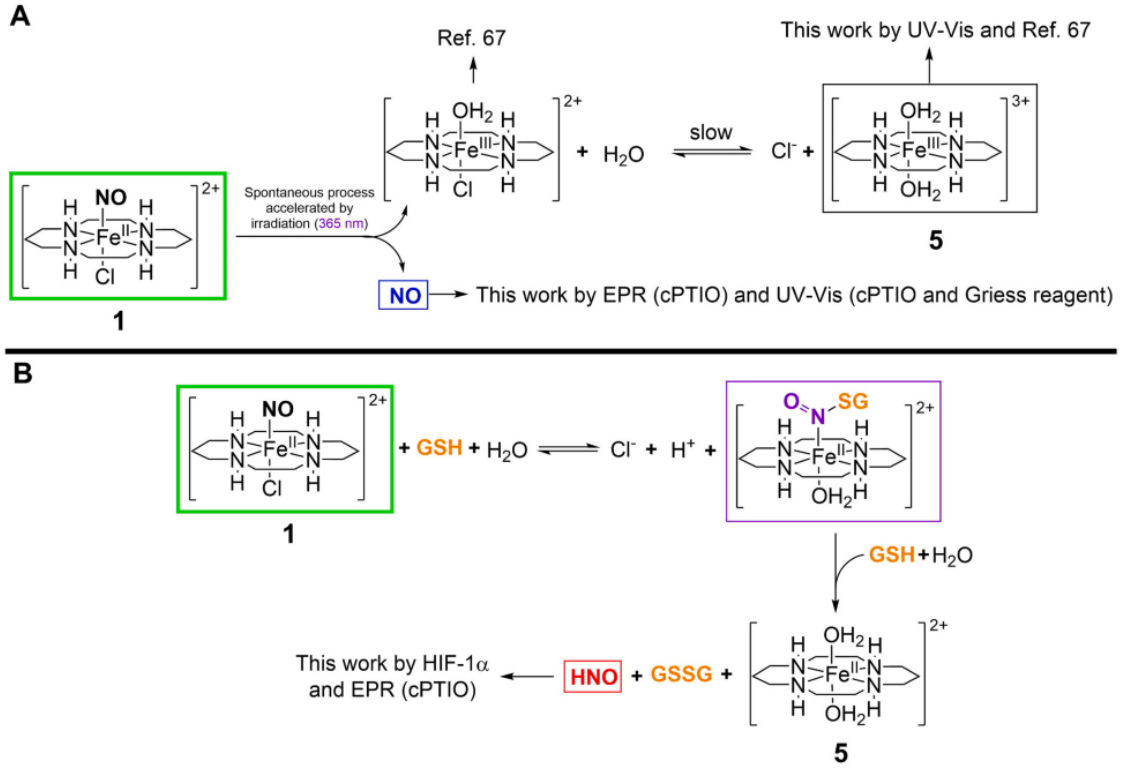

Scheme 1. Mechanistic proposal for the stimulated release of NO (A, spontaneous process accelerated by light) and HNO (B, glutathione) by the nitrosyl complex **1** (Fe-NO).

3.2. Photorelease of NO

To investigate if light could induce NO or HNO release, a similar set of qualitative studies were conducted with complex **1**. First of all, the cPTIO probe was combined with the nitrosyl complex in 0.1 M phosphate buffer pH 7.4 solution and irradiated for *ca.* 20 min with 365 nm light, at 25 °C. A much faster UV–Vis spectroscopic change was observed with a typical decrease in the bands at 360 and 560 nm, along with the concomitant appearance of a weak shoulder around 440 nm (Supporting Information Fig. S6).

cPTIO has been widely used by the scientific community not only for the detection of NO, but also for its ability to distinguish NO from HNO [65,84–86]. The reaction of cPTIO with NO generates cPTI species, which lacks a band at 560 nm and shows another one close to 440 nm. In contrast, the reaction of HNO with cPTIO produces usually cPTIO-H that does not present any absorption band from 420 up to 700 nm (Supporting information Fig. S7) [86]. The complex **1** and cPTIO were photolyzed separately under the same conditions, where no changes were seen (Supporting Information Fig. S7). The spectroscopic profile of cPTIO during photolysis of the nitrosyl complex was typical of a reaction with NO (Fig. 4 and Supporting Information Fig. S6).

This photochemical reaction was also monitored by the EPR technique using cPTIO in 0.1 μM phosphate buffer pH 7.4 solution. In Fig. 4 shows the EPR spectra of cPTIO in the presence of complex **1**, before and after irradiation at 365 nm for 15 min. This light irradiation resulted in the modification of the typical cPTIO spectrum with five lines (g = 2.006 and $a_N^{1,3}$ = 8.1 G) to the corresponding spectrum of cPTI with seven lines. The more complex spectral profile in the cPTI product is a consequence of the presence of non-symmetric nitrogen atoms in the structure, which leads to the appearance of different hyperfine

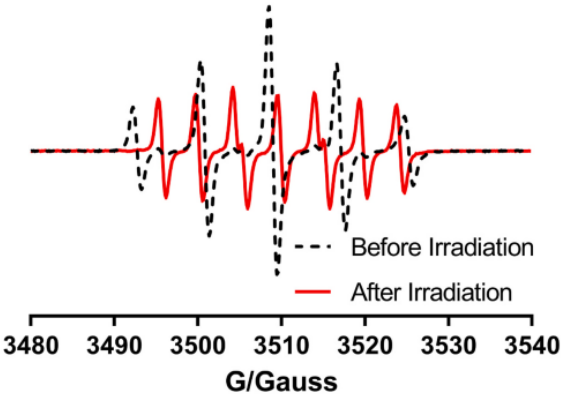

Fig. 4. EPR monitoring of the reaction of **1** (400 μM) with light (365 nm) using cPTIO (200 μM) in 0.1 M phosphate buffer pH 7.4 solution at 25 °C. Dashed line (before irradiation) and solid line (after irradiation).

splitting constants for ^{14}N (g = 2.006 and a_N^1 = 9.8 G and a_N^3 = 4.4 G) [87]. This evidence supports a direct reaction between cPTIO and NO as well reported in the literature [86,88].

The structural and electronic properties of the *trans*-[Fe(cyclam)(NO)Cl]$^{2+}$ complex were investigated using density functional theory (DFT) and time-dependent DFT (TD-DFT). All calculations were in good agreement with the experimental data, including the single-crystal X-ray structure (see Supporting Information). The light irradiation of the metal complex **1** at 365 nm promotes electronic transitions to

molecular orbitals with π*-antibonding character centered on the Fe^{II}–NO^+ bond (Table S2), which might reduce the bonding strength, leading to NO release. Similar photochemical behavior was reported for other metal nitrosyl complexes where photolabilization involves MLCT (Metal-to-ligand charge-transfer) transitions [89]. For nitrosyl complexes, TD-DFT calculations [45,89] indicate that both LLCT (Ligand-to-ligand charge-transfer) and MLCT transitions involve a dπ(Fe)-antibonding π*(NO) molecular orbital with an accepting character.

In addition to that, complex **5** was previously identified as one of the photolysis products of **1** [67]. A series of controls were also done using cPTIO with and without the metal complexes, and also in the presence or absence of light, which supported the photoproduction of NO (Supporting Information Fig. S8). Also, the indirect detection of NO after photoirradiation of **1** using Griess reagent was observed (Supporting Information Fig. S9) [81]. The inclusion of a dark control demonstrated that light irradiation greatly accelerates NO release, indicating, in contrast, that thermal release does not contribute significantly to the photochemical process. Altogether, these results support the fact that NO is released from **1** upon light irradiation (365 nm).

3.3. Reaction with glutathione

Due to the large intracellular GSH concentration in cancer cells and reports of its reactivity with nitrosyl metal complexes, we next investigated complex **1** reaction with GSH to produce HNO. A qualitative analysis of the reaction of GSH with **1** was performed using the FTIR-ATR technique. In this experiment, the NO^+ stretching band at 1894 cm^{-1} disappeared within 5 min after addition of GSH, illustrating a fast reaction (Supporting Information Fig. S10).

Next, GSH stimulation of **1** in the presence of cPTIO probe in 0.1 M phosphate buffer solution (pH 7.4) was then investigated. This reaction was monitored for 18 min, during which time the cPTIO EPR signal (g = 2.006 and $a_N^{1,3}$ = 8.1 G) rapidly disappeared (Fig. 5A) when compared to the GSH-cPTIO control solution, which (Supporting Information Fig. S11) showed a very modest change. Qualitative curves following the maximum relative intensity of each spectrum were prepared to illustrate the effect of GSH on the cPTIO spectrum, and the rapid decrease in the signal due to the reaction involving the nitrosyl metal complex (Fig. 5B).

Our data show clearly a decrease of the EPR signal of cPTIO promoted by the reaction of **1** with GSH. The cPTIO in the presence of HNO reacts to produce the non-radical product cPTIOH. Therefore, this result supports the quick generation of HNO under such conditions [90]. This reaction may have key implications on the biological fate of this compound with *in vivo* activation. Other nitrosyl complexes exhibited similar behavior upon reaction with GSH, where HNO was produced [65,91]. Recently, it was shown that HNO can also be produced by direct reaction of free NO with glutathione [23]. Despite this careful and detailed *in vitro* study, one may raise question the possibility of the occurrence of this reaction *in vivo*. Actually, if the reaction took place *in vivo*, where up to 10 mM of GSH is found, we would expect any NO donor to behave mostly as an HNO donor. Given that this behavior has not been extensively investigated, this point should be approached with caution. To further investigate this reaction, we carried out stopped-flow studies.

3.4. Fast kinetic study

The reaction between complex **1** and GSH was studied by stopped-flow kinetics and UV–Vis techniques in 0.5 M phosphate buffer pH 7.4 solution, at 37 °C where it was found that the spectrum of the nitrosyl complex changed significantly within 5 s in the presence of GSH. The appearance of a transition electronic band at 541 nm was observed, which remained unchanged throughout the process, sustaining an elementary process (Fig. 6). A pseudo-first-order reaction fit yielded a k_{obs} value of 6.31 ± 0.43 s^{-1} for the band appearing at 541 nm. The following decrease of this band was studied by conventional UV–Vis spectroscopy. The first spectrum profile was similar to the one obtained from the stopped-flow experiment, indicating that the increase of this band can only be observed *via* a fast technique such as stopped-flow. The decrease of the 541 nm band was monitored by conventional UV–Vis spectroscopy over 11 h. These data were fit with a first-order reaction equation, where a k_{obs} of 6.93 × 10^{-5} ± 0.96 × 10^{-5} s^{-1} was determined.

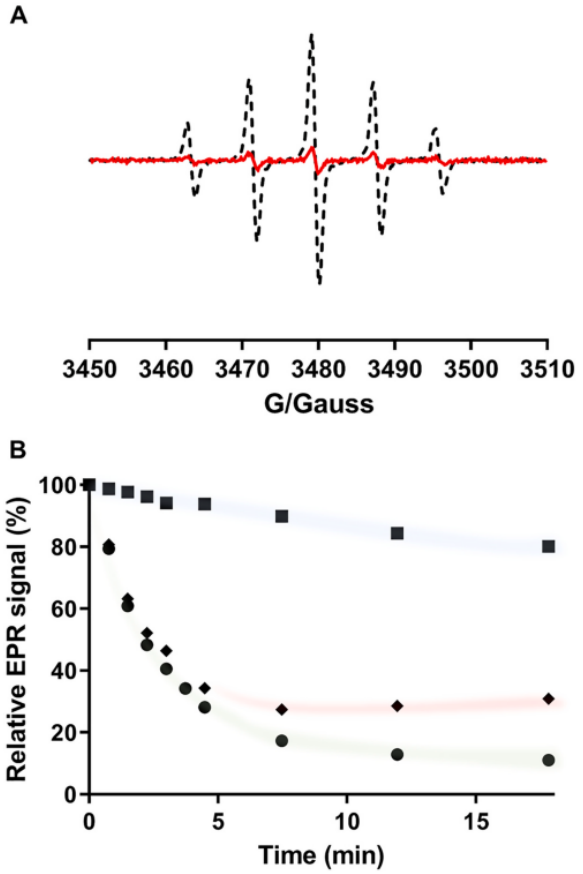

Fig. 5. EPR monitoring of the reaction of **1** (400 μM) with GSH (4 mM) using cPTIO (200 μM) as probe, in 0.1 mM phosphate buffer pH 7.4 solution, at 25 °C, and aerobic conditions. A. EPR spectra right before (dashed line) and after (solid line) 18 min of reaction. B. A trend of the EPR signal of reaction of cPTIO with *trans*-$[Fe(cyclam)(NO)Cl]^{2+}$ and GSH (circles) for 18 min; control reaction of GSH with cPTIO (square); result of the subtraction of the first and second measurements described above (diamond).

Based on kinetics and computational studies, the literature reported the formation of the intermediate complex $[Fe(CN)_5N(O)SH]^{3-}$ from the reaction of sodium nitroprusside (SNP) with H_2S. This species is responsible for the appearance of an electronic absorption band with a maximum at 535 nm at pH 7.4 [18]. A similar observation was previously reported for the reaction of cysteine, with another nitrosyl complex [41,92]. The reaction of SNP with cysteine led to the formation of an adduct species characterized by a new absorption band with maximum at 520 nm. The mechanism proposed for this reaction was based on the existence of an adduct intermediate of generic structure $[(CN)_5FeN\text{-}(O)L]^{n-}$, where L is a nucleophile (*e.g.* GSH). This intermediate adduct would further decompose releasing cystine and NO,

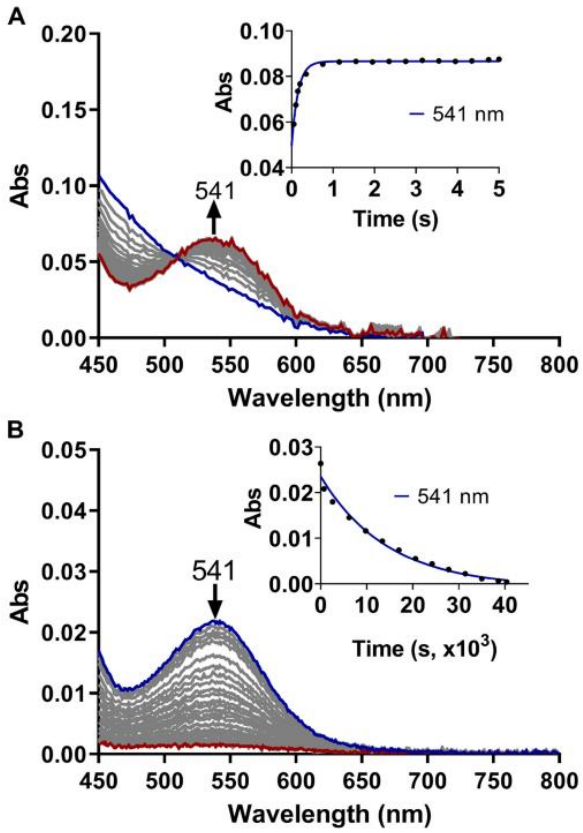

Fig. 6. Spectral changes investigated by stopped-flow measurement during the reaction of *trans*-[Fe(cyclam)(NO)Cl]$^{2+}$ (5 mM) with GSH (150 mM) (A) and the same reaction between of *trans*-[Fe(cyclam)(NO)Cl]$^{2+}$ (300 μM) with GSH (9 mM) by UV–Vis (B) in 0.5 M phosphate buffer pH 7.4 solution at 37 °C and under aerobic conditions. Inset: kinetic curve monitored at 541 nm (first order equation fit, in A k_{obs} = 6.31 s^{-1}, R^2 = 0.9936, in B k_{obs} = 6,93 × 10^{-5}, R^2 = 0.9830).

suggesting that cysteine is oxidized and NO^+ is reduced without formation of a nitrosothiol intermediate [92,93]. Thus, the presence of the transient band at 541 nm indicates that the release of the nitrosyl ligand, triggered by reaction with GSH, might occur through a new intermediate adduct complex in agreement with other nitrosyl complexes.

3.5. HIF-1α stability assay as a biological validation of HNO production

One biological molecule employed to discern the effects of NO and HNO species pertains to their effect on HIF-1α stability [8,65,94]. HIF-1α is a subunit of the HIF-1 transcription factor, which regulates the cellular response to oxygen and other metabolic processes. Under conditions of normoxia, HIF-1α is maintained at low levels due to a continuous process of labeling for protein degradation. Lower levels of oxygen create a hypoxic environment preventing HIF-1α labeling and degradation. Once accumulated, HIF-1α translocates to the nucleus, where it undergoes heterodimerization with the subunit HIF-1β forming the active HIF-1 transcription factor that binds to hypoxia response elements. The targeted genes regulate many key processes such as angiogenesis and cellular metabolism. In cancer, the deregulation of HIF-1α and/or its high expression promotes tumor growth and metastasis, through altered tumor angiogenesis, cell metabolism and survival in response to hypoxia. All these aspects make HIF-1α an exciting potential drug target in cancer chemotherapy [29,65].

Studies have demonstrated a role of NO in the stabilization of HIF-1α under normoxic conditions [95,96]. In contrast, HNO was shown to block HIF-1α stabilization induced by both hypoxia and NO in room air. Sousa et al. demonstrated that a nitrosyl complex **2** limited HIF-1α stabilization, which was mediated by thiol-induced HNO production [65].

Here, we investigated the effects of complex **1** on NO- or hypoxia-induced HIF-1α protein levels in MB-231 or MCF-7 cancer cells. These breast cancer cells were pre-treated for 30 min with increasing concentrations of **1** (1 to 20 μM, identified as Fe-NO), then treated with 100 μM of SPER/NO, a known NO donor, for 4 h or hypoxia at 1.1% oxygen, for 2 h at 37 °C. The iron complex clearly limited SPER/NO-induced HIF-1α stabilization (Fig. 7A), thus ruling out NO production by complex **1**. Indeed, the abated HIF-1α levels shown in Fig. 7A could be explained by the capacity of nitrosyl complexes to release HNO, as previously suggested by *in vitro* assays with a ruthenium-based complex and cPTIO [65].

The complex **1** also limited HIF-1α accumulation under hypoxic condition (Fig. 7C), however, it was less efficient when compared to the studies carried out using SPER/NO. Deferoxamine (10 μM), a commonly used iron chelator, was also employed to investigate a role of free iron in HIF-1α modulation. In contrast to the effects of complex **1**, the precursor molecule, *trans*-[Fe(cyclam)Cl_2]$^+$ (**3**, Fe-ctrl), enhanced HIF-1α stability under hypoxic conditions, which was almost completely reversed in the presence of deferoxamine (Fig. 7D). Given that deferoxamine also increased HIF-1α levels under hypoxic conditions, and chelators disrupt iron homeostasis and cellular metabolism, which promotes HIF-1α stabilization [97,98], these results warrant further investigation. Moreover, it is unclear if this chelation caused an overwhelming effect beyond that promoted by these complexes, however prolyl hydroxylase activity requires iron, which may have been modulated by deferoxamine. Nonetheless, these results further support that the overall effect of nitrosyl complex is due to HNO production *in vivo*.

As HIF-1α mediates the induction of angiogenesis, we further explored potential anti-angiogenic effects of our nitrosyl iron complex **1**. HUVEC cells were seeded in the presence and absence of **1** (Fe-NO) and **3** (Fe-ctrl), then incubated for 5 h, after which endothelial tube formation was assessed. As shown in Fig. 8, when compared to a Sham Control, 20 μM of **1** (Fe-NO) reduced endothelial tube formation by approximately 50%. In contrast, the control complex **3** (Fe-ctrl) had no significant anti-angiogenic effects. These results demonstrate that HNO released by complex **1** limits angiogenesis, as previously observed with a ruthenium-based complex. Importantly, this effect has not been reported with a nitrosyl iron complex [65].

3.6. Vasodilation assay

NO and HNO can exhibit great vasodilating properties, which might suggest another possible application of our nitrosyl complex. Moreover, there are only a few promising iron-based nitrosyl complexes available for this purpose. Oxacom®, a dinitrosyl iron complex (DNIC) containing glutathione as a ligand, is one relevant example of a hypotensive drug without reported adverse effects reported so far; however, this formulation is still in phase I/II clinical trials [37,99–101]. Sodium nitroprusside, a ferrate complex ($Na_2[Fe(CN)_5NO]\cdot 2H_2O$, SNP) is the only iron complex in clinical use. However, it has major limitations due to rapid NO release and toxicity associated with the release of cyanide ions [39,40,54].

The complex **1** was studied as a vasodilator agent using rat aortic rings precontracted with phenylephrine. In this dose-response study, SNP was used as a positive control. Fig. 9 shows a dose-response curve of aorta relaxation.

Relaxation potency was reported as IC_{50} values, corresponding to the minimum concentration of compound required to cause 50% of

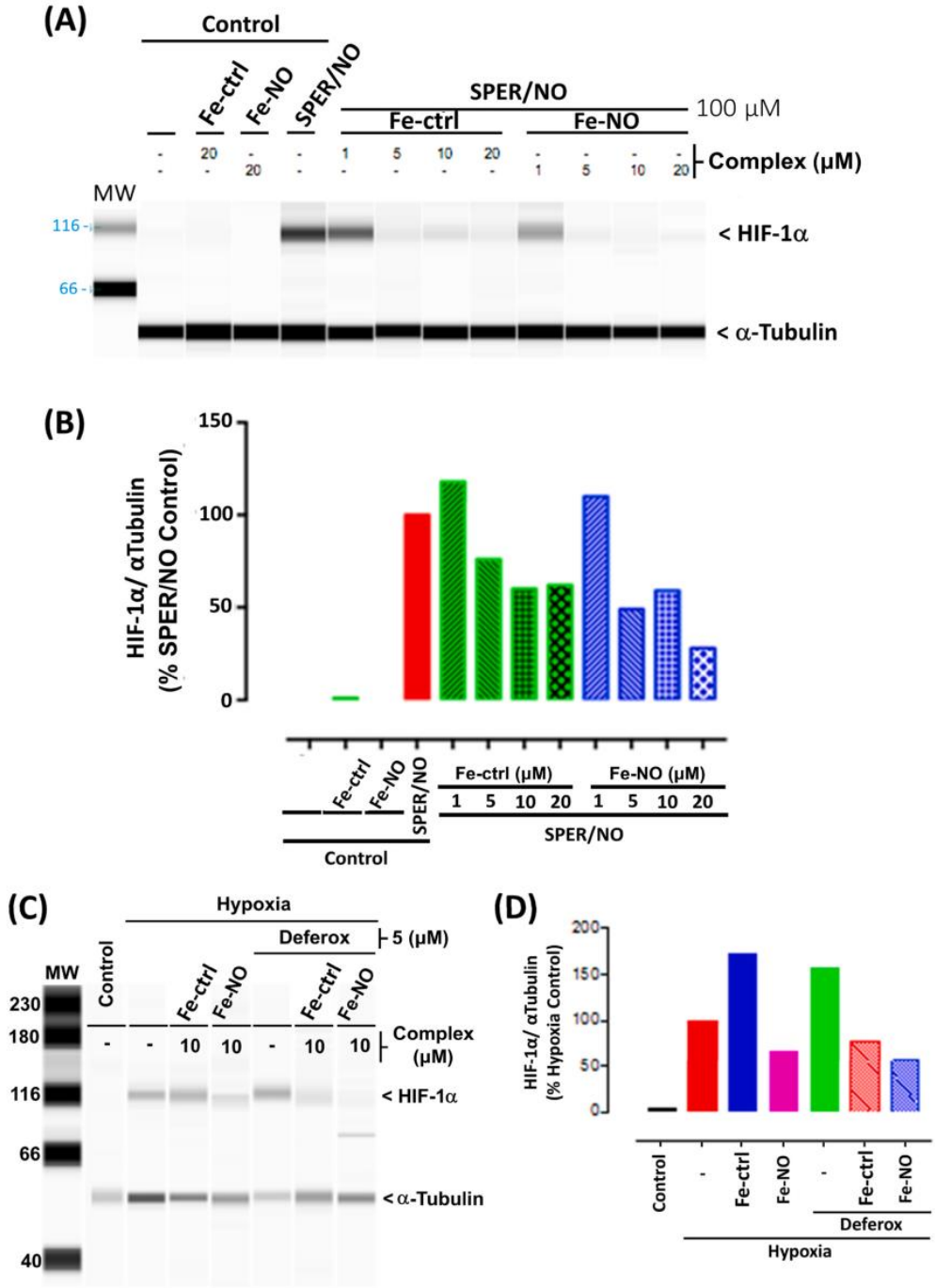

Fig. 7. Effect of complex **1** (Fe-NO) on SPER/NO- or hypoxia-induced HIF-1α stabilization in breast cancer cells. (A) WES analysis of HIF-1α protein levels in MB-231 breast cancer cells pre-treated with 20, 10, 5 and 1 µM of **1** (Fe-NO) and **3** (Fe-ctrl) for 30 min, followed by treatment with 100 µM SPER/NO for 4 h. (B) Quantitation of WES analysis shown in panel (A). (C) WES analysis of HIF-1α protein levels in MCF-7 breast cancer cells treated with 10 µM of **1** and **3** under hypoxic conditions (1.1% oxygen) for 1.5 h. Deferoxamine was used at 10 µM to chelate traces of free iron. (D) Quantitation of WES shown in panel (C).

vasodilatation, which was 24 nM and 910 nM for SNP and **1**, respectively. These results showed that nitrosyl complex **1** is less effective than SNP under these working conditions. However, this was expected based on *in vitro* measurements of a slow NO release. Indeed, this moderate activity is an important feature and possibly an advantage over SNP as this behavior may be indicative of a more controlled

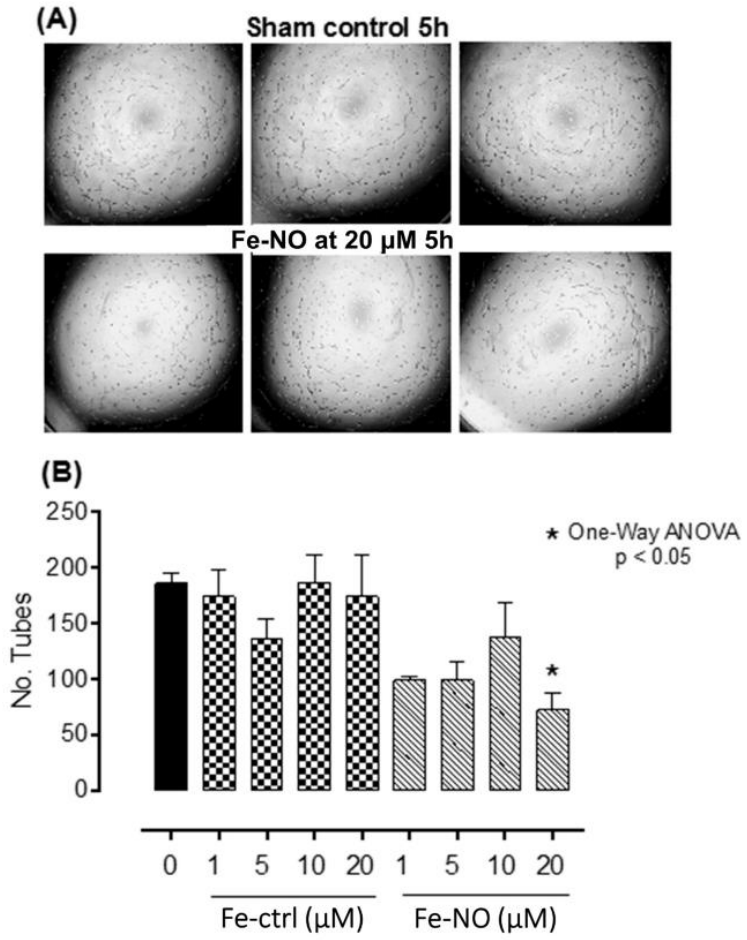

Fig. 8. Anti-angiogenic effects of **1** (Fe-NO) in HUVEC cells. (A) Anti-angiogenic effects of 20 μM **1** (Fe-NO) as demonstrated by reduced endothelial tube formation when compared to a Sham Control. (B) Quantitation of tube formation shown in panel (A) and comparison with results obtained with **3** (Fe-ctrl).

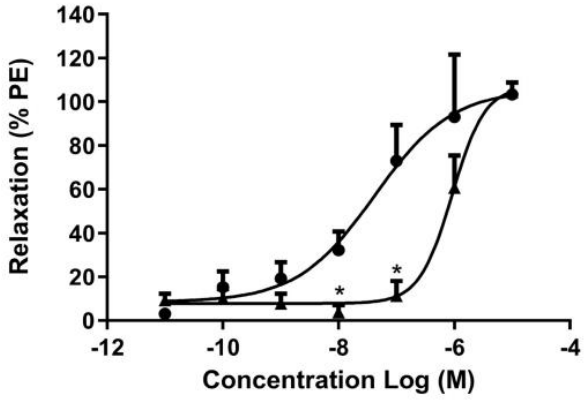

Fig. 9. Relaxation promoted by the **1** (Fe-NO, triangles) and SNP (circles) in rat aortic rings pre-contracted with phenylephrine (1.0 μM). Relaxation responses are expressed as the percentage of relaxation *versus* concentration of tested compounds (all measurements were carried out in seven independent aortas, $p < 0.05$, SNP *vs.* **1** (Fe-NO)).

release of NO, thereby avoiding hypotension issues caused by the rapid NO release associated with SNP, as well as the side effects associated with cyanide [39,102], which cannot be the case for complex **1**. Altogether these results indicate that complex **1** is a promising model of new antihypertensive agents, possibly with lower side effects than SNP.

3.7. Cytotoxicity

Nitric oxide has shown dual effects on cancer cells, either inducing or blocking cancer progression in a concentration-dependent manner. In general, high concentrations of NO lead to inhibition of cell growth and induce cell death by apoptosis, while low concentrations promote cell survival and proliferation [103]. This dichotomous behavior has prompted a keen interest in modulation of NO release by novel NO donors [104]. As previously described, HNO donors may also have promising anti-angiogenic and anti-stemness activities on tumors, which also warrants the design and investigation of novel HNO donating compounds.

Here, we measured the cell viability for B16-F10 [105] and HUH-7 [106] cancer cells in the presence of complex **1**, (Supporting information, Fig. S12). The obtained high IC_{50} values (above 100 μM) are indicative of a possible reduced cytotoxicity, which may be relevant for cardiovascular applications, without discarding a potential use as an

anti-angiogenic agent or neoadjuvant in cancer therapy.

3.8. Proposed mechanism for induced release of NO and HNO

Our experimental data support that **1** decomposes spontaneously in solution by an intramolecular redox process, where the NO^+ ligand is reduction by the metal center, causing the production of the aqua ferric complex **5** and free NO^0, as well as, the UV light irradiation can accelerate this process. Upon illumination at 365 nm, the electronically excited state of **1** decays by a non-radiative pathway of releasing of NO^0 and production of **5**, in line with previous works (Scheme 1A) [67]. In addition, glutathione is a second route of stimulus, which was shown here to promote the release of HNO. The reaction of nitrosyl complexes with GSH has been investigated and intermediate species were proposed.

Similarly to those previous works, the nitrosyl complex **1** may form an adduct intermediate (*trans*-[Fe(cyclam)(Cl)N(*O*)SG]$^+$) (Scheme 1B). This adduct, analogously with the *trans*-[Ru(cyclam)(NO)Cl]$^{2+}$ complex [107], can exchange the Cl^- ligand by a water molecule, producing the second intermediate *trans*-[Fe(cyclam)(H_2O)N(*O*)SG]$^+$. The latter intermediate can then react directly with another GSH molecule, producing the *trans*-[Fe(cyclam)(H_2O)N(O)($SG)_2$] adduct, which was observed as in the case of other nitrosyl metal complexes [108]. This second intermediate species, decomposes immediately generating HNO, the aqua complex **5** and oxidized glutathione (GSSG) [92].

4. Final consideration

More than a decade after the synthesis of the *trans*-[Fe(cyclam)(NO)Cl]$^{2+}$ complex, a series of systematic studies on its reactivity definitely reveal its promising potential as NO/HNO donor. This compound has demonstrated spontaneous slow release of NO, which can be highly accelerated upon moderate UV light irradiation. On the other hand, a fast reaction with glutathione (GSH) favors a major production of HNO, which may have beneficial physiological effects, including abated angiogenesis through HIF-1α destabilization in a tumor microenvironment. Importantly, other thiols including cysteine and H_2S, eventually found in the biological medium, might also promote HNO production through reaction with this complex. Vasodilation assays showed an IC_{50} of 910 nM, which may provide a therapeutic advantage when compared to that of SNP (24 nM). In addition, the high IC_{50} value measured during cell viability assays, suggests potentially lower cytotoxicity of this metal complex and the absence of cyanide ion would also be advantageous in a clinical setting. In summary, this compound deserves further biological studies to uncover its full therapeutic potential, as it represents the first iron nitrosyl-type compound to exhibit all of the mentioned pharmacological activities.

Abbreviations

ATR	attenuated total reflectance
bpy	2,2′-bipyridine
cPTIO	2-(4-carboxyphenyl)-4,4,5,5-tetramethylimidazoline-1-oxyl-3-oxide potassium salt
Cyclam	1,4,8,11-tetraazacyclotetradecane
Deferoxamine	*N*-[5-[[4-[5-[acetyl(hydroxy)amino]pentylamino]-4-oxobutanoyl]-hydroxyamino]pentyl]-*N*′-(5-aminopentyl)-*N*′-hydroxybutanediamide
DFT	density functional theory
DTPA	diethylenetriaminepentaacetic acid
DMEM	Dulbecco's Modified Eagle Medium
EPR	electron paramagnetic resonance
FBS	heat-inactivated fetal bovine serum
FCS	fetal calf serum
GSH	glutathione
GSSG	oxidized glutathione
HIF-1	hypoxia-inducible factor-1
HNO	nitroxyl
HREs	hypoxia response elements
IC	cell viability
LLCT	ligand-to-ligand charge-transfer
Mb-Fe^{3+}	met-myoglobin
MLCT	metal-to-ligand charge-transfer
MTT	3-(4,5-dimethylthiazol-2-yl)-2,5-diphenyltetrazolium-bromide
NO	nitric oxide
Piloty's acid	benzenesulphonydroxamic acid
SPER/NO	N-[4-[1-(3-aminopropyl)-2-hydroxy-2-nitrosohydrazino] butyl]-1,3-propanediamine
SDS	sodium dodecyl sulfate
SNP	sodium nitroprusside
TD-DFT	time-dependent DFT
WES	automated capillary Western blot

Authors contributions

EMC carried out synthesis, designed the chemical experiments and carried out spectroscopic and electrochemical studies, has also analyzed and interpreted data, wrote the paper. LAR and DAW planned and carried out HIF and tube formation experiments, discussed results and wrote the paper. FSGJ has measured NO using selective electrode and discussed the results. PHBC and NRFN designed and carried out vasodilation assays, interpreted the results and wrote the paper. MJCM and DLP designed and carried out cytotoxicity assays. EL designed experiment and interpreted results of nitrite measurements. TFP carried out DFT analysis, interpreted data and wrote the paper. DWF, VBG and RC planned and assisted on EPR data acquisition, in addition, VBG and RC helped in the discussion of the mechanism and wrote the paper. EHSS and LGFL designed experiments, analyzed and interpreted data, wrote the paper.

Declaration of competing interest

The authors declare no competing financial interest.

Acknowledgements

The authors are thankful to CNPq (L. G. F. Lopes 303355/2018-2, E. H. S. Sousa 308383/2018-4, Universal 403866/2016-2; T. F. Paulo, Universal 428741/2016-9), FUNCAP (PRONEX PR2 0101-00030.01.00/15 SPU N°: 3265612/2015) for financial support. This study was also financed in part by the Coordenação de Aperfeiçoamento de Pessoal de Nível Superior - Brasil (CAPES) - Finance Code 001 and CAPES/COFECUB (88887.130198/2017-01) as well as the NIH Intramural Research Programs and Cancer and Inflammation Program (LAR and DAW).

Appendix A. Supplementary data

Electronic supplementary information (ESI): Notes, details of methods and additional data (Fig. and table: Fig. S1 to S13 and Tables S1 and S2) can be found in the supporting information. Supplementary data to this article can be found online at doi:https://doi.org/10.1016/j.jinorgbio.2020.111133.

References

[1] D.D. Thomas, L.A. Ridnour, J.S. Isenberg, W. Flores-Santana, C.H. Switzer, S. Donzelli, P. Hussain, C. Vecoli, N. Paolocci, S. Ambs, C.A. Colton, C.C. Harris, D.D. Roberts, D.A. Wink, Free Radic. Biol. Med. 45 (2008) 18–31, https://doi.org/10.1016/j.freeradbiomed.2008.03.020.

[2] L.J. Ignarro, B.A. Freeman (Eds.), Nitric Oxide Biology and Pathobiology, Elsevier

Inc, 2017.
[3] J.A. McCleverty, Chem. Rev. 104 (2004) 403–418, https://doi.org/10.1021/cr020623q.
[4] J.K.Y. Tse, ACS Chem. Neurosci. 8 (2017) 1438–1447, https://doi.org/10.1021/acschemneuro.7b00176.
[5] K.M. Miranda, Coord. Chem. Rev. 249 (2005) 433–455, https://doi.org/10.1016/j.ccr.2004.08.010.
[6] H.N. Sabbah, C.G. Tocchetti, M. Wang, S. Daya, R.C. Gupta, R.S. Tunin, R. Mazhari, E. Takimoto, N. Paolocci, D. Cowart, W.S. Colucci, D.A. Kass, Circ. Heart Fail. 6 (2013) 1250–1258, https://doi.org/10.1161/CIRCHEARTFAILURE.113.000632.
[7] H.T. Nagasawa, S.P. Kawle, J.A. Elberling, E.G. DeMaster, J.M. Fukuto, J. Med. Chem. 38 (1995) 1865–1871, https://doi.org/10.1021/jm00011a005.
[8] A.J. Norris, M.R. Sartippour, M. Lu, T. Park, J.Y. Rao, M.I. Jackson, J.M. Fukuto, M.N. Brooks, Int. J. Cancer 122 (2008) 1905–1910, https://doi.org/10.1002/ijc.23305.
[9] A.B. Seabra (Ed.), Nitric Oxide Donors Novel Biomedical Applications and Perspectives, Elsevier Inc, 2017.
[10] P.G. Wang, M. Xian, X. Tang, X. Wu, Z. Wen, T. Cai, A.J. Janczuk, Chem. Rev. 102 (2002) 1091–1134, https://doi.org/10.1021/cr000040l.
[11] H. Nakagawa, J. Inorg. Biochem. 118 (2013) 187–190, https://doi.org/10.1016/j.jinorgbio.2012.10.004.
[12] D.A. Guthrie, A. Ho, C.G. Takahashi, A. Collins, M. Morris, J.P. Toscano, J. Org. Chem. 80 (2015) 1338–1348, https://doi.org/10.1021/jo502330w.
[13] F. Doctorovich, P.J. Farmer, M.A. Marti (Eds.), The Chemistry and Biology of Nitroxyl (HNO), Elsevier, 2017.
[14] C. Oliveira, S. Benfeito, C. Fernandes, F. Cagide, T. Silva, F. Borges, Med. Res. Rev. 38 (2018) 1159–1187, https://doi.org/10.1002/med.21461.
[15] J.F. DuMond, S.B. King, Antioxid. Redox Signal. 14 (2011) 1637–1648, https://doi.org/10.1089/ars.2010.3838.
[16] D.R. Truzzi, D.W. Franco, Inorg. Chim. Acta 421 (2014) 74–79, https://doi.org/10.1016/j.ica.2014.05.010.
[17] M.R. Walter, S.P. Dzul, A.V. Rodrigues, T.L. Stemmler, J. Telser, J. Conradie, A. Ghosh, T.C. Harrop, J. Am. Chem. Soc. 138 (2016) 12459–12471, https://doi.org/10.1021/jacs.6b05896.
[18] M.R. Filipovic, M. Eberhardt, V. Prokopovic, A. Mijuskovic, Z. Orescanin-Dusic, P. Reeh, I. Ivanovic-Burmazovic, J. Med. Chem. 56 (2013) 1499–1508, https://doi.org/10.1021/jm3012036.
[19] T.T. Lu, C.H. Chen, W.F. Liaw, Chem. Eur. J. 16 (2010) 8088–8095, https://doi.org/10.1002/chem.201000524.
[20] S.A. Dillinger, H.W. Schmalle, T. Fox, H. Berke, Dalton Trans. (2007) 3562–3571, https://doi.org/10.1039/b702461d.
[21] M. Eberhardt, M. Dux, B. Namer, J. Miljkovic, N. Cordasic, C. Will, T.I. Kichko, J. De la Roche, M. Fischer, S.A. Suárez, D. Bikiel, K. Dorsch, A. Leffler, A. Babes, A. Lampert, J.K. Lennerz, J. Jacobi, M.A. Martí, F. Doctorovich, E.D. Högestätt, P.M. Zygmunt, I. Ivanovic-Burmazovic, K. Messlinger, P. Reeh, M.R. Filipovic, Nat. Commun. 5 (4381) (2014), https://doi.org/10.1038/ncomms5381.
[22] S.A. Suarez, N.I. Neuman, M. Munoz, L. Alvarez, D.E. Bikiel, C.D. Brondino, I. Ivanovic-Burmazovic, J. Miljkovic, M.R. Filipovic, M.A. Marti, F. Doctorovich, J. Am. Chem. Soc. 137 (2015) 4720–4727, https://doi.org/10.1021/ja512343w.
[23] S.A. Suarez, M. Munoz, L. Alvarez, M.F. Venancio, W.R. Rocha, D.E. Bikiel, M.A. Marti, F. Doctorovich, J. Am. Chem. Soc. 139 (2017) 14483–14487, https://doi.org/10.1021/jacs.7b06968.
[24] W. Flores-Santana, D.J. Salmon, S. Donzelli, C.H. Switzer, D. Basudhar, L. Ridnour, R. Cheng, S.A. Glynn, N. Paolocci, J.M. Fukuto, K.M. Miranda, D.A. Wink, Antioxid. Redox Signal. 14 (2011) 1659–1674, https://doi.org/10.1089/ars.2010.3841.
[25] C.L. Bianco, J.P. Toscano, M.D. Bartberger, J.M. Fukuto, Arch. Biochem. Biophys. 617 (2017) 129–136, https://doi.org/10.1016/j.abb.2016.08.014.
[26] E.G. DeMaster, B. Redfern, H.T. Nagasawa, Biochem. Pharmacol. 55 (1998) 2007–2015, https://doi.org/10.1016/s0006-2952(98)00080-x.
[27] J.P. Froehlich, J.E. Mahaney, G. Keceli, C.M. Pavlos, R. Goldstein, A.J. Redwood, C. Sumbilla, D.I. Lee, C.G. Tocchetti, D.A. Kass, N. Paolocci, J.P. Toscano, Biochemistry 47 (2008) 13150–13152, https://doi.org/10.1021/bi801925p.
[28] B.E. Lopez, D.A. Wink, J.M. Fukuto, Arch. Biochem. Biophys. 465 (2007) 430–436, https://doi.org/10.1016/j.abb.2007.06.017.
[29] G.N. Masoud, W. Li, Acta Pharm. Sin. B 5 (2015) 378–389, https://doi.org/10.1016/j.apsb.2015.05.007.
[30] G.M. Burslem, H.F. Kyle, A. Nelson, T.A. Edwards, A.J. Wilson, Chem. Sci. 8 (2017) 4188–4202, https://doi.org/10.1039/c7sc00388a.
[31] T.T. Lu, Y.M. Wang, C.H. Hung, S.J. Chiou, W.F. Liaw, Inorg. Chem. 57 (2018) 12425–12443, https://doi.org/10.1021/acs.inorgchem.8b01818.
[32] N. Bicer, E. Yildiz, A.A. Yegani, F. Aksu, New J. Chem. 42 (2018) 8098–8104, https://doi.org/10.1039/c7nj04223j.
[33] W.A. Wani, U. Baig, S. Shreaz, R.A. Shiekh, P.F. Iqbal, E. Jameel, A. Ahmad, S.H. Mohd-Setapar, M. Mushtaque, L.T. Hun, New J. Chem. 40 (2016) 1063–1090, https://doi.org/10.1039/c5nj01449b.
[34] E.H.S. Sousa, F.G.M. Vieira, J.S. Butler, L.A. Basso, D.S. Santiago, I.C. Diogenes, L.G.F. Lopes, P.J. Sadler, J. Inorg. Biochem. 140 (2014) 236–244, https://doi.org/10.1016/j.jinorgbio.2014.08.002.
[35] J. Laborde, C. Deraeve, F.G.M. Vieira, A. Sournia-Saquet, L. Rechignat, A.D. Villela, B.L. Abbadi, F.S. Macchi, K. Pissinate, C.V. Bizarro, P. Machado, L.A. Basso, G. Pratviel, L.G.F. Lopes, E.H.S. Sousa, V. Bernardes-Genisson, J. Inorg. Biochem. 179 (2018) 71–81, https://doi.org/10.1016/j.jinorgbio.2017.11.013.
[36] J. Keiser, M. Vargas, R. Rubbiani, G. Gasser, C. Biot, Parasites Vectors 7 (424) (2014), https://doi.org/10.1186/1756-3305-7-424.
[37] A.F. Vanin, N.A. Sanina, V.A. Serezhenkov, D.S. Burbaev, V.I. Lozinsky, S.M. Aldoshin, Nitric Oxide 16 (2007) 82–93, https://doi.org/10.1016/j.niox.2006.07.005.
[38] Y.P. Vedernikov, P.I. Mordvintcev, I.V. Malenkova, A.F. Vanin, Eur. J. Pharmacol. 211 (1992) 313–317, https://doi.org/10.1016/0014-2999(92)90386-i.
[39] T.C. Buzinari, J.C. Oishi, T.F. De Moraes, I.P. Vatanabe, H.S. Selistre-de-Araujo, C.R. Pestana, G.J. Rodrigues, Eur. J. Pharm. Sci. 105 (2017) 144–149, https://doi.org/10.1016/j.ejps.2017.04.022.
[40] D.G. Hottinger, D.S. Beebe, T. Kozhimannil, R.C. Prielipp, K.G. Belani, J. Anaesthesiol. Clin. Pharmacol. 30 (2014) 462–471, https://doi.org/10.4103/0970-9185.142799.
[41] F.O.N. Silva, M.C.L. Candido, A.K.M. Holanda, I.C.N. Diogenes, E.H.S. Sousa, L.G.F. Lopes, J. Inorg. Biochem. 105 (2011) 624–629, https://doi.org/10.1016/j.jinorgbio.2011.02.004.
[42] F.O.N. Silva, E.C.C. Gomes, T.S. Francisco, A.K.M. Holanda, I.C.N. Diógenes, E.H.S. Sousa, L.G.F. Lopes, E. Longhinotti, Polyhedron 29 (2010) 3349–3354, https://doi.org/10.1016/j.poly.2010.09.009.
[43] A.P. Sousa, A.F. Fernandes, I.A. Paz, N.R.F. Nascimento, J. Ellena, E.H.S. Sousa, L.G.F. Lopes, A.K.M. Holanda, J. Braz, Chem. Soc. 28 (2017) 2117–2129, https://doi.org/10.21577/0103-5053.20170057.
[44] N. Levin, J. Perdomenico, E. Bill, T. Weyhermuller, L.D. Slep, Dalton Trans. 46 (2017) 16058–16064, https://doi.org/10.1039/c7dt03142d.
[45] C.D.S. Silva, I.A. Paz, F.D. Abreu, A.P. de Sousa, C.P. Verissimo, N.R.F. Nascimento, T.F. Paulo, D. Zampieri, M.N. Eberlin, A.C.S. Gondim, L.C. Andrade, I.M.M. Carvalho, E.H.S. Sousa, L.G.F. Lopes, J. Inorg. Biochem. 182 (2018) 83–91, https://doi.org/10.1016/j.jinorgbio.2018.02.005.
[46] P.C. Ford, J. Bourassa, K. Miranda, B. Lee, I. Lorkovic, S. Boggs, S. Kudo, L. Laverman, Coord. Chem. Rev. 171 (1998) 185–202, https://doi.org/10.1016/s0010-8545(98)90031-5.
[47] C.F. Works, C.J. Jocher, G.D. Bart, X. Bu, P.C. Ford, Inorg. Chem. 41 (2002) 3728–3739, https://doi.org/10.1021/ic020248k.
[48] A.A. Eroy-Reveles, Y. Leung, C.M. Beavers, M.M. Olmstead, P.K. Mascharak, J. Am. Chem. Soc. 130 (2008) 4447–4458, https://doi.org/10.1021/ja710265j.
[49] R. Kumar, S. Kumar, M. Bala, A. Ratnam, U.P. Singh, K. Ghosh, J. Organomet. Chem. 863 (2018) 77–83, https://doi.org/10.1016/j.jorganchem.2018.02.010.
[50] N.A. Sanina, R.A. Manzhos, N.S. Emel'yanova, N.E. Kupchinskaya, A.G. Krivenko, S.M. Aldoshin, J. Mol. Struct. 1181 (2019) 253–260, https://doi.org/10.1016/j.molstruc.2018.12.112.
[51] A.C. Roveda Jr., W.G. Santos, M.L. Souza, C.N. Adelson, F.S. Goncalves, E.E. Castellano, C. Garino, D.W. Franco, D.R. Cardoso, Dalton Trans. 48 (2019) 10812–10823, https://doi.org/10.1039/c9dt01432b.
[52] I. Sasaki, S. Amabilino, S. Mallet-Ladeira, M. Tassé, A. Sournia-Saquet, P.G. Lacroix, I. Malfant, New J. Chem. 43 (2019) 11241–11250, https://doi.org/10.1039/c9nj02398d.
[53] C.K. Chiang, K.T. Chu, C.C. Lin, S.R. Xie, Y.C. Liu, S. Demeshko, G.H. Lee, F. Meyer, M.L. Tsai, M.H. Chiang, C.M. Lee, J. Am. Chem. Soc. 142 (2020) 8649–8661, https://doi.org/10.1021/jacs.9b13837.
[54] P.M. Silva Filho, I.A. Paz, N.R.F. Nascimento, C.F. Santos, V.R. Araujo, C.P. Aquino, T.S. Ribeiro, I.F. Vasconcelos, L.G.F. Lopes, E.H.S. Sousa, E. Longhinotti, Mol. Pharm. 16 (2019) 2912–2921, https://doi.org/10.1021/acs.molpharmaceut.9b00110.
[55] B.J. Heilman, J. St John, S.R. Oliver, P.K. Mascharak, J. Am. Chem. Soc. 134 (2012) 11573–11582, https://doi.org/10.1021/ja3022736.
[56] Y.H. Li, M. Guo, S.W. Shi, Q.L. Zhang, S.P. Yang, J.G. Liu, J. Mater. Chem. B 5 (2017) 7831–7838, https://doi.org/10.1039/c7tb02059g.
[57] A.S. Leitão Jr., R.M. Campos, J.B.G Cerqueira, M.C. Fonteles, C.F. Santos, G. Nucci, E.H.S Sousa, L.G.F Lopes, L.F. Gonzaga-Silva, N.R.F Nascimento, Int. J. Impot. Res. 28 (2016) 20–24, https://doi.org/10.1038/ijir.2015.27.
[58] M.W.S. Campelo, R.B. Oria, L.G.F. Lopes, G.A.C. Brito, A.A. Santos, R.C. Vasconcelos, F.O.N. Silva, B.N. Nobrega, M.T. Bento-Silva, P.R.L. Vasconcelos, Neurochem. Res. 37 (2012) 749–758, https://doi.org/10.1007/s11064-011-0669-x.
[59] A.C. Rossaneis, D.T. Longhi-Balbinot, M.M. Bertozzi, V. Fattori, C.Z. Segato-Vendrameto, S. Badaro-Garcia, T.H. Zaninelli, L. Staurengo-Ferrari, S.M. Borghi, T.T. Carvalho, A.J.C. Bussmann, F.S. Gouveia Jr., L.G.F. Lopes, R. Casagrande, W.A. Verri Jr., Front. Pharmacol. 10 (2019) 229, https://doi.org/10.3389/fphar.2019.00229.
[60] N.R.F. Nascimento, F.L.N. Aguiar, C.F. Santos, A.M.L. Costa, D.J. Hardoim, K.S. Calabrese, F. Almeida-Souza, E.H.S. Sousa, L.G.F. Lopes, M.J. Teixeira, V.S. Pereira, R.S.N. Brilhante, M.F.G. Rocha, Acta Trop. 192 (2019) 61–65, https://doi.org/10.1016/j.actatropica.2019.01.021.
[61] J.J.N. Silva, P.M.M. Guedes, A. Zottis, T.L. Balliano, F.O.N. Silva, L.G.F. Lopes, J. Ellena, G. Oliva, A.D. Andricopulo, D.W. Franco, J.S. Silva, Br. J. Pharmacol. 160 (2010) 260–269, https://doi.org/10.1111/j.1476-5381.2010.00576.x.
[62] A.P.M. Santana, B.M. Tavares, L.T. Lucetti, F.S. Gouveia Jr., R.A. Ribeiro, P.M.G. Soares, E.H.S. Sousa, L.G.F. Lopes, J.V.R. Medeiros, M.H.L.P. Souza, Nitric Oxide 45 (2015) 35–42, https://doi.org/10.1016/j.niox.2015.02.002.
[63] L. Staurengo-Ferrari, S.S. Mizokami, J.J. Silva, F.O.N. Silva, E.H.S. Sousa, L.G.F. Lopes, M.L. Matuoka, S.R. Georgetti, M.M. Baracat, R. Casagrande, W.R. Pavanelli, W.A. Verri Jr., Pharmacol. Biochem. Behav. 105 (2013) 157–165, https://doi.org/10.1016/j.pbb.2013.02.006.
[64] W.R. Pavanelli, J.J.N. Silva, C. Panis, T.M. Cunha, I.C. Costa, M.C.N.D. Menezes, F.J.A. Oliveira, L.G.F. Lopes, R. Cecchini, F.Q. Cunha, M.A.E. Watanabe, E.N. Itano, Mycopathologia 172 (2011) 95–107, https://doi.org/10.1007/s11046-011-9416-8.
[65] E.H.S. Sousa, L.A. Ridnour, F.S. Gouveia Jr., C.D.S. Silva, D.A. Wink, L.G.F. Lopes,

P.J. Sadler, ACS Chem. Biol. 11 (2016) 2057–2065, https://doi.org/10.1021/acschembio.6b00222.
[66] D. Michael, P. Mingos, Nitrosyl Complexes in Inorganic Chemistry, Biochemistry and Medicine I, Springer, Berlin, Heidelberg, 2014.
[67] A.K.M. Holanda, F.O.N. da Silva, I.M.M. Carvalho, A.A. Batista, J. Ellena, E.E. Castellano, Í.S. Moreira, L.G.F. Lopes, Polyhedron 26 (2007) 4653–4658, https://doi.org/10.1016/j.poly.2007.05.036.
[68] M.P. Gamcsik, M.S. Kasibhatla, S.D. Teeter, O.M. Colvin, Biomarkers 17 (2012) 671–691, https://doi.org/10.3109/1354750X.2012.715672.
[69] P.K. Chan, C.K. Poon, J. Chem. Soc. Dalton Trans. 0 (1976) 858–862, https://doi.org/10.1039/DT9760000858.
[70] F. Jensen, Introduction to computational chemistry, 2nd ed., John Wiley & Sons, UK, 2007.
[71] P.J. Hay, W.R. Wadt, J. Chem. Phys. 82 (1985) 299–310, https://doi.org/10.1063/1.448975.
[72] C. Rong, S. Lian, D. Yin, B. Shen, A. Zhong, L. Bartolotti, S. Liu, J. Chem. Phys. 125 (2006) 1–7, https://doi.org/10.1063/1.2378830.
[73] W.R. Wadt, P.J. Hay, J. Chem. Phys. 82 (1985) 284–298, https://doi.org/10.1063/1.448800.
[74] G. Frenking, W. Koch, J. Chem. Phys. 84 (1986) 3224–3229, https://doi.org/10.1063/1.450832.
[75] A.L. Miguel, Neepa T. Marques, Maitra Fernando M.S., Nogueira Eberhard K.U., Gross, Angel Rubio, Fundamentals of Time-Dependent Density Functional Theory, Springer, Berlin, Heidelberg, 2012.
[76] T. Lu, F. Chen, J. Comput. Chem. 33 (2012) 580–592, https://doi.org/10.1002/jcc.22885.
[77] N.M. O'Boyle, A.L. Tenderholt, K.M. Langner, J. Comput. Chem. 29 (2008) 839–845, https://doi.org/10.1002/jcc.20823.
[78] R.G. Aga, M.N. Hughes, E. Inc (Ed.), Methods in Enzymology, 436 2008, pp. 35–48, , https://doi.org/10.1016/S0076-6879(08)36003-0.
[79] A. Castro-Forero, D. Jiménez, J. López-Garriga, M. Torres-Lugo, J. Appl. Polym. Sci. 107 (2008) 881–890, https://doi.org/10.1002/app.26289.
[80] C.K. Poon, W.M. Andrew, Inorg. Chem. 18 (1979) 1277–1283, https://doi.org/10.1021/ic50195a021.
[81] N.S. Bryan, M.B. Grisham, Free Radic. Biol. Med. 43 (2007) 645–657, https://doi.org/10.1016/j.freeradbiomed.2007.04.026.
[82] S. Amabilino, M. Tasse, P.G. Lacroix, S. Mallet-Ladeira, V. Pimienta, J. Akl, I. Sasaki, I. Malfant, New J. Chem. 41 (2017) 7371–7383, https://doi.org/10.1039/c7nj00866j.
[83] K. Ghosh, R. Kumar, K. Kumar, A. Ratnam, U.P. Singh, RSC Adv. 4 (2014) 43599–43605, https://doi.org/10.1039/c4ra04767b.
[84] N. Hogg, Free Radic. Biol. Med. 49 (2010) 122–129, https://doi.org/10.1016/j.freeradbiomed.2010.03.009.
[85] E. Orlowska, M.V. Babak, O. Dömötör, E.A. Enyedy, P. Rapta, M. Zalibera, L. Bučinský, M. Malček, C. Govind, V. Karunakaran, Y.C.S. Farid, T.E. McDonnell, D. Luneau, D. Schaniel, W.H. Ang, V.B. Arion, Inorg. Chem. 57 (2018) 10702–10717, https://doi.org/10.1021/acs.inorgchem.8b01341.
[86] U. Samuni, Y. Samuni, S. Goldstein, J. Am. Chem. Soc. 132 (2010) 8428–8432, https://doi.org/10.1021/ja101945j.
[87] T. Akaike, M. Yoshida, Y. Miyamoto, K. Sato, M. Kohno, K. Sasamoto, K. Miyazaki, S. Ueda, H. Maeda, Biochemistry 32 (1993) 827–832, https://doi.org/10.1021/bi00054a013.
[88] A.A. Bobko, V.V. Khramtsov, Nitric Oxide 40 (2014) 92–98, https://doi.org/10.1016/j.niox.2014.05.013.
[89] E. Tfouni, M. Krieger, B.R. McGarvey, D.W. Franco, Coord. Chem. Rev. 236 (2003) 57–69, https://doi.org/10.1016/S0010-8545(02)00177-7.
[90] A.A. Bobko, A. Ivanov, V.V. Khramtsov, Free Radic. Biol. Med. 47 (2013) 74–81, https://doi.org/10.3109/10715762.2012.746460.
[91] M.A. Rhine, B.C. Sanders, A.K. Patra, T.C. Harrop, Inorg. Chem. 54 (2015) 9351–9366, https://doi.org/10.1021/acs.inorgchem.5b00883.
[92] F. Roncaroli, J.A. Olabe, Inorg. Chem. 44 (2005) 4719–4727, https://doi.org/10.1021/ic048156d.
[93] J.N. Bates, M.T. Baker, R. Guerra, D.G. Harrison, Biochem. Pharmacol. 42 (1991) S157–S165, https://doi.org/10.1016/0006-2952(91)90406-U.
[94] H.J. Sun, W.T. Lee, B. Leng, Z.Y. Wu, Y. Yang, J.S. Bian, Antioxid. Redox Signal. 32 (2020) 331–349, https://doi.org/10.1089/ars.2019.7904.
[95] E. Metzen, J. Zhou, W. Jelkmann, J. Fandrey, B. Brüne, Mol. Biol. Cell 14 (2003) 3470–3481, https://doi.org/10.1091/mbc.e02-12-0791.
[96] R. Chowdhury, L.C. Godoy, A. Thiantanawat, L.J. Trudel, W.M. Deen, G.N. Wogan, Chem. Res. Toxicol. 25 (2012) 2194–2202, https://doi.org/10.1021/tx300274a.
[97] Y. Ikeda, S. Tajima, S. Yoshida, N. Yamano, Y. Kihira, K. Ishizawa, K. Aihara, S. Tomita, K. Tsuchiya, T. Tamaki, Atherosclerosis 215 (2011) 339–347, https://doi.org/10.1016/j.atherosclerosis.2011.01.009.
[98] V.I. Holden, S. Lenio, R. Kuick, S.K. Ramakrishnan, Y.M. Shah, M.A. Bachman, Infect. Immun. 82 (2014) 3826–3836, https://doi.org/10.1128/IAI.01849-14.
[99] V.P. Mokh, A.P. Poltorakov, V.A. Serezhenkov, A.F. Vanin, Nitric Oxide 22 (2010) 266–274, https://doi.org/10.1016/j.niox.2010.01.002.
[100] E.I. Chazov, O.V. Rodnenkov, A.V. Zorin, V.L. Lakomkin, V.V. Gramovich, O.N. Vyborov, A.G. Dragnev, A.A. Timoshin, L.I. Buryachkovskaya, A.A. Abramov, V.P. Massenko, E.V. Arzamastsev, V.I. Kapelko, A.F. Vanin, Nitric Oxide 26 (2012) 148–156, https://doi.org/10.1016/j.niox.2012.01.008.
[101] H.Y. Hsiao, C.W. Chung, J.H. Santos, O.B. Villaflores, T.T. Lu, Dalton Trans. 48 (2019) 9431–9453, https://doi.org/10.1039/c9dt00777f.
[102] S. Ikeda, J.F. Schweiss, P.A. Frank, S.M. Homan, Anesthesiology 66 (1987) 381–385.
[103] S. Huerta, S. Chilka, B. Bonavida, Int. J. Oncol. 33 (2008) 909–927, https://doi.org/10.3892/ijo_00000079.
[104] J. Zhao, S. Gou, Y. Sun, R. Yin, Z. Wang, Chem. Eur. J. 18 (2012) 14276–14281, https://doi.org/10.1002/chem.201201605.
[105] W.W. Overwijk, N.P Restifo, Current Protocols in Immunology Chapter 20, pp. Unit-20.1.1-20.1.29 (2001), https://doi.org/10.1002/0471142735.im2001s39.
[106] H.L. Lu, F. Liao, J. Immunol. 191 (2013) 3264–3276, https://doi.org/10.4049/jimmunol.1300512.
[107] D.R. Lang, J.A. Davis, L.G.F. Lopes, A.A. Ferro, L.C.G. Vasconcellos, D.W. Franco, E. Tfouni, A. Wieraszko, M.J. Clarke, Inorg. Chem. 39 (2000) 2294–2300, https://doi.org/10.1021/ic9912979.
[108] M.L. Souza, A.C. Roveda Jr., J.C.M. Pereira, D.W. Franco, Coord. Chem. Rev. 306 (2016) 615–627, https://doi.org/10.1016/j.ccr.2015.03.008.

3.4 Supporting information

3.4.1 DFT studies (Results and discussion)

The structural and electronic properties of *trans*-[Fe(cyclam)(NO)Cl]$^{2+}$ complex (1) were investigated using density functional theory (DFT) and time-dependent DFT (TD-DFT). Electronic transitions contributions were subsequently determined, which were used to guide interpretation of UV-Vis electronic absorption spectrum and photochemical processes. The optimized geometry of **1** obtained by DFT was compared with experimental data (Fig. S1 and Table S1).[1]

Figure S1 - DFT optimized structure of the complex *trans*-[Fe(cyclam)(Cl)(NO)]$^{2+}$.

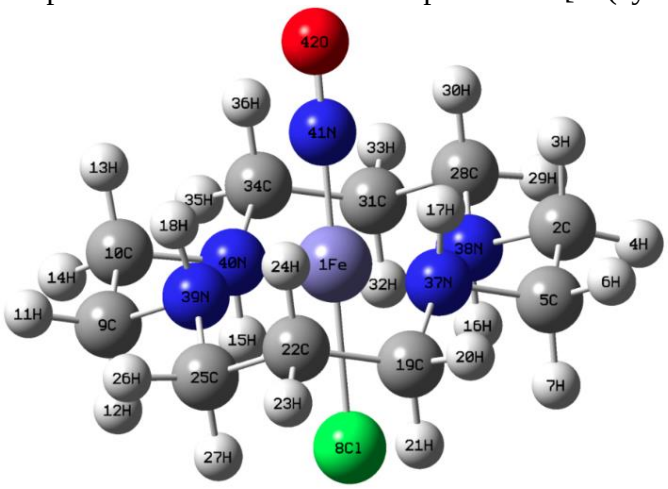

Reference: Elaborated by the author.

Table S1 - Bond lengths (Å) and angles (°) of the *trans*-[Fe(cyclam)(NO)Cl]Cl_2: experimental and optimized.

	Experimental	**Optimized**	**Deviation (±)**
Bond lengths (Å)			
Fe–N(1)	1.682(3)	1.648	0.017
Fe–N(2)	2.012(3)	2.057	0.023
Fe–N(3)	2.009(3)	2.058	0.025
Fe–N(4)	1.999(3)	2.029	0.015
Fe–N(5)	2.006(3)	2.029	0.012
Fe–Cl(1)	2.248(1)	2.305	0.029
O(1)–N(1)	1.091(4)	1.135	0.022
N(2)–C(1)	1.482(5)	1.495	0.007
N(2)–C(10)	1.487(5)	1.495	0.004
N(3)–C(3)	1.484(5)	1.495	0.006
N(3)–C(4)	1.487(5)	1.495	0.004
N(4)–C(6)	1.485(5)	1.491	0.003
N(4)–C(5)	1.491(5)	1.492	0.001
N(5)–C(9)	1.476(5)	1.492	0.008

Table S1. *Continuation.*

	Experimental	Optimized	Deviation (±)
Bond lengths (Å)			
N(5)–C(8)	1.484(5)	1.491	0.004
C(1)–C(2)	1.516(6)	1.527	0.006
C(2)–C(3)	1.522(6)	1.527	0.003
C(4)–C(5)	1.493(6)	1.519	0.013
C(6)–C(7)	1.519(6)	1.528	0.009
C(7)–C(8)	1.510(6)	1.528	0.009
C(9)–C(10)	1.498(5)	1.519	0.011
Bond Angle (°)			
N(1)–Fe–Cl(1)	178.63(11)	178.44	0.10
N(1)–Fe–N(2)	91.53(13)	92.45	0.46
N(1)–Fe–N(5)	91.40(14)	93.42	1.01
N(2)–Fe–Cl(1)	88.44(9)	88.62	0.09
N(3)–Fe–Cl(1)	87.94(10)	88.60	0.33
N(3)–Fe–N(2)	95.36(13)	95.08	0.14
N(4)–Fe–Cl(1)	86.50(10)	85.61	0.45
N(4)–Fe–N(2)	174.80(12)	174.19	0.31
N(4)–Fe–N(3)	85.61(13)	85.45	0.08
N(4)–Fe–N(5)	93.41(13)	93.38	0.02
N(5)–Fe–N(3)	175.13(13)	174.08	0.53
N(5)–Fe–N(2)	85.20(12)	85.50	0.15
N(5)–Fe–Cl(1)	87.24(9)	85.52	0.86
O(1)–N(1)–Fe	177.4(3)	179.3	0.95
C(1)–N(2)–Fe	118.9(3)	117.6	0.65
C(10)–N(2)–Fe	107.6(2)	107.2	0.20
C(1)–N(2)–C(10)	112.5(3)	112.6	0.05
C(3)–N(3)–Fe	119.0(3)	117.7	0.65
C(4)–N(3)–Fe	107.7(2)	107.1	0.30
N(1)–Fe–N(3)	93.43(14)	92.44	0.50
N(1)–Fe–N(4)	93.51(13)	93.31	0.10
C(3)–N(3)–C(4)	112.7(3)	112.7	0
C(5)–N(4)–Fe	107.8(2)	107.8	0.0
C(6)–N(4)–Fe	117.4(2)	117.8	0.20
C(6)–N(4)–C(5)	112.5(3)	113.6	0.55
C(8)–N(5)–Fe	117.2(2)	117.9	0.35
C(9)–N(5)–Fe	107.9(2)	107.7	0.10
C(9)–N(5)–C(8)	112.9(3)	113.5	0.30
N(2)–C(1)–C(2)	112.0(3)	112.4	0.20
C(1)–C(2)–C(3)	113.8(3)	114.5	0.35
N(3)–C(3)–C(2)	112.8(3)	112.7	0.05
N(3)–C(4)–C(5)	108.0(3)	108.6	0.30
N(4)–C(5)–C(4)	108.0(3)	108.2	0.10
N(4)–C(6)–C(7)	111.3(3)	112.4	0.55
C(8)–C(7)–C(6)	115.0(3)	115.4	0.20
N(5)–C(8)–C(7)	112.6(3)	112.6	0
N(5)–C(9)–C(10)	107.7(3)	108.2	0.25
N(2)–C(10)–C(9)	107.7(3)	108.8	0.55

Reference: Elaborated by the author.

The computed geometrical parameters of such complex are in excellent agreement with crystallographic data obtained by single crystal X-ray diffraction. Interestingly, a Fe-N-O angle of 179.3° calculated by DFT was very close to 177.4° found by X-ray data. This value indicated nitrosyl ligand primarily exhibits major NO^+ character as previously reported.[2] Additionally, a plane containing O-N-Fe-Cl is not perfectly perpendicular to the one containing the nitrogen atoms of the cyclam ligand. This distortion occurs due to interactions of the hydrogens of cyclam with axial ligands.[1]

A comparison of experimental and theoretical electronic spectra of **1** is shown in supporting Fig. S2, where satisfactory agreement was observed. These calculations provided support of assigned electronic transitions based on the character of the molecular orbitals involved in this process (see Tables S2 and Fig. S3-S4).

Figure S2 - Experimental (—), theoretical (---) electronic spectra of the *trans*-[Fe(cyclam)(NO)Cl]$^{2+}$ complex ion in water and vertical electronic transitions calculated by TD-DFT (—).

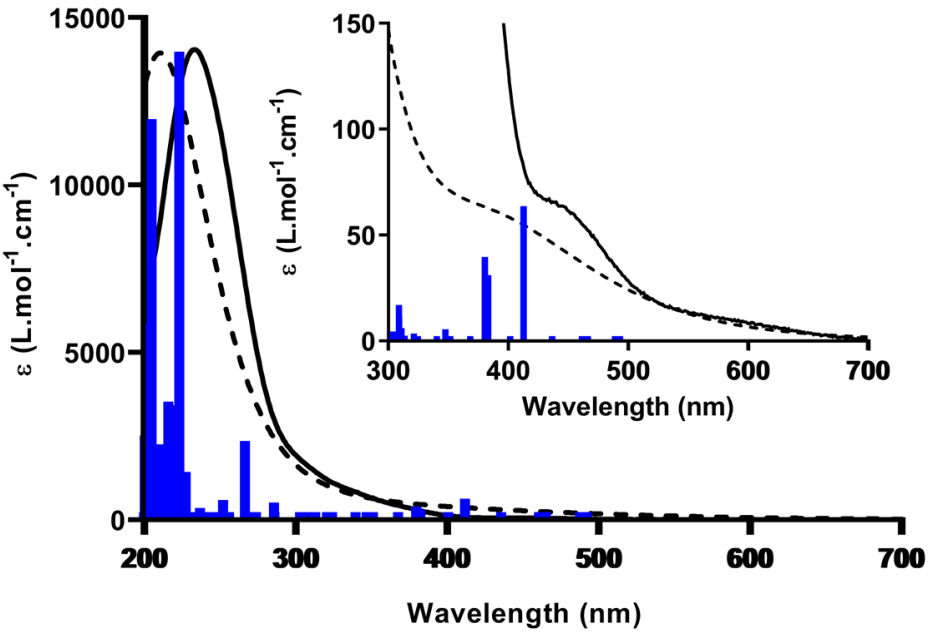

Reference: Elaborated by the author.

Table S2 - Selected electronic transitions of the *trans*-[Fe(cyclam)(NO)Cl]$^{2+}$ obtained by TD-DFT and experimentally measured in water.

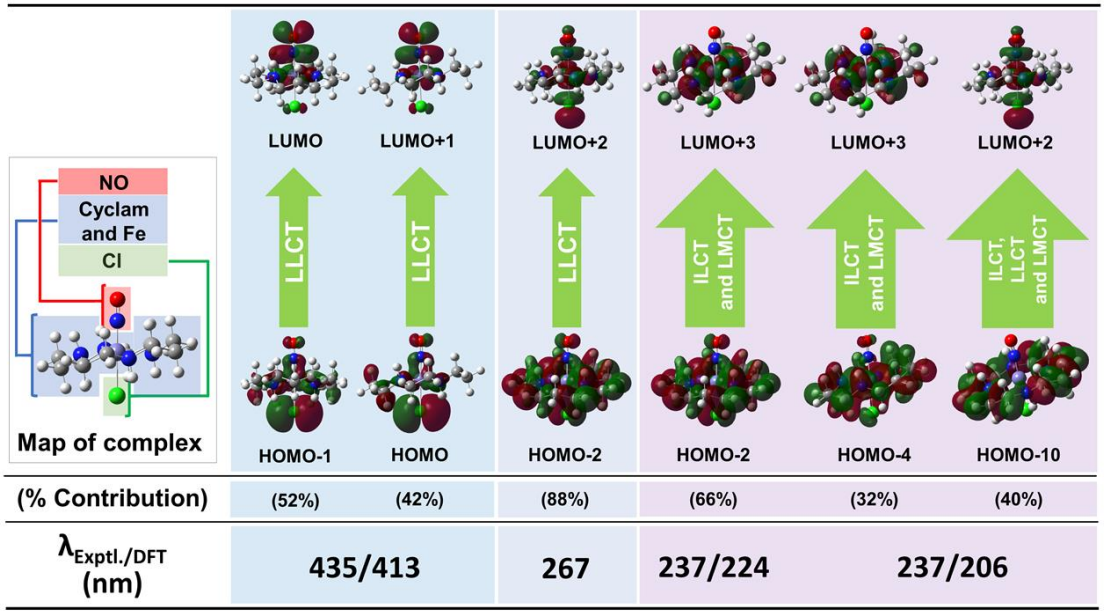

LLCT = ligand-to-ligand-charge-transfer transition; ILCT = intraligand-charge-transfer transition; ligand-metal charge transfer (LMCT).

Reference: Elaborated by the author.

Figure S3 - Molecular orbitals involved in the main electronic transitions of *trans*-[Fe(cyclam)(Cl)(NO)]$^{2+}$.

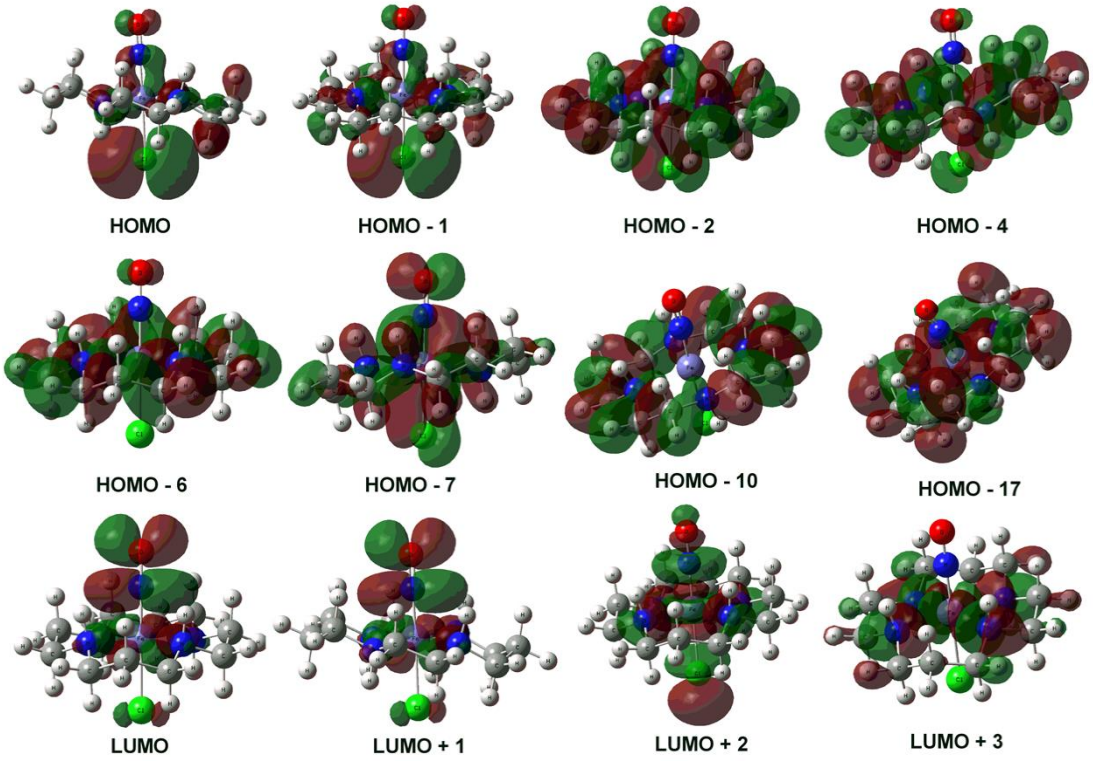

Reference: Elaborated by the author.

Figure S4 - Percent contributions of selected molecular orbitals of *trans*-[Fe(cyclam)(Cl)(NO)]$^{2+}$.

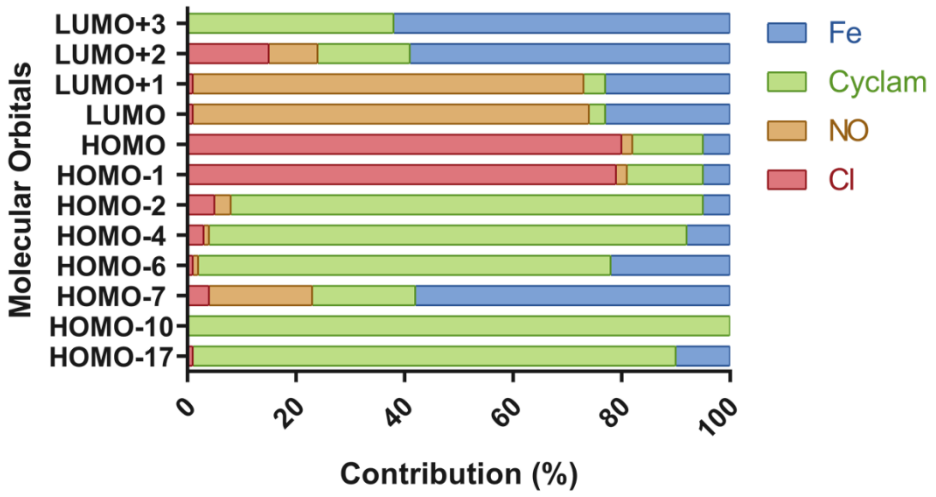

Reference: Elaborated by the author.

Interestingly, the very low-intensity band at 435 nm resulted mainly from isoenergetic transitions originating from the highest occupied molecular orbitals (HOMO and HOMO-1) centered mainly on Cl^- ligand to the lowest unoccupied molecular orbitals (LUMO and LUMO+2) associated primarily with the $NO^\bullet$ moiety (π^*(NO)) (see Fig. S2 and S3). Considering the participation of these relevant MO, this absorption band can be assigned mainly as a ligand-to-ligand charge transfer (LLCT). The most intense band at 237 nm is associated with the transitions (HOMO-2 → LUMO+3 and HOMO-4 → LUMO+3). HOMO-2 and HOMO-4 are centered on the cyclam ligand while LUMO+3 is centered on σ-antibonding p(cyclam)-d(Fe) MO, which characterizes this transition as an intraligant charge transfer (ILCT). The latter has further contribution of the transition from HOMO-10 also centered on cyclam to LUMO-2 delocalized over the entire complex ion (σ-antibonding d(Ru)-p(all ligands) MO), this transition presents an mixture of ILCT and LLCT.

We did not have observed any metal-to-ligand charge transfer (MLCT) transitions, which are expected to nitrosyl Fe^{II} complexes. This can be explained by the very strong π-acceptor bonding of NO^+, which may stabilize significantly the iron-based orbitals. This supports the hypothesis that the character of Fe^{III} is very expressive in a NO^+ complex.

3.4.2 Thermal stability

Figure S5 - Electronic spectra of aqueous solution of Griess reagent (50 mM) and *trans*-$[Fe(cyclam)Cl_2]^{2+}$ (2 mM) after 24 hours in water at 37 ºC, under aerobic conditions.

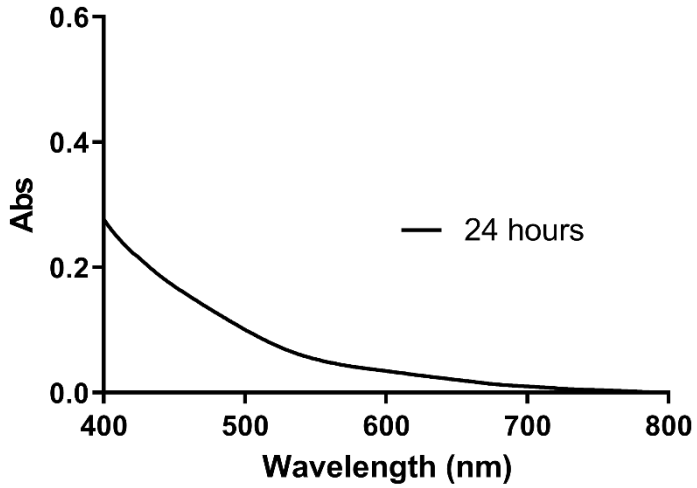

Reference: Elaborated by the author.

3.4.3 Photorelease of NO•

Figure S6 - Probing the photorelease of NO•/HNO. Spectroscopic changes of a mixture of cPTIO (100 μM), complex *trans*-$[Fe(cyclam)(NO)Cl]^{2+}$ (200 μM) in 0.1 M phosphate buffer pH 7.4 solution, containing DTPA (100 μM), during light irradiation at 365 nm for 20 min, at room temperature (ca. 25 ºC) and aerobic conditions. Inset: kinetic curves at 560 nm (first order equation fit, k_{obs} = 379.3 x 10^{-3} min^{-1}, R^2 = 0.9967).

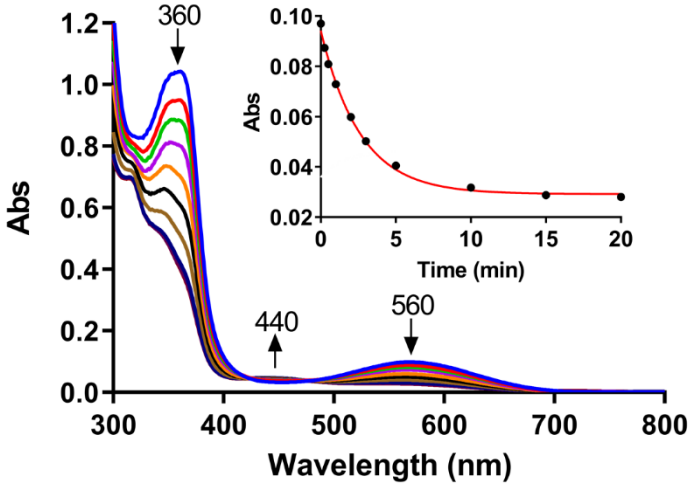

Reference: Elaborated by the author.

Figure S7 - Electronic spectra of cPTIO (—), cPTI (—) (resulted of cPTIO in reaction with NO•, from a NO• saturated solution), cPTIO-H (—) (resulted of cPTIO in reaction with HNO by using Angeli's salt (200 μM)), *trans*-[Fe(cyclam)(NO)Cl]$^{2+}$ (—) (200 μM) after 30 min of light irradiation at 365 nm and cPTIO (—) after 30 min of light irradiation at 365 nm. All electronic spectra were obtained in 0.1 M phosphate buffer pH 7.4 solution at 37 ºC, under aerobic conditions. The concentration of cPTIO used in all assays was 100 μM.

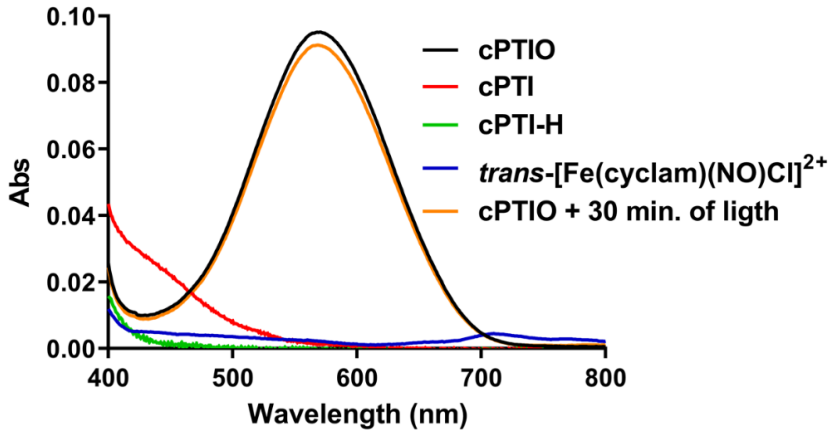

Reference: Elaborated by the author.

Figure S8 - EPR monitoring of the reaction of *trans*-[Fe(cyclam)(NO)Cl]$^{2+}$ (400 µM) with light (365 nm) using cPTIO (200 µM) as probe, in 0.1 M phosphate buffer pH 7.4 solution at 25 ºC. A. Reaction in the presence of light (365 nm) without complex. B. Reaction with complex in absence of light. C. Reaction of *trans*-[Fe(cyclam)Cl_2]$^+$ (400 µM) with cPTIO (200 µM) in absence of light, 0.1 M phosphate buffer pH 7.4 solution at 25 ºC. All spectra were measured under aerobic conditions.

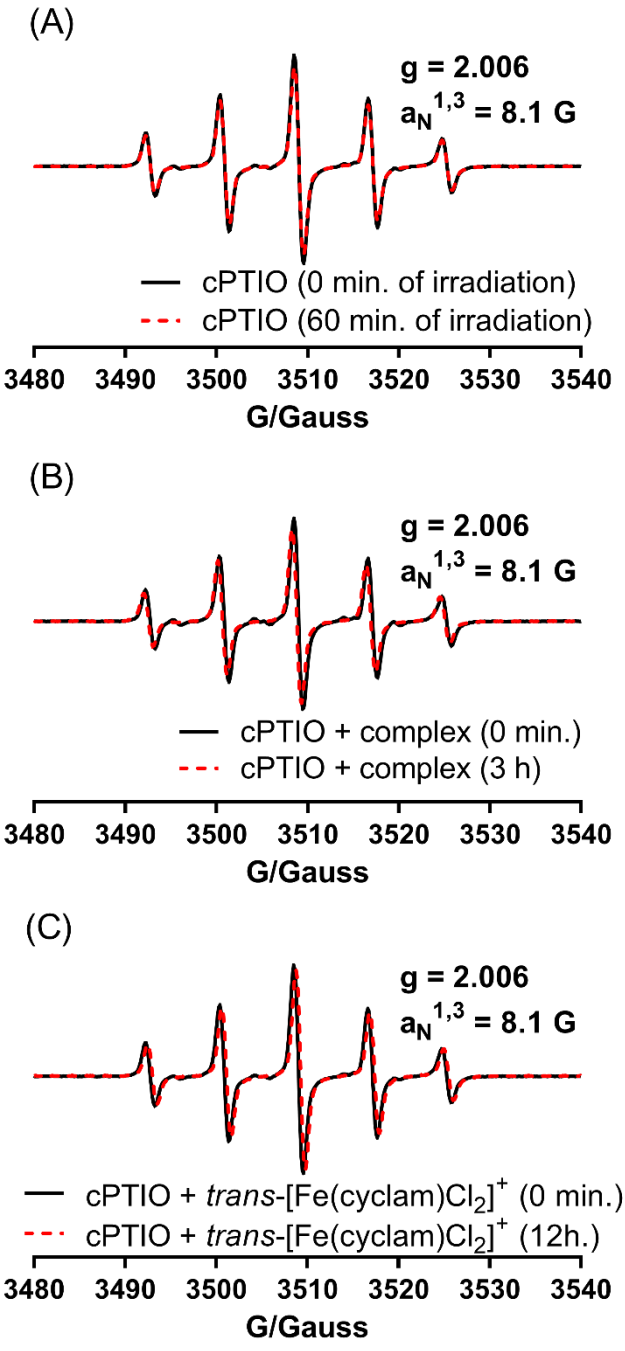

Reference: Elaborated by the author.

Figure S9 – Electronic spectra of aqueous solution of Griess reagent (50 mM) and *trans*-[Fe(cyclam)(NO)Cl]$^{2+}$ (2 mM) before irradiation (gray), with 15 min of irradiation (λ_{irrd} = 365 nm) (black) and 15 min without irradiation (dotted) at room temperature (ca. 25 ºC), under aerobic conditions. Inset: Solution before and after irradiation.

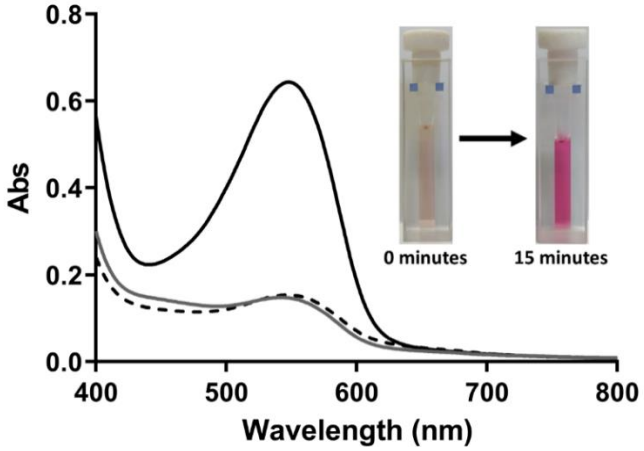

Reference: Elaborated by the author.

3.4.4 Reaction with glutathione

Figure S10 - Investigation of the reaction of *trans*-[Fe(cyclam)(NO)(Cl)]$^{2+}$ (10 mM) with glutathione (GSH, 100 mM) in 0.1 M phosphate buffer pH 7.4 solution monitored by FTIR-ATR at 25 ºC, under aerobic conditions. Phosphate buffer (—), GSH (—), complex *trans*-[Fe(cyclam)(NO)(Cl)]$^{2+}$ (—) and mixture containing the complex and GSH after 5 min of reaction (—).

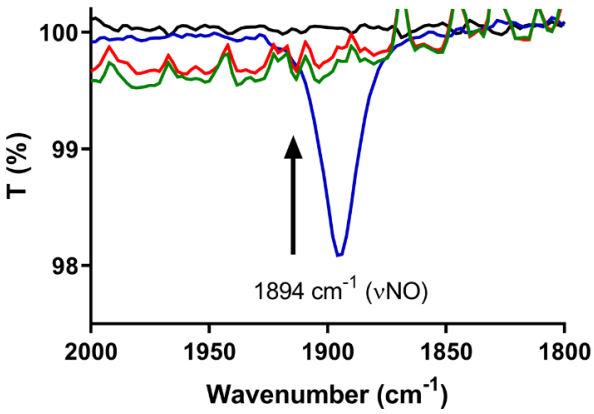

Reference: Elaborated by the author.

Figure S11 - EPR monitoring of the reaction of GSH (4 mM), cPTIO (200 µM), containing DTPA (400 µM) at 25 ºC, under aerobic conditions. All spectra were recorded during 18 min at intervals of ca. 10 seconds.

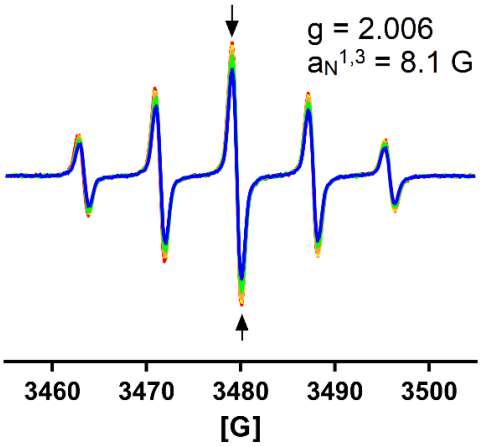

Reference: Elaborated by the author.

3.4.5 Cytotoxicity

Figure S12 - Cell viability curves (%) vs. concentration (µM) of the complex *trans*-$[Fe(cyclam)(NO)Cl]^{2+}$ to a cell line (A) B16-F10 (mouse melanoma, IC_{50} = 202.7 µM. R^2 = 0.9994) and (B) HUH-7 (human hepatocarcinoma, IC_{50} = 142.9 µM. R^2 = 0.9965).

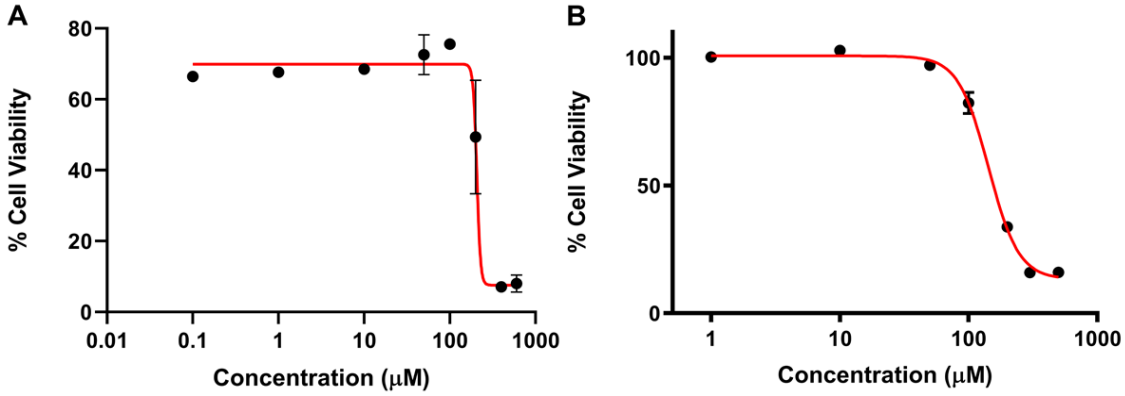

Reference: Elaborated by the author.

Abbreviations

ATR	Attenuated total reflectance
cPTIO	2-(4-carboxyphenyl)-4,4,5,5-tetramethylimidazoline-1-oxyl-3-oxide potassium salt
Cyclam	1,4,8,11-tetraazacyclotetradecane
DFT	Density functional theory
DTPA	Diethylenetriaminepentaacetic acid

EPR	Electron paramagnetic resonance
GSH	Glutathione
HNO	Nitroxyl
HOMO	Highest occupied molecular orbital
IC	Cell viability
ILCT	Intraligand-charge-transfer transition
LLCT	Ligand-to-ligand charge-transfer
LMCT	Ligand-metal charge transfer
LUMO	Lowest unoccupied molecular orbital
Mb-Fe^{3+}	met-Myoglobin
MLCT	Metal-to-ligand charge-transfer
MO	Molecular orbital
$NO^{\bullet}$	Nitric oxide
TD-DFT	Time-dependent DFT

Reference

1. HOLANDA, A. K. M.; SILVA, F. O. N.; CARVALHO, I. M. M.; BATISTA, A. A.; ELLENA, J.; CASTELLANO, E. E.; MOREIRA, Í. S.; LOPES, L. G. F. Crystal structure, electrochemical and photochemical studies of the *trans*-[Fe(cyclam)(NO)Cl]Cl_2 complex (cyclam=1,4,8,11-tetraazacyclotetradecane). **Polyhedron**, v. 26, p. 4653-4658, 2007.

2. DZIĘGIELEWSKI, J. O.; MACHURA, B. The x-ray crystal structure of [Re(NO)(Ph)Br_3(PPh_3)] complex. **Polyhedron**, v. 15, p. 3713–3716, 1996.

3.5 Unpublished results associated with the article

Besides the results presented in article 1, some other studies were performed aiming at HNO detection from the *trans*-[Fe(cyclam)(NO)Cl]$^{2+}$ in thermal- and photo-decomposition conditions by using metmyoglobin (Mb-Fe^{III}) as a probe. The stability of the iron complexes (*trans*-[Fe(cyclam)(NO)Cl]$^{2+}$ and *trans*-[Fe(cyclam)Cl_2]$^{+}$), in the presence of the chelating pentetic acid (DTPA), were also carried out. Finally, the photostability of the nitrosyl complex *trans*-[Fe(cyclam)(NO)Cl]Cl_2, in the solid state, was tested as well. These results are described and discussed below.

3.5.1 Experimental section

Thermal- and photo- stability of the trans-[Fe(cyclam)(NO)Cl]$^{2+}$ in the presence of metmyoglobin (Mb-Fe^{III})

The thermal stability of the *trans*-[Fe(cyclam)(NO)Cl]$^{2+}$ complex, in the presence of metmyoglobin (Mb-Fe^{III}), was monitored by UV–Vis spectroscopy for ca. 24 h at 37 ºC, using 134 μM of the nitrosyl complex and 6.7 μM of the Mb-Fe^{III} dissolved in 0.1 M phosphate buffer pH 7.4 solution, under anaerobic conditions. The solutions were prepared in an argon atmosphere with the aid of an inert gas glove box. This study was also performed with Angeli's salt (27 μM) and Mb-Fe^{III} (6.7 μM) for comparative purposes. The experiment with Angeli's salt was monitored for ca. 1 h at 37 ºC.

The study of NO/HNO photorelease was carried out using light irradiation at 365 nm and Mb-Fe^{III} as NO/HNO probe. The solution containing 4.6 μM of Mb-Fe^{III} and 100.0 μM of the nitrosyl complex was prepared in anaerobic phosphate buffer (0.1 M, pH 7.4), and monitored for 1.5 h at 37 ºC by absorption spectroscopy in UV-Vis region. This experiment was also prepared in an argon atmosphere with the aid of an inert gas glove box.

Thermal stability in the presence of pentetic acid (DTPA)

The stability of the nitrosyl complex in the presence of pentetic acid (DTPA), was studied by UV–Vis spectroscopy using a solution composed of *trans*-[Fe(cyclam)(NO)Cl]$^{2+}$ (2 mL at 50 μM) and of DTPA (2 mL at 75 μM), in 0.1 M phosphate buffer (pH 7.4). This study was also performed using a solution of *trans*-[Fe(cyclam)Cl_2]$^{+}$ complex (2 mL at 100 μM) and DTPA (2 mL at 150 μM), under the same conditions. The solutions of these complexes were prepared and monitored for ca. 4 h at 37 ºC under aerobic conditions.

Photodecomposition in solid state

The photostability of the nitrosyl complex, in solid state, was studied by FTIR using *trans*-[Fe(cyclam)(NO)Cl]Cl_2 salt, dispersed in KBr pellet, and irradiation at 365 nm. The study was monitored based upon the presence of the band at 1888 cm^{-1}, assigned to the ν(NO^{+}), measured over a period of 6 h under aerobic conditions.

3.5.2 Synthetic procedures

Precursor trans-[Fe(cyclam)Cl_2](PF$_6$) complex

A solution of *cis*-[Fe(cyclam)Cl_2]Cl (0.100 g, 0.214 mmol), in methanol/water (50%) was heated (80 ºC) and mixed for 30 min then a change of color from yellow to green

was observed. A saturated solution of NH_4PF_6 in methanol was added dropwise. The green solid formed was filtered, washed with ice-cold methanol, and dried by vacuum.

Yield = 40% (0.040 g), green solid. **IR** symmetric stretching (ν_s), symmetric bending (δ_s) and twisting (τ) (cm^{-1}): 3255 – 3208 (ν_s N-H), 2980 - 2925 (ν_s C-H), 1483 – 1430 (δ_s CH_2), 1331 – 1280 (τ CH_2), 1122 – 1020 (ν_s C-N), 835 and 561 (ν_s P-F). **UV-Vis** (H_2O) λ_{max}/nm ($\varepsilon/M^{-1}cm^{-1}$) = 238 (7635), 300, (2019), 355 (1096). **Cyclic voltammetry** in CF_3COOH/CF_3COONa solution 0.1 M (pH 3.2), V = 0.1 V s^{-1}: $E_{1/2}$ = 0.291 V *vs* NHE.

Nitrosyl trans-[Fe(cyclam)(NO)Cl]Cl_2 complex

To a solution of *cis*-[Fe(cyclam)Cl_2]Cl (0.100 g, 0.214 mmol), in degassed water (10 mL), it was bubbled NO gas for 60 min. The solution was concentrated by vacuum and, then, added dropwise to a mixture of ethanol/diethyl ether (70 mL, 1:1). The resulting yellow precipitate was kept overnight (16 h) at -20 ºC before it was collected by filtration, washed with ethanol/diethyl ether (1:1) ice-cold solution, and dried in a vacuum desiccator. CAUTION: since the complex is moderately light sensitive, it must be stored in a vacuum desiccator protected from light to extend their lifetime.

Yield = 80% (0.080 g), yellow white solid. **IR** symmetric stretching (ν_s), symmetric bending (δ_s) and twisting (τ) (cm^{-1}): 3092 (ν_s N-H), 3012 – 2857 (ν_s C-H), 1888 (ν_s NO), 1452 (δ_s CH_2), 1380 – 1290 (τ CH_2), 1100 – 1044 (ν_s C-N), 835 and 885 (τ N-H), 812 (τ CH_2). **UV-Vis** (H_2O) λ_{max}/nm ($\varepsilon/M^{-1}cm^{-1}$) = 232 (14025), 438, (66). **Cyclic voltammetry** in CF_3COOH/CF_3COONa solution 0.1 M (pH 3.2), V = 0.1 V s^{-1}: $E_{1/2}$ = 0.292 and 0.595 V *vs* NHE, E_{pa} = 0.905 V and E_{pc} = -0.375 V *vs* NHE.

3.5.3 Results and discussion

Thermal- and photo- stability of the trans-[Fe(cyclam)(NO)Cl]Cl_2 in the presence of metmyoglobin (Mb-Fe^{III})

Metmyoglobin (Mb-Fe^{III}) can be used as a probe for nitric oxide (NO) and nitroxyl (HNO) detection. While the reaction of Mb-Fe^{III} with HNO directly generates the NO-MbFe^{II} adduct, k = 2.7 x 10^5 M^{-1} s^{-1} (Scheme 16),[328] that of NO and Mb-Fe^{III} produces the NO-MbFe^{II} adduct via three steps; (i) formation of NO-MbFe^{III} adduct (unstable species), k = 5.3 x 10^4 M^{-1} s^{-1}, (ii) reaction between NO-MbFe^{III} and OH^- generating nitrite (NO_2^-) and Mb-Fe^{II}, k = 3.2 x 10^2 M^{-1} s^{-1}, (iii) and myoglobin (Mb-Fe^{II}) reaction with NO finally producing NO-MbFe^{II}, k = 1.7 x 10^7 M^{-1} s^{-1} (Scheme 16).[109, 329] Thus, the thermal- and photo-

stability of the ion *trans*-[Fe(cyclam)(NO)Cl]$^{2+}$ was studied in the presence of Mb-Fe^{III} aiming at the discrimination of NO and HNO.

Scheme 16 - Production of the NO-MbFe^{II} adduct through reacting with NO$^{\bullet}$ or HNO.

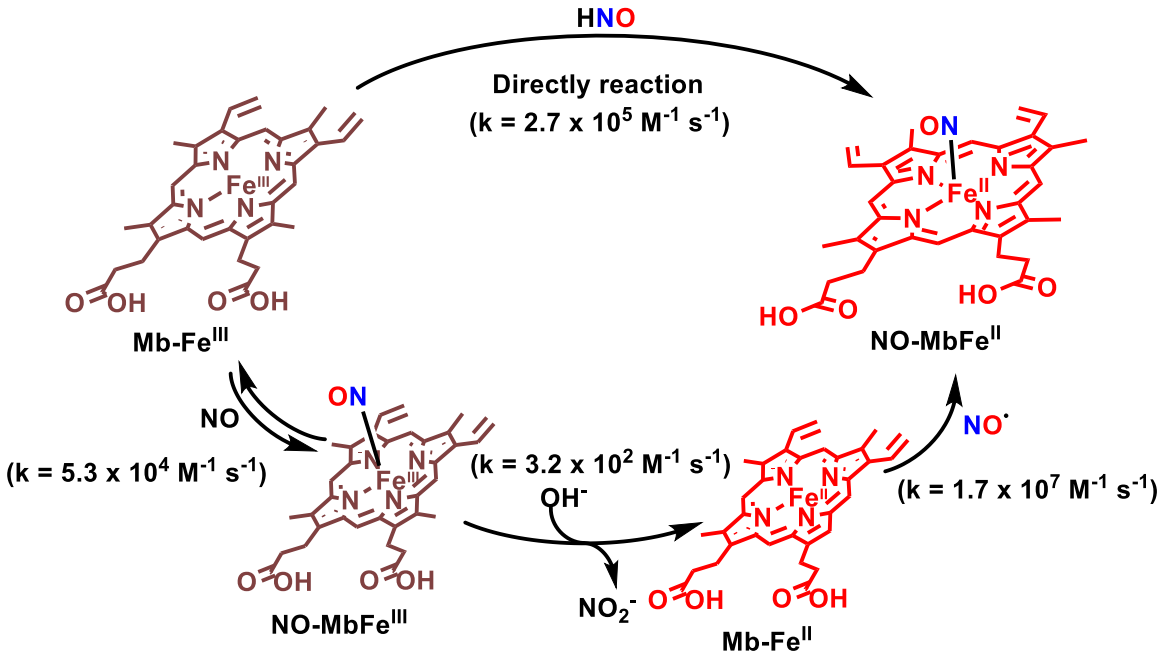

Reference: Adapted from 109, 328 and 329.

First of all, a control experiment using Mb-Fe^{III} and Angeli's salt, a well established direct HNO donor, was performed under physiological conditions (degassed phosphate buffer 0.1 M, pH 7.4, at 37 ºC), to obtain the UV-Vis spectral profile of the NO-MbFe^{II} adduct (Figure 28). All anaerobic experiments were prepared in an inert gas glove box. Before the spectrophotometer analysis, the cuvettes containing the samples were efficiently sealed to prevent the entry of atmospheric air. The main differences observed in the initial and final UV-Vis spectra of the heme-protein were the displacement of the Soret band, from 408 to 420 nm, and Q bands, from 506 and 634 nm, to 548 and 580 nm, respectively. These modifications are indicative of the Mb-Fe^{III} conversion to the NO-MbFe^{II} form.[328]

Figure 28 - Spectral variation in the UV-Vis region for a mixture containing Mb-Fe^{III} (6.7 μM) and Angeli's salt (27 μM), in anaerobic phosphate buffer (0.1 M, pH 7.4, at 37 ºC). Solution before (grey) and after 1 h (black) of reaction. A = Full spectra (Soret band) and B = Spectra zoom between 450 and 700 nm (Q bands).

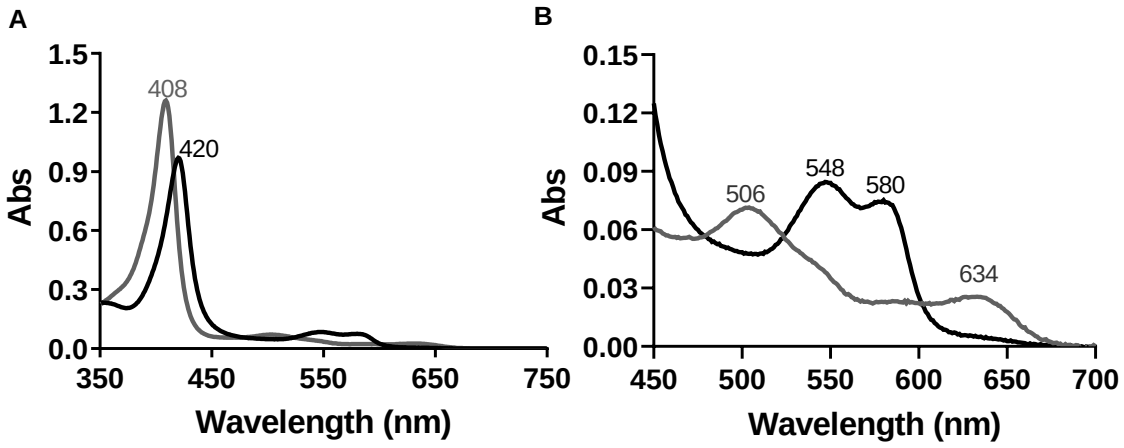

Reference: Elaborated by the author.

The study of the *trans*-[Fe(cyclam)(NO)Cl]$^{2+}$ complex in the presence of Mb-Fe^{III}, under the same conditions of the control experiment (anaerobic phosphate buffer solution, 0.1 M, pH 7.4, at 37 ºC), was monitored by UV-Vis for 24 h (Figure 29). The results did not indicate significant changes in the Mb-Fe^{III} spectrum over the time (24 h). Since the reaction of Mb-Fe^{III} with NO is about fivefold slower than that with HNO, these results suggest a potential NO release, via thermal decomposition of the nitrosyl iron complex under physiological conditions, thus corroborating with the published results.

Figure 29 - Spectral variation in the UV-Vis region for a mixture containing Mb-Fe^{III} (6.7 μM) and *trans*-[Fe(cyclam)(NO)Cl]$^{2+}$ complex (134.0 μM), in anaerobic phosphate buffer (0.1 M, pH 7.4, at 37 ºC). Solution before (gray) and after 24 h (black) of reaction. A = Full spectra (Soret band) and B = Spectra zoom between 450 and 700 nm (Q bands).

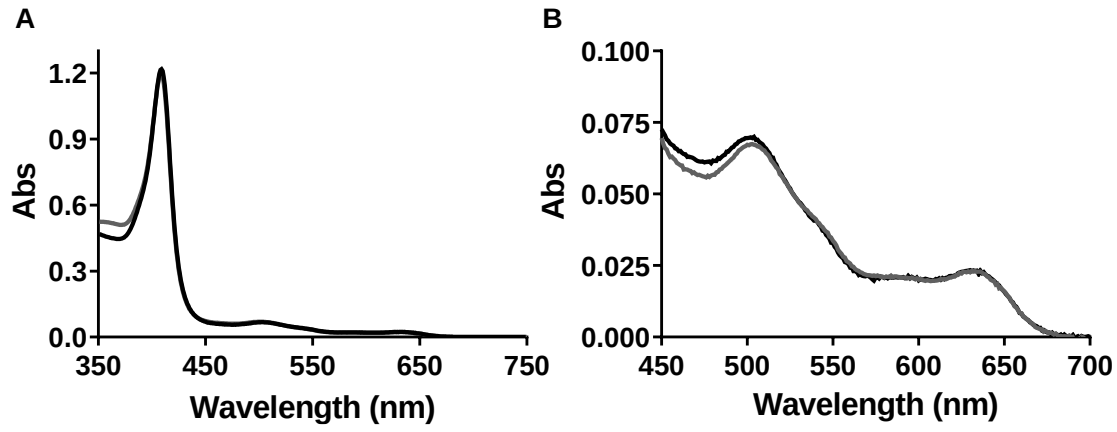

Reference: Elaborated by the author.

In photodecomposition study, a mixture containing the nitrosyl complex and Mb-Fe^{III}, in anaerobic solution of phosphate buffer (0.1 M pH 7.4 at 37 °C), was monitored before and after 1.5 h of irradiation (365 nm), by absorption spectroscopy in the UV-Vis region (Figure 30). No evidences of the NO-Mb-Fe^{II} adduct was observed over the time (1.5 h). Since the reaction of the oxidized protein with HNO is substantially faster, this result suggests that HNO was not produced in this experiment.

Figure 30 - Spectral variation in the UV-Vis region for an anaerobic solution of Mb-Fe^{III} (4.6 μM) and *trans*-[Fe(cyclam)(NO)Cl]$^{2+}$ (100.0 μM), in phosphate buffer 0.1 M, pH 7.4, at 37 ºC. Mixture before (gray) and after 1.5 h (black) of irradiation (365 nm). A = Full spectra (Soret band) and B = Spectra zoom between 450 and 700 nm (Q bands).

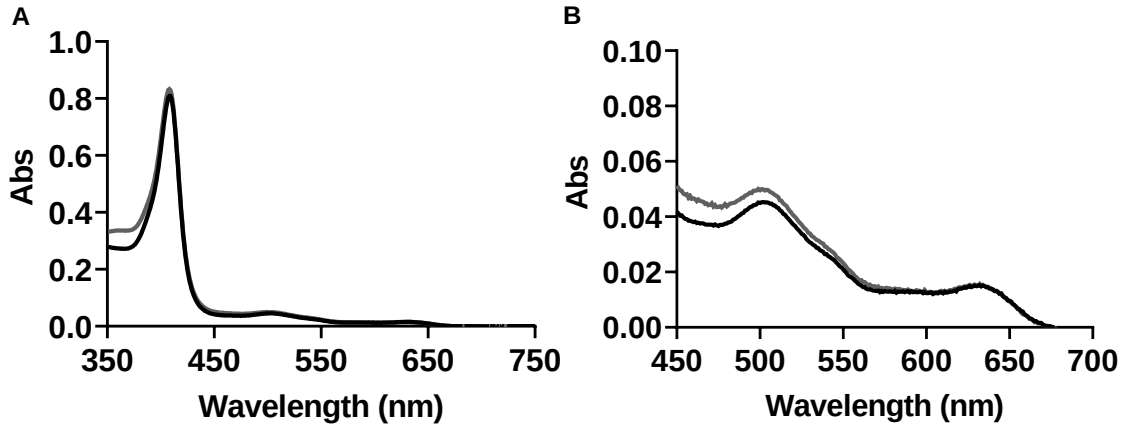

Reference: Elaborated by the author.

trans-[Fe(cyclam)(NO)Cl]Cl_2 stability in the presence of pentetic acid (DTPA)

Aiming to inhibit potential interferences of free iron ions in solution, some experiments were performed in the presence of chelating agents, pentetic acid (DTPA) or deferoxamine. For that, control experiments to examine the potential influence of the use of DTPA in the assays were performed. In this context, the stabilities of the *trans*-[Fe(cyclam)(NO)Cl]$^{2+}$ and *trans*-[Fe(cyclam)Cl_2]$^{+}$ complexes, alone and in the presence of DTPA, were monitored for 4 h via electronic absorption spectroscopy, in UV-Vis region, in phosphate buffer solutions (0.1 M, pH 7.4 at 37 °C). In the study involving the *trans*-[Fe(cyclam)(NO)Cl]$^{2+}$ and DTPA, it was observed a decrease of the band at 235 nm (Figure 31A) assigned to intraligand-charge-transfer transition (ILCT) of the cyclam ligand and ligand-metal charge transfer (LMCT) from the cyclam ligand to Fe^{II} metal center. The mixture of the *trans*-[Fe(cyclam)Cl_2]$^{+}$ and DTPA showed a hyperchromic and hypsochromic effect of the band at 320 nm related to the iron complex (Figure 31B). Similar results were obtained in the thermal stability experiments of the *trans*-[Fe(cyclam)(NO)Cl]$^{2+}$ and *trans*-

$[Fe(cyclam)Cl_2]^+$ (see the chapter 1 - Thermal stability and NO release section), indicating that, in fact, the spectral changes observed are related to the spontaneous thermal decomposition of the iron complexes in solution, and do not arise from the presence of free iron ions. Since the spectral records, in the presence and absence of DTPA, showed similar profiles and trends, we conclude that DTPA did not influence the thermal decomposition of the complexes nor influence the other experiments.

Figure 31 - Thermal stability of the iron complexes in the presence of DTPA. A. Spectroscopic changes for *trans*-$[Fe(cyclam)(NO)Cl]^{2+}$ (50 μM) solution in the presence of DTPA (75 μM), inset shows the kinetic curve based on changes at 235 nm. B. Spectroscopic changes for *trans*-$[Fe(cyclam)Cl_2]^+$ (100 μM) solution in the presence of DTPA (150 μM), inset shows the kinetic curve at 320 nm. The spectra were monitored by electronic spectroscopy for ca. 4 h in 0.1 M phosphate buffer (pH 7.4) solution at 37 ºC, under aerobic conditions. Final spectrum in black.

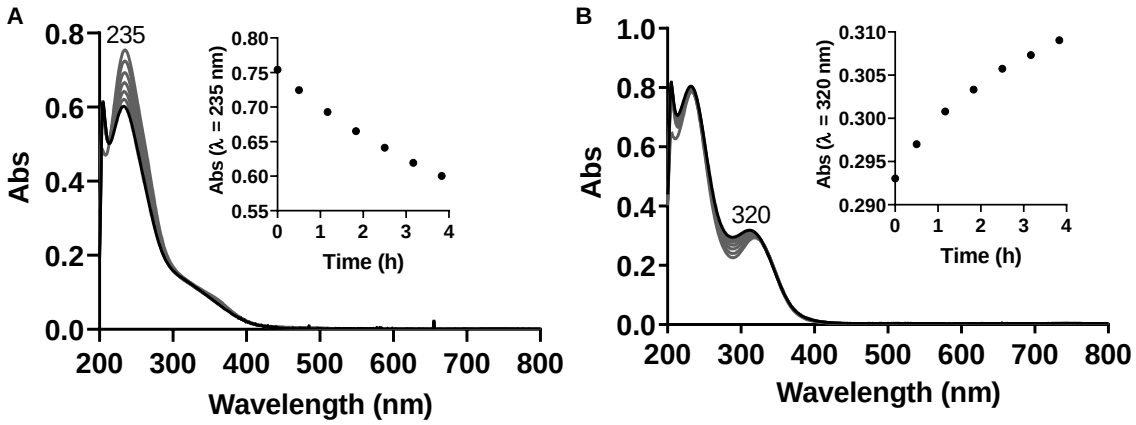

Reference: Elaborated by the author.

Photostability study of the trans-[Fe(cyclam)(NO)Cl]Cl_2 in solid state

To verify the stability of the *trans*-$[Fe(cyclam)(NO)Cl]Cl_2$, in solid state, when subjected to irradiation (365 nm), the nitrosyl complex, dispersed in KBr pellet, was irradiated at different times and then the respective spectra in the infrared region were recorded (Figure 32). It was observed that over the irradiation time, the stretch corresponding to the ligand NO^+ (1888 cm^{-1}) disappears, indicating that also in a solid state, the irradiation at 365 nm can induce the decomposition of the nitrosyl complex.

Figure 32 - Irradiation of the *trans*-[Fe(cyclam)(NO)Cl]Cl_2 at 365 nm (6 h), in KBr pellet, monitoring by FTIR.

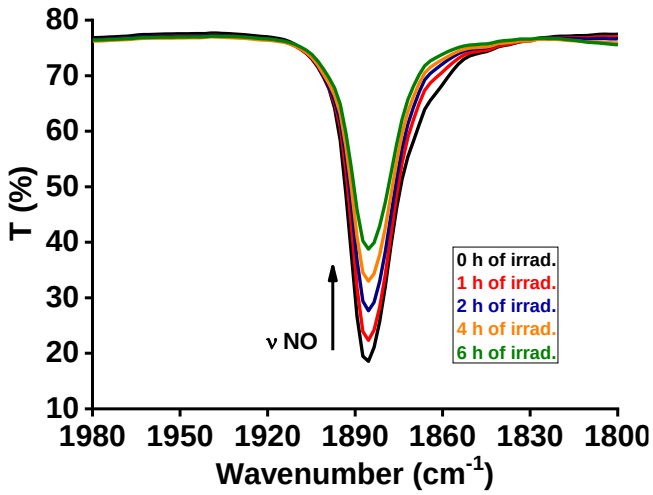

Reference: Elaborated by the author.

3.6 Conclusion

The results shown in this section provide important information about the reactivity of the nitrosyl complex. The thermal stability and photoirradiation studies, involving Mb-Fe^{III} and *trans*-$[Fe(cyclam)(NO)Cl]^{2+}$ complex, indicated that the HNO was not detected in both experiments, corroborating with the experiments reported in the publication. The presence of the DTPA chelator was not able to induce significant changes in the standard spectra of the *trans*-$[Fe(cyclam)(NO)Cl]^{2+}$ and *trans*-$[Fe(cyclam)Cl_2]^{+}$ complexes, indicating that the presence of DTPA did not influence the experimental responses obtained. In addition, it was shown that the nitrosyl complex *trans*-[Fe(cyclam)(NO)Cl]Cl_2, in solid state, can be photodecomposed by irradiation at 365 nm, mainly affecting the interaction between the metallic center and the ligand NO^{+}.

4 PART 2 – PENTACYANOFERRATE COMPLEXES: HYDROXAMIC ACID AS THERAPEUTIC PLATFORMS

Hydroxamic acids display several chemical and biological properties,[119,293,330,331] many of which attributed to their ability to release NO•/HNO under oxidative conditions. The pharmacological effects aligned with the HNO and NO• metabolites are diverse, the releasing moiety may also display physiological roles, which illustrates the potential use of these agents in the development of new drugs.[297,331,332] In this part of the thesis, we focused on the oxidative study of these organic molecules. From a fundamental perspective, the chapter 2 describes the oxidative mechanism involving three azine hydroxamic acid derivatives, while in the chapter 3 we explore the antituberculosis and cardiovascular properties of new Fe^{II} hydroxamic acid complexes under oxidative conditions. HNO release is one of the key points of these two studies.

4.1 Introduction

The reaction between diethyl oxalate and hydroxylamine, producing the compound oxalohydroxamic acid (Scheme 17), carried out by H. Lossen in 1869, marks the beginning of hydroxamic acid chemistry.[330,333] From this milestone, a series of studies have begun involving new synthetic approaches and possible applications in organic and inorganic chemistry, and biochemistry as bioactive molecules.[119,293]

Scheme 17 - Oxalohydroxamic acid synthesis by Lossen.

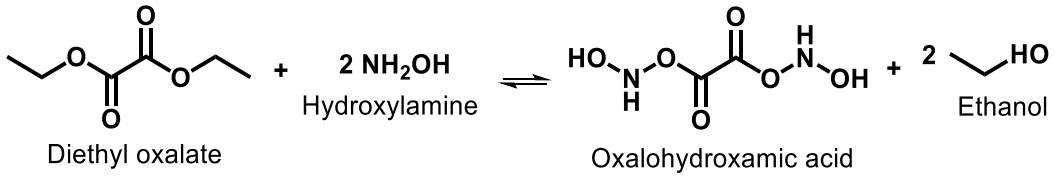

Reference: Adapted from 330 and 333.

It was mentioned earlier that hydroxamic acids are able to release NO•/HNO under oxidative conditions and many of their chemical and biological properties are attributed to this ability.[119]

In the introduction of this thesis, we report that isoniazid (INH), pyrazinamide (PZA) and delamanid are all pro-drugs used in antituberculosis treatments.[187] The

pharmacological action of these drugs is dependent on an activation step mediated by enzymes present in *Mtb*. INH is activated through an oxidative process mediated by the mycobacterial catalase-peroxidase enzyme, KatG, generating the isonicotinoyl radical intermediate that reacts with NAD(H) yielding an INH-NADH adduct, the ultimate active metabolite against *Mtb* (Scheme 18).[31] On the other hand, the PZA activation occurs via a hydrolysis process mediated by the pyrazinamidase enzyme, PncA, yielding pyrazinoic acid as the active metabolite (Scheme 18).[187] Delamanid is also proposed as a pro-drug that requires enzymatic activation. It has been suggested that its main active metabolite against *Mtb* is HNO, this latter resulting from a reductive decomposition of the nitroimidazole group by a mycobacterial nitroreductase enzyme (Ddn) (Scheme 18).[31]

Scheme 18 - Enzymatic activation of INH, PZA and delamanid.

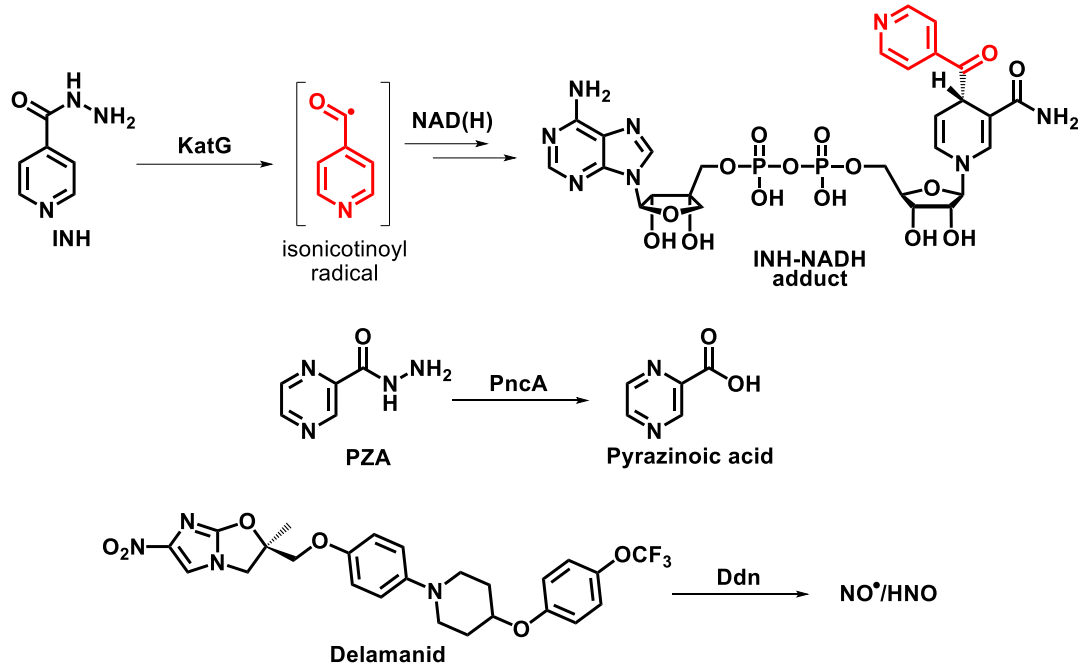

Reference: Adapted from 31 and 187.

Nevertheless, the emergence of multidrug-resistant strains of *Mtb* has limited the use of drugs such as INH and PZA in TB therapy. In most cases, the resistance mechanism is associated with mutations in the gene that encodes for the enzymes responsible for activating drugs, as a result, mycobacteria can no longer oxidize the drugs.[187] Multidrug-resistant tuberculosis (MDR-TB) has opened up opportunities to develop new strategies to control TB. Delamanid is an example of a new pro-drug developed for use in MDR-TB cases. However, the possible strategies are not limited to organic compounds only. Motivated by a potential

therapeutic approach using metal complexes, Sousa and collaborators,[31] developed a strategy based on the pentacyanoferrate(II) complex of INH, called IQG607. In summary, IQG607, when oxidized to Fe^{III} by $H_2O_2/O_2^{\bullet-}$, produces isonicotinoyl radical, a key tool in the anti-TB action of INH (Figure 33). During this oxidation process, isonicotinic acid and isonicotinamide are also formed as final metabolites. Furthermore, this complex has shown an efficient inhibition of the InhA enzyme *in vitro*, even in the absence of KatG, accompanied by a very low MIC (0.2 µg/mL) against *Mtb*.[31] This approach could be very important, especially in cases of acquired resistance to INH, since this process would overcome the enzymatic activation of INH promoted by KatG. Thus, the use of the pentacyanoferrate(II) moiety as an alternative to enable drug activation has stimulated its use with other molecules of biological interest such as hydroxamic acids.

Figure 33 - Proposal of the redox metal-mediated activation of IQG607 in *Mtb*, extracted from the reference.

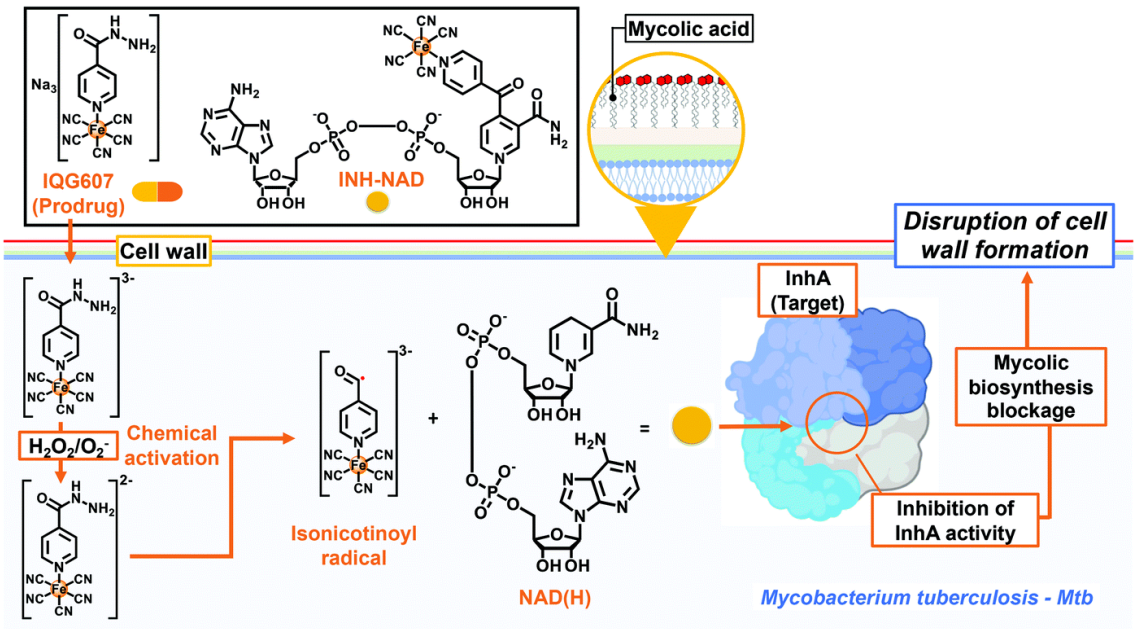

Reference: Extracted from 31.

In light of what was discussed, the development of new therapeutic platforms capable of releasing HNO, through chemical activation mediated by metal-complexes, is a promising strategy. This part of the thesis presents the development and biological study of three new pentacyanoferrate (II) complexes containing pyrazino-, isonicotino-, and nicotino-hydroxamic acids as the sixth ligand.

Prior to the synthesis of Fe^{II} complexes, we have judged necessary to study the ability of ligands alone to release $NO^{\bullet}$/HNO in oxidative conditions to better appreciate the

interest to complex the hydroxamic acids (NO•/HNO donors) to a inorganic moiety [-$Fe(CN)_5$]. Thus, the first article presents a study of three hydroxamic acid derivatives with oxidizing agents such as hexacyanoferrate(III) complex and H_2O_2. In this study, when hexacyanoferrate(III) complex was used as oxidizing agent, it was possible to identify HNO as one of the final products of these reactions and *N*,*O*-di(di)azinoylhydroxylamine as intermediate. In the presence of H_2O_2 alone, hydroxamic acids are not oxidized. The aim of this article is to highlight the ability of hydroxamic acids to act as HNO donors, and to provide more clarity as to its mechanism.

The second article aims at the synthesis of pentacyanoferrate(II)-type complexes with the pyrazino- and isonicotino-hydroxamic acids as ligands, which are pyrazinamide's and isoniazid's analogs, respectively. The study of their oxidation mechanism and their potential to release HNO and another active metabolite (pyrazinoic acid or isonicotinoyl radical) was conducted. Finally, the antimycobacterial activity against the *Mtb* H37Rv and the vasodilator activity of these complexes were also investigated.

4.2 Chapter 2 - Mechanistic study of oxidative activation of aryl hydroxamic acids

4.2.1 Article 2: New Journal of Chemistry, 2020, 44, 11965-11973 - Résumé de l'article en français:

Mechanistic insights into the in vitro metal-promoted oxidation of (di)azine hydroxamic acids: evidence of HNO release and *N,O*-di(di)azinoyl hydroxylamine intermediate

Edinilton Muniz Carvalho, Lionel Rechignat, Eduardo Henrique Silva Sousa, Luiz Gonzaga de França Lopes, Remi Chauvin, Vania Bernardes-Génisson.

New Journal of Chemistry, ***2020***, *44, 11965-11973.*

Le nitroxyle (HNO) est un acide inorganique faible (pKa = 11,4) et instable qui présente plusieurs activités biologiques importantes qui sont pourtant encore très mal comprises.[75] L'une des principales propriétés pharmacologiques de HNO est son action bénéfique sur le système cardiovasculaire.[334] HNO présente aussi une activité antiangiogénique, en opposition à son cousin NO• qui lui favorise l'angiogenèse. Cette dernière propriété citée de HNO ouvre des opportunités intéressantes pour la thérapie contre le cancer.[335] Étant donné que HNO ne peut pas être directement utilisé *in vivo* en raison de sa forte instabilité en milieu aqueux (dimérisation et déshydratation donnant du protoxyde d'azote, N_2O, schème 19)[336] et une forte réactivité vis-à-vis des biomolécules nucléophiles (principalement avec des composés soufrés),[337] toutes les études concernant les propriétés biologiques de HNO ou son emploi comme agent thérapeutique nécessitent des composés donneurs de HNO.

Schème 19 - Réactions de HNO en milieu aqueux ou biologique.

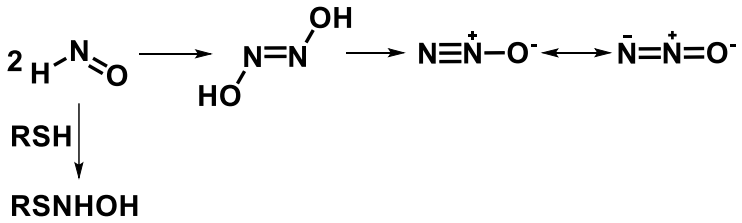

Référence : Extrait de 75.

Le HNO a été décrit comme l'un des principaux produits de l'oxydation de l'acide hydroxamique médiée par divers agents oxydants ($NaIO_4$, metaloenzymas, $Na_3[Fe^{II}(CN)_5NH_3]$ / oxydante, $K_3[Fe^{III}(CN)_6]$, ˙OH, ˙N_3, etc.). Toutefois, le mécanisme exact de cette réaction d'oxydation dans des conditions physiologiques de pH ainsi que la caractérisation directe ou indirecte des éventuels intermédiaires générés, restent encore à être élucidés et font ainsi objet d'étude. Compte tenu du fort potentiel des acides hydroxamiques à générer de HNO, l'élucidation de leur mécanisme d'oxydation dans des conditions physiologiques de pH est cruciale pour assister à la conception de nouvelles molécules donneuses de HNO plus performantes. Dans le premier chapitre de cette deuxième partie (chapitre 2), nous avons examiné l'oxydation intermoléculaire directe des dérivés : acide hydroxamique isonicotinique (**1**), nicotinique (**2**) et pyrazinique (**3**), médiée par le ferricyanure de potassium ($K_3[Fe^{III}(CN)_6]$) à pH = 7.4, ainsi qu'élucidé les structures des intermédiaires et des produits finaux formés (Schème 20).

Schème 20 - Réaction d'activation oxydative de l'acide hydroxamique isonicotinique (**1**), nicotinique (**2**) et pyrazinique (**3**), par l'ion $[Fe^{III}(CN)_6]^{3-}$ à pH = 7.4.

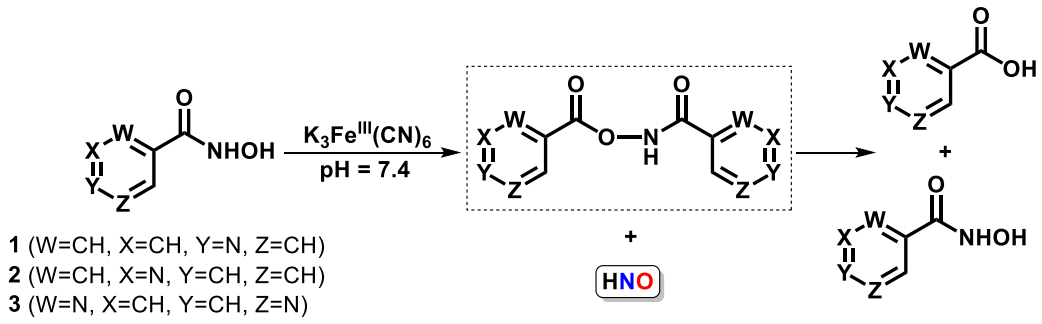

Référence : Élaboré par l'auteur.

L'oxydation des acides hydroxamiques **1-3** (1 éq.) par $[Fe(CN)_6]^{3-}$ (2,5 éq.) réalisée dans une solution tampon phosphate (D_2O, pH = 7,4) a été initialement suivie par RMN ^{1}H. Cette étude a révélé qu'après 1 h de réaction, il existe une conversion partielle du produit de départ (50%, 56% et 38% pour **1**, **2** et **3**, respectivement). L'analyse spectrale de RMN ^{1}H montre, en plus des signaux relatifs au produit de départ restante, l'apparition d'un nouveau composé, possédant des signaux aromatiques dupliqués. Ce nouveau composé, au fil du temps, a tendance à disparaître en faveur de la formation d'un composé final présentant des signaux à 7,61–8,70 et 7,91 ppm pour **1**, 8,42 et 8,68 ppm pour **2** et 8,70–9,04 et 9,15 ppm pour **3,** qui ont pu être reconnus comme étant caractéristiques des acides carboxyliques correspondants sous forme déprotonée (carboxylate). Cette proposition a été confirmée par

comparaison avec les données de RMN ^{1}H obtenues à partir d'échantillons authentiques de sels d'acides carboxyliques. Ces résultats confirment ainsi que l'acide carboxylique est le produit final de l'oxydation - métabolite potentiel - de l'acide hydroxamique. Après 312 h de réaction, les spectres RMN ^{1}H indiquent essentiellement des pics correspondant à la structure du carboxylate. Sur la base de ces résultats, nous postulons que l'oxydation des acides hydroxamiques dans de telles conditions se produit d'abord en produisant un radical nitroxyde instable (oxydation monoélectronique de l'acide hydroxamique), qui est converti, après dimérisation, en HNO et une *N*,*O*-di(di)azinoylhydroxylamine, ce qui explique la duplication de signaux aromatiques observés en RMN ^{1}H (Schème 21). L'intermédiaire diacylhydroxylamine pourrait en effet être hydrolysé pour produire les acides carboxyliques correspondants et l'acide hydroxamique de départ qui subirait de nouveau une étape d'oxydation.

Schème 21 - Hypothèses mécanistiques pour la libération de HNO via oxydation des acides hydroxamiques.

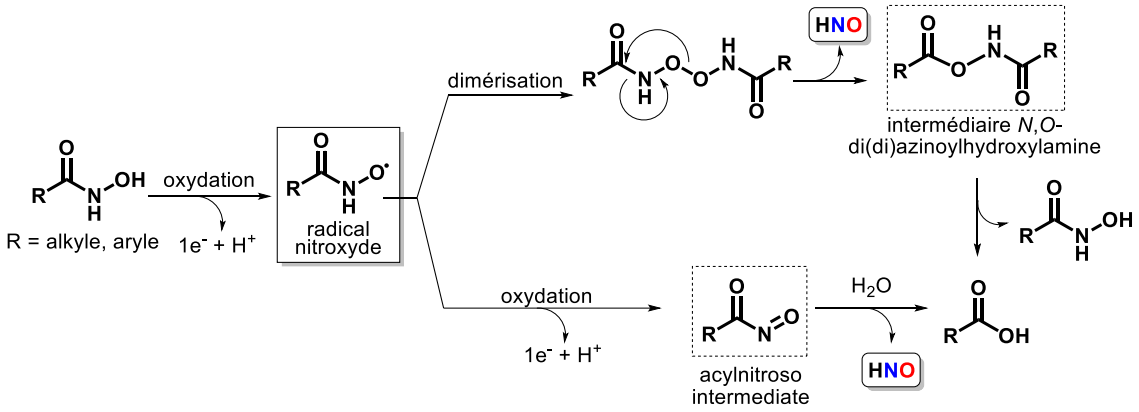

Référence : Élaboré par l'auteur.

La possibilité d'une oxydation supplémentaire du radical nitroxyde (oxydation à 2 électrons) conduisant à la formation d'un intermédiaire nitrosocarbonylé devrait être aussi considérée puisque ce dernier pourrait réagir facilement avec H_2O se décomposant en acide carboxylique correspondant et HNO (Schème 21).[119] Cependant, les spectres RMN ^{1}H montrent qu'après 1 h de réaction la conversion de l'acide hydroxamique de départ conduit uniquement or très majoritairement à l'intermédiaire *N*,*O*-di(di)azinoylhydroxylamine correspondant ; le produit acide carboxylique correspondant, qui pourrait être formé à partir d'un éventuel intermédiaire nitrosocarbonylé avec de l'eau, n'étant pas détecté en début de

réaction. Ensemble, ces résultats suggèrent que l'intermédiaire nitrosocarbonylé n'est pas impliqué dans la formation de HNO et d'acide carboxylique.

Pour tenter de caractériser l'intermédiaire proposé, les réactions d'oxydation des acides hydroxamiques **1**-**3** ont été répétées sur une échelle préparative (acide hydroxamique (0,72 mmol) et $K_3[Fe^{III}(CN)_6]$ (2,5 éq.)) et arrêtées après 24 h. Le nouveau produit a été isolé puis caractérisé par des techniques de RMN (^1H et ^{13}C) et SM (basse et haute résolution (HR)). Pour le dérivé **1**, l'analyse RMN ^1H a montré un produit présentant quatre doublets à 8,91 (d, 1H), 8,81 (d, 1H), 7,99 (d, 1H) et 7,79 (d, 1H) ppm. Par RMN ^{13}C, on constate la présence de deux signaux à 167,7 et 166,0 ppm compatible avec le carbone quaternaire de deux groupes carbonylés différents, quatre signaux à 149,7, 147,8, 123,4 et 122,7 ppm dus à des CH aromatiques et deux pics à 146,0 et 137,5 ppm désignés comme étant les Cq des noyaux aromatiques. L'ensemble des données corrèle très bien avec la structure *N*,*O*-diisonicotinoylhydroxylamine (Schéme 21, composé **4**) proposée pour l'intermédiaire. L'analyse SM (DCI-CH_4) n'a pas permis l'identification du pic ion moléculaire de cet intermédiaire (composé **4**). Par contre, la détection des pics à *m/z* = 199, attribués à l'amide **13** [M^+] (Schéme 21), *m/z* = 124, attribué à l'acide **7a** [$M^+ + 1$] (Schème 22), et principalement à *m/z* = 123 qui a été attribué à l'amide **10** [$M^+ + 1$] (Schème 22) sont des forts indices d'être des fragments de l'intermédiaire di(di)azinoylhydroxylamine proposé. En effet, l'amide *m/z* = 123 pourrait être issu d'une étape de decarboxylation (perte de CO_2) de **4**. Par SMHR (mode positif ESI), un petit pic à *m/z* = 244,0726 a pu finalement être détecté et la masse exacte correspond bien à celle de la formule brute de **4** plus une unité [$M^+ + 1$].

Schème 22 - Voies de fragmentation par SM des intermédiaires proposés, *N*,*O*-di(di) azinoylhydroxylamines, issus de l'oxydation des acides (di)azine hydroxamiques.

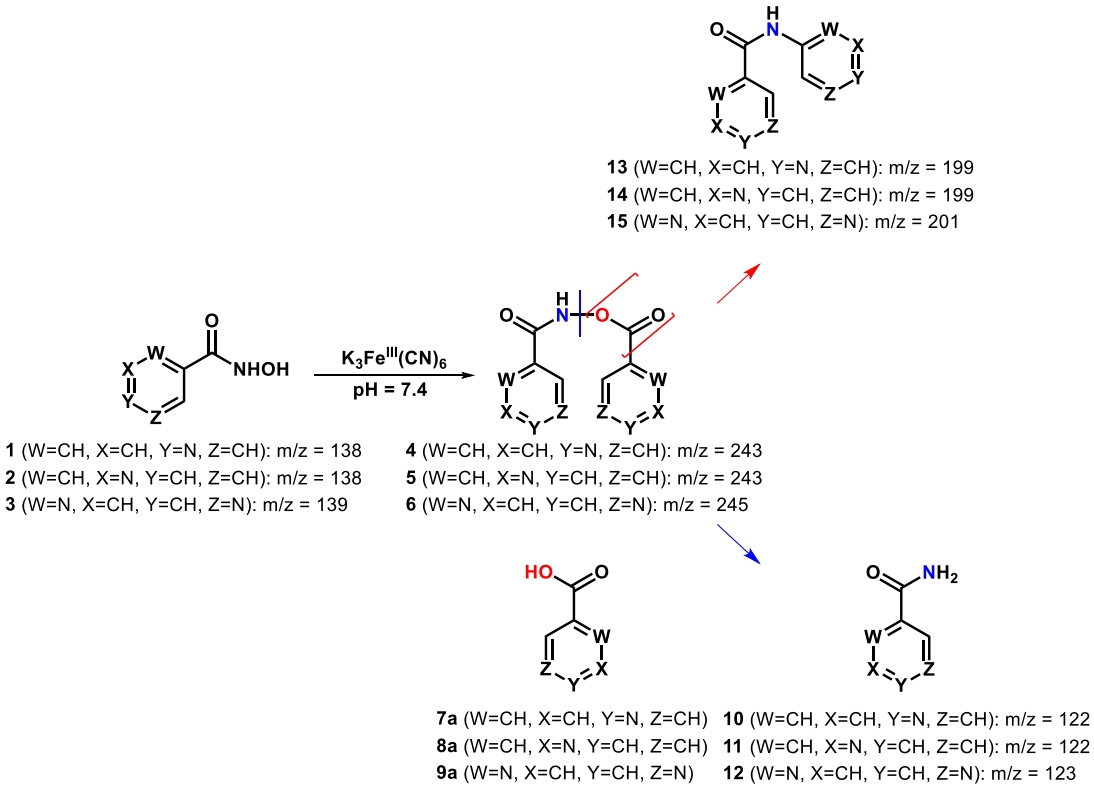

Référence : Élaboré par l'auteur.

La RMN ^{1}H de la même réaction d'oxydation mais utilisant le composé **2** comme substrat a montré 8 signaux attribuables aux hydrogènes aromatiques (9,18, 9,00, 8,86, 8,68, 8,39, 8,18, 7,62, 7,49 ppm) du composé **5** (Schème 22). Par contre, le spectre de masse (DCI-CH_4) du produit issu de la réaction d'oxydation de **2** a montré, des pics à *m/z* = 215 (composé **14** [M + $CH_4^{+\bullet}$]) et à *m/z* = 200 (composé **14**, [M + H^+]), caractéristique d'une fragmentation de **5** (Schème 22). De plus, l'analyse de masse de haute résolution (mode positif ESI) a permis de détecter d'un pic à *m/z* = 244,0726 correspondant au ion moléculaire [M + H^+] du composé **5**.

Contrairement aux études présentées pour les molécules **1** et **2**, le spectre RMN ^{1}H de l'oxydation de **3** était plus spéculatif en raison de chevauchements de signaux, ne contribuant pas de façon significative à supporter la structure supposée pour l'intermédiaire **6**. Par contre, dans le cas de l'oxydation de **3** ($K_3[Fe^{III}(CN)_6]$ + H_2O_2) étudiée par SM haute résolution (mode positif ESI),[320] il a été possible de détecter un pic de l'ion moléculaire à *m/z* = 246,0619 ([M + H^+]) cohérent avec la structure proposée pour le composé **6** (schéma 21). L'ensemble de ces caractérisations supporte *N*,*O*-di(di)azinoylhydroxylamine comme étant

l'intermédiaire formé lors de l'étape d'oxydation des acides hydroxamiques in milieu aqueux et à pH physiologique.

Outre les résultats de mise en évidence de l'intermédiaire *N*,*O*-di(di)azinoylhydroxylamine, nous avons aussi démontré qu'en présence de méthylamine cet intermédiaire est capable d'agir comme un agent acylant conduisant la formation de dérivés de type *N*-méthylamide.

Enfin, les résultats des études spectroscopiques (UV-Vis et EPR), en utilisant le piège cPTIO, du suivi de la réaction d'oxydation des acides hydroxamiques par l'ion Fe^{III}, supportent fortement la proposition de formation de HNO. En effet, les réactions des acides hydroxamiques avec l'ion $[Fe^{III}(CN)_6]^{3-}$, en présence de cPTIO, ont conduit à une diminution du quintuplet caractéristique du cPTIO présent dans le spectre de RPE et à une diminution de sa bande à 541 nm (UV-Vis). Les modifications observées lors de ces expériences, peuvent être corrélées à une réaction du cPTIO avec HNO.[324] Toutes ces approches expérimentales corroborent à une nouvelle perspective sur le mécanisme oxydatif des acides hydroxamiques aromatiques in milieu aqueux à pH physiologique.

4.3 Article 2: New Journal of Chemistry, 2020, 44, 11965-11973 – Printed

NJC

ROYAL SOCIETY OF CHEMISTRY

PAPER

View Article Online
View Journal | View Issue

Cite this: *New J. Chem.*, 2020, 44, 11965

Mechanistic insights into the *in vitro* metal-promoted oxidation of (di)azine hydroxamic acids: evidence of HNO release and *N,O*-di(di)azinoyl hydroxylamine intermediate†

Edinilton Muniz Carvalho, [abc] Lionel Rechignat, [ab] Eduardo Henrique Silva de Sousa, [c] Luiz Gonzaga de França Lopes, *[c] Remi Chauvin [ab] and Vania Bernardes-Génisson *[ab]

Received 12th February 2020,
Accepted 24th June 2020

DOI: 10.1039/d0nj00753f

rsc.li/njc

The oxidant-dependent ability of hydroxamic acids to release nitroxyl (HNO), a small inorganic molecule endowed with various biological properties, is addressed from a mechanistic standpoint. Indeed, the exact mechanism of the hydroxamic acid oxidation in physiological conditions and the direct or indirect characterization of the intermediates remain elusive. In this work, intermolecular oxidation of isonicotino-, nicotino- and pyrazino-hydroxamic acids with $K_3[Fe^{III}(CN)_6]$ at physiological pH (7.4), was monitored by ^{1}H NMR, MS, EPR and UV-vis techniques. While nitrosocarbonyl (di)azine intermediates, (di)Az-C(O)-NO, could be *a priori* envisaged, it was in fact the corresponding *N,O*-di(di)azinoylhydroxylamines (AzC(O)NHOC(O)Az) and HNO that were identified, the first by ^{1}H NMR and the second on the basis of EPR and UV-vis experiments using the [2-(4-carboxyphenyl)-4,4,5,5-tetramethylimidazoline-1-oxyl-3-oxide] (cPTIO) spin trap. The decomposition of the unstable *N,O*-di(di)azinoylhydroxylamine intermediates in aqueous buffer media was shown to generate the corresponding carboxylic acids as final organic products, envisaged as possible *in vivo* metabolites. The same oxidation experiments performed in the presence of methylamine led to the corresponding *N*-methyl amides suggesting that, unlike hydroxamic acids, *N,O*-di(di)azinoylhydroxylamines act as acylating agents in physiological pH conditions.

1. Introduction

Nitroxyl or azanone (HNO) is an unstable inorganic weak acid ($pK_a = 11.4$),[1,2] which can also be considered as the protonated form of the one-electron reduction product of the nitric oxide radical (NO•). Nitroxyl displays several important biological activities,[3] remaining, however, poorly understood. One of the main pharmacological properties of HNO is its beneficial influence on the cardiovascular system. HNO, which is indeed known to induce vasodilation,[4,5] exhibit positive inotropic/lusitropic effects[6,7] and inhibit platelet aggregation,[8] is thus envisaged to play a key role for the treatment of patients with heart failure. HNO also exhibits an anti-angiogenic activity, as opposed to its sibling NO that promotes angiogenesis. This HNO property has opened many potential pharmacological applications including in cancer therapy.[9] Since HNO cannot be directly employed *in vivo* due its high irreversible instability in aqueous media (dimerization and dehydration giving nitrous oxide, N_2O, Scheme 1)[1,2] and high reactivity towards nucleophilic bio-molecules (mainly with sulfur compounds),[3,10] all studies on biological properties of HNO or its use as a therapeutic agent require the design of HNO donor compounds. Hence research into the development of different classes of pro-drugs, with the ability to release HNO under physiological conditions and in a tunable manner, attracts the attention of the scientific community. Among the different classes of HNO donors,[11] one can mention the hydroxamic acid function –C(O)NHOH, which is prone to generate HNO upon reaction with various oxidizing agents ($NaIO_4$, metalloenzymes, $Na_3[Fe^{II}(CN)_5NH_3]$/oxidant, $K_3[Fe^{III}(CN)_6]$, radicals generated by radiolysis such as •OH, $^•N_3$, *etc.*).[12] However, the exact mechanism of the hydroxamic acid oxidation in physiological conditions and the direct or indirect characterization of the transient intermediates,

[a] *CNRS, Laboratoire de Chimie de Coordination, LCC, UPR 8241, 205 Route de Narbonne, BP 44099, F-31077 Toulouse, Cedex 4, France. E-mail: vania.bernardes-genisson@lcc-toulouse.fr*
[b] *Université de Toulouse, Université Paul Sabatier, UPS, 118 Route de Narbonne, F-31062, Toulouse, Cedex 9, France*
[c] *Laboratório de Bioinorgânica, Universidade Federal do Ceará, Departamento de Química Orgânica e Inorgânica, Campus Pici, Fortaleza, CE 60455-760, Brazil. E-mail: lopeslu@dqoi.ufc.br*

† Electronic supplementary information (ESI) available: Experimental synthesis protocols and ^{1}H NMR, MS, UV-vis and EPR spectra of relevant species. See DOI: 10.1039/d0nj00753f

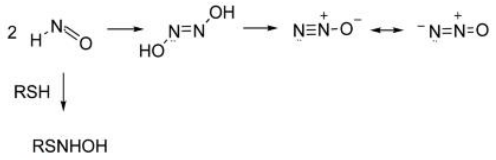

Scheme 1 Reactions of HNO in aqueous or biological media.

generated by an oxidative process in aqueous media, still constitute a matter of study.[12–14]

Taking into account the potential of hydroxamic acids to act as HNO donors for therapeutic treatments, the elucidation of their oxidation mechanism in physiological pH conditions is crucial to improve their properties as possible pro-drugs able to release HNO in a controllable way. Recently, we have developed a pentacyanoferrate(II) complex of pyrazinohydroxamic acid and have investigated *in vitro* its oxidation in the presence of H_2O_2 as well as its ability to release simultaneously HNO and the corresponding carboxylic acid (pyrazinoic acid) as the antituberculosis active metabolites of the delamanid and pyrazinamide drugs, respectively.[15] It has been proposed that oxidation of the pentacyanoferrate(II) complex

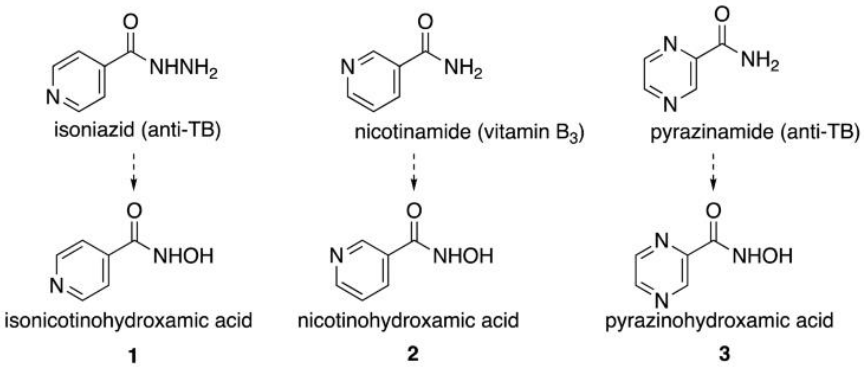

Scheme 2 Hydroxamic derivatives of isonicotinic hydrazine (isoniazid), nicotinamide, and pyrazinamide.

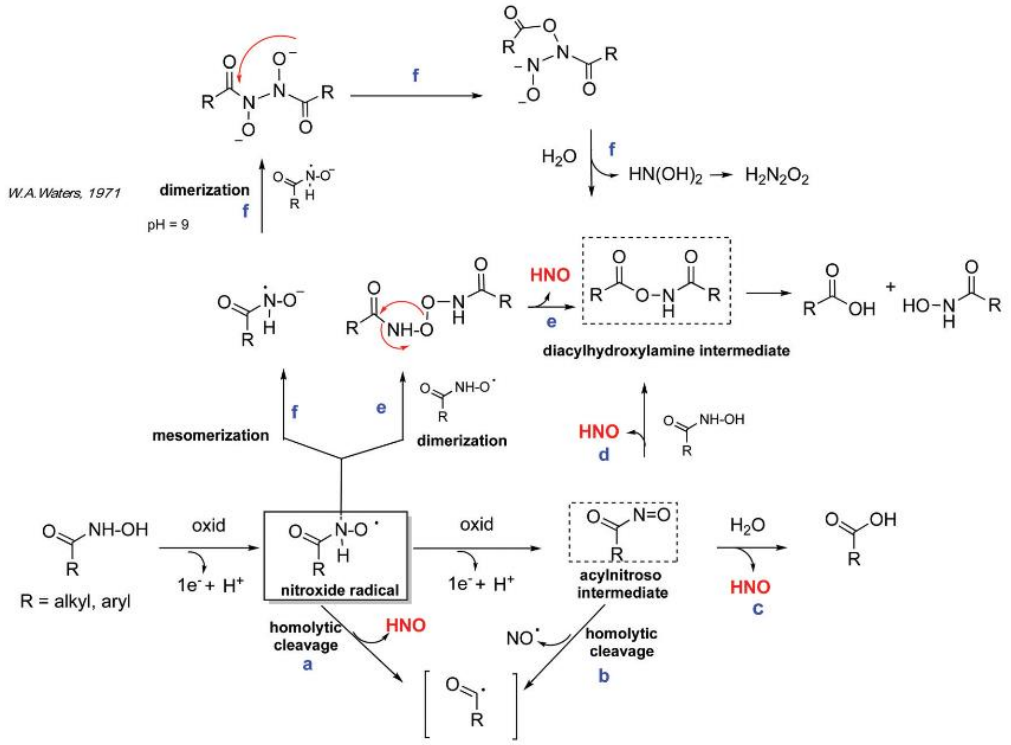

Scheme 3 Possible pathways and intermediates for the oxidation of hydroxamic acids (adapted from ref. 13).

of pyrazinohydroxamic acid proceeds *via* intramolecular (Fe^{III})-mediated oxidation of the C(O)NHOH function after initial oxidation of the Fe^{II} center into Fe^{III} center by H_2O_2.

In the present study, we examine if the direct intermolecular oxidation of isonicotino- (**1**), nicotino- (**2**), and pyrazino- (**3**) hydroxamic acids promoted by potassium ferricyanide

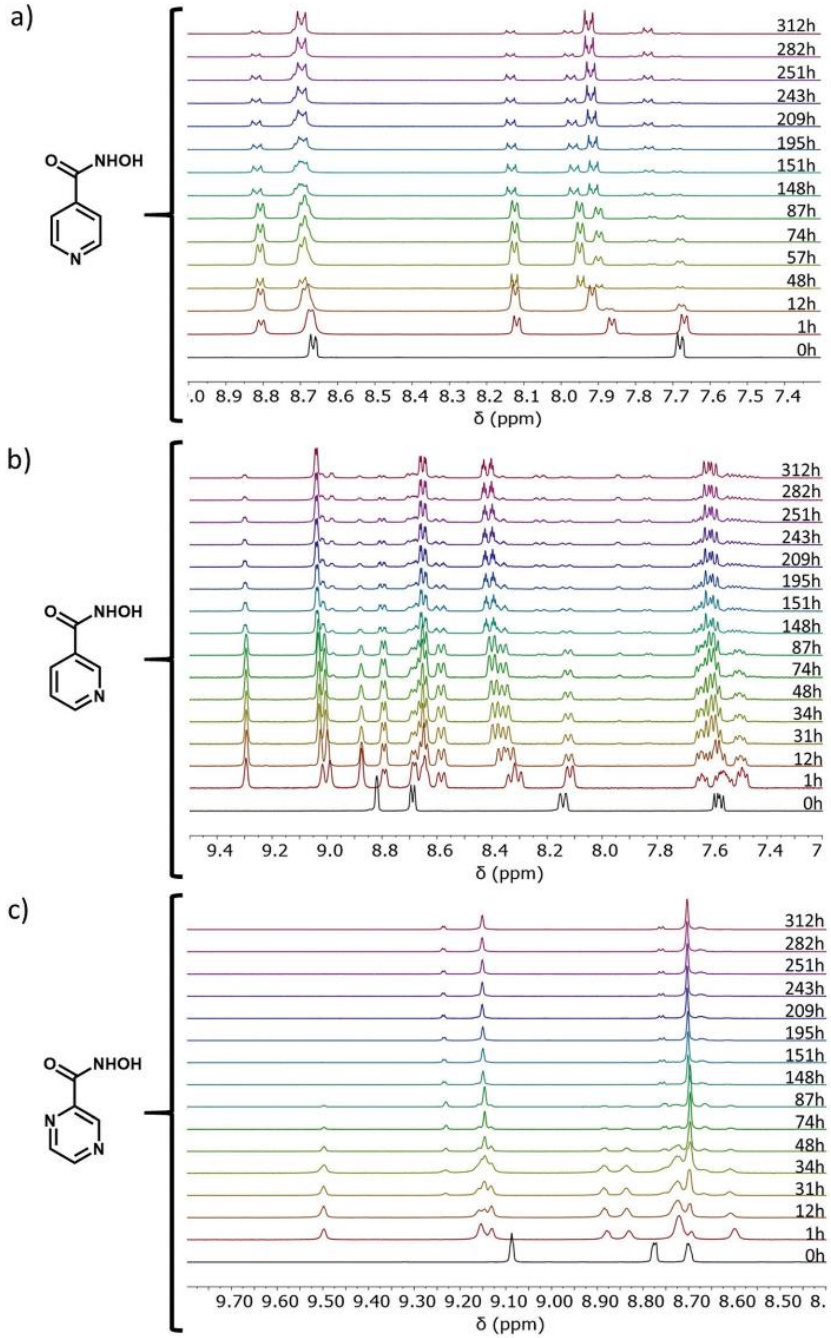

Fig. 1 ^1H NMR monitoring of $K_3[Fe^{III}(CN)_6]$-mediated oxidation of isonicotinohydroxamic acid **1** (24 mM, a) nicotinohydroxamic acid **2** (24 mM, b) and pyrazinohydroxamic acid **3** (24 mM, c) by $K_3[Fe^{III}(CN)_6]$ (60 mM) in a sodium phosphate D_2O buffer solution (pH = 7.4) at room temperature. The spectrum at 0 h corresponds to the reaction medium before addition of $K_3[Fe^{III}(CN)_6]$.

($K_3[Fe^{III}(CN)_6]$) at pH = 7.4 (Scheme 2) occurs and leads to the same final metabolites.

2. Results and discussion

The hexacyanoferrate(III) ion is a mild oxidizing species, which operates by abstracting one electron from a substrate through an outer sphere (intermolecular) pathway. This reagent allows oxidative processes[16] without atom transfer. Its use is relevant for a mechanistic study that could corroborate our previous results on the oxidation of the pyrazinohydroxamic acid acting as a *N*-ligand at a $Fe^{II}(CN)_5^{3-}$ center, for which an oxidation of the hydroxamic portion is proposed *via* an action of a Fe^{III} center generated by oxidation of the Fe^{II} center by H_2O_2.

It has been reported that one-electron oxidation of hydroxamic acids leads to the unstable nitroxide radical $RCONHO^{\bullet}$.[13,14,17] The fate of this radical is, however, uncertain: several alternative theoretical routes have been proposed,[14,16] and conceivable intermediates are *a priori* too unstable to be fully characterized (Scheme 3). On the one hand, the nitroxide radical could undergo a homolytic cleavage to form HNO and the aroyl radical (pathway a), or quickly dimerize, then rearrange to a *N*,*O*-diacylhydroxylamine intermediate (pathway e and f, the latter proposed by W. A. Waters).[12] On the other hand, it is proposed that the nitroxide radical readily undergoes a second oxidation to give the nitrosocarbonyl derivative, for which, however, direct evidence and complete spectral characterization in aqueous solution are lacking.[18,19] Such species are highly reactive and can decompose by either nucleophilic addition/HNO elimination (pathway c and d), or homolytic cleavage releasing $NO^{\bullet}$ and an aroyl radical (pathway b) (Scheme 3). In the first issue, it must be reminded that direct identification of HNO is still a real challenge. In the following are reported mechanistic investigations of the oxidation of isonicotino- (**1**), nicotino- (**2**) and pyrazino- (**3**) hydroxamic acids by $K_3[Fe(CN)_6]$ in aqueous buffer solution using ^{1}H NMR, MS, EPR and UV-vis techniques.

2.1 Monitoring of Fe^{III}-mediated oxidation of heteroarylhydroxamic acids by ^{1}H NMR

Oxidation of isonicotino-, nicotino-, and pyrazino-hydroxamic acids (1 eq.) by $K_3[Fe(CN)_6]$ (2.5 eq.) carried out in a sodium phosphate D_2O buffer solution (pH = 7.4), was monitored by ^{1}H NMR spectroscopy for 312 h (Fig. 1). ^{1}H NMR spectroscopy was also used to determine the *in situ* relative ratio of various products.

After 1 h, ^{1}H NMR analysis indicated a partial conversion of the starting material (50%, 56% and 38% for **1**, **2**, and **3**, respectively), mainly into a single primary product evidenced through a duplication of all aromatic signals (Fig. 1). Over time, the primary product tends to disappear (not completely), while giving another product characterized by new ^{1}H NMR data: 7.61–8.70 and 7.91 ppm from **1**, 8.42 and 8.68 ppm from **2**, 8.70–9.04 and 9.15 ppm from **3** (Fig. 1). Even though these data are slightly shifted with respect to authentic samples of the corresponding carboxylates (Fig. 2), signal patterns remain the same, in particular showing an overlap for the two vicinal aromatic protons of the pyrazine ring (Fig. 1). These oxidative protocols were repeated using pure D_2O as solvent: in these conditions, the reactions were found to proceed at slower rate, and the ^{1}H NMR chemical shifts measured at t = 226 h were in agreement with those of the corresponding carboxylate form (Fig. S1, ESI†). These results support our proposal that the carboxylic acid is the ultimate oxidation product – potential metabolite – of the hydroxamic acid (Fig. 2).

Thus, we propose that the intermediate product, tentatively assigned to the di(di)azinoylhydroxylamine structure of Scheme 4,

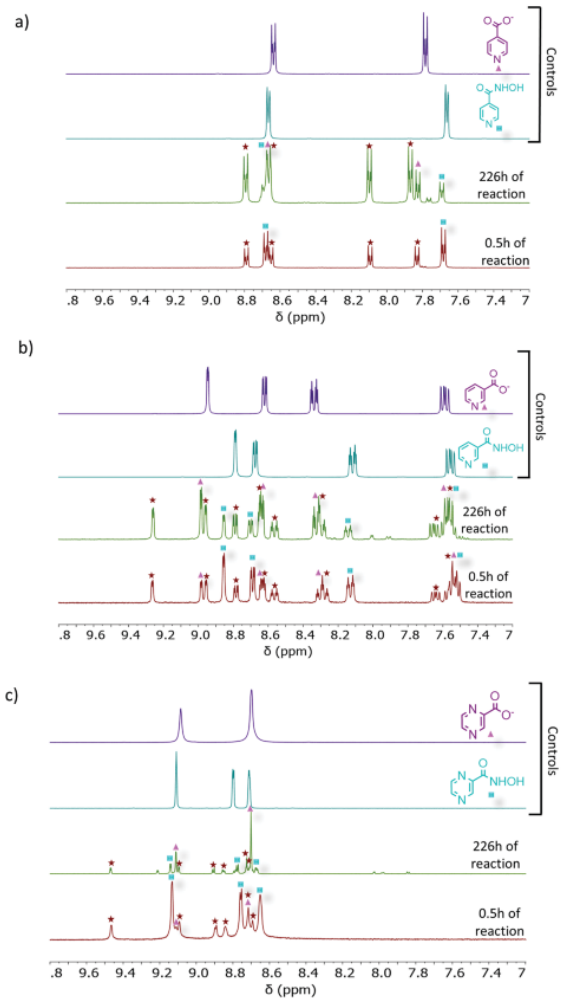

Fig. 2 ^{1}H NMR spectra of the $K_3[Fe^{III}(CN)_6]$-mediated oxidation of (a) isonicotinohydroxamic acid (b) nicotinohydroxamic acid and (c) pyrazino-hydroxamic acid at 0.5 h and 226 h using $K_3[Fe^{III}(CN)_6]$ in D_2O, at room temperature and authentic samples of (a) isonicotinohydroxamic acid and sodium isonicotinoate, (b) nicotinohydroxamic acid and sodium nicotinoate and (c) pyrazinohydroxamic acid and sodium pyrazinoate. Symbols: blue squares: starting hydroxamic acid, red stars: intermediate product, pink triangle: final carboxylic acid under carboxylate salt form.

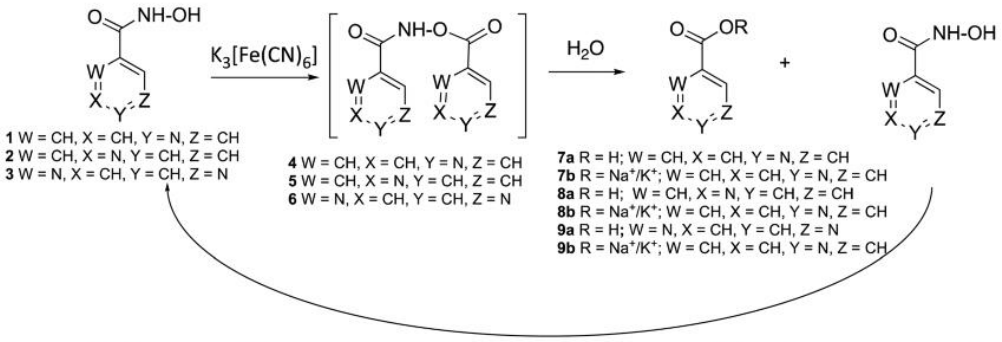

Scheme 4 Products suggested to appear during oxidation of (di)azine carbohydroxamic acids with a five-fold excess of potassium ferricyanide.

is hydrolyzed to the corresponding carboxylic acid and the starting hydroxamic acid after a nucleophilic attack at the most electrophilic carbonyl group (Scheme 4). As indicated on the ^{1}H NMR spectra, the amount of hydroxamic acid remains lower than that of the carboxylic acid because the former is oxidized again by the four-fold excess of $K_3[Fe(CN)_6]$, yielding *de novo* the intermediate di(di)azinoylhydroxylamine product.

After 312 h in buffer solution (Fig. 1), ^{1}H NMR spectra showed essentially peaks corresponding to the carboxylate structure (79%, 80% and 76% yield for isonicotinoic, nicotinoic and pyrazinoic acid from **1**, **2** and **3**, respectively).

On the basis of these results, we postulate that oxidation of (di)azine hydroxamic acids under such mild conditions occurs by first giving an unstable nitroxide radical, which is converted, after dimerization, to HNO and a *N*,*O*-di(di)azinoylhydroxylamine

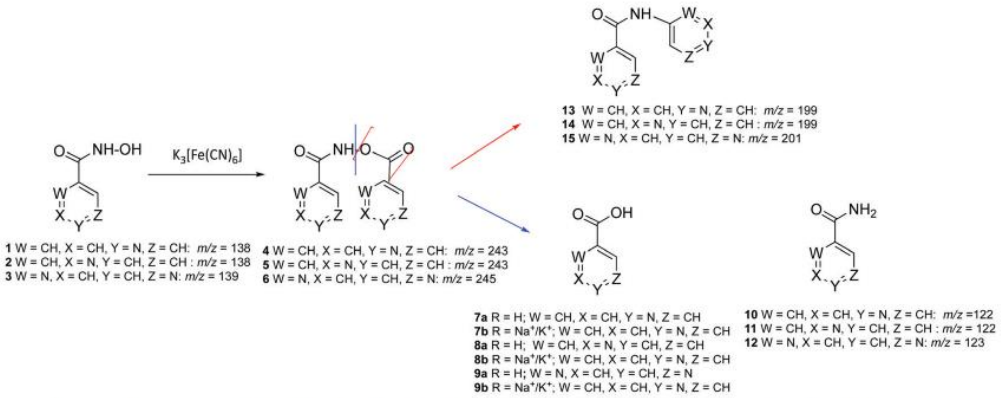

Fig. 3 MS fragmentation of the proposed *N*,*O*-di(di)azinoylhydroxylamine intermediates in the oxidation of (di)azine hydroxamic acids.

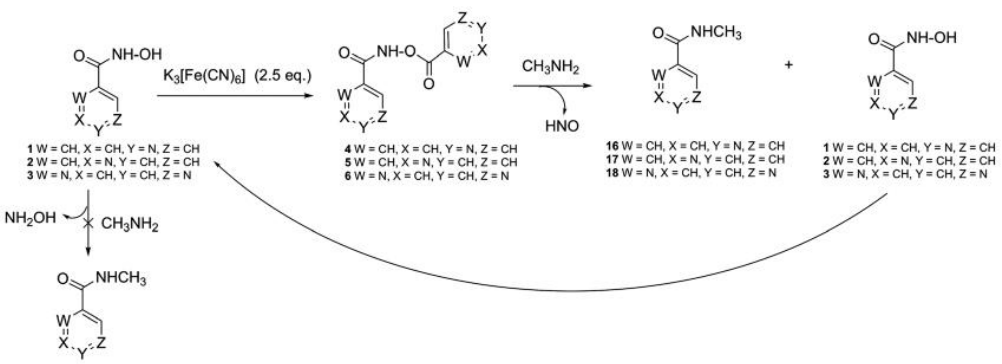

Scheme 5 Oxidation of (di)azine carbohydroxamic acids in the presence of methyl amine.

(Scheme 3, pathway e). The formation of the latter species could explain the duplication of the aromatic signals observed on ^{1}H NMR spectra.

As already mentioned, it could also be envisaged that the nitroxide radical undergoes a second oxidation leading to a transient nitrosocarbonyl (di)azine, which would readily react with any available nucleophile occurring in the medium. Thereby, reaction of the nitrosocarbonyl (di)azine with remaining hydroxamic acid would also lead to *N*,*O*-di(di)azinoylhydroxylamine and HNO (pathway d). In these conditions, one would also expect the nitrosocarbonyl (di)azine to react with H_2O, breaking down into the corresponding carboxylic acid and HNO (pathway c). However, ^{1}H NMR analysis of the reaction after 1 h showed that the conversion of the starting material (see *e.g.* **1**, Fig. 1 and 2) leads initially only to the putative *N*,*O*-di(di)azinoylhydroxylamine intermediate **4** whereas the corresponding carboxylic acid product had not yet begun to be produced. All together, these results suggest that no nitrosocarbonyl (di)azine is involved in the formation of the *N*,*O*-di(di)azinoylhydroxylamine and carboxylic acid. This scenario is also in total agreement with the work carried out by A. Cerami *et al.* from benzene hydroxamic acid.[14]

2.2 Identification of intermediates in Fe^{III}-mediated oxidation of (di)azine hydroxamic acids

In an attempt to characterize the proposed intermediates, the reaction of isonicotinohydroxamic acid was repeated at a preparative scale (0.72 mmol, using 2.5 eq. $K_3[Fe^{III}(CN)_6]$) and stopped after 24 h. The new product was isolated and then characterized by ^{1}H NMR, ^{13}C NMR and MS techniques. For the isonicotinic derivative, ^{1}H NMR analysis showed a product exhibiting four doublets at 8.91 (d, 1H), 8.81 (d, 1H), 7.99 (d, 1H) and 7.79 (d, 1H) ppm, confirming the results of the ^{1}H NMR monitoring experiment. Moreover, the ^{13}C NMR spectrum revealed the presence of two different carbonyl groups (167.7 and 166.0 ppm), four CH (149.7, 147.8, 123.4 and 122.7 ppm) and two Cq (146.0 and 137.5 ppm) centers, which correlate with the dissymmetric *N*,*O*-diisonicotinoylhydroxylamine structure (**4**). Analysis by mass spectrometry (MS, DCI–CH_4) did not allow the identification of the molecular ion peak but allowed the detection of three peaks at *m*/*z* = 199, *m*/*z* = 124 and *m*/*z* = 123 assigned to the amide **13** [M^+], acid **7a** [$M^+ + 1$] and amide **10** [$M^+ + 1$] (Fig. 3), respectively. The amide **13** would result from a decarboxylation of **4**, while the acid **7a** and amide **10** would result from a cleavage of the hydroxamic N–O bond (Fig. S2, ESI†). By HRMS (ESI-positive mode), a small peak at *m*/*z* = 244.0726 corresponding to **4** ([$M^+ + 1$]) was detected. In the nicotinic or pyrazinic series, a mixture of compounds was obtained, containing the intermediate **5** or **6** along with the starting material **2** or **3** and the corresponding carboxylic acids. The ^{1}H NMR spectrum of the nicotinic intermediate showed signals clearly attributable to all the non-equivalent aromatic CH groups of **5** (9.18, 9.00, 8.86, 8.68, 8.39, 8.18, 7.62, 7.49 ppm), while that of the pyrazinic product **6** was slightly more speculative because of signal overlaps. The mass spectrum (DCI–CH_4) of the nicotinic products (from **2**) showed, besides peaks relative to the nicotinic acid impurity, peaks at *m*/*z* = 215, *m*/*z* = 200 and *m*/*z* = 123, attributable to the secondary amide **14** ([$M + CH_4^{+\bullet}$], [$M + H^+$]) and primary amide **11** ([$M + H^+$]), respectively. As observed in the isonicotinic series (from **1**), in the nicotinic series (from **2**) HRMS (ESI-positive mode) allowed detection of a peak consistent with the structure **5** at *m*/*z* = 244.0726 ([$M + H^+$]). In the pyrazinic series (from **3**), MS (DCI–CH_4) revealed peaks at *m*/*z* = 230, 217 and 202 assignable to the secondary amide **15** ([$M + C_2H_5^+$], [$M + CH_3^+$] and [M+ H^+], respectively), and at *m*/*z* = 124 assignable to the primary amide **12** ([$M + H^+$]). Oxidation of **3** in the presence of $K_3[Fe^{III}(CN)_6]$ and H_2O_2 (conditions already used for oxidation of the pyrazinohydroxamic acid-[$Fe^{II}(CN)_5$ complex])[15] allowed detection of the molecular ion peak of *N*,*O*-dipyrazinoylhydroxylamine **6** by HRMS-ESI$^+$ at *m*/*z* = 246.0619 ([$M + H^+$]), and this in spite of the harsher conditions. In summary, the presence of the molecular ion peaks for the di(di)azinoylhydroxylamines **4–6** and secondary carboxamides **13–15** supports the proposed mechanism.

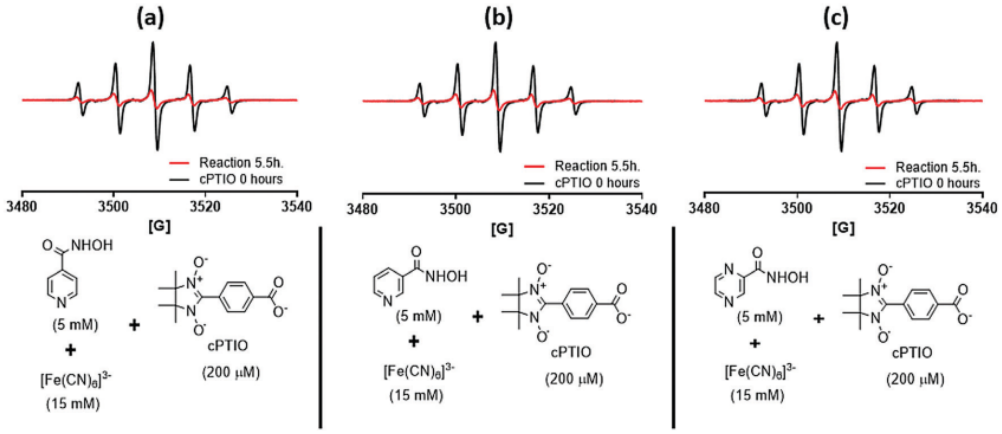

Fig. 4 EPR spectra of the reaction of (a) isonicotinohydroxamic acid, (b) nicotinohydroxamic acid and (c) pyrazinohydroxamic acid with $K_3[Fe^{III}(CN)_6]$ (15 mM) in the presence of cPTIO (200 μM) for 5.5 h in 40 mM phosphate buffer (pH 7.4), at room temperature.

2.3 Fe^{III}-mediated oxidation of (di)azine hydroxamic acids in the presence of methylamine

With the view to controlling the apparent electrophilic *trans*-acylation reactivity of the postulated *N*,*O*-di(di)azinoylhydroxylamine intermediates, the reaction with $K_3[Fe^{III}(CN)_6]$ was performed in the presence of an excess of methylamine (10 eq.) as a potential nucleophile. From the three hydroxamic acids **1–3**, a selective reaction was observed, allowing isolation of the *N*-methyl carboxamides **16–18** with *ca.* 70% yield, as confirmed by ^{1}H NMR, ^{13}C NMR, IR and HRMS analyses (Scheme 5). It is noteworthy that control experiment of the hydroxamic acids **1–3** with methylamine in the absence of $K_3[Fe^{III}(CN)_6]$ did not produce the corresponding carboxamides by elimination of NH_2OH. The requirement of $K_3[Fe^{III}(CN)_6]$ suggests the occurrence of the intermediates **4–6**, as mentioned above, which could react as an acyl donor towards methylamine.

2.4 Monitoring of Fe^{III}-mediated oxidation of (di)azine carbohydroxamic acids by EPR

In order to test whether the oxidation of hydroxamic acids promoted by $K_3[Fe^{III}(CN)_6]$, in physiological pH condition, is accompanied by HNO release, the nitronyl nitroxide radical [2-(4-carboxyphenyl)-4,4,5,5-tetramethylimidazoline-1-oxyl-3-oxide] (cPTIO) was employed. This spin trap probe is currently used to discriminate between the NO$^\bullet$ radical and HNO using electronic paramagnetic resonance (EPR).[20] The NO$^\bullet$ radical reacts with cPTIO by deoxygenation, giving $NO_2^\bullet$ and the cPTI radical (Fig. S3, ESI†), which exhibits a more complex EPR signal (septet pattern). In contrast, HNO readily reduces cPTIO into the corresponding nitronyl hydroxylamine (cPTIO-H) that is an EPR-silent diamagnetic species, inducing a decrease of the initial cPTIO EPR signal (Fig. S3, ESI†).

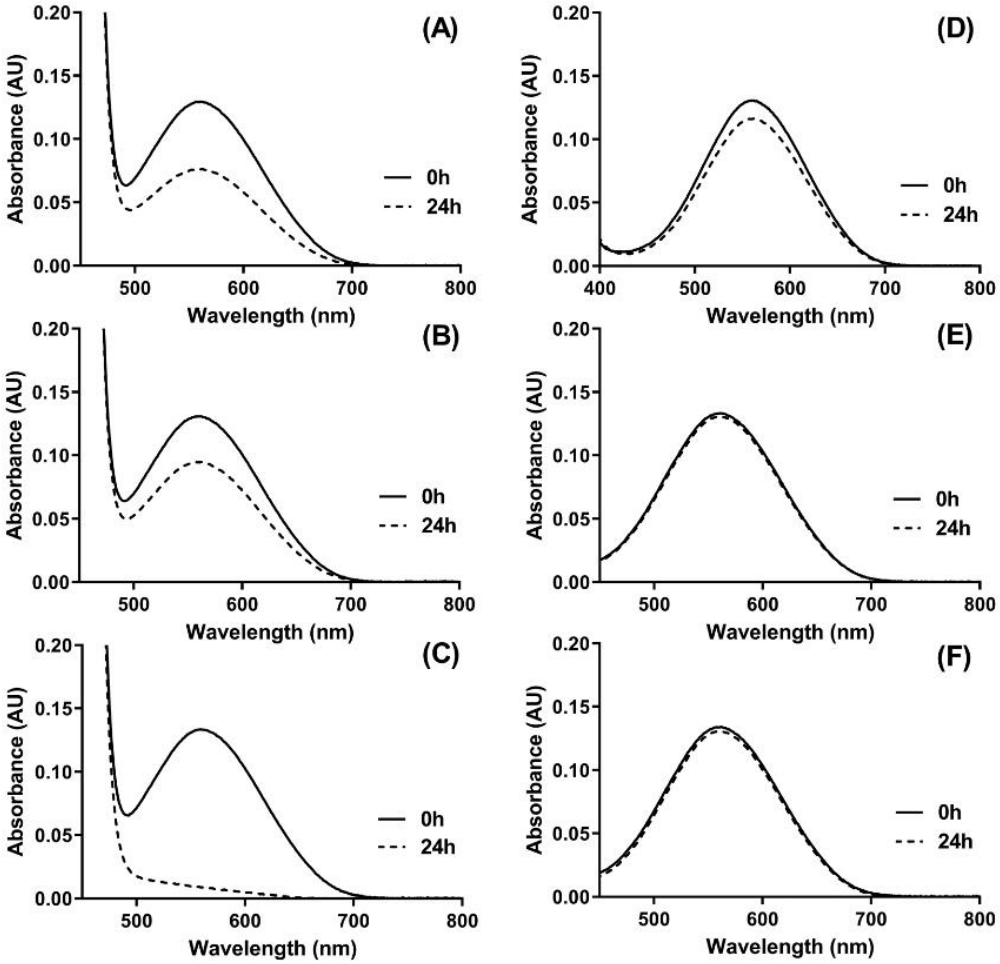

Fig. 5 Electronic absorption spectra of cPTIO in oxidative reaction mixtures or with hydroxamic acids alone. Panels on the left show spectra of the reaction between isonicotino- (A), nicotino- (B) and pyrazino- (C) hydroxamic acids (750 μM) with $K_3[Fe^{III}(CN)_6]$ (15 mM) in the presence of cPTIO (150 μM). Panels on the right show the spectra of cPTIO (150 μM) in the presence of isonicotino- (D), nicotino- (E) and pyrazino- (F) hydroxamic acids (750 μM). All reactions were monitored at 0 and 24 h in 40 mM phosphate buffer (pH 7.4), at room temperature.

Reactions of the hydroxamic acids **1**, **2** and **3** (5 mM) with $K_3[Fe^{III}(CN)_6]$ (15 mM), in phosphate buffer (40 mM, pH = 7.4) and in the presence cPTIO (200 μM), were carried out for 5.5 h and analyzed by EPR. The stability of cPTIO in the reaction conditions was first checked by EPR: alone or in the presence of hydroxamic acid, cPTIO was found to be stable without modification of the signal (Fig. S4a, ESI†). In the presence of $[Fe^{III}(CN)_6]^{3-}$ or $[Fe^{II}(CN)_6]^{4-}$, two complex ions expected to occur during the redox reaction, a decrease of the cPTIO EPR signal by 65% or 30%, respectively, was observed (Fig. S4a, ESI†). In the reaction mixture, where hydroxamic acid, $[Fe^{III}(CN)_6]^{3-}$/$[Fe^{II}(CN)_6]^{4-}$ and cPTIO co-exist, the EPR signal corresponding to the cPTIO radical was almost completely abolished (85% of reduction) after 5.5 h (Fig. 4). This result disclosed that the cPTIO signal decrease is accelerated with the concomitant presence of hydroxamic acid and $K_3[Fe^{III}(CN)_6]$, and suggesting that HNO is indeed released during oxidation of hydroxamic acids promoted by $K_3[Fe^{III}(CN)_6]$.

2.5 Monitoring of Fe^{III}-mediated oxidation of (di)azine carbohydroxamic acids by UV-vis

The release of HNO during the oxidation of the (di)azine hydroxamic acids **1–3** promoted by $K_3[Fe^{III}(CN)_6]$, in the presence of cPTIO was also studied by UV-vis spectroscopy. cPTIO exhibits characteristic electronic absorptions at 360 and 560 nm. Since no other reaction component absorbs around 560 nm (in contrast to the 360 nm region), this wavelength was chosen for monitoring. The evolution of this band was first followed in the sole presence of $K_3[Fe^{III}(CN)_6]$ or hydroxamic acids. No significant interaction was evidenced between $[Fe^{III}(CN)_6]^{3-}$ and cPTIO (Fig. S5, ESI†), or hydroxamic acids and cPTIO (Fig. 5D–F). In the oxidative reaction conditions (hydroxamic acid + $K_3[Fe^{III}(CN)_6]$ + cPTIO), monitoring over 24 h showed a decline of the absorption band at 560 nm for the three substrates **1–3** (Fig. 5A–C). These observations confirm the consumption of cPTIO under the given conditions, while the disappearance of the EPR signal indicated that it is accompanied by the generation of HNO (see above section).

3. Conclusion

In this work, it was shown that (di)azine carbohydroxamic acids generate HNO at physiological pH upon oxidation by $K_3[Fe^{III}(CN)_6]$ through an intermolecular/outer-sphere process, as it was previously shown upon oxidation by H_2O_2 through an intramolecular/inner-sphere process.[15] However, in contrast to what is often reported, HNO was not generated from the putative nitrosocarbonyl (di)azine, which would be formed after two oxidation steps of hydroxamic acid. Instead, HNO is released through a one-electron oxidation of the hydroxamic acid along with the *N*,*O*-di(di)azinoylhydroxylamine intermediate. This intermediate was characterized by NMR, MS, UV techniques and proved to be quite reactive, breaking down into the corresponding carboxylic acid and hydroxamic acid, which is then re-oxidized. So, globally, one molecule of hydroxamic acid generates one molecule of HNO. Since oxidation processes of arene hydroxamic acids going through either nitrosocarbonyl or *N*,*O*-di(di)aroylhydroxylamine intermediates, can have similar features in terms of (i) stoichiometry of HNO release, (ii) electrophilic reactivity of the intermediate and (iii) chemical nature of the final carboxylic products, a particular attention should be addressed to such mechanistic proposals. Computational studies would deserve to be considered to discriminate between the intrinsically highly reactive nitrosocarbonyl and *N*,*O*-diaroylhydroxylamine intermediates.

Conflicts of interest

There are no conflicts to declare.

Acknowledgements

We are thankful to CAPES (PROEX 23038.000936/2018-46), Capes/Cofecub (88887.130198/2017-01/Ph-C 883-17), CNPq (L. G. F. Lopes 303355/2018-2; E. H. S. Sousa 308383/2018-4, Universal 403866/2016-2), FUNCAP (PRONEX PR2 0101-00030.01.00/15 SPU No. 3265612/2015) for financial support. This study was also financed in part by the Coordenação de Aperfeiçoamento de Pessoal de Nível Superior – Brasil (CAPES) – Finance Code 001.

References

1 F. Doctorovich, D. Bikiel, J. Pellegrino, S. A. Suárez, A. Larsen and M. A. Martí, *Coord. Chem. Rev.*, 2011, **255**, 2764–2784.
2 V. Shafirovich and S. V. Lymar, *Proc. Natl. Acad. Sci. U. S. A.*, 2002, **99**, 7340–7345.
3 J. C. Irvine, R. H. Ritchie, J. L. Favaloro, K. L. Andrews, R. E. Widdop and B. K. Kemp-Harper, *Trends Pharmacol. Sci.*, 2008, **29**, 601–608.
4 J. C. Irvine, J. L. Favaloro and B. K. Kemp-Harper, *Hypertension*, 2003, **41**, 1301–1307.
5 J. C. Irvine, J. L. Favaloro, R. E. Widdop and B. K. Kemp-Harper, *Hypertension*, 2007, **49**, 885–892.
6 N. Paolocci, T. Katori, H. C. Champion, M. E. John, K. M. Miranda, J. M. Fukuto, D. A. Wink and D. A. Kass, *Proc. Natl. Acad. Sci. U. S. A.*, 2003, **100**, 5537–5542.
7 N. Paolocci, W. F. Saavedra, K. M. Miranda, C. Martignani, T. Isoda, J. M. Hare, M. G. Espey, J. M. Fukuto, M. Feelisch, D. A. Wink and D. A. Kass, *Proc. Natl. Acad. Sci. U. S. A.*, 2001, **98**, 10463–10468.
8 E. Bermejo, D. A. Sáenz, F. Alberto, R. E. Rosenstein, S. E. Bari and M. A. Lazzari, *Thromb. Haemostasis*, 2005, **94**, 578–584.
9 M. E. Shoman and O. M. Aly, *Curr. Top. Med. Chem.*, 2016, **16**, 2462–2470.
10 M. D. Bartberger, J. M. Fukuto and K. N. Houk, *Proc. Natl. Acad. Sci. U. S. A.*, 2001, **98**, 2194–2198.
11 (*a*) A. Porcheddu, L. De Luca and G. Giacomelli., *Synlett*, 2009, 2149–2153; (*b*) A. D. Sutton, M. Williamson, H. Weismiller and J. P. Toscano, *Org. Lett.*, 2012, **14**, 472–475; (*c*) X. Sha, T. S. Isbell, R. P. Patel, C. S. Day and S. B. King, *J. Am. Chem. Soc.*, 2006, **128**, 9687–9692; (*d*) M. E. Shoman, J. F. Du Mond, T. S. Isbell,

J. H. Crawford, A. Brandon, J. Honovar, D. A. Vitturi, C. R. White, R. P. Patel and S. B. King, *J. Med. Chem.*, 2011, **54**, 1059–1070; (*e*) D. A. Guthrie, A. Ho, C. G. Takahashi, A. Collins, M. Morris and J. P. Toscano, *J. Org. Chem.*, 2015, **80**, 1338–1348; (*f*) D. A. Guthrie, S. Nourian, C. G. Takahashi and J. P. Toscano, *J. Org. Chem.*, 2015, **80**, 1349–1356; (*g*) A. El-Armouche, A. Wahab, K. Wittköpper, T. Schulze, F. Böttcher, L. Pohlmann, S. B. King, J. F. DuMond, C. Gerloff, R. H. Böger, T. Eschenhagen, L. Carrier and S. Donzelli, *Biochem. Biophys. Res. Commun.*, 2010, **402**, 340–344.

12 T. R. Oliver and W. A. Waters, *J. Chem. Soc. B*, 1971, 677–681.

13 M. M. Gutiérrez, A. E. Almaraz, S. E. Bari, J. A. Olabe Iparraguirre and V. T. Amorebieta, *J. Coord. Chem.*, 2015, **68**, 3236–3246.

14 S. H. Blobstein, R. W. Grady, S. R. Meshnick and A. Cerami, *Biochem. Pharmacol.*, 1978, **27**, 2939–2945.

15 Results not yet published.

16 J. M. Leal, B. Garcia and P. L. Domingo, *Coord. Chem. Rev.*, 1998, **173**, 79–131.

17 U. Samuni, E. Mainon and S. Goldstein, *J. Coord. Chem.*, 2018, **71**, 1728–1737.

18 E. Maimon, A. Lerner, A. Samuni and S. Goldstein, *J. Phys. Chem.*, 2018, **122**, 7006–7013.

19 E. Maimon, A. Samuni and S. Goldstein, *J. Phys. Chem.*, 2018, **122**, 3747–3753.

20 A. A. Bobko and V. V. Khramtsov, *Nitric oxide*, 2014, **40**, 92–98.

4.4 Support information

4.4.1 Experimental section

*General Protocol for the ^1H NMR following of the $K_3[Fe^{III}(CN)_6]$ mediated oxidation of (di)azine hydroxamic acids **1**, **2** and **3***

The isonicotinohydroxamic acid (1 eq.) was added in phosphate buffer solution (0.1 M, pH 7.4) (3 mL). After solubilization of the substrate, $K_3[Fe(CN)_6]$ (2.5 eq.) was added to the hydroxamic acid solution. The mixture was stirred at room temperature and analyzed by ^{1}H NMR spectroscopy for 322 h.

*General protocol for the synthesis of N,O-diaroylhydroxylamines **4**, **5** and **6***

The hydroxamic acid (1 eq.) was added in phosphate buffer (0.1 M, pH 7.4) (3 mL). After solubilization of the substrate, $K_3[Fe(CN)_6]$ (2.5 eq.) was added to hydroxamic acid solution. The mixture was stirred at room temperature for 24 h. The mixture was extracted with EtOAc. The organic phase was concentrated under reduced pressure, and the solid residue was dried under vacuum before characterization.

*N,O-diisonicotinoylhydroxylamine (**4**)*

From isonicotinohydroxamic acid (0.100 g, 0.734 mmol) and $K_3[Fe(CN)_6]$ (0.604 g, 1.835 mmol). **^{1}H NMR** (400 MHz, DMSO-d_6) δ (ppm): 8.91(d, J = 4.4 Hz, 2H), 8.81 (d, J = 4.4 Hz, 2H), 7.98 (d, J = 4.4 Hz, 2H) and 7.79 (d, J = 4.4 Hz, 2H) (400 MHz, D_2O) δ (ppm): 8.80 (tt, J = 4.6, 1.6 Hz, 4H), 8.22 (dt, J = 5.2, 1.6 Hz, 2H), 8.13 (dt, J = 4.6, 1.6 Hz, 2H). **^{13}C NMR** (101 MHz, DMSO-d_6) δ (ppm): 167.7 (C=O), 166.0 (C=O), 149.7 (CH x 2), 147.8 (CH x 2), 146.0 (C), 137.5 (C), 123.4 (CH x 2), 122.7 (CH x 2). **IR** Symmetric stretching (ν_s), Antisymmetric stretching (ν_{as}), Symmetric bending (δ_s) and Twisting (τ) (cm^{-1}): 3465-3297 (ν_s N-H), (ν_s C-H), 1719 (ν_s C=O/ bonding to O), 1592 (ν_s C=O/ bonding to N) 1560 - 1499 (ν_s C=N, ν_sC=C), 1420 (δ_s N-H), 1269 (δ_s C-H), 1059 - 1015 (ν_{as} C=N), 854 (τ C-H). **HRMS** (ESI): *m/z* calcd. for $C_{12}H_9N_3O_3$: 244.0722 found: 244.0726.

*N,O-dinicotinoylhydroxylamine (**5**)*

From nicotinohydroxamic acid (0.100 g, 0.734 mmol) and $K_3[Fe(CN)_6]$ (0.604 g, 1.84 mmol). **^{1}H NMR** (400 MHz, DMSO-d_6) δ (ppm): 9.17 (dd, J = 2.2, 0.9 Hz, 1H), 9.00 (dd, J = 2.3, 0.9 Hz, 1H), 8.86 (dd, J = 4.8, 1.7 Hz, 1H), 8.68 (dd, J = 4.8, 1.7 Hz, 1H), 8.39 (dt, J = 8.0, 2.0

Hz, 1H), 8.18 (dt, *J* = 7.9, 2.0 Hz, 1H), 7.62 (ddd, *J* = 8.0, 4.9, 0.9 Hz, 1H), 7.50 – 7.45 (m, 1H). **HRMS** (ESI^+): *m/z* calcd. for $C_{12}H_9N_3O_3$: 244.0722, found: 244.0726.

*N,O-dipyrazinoylhydroxylamine (**6**)*

From pyrazinohydroxamic acid (0.100 g, 0.719 mmol) and $K_3[Fe(CN)_6]$ (0.592 g, 1.797 mmol). MS (DCI/CH_4): *m/z* = 230 [M**9** + $C_2H_5^+$], 217 [M**9** + CH_3^+], 202 [M**9** + H^+] and *m/z* = 124 [M**14** + H^+].

*General protocol for the synthesis of N-methylisonicotinamide, N-methylnicotinamide, and N-methylpyrazinamide **16**, **17** and **18***

The hydroxamic acid (1 eq.) and NH_2CH_3 40% in water (10 eq.) was added to a phosphate buffer solution (0.1 M, pH 7.4) (3 mL). After solubilization of the substrate, $K_3[Fe(CN)_6]$ (2.5 eq.) was added to hydroxamic acid solution. The mixture was stirred at room temperature for 2 h. The solvent was removed by evaporation under reduced pressure. The crude material was purified by silica gel flash column chromatography using a mixture of MeOH/DCM (0-100 / 10-90) as eluent.

*N-methylisonicotinamide (**16**)*

From isonicotinohydroxamic acid (0.10 g, 0.734 mmol), NH_2CH_3 40% in water (0.228 g, 7.35 mmol) and $K_3[Fe(CN)_6]$ (0.604 g, 1.84 mmol). **Yield** = 79% (0.078 g), white solid. **^{1}H NMR** (400 MHz, DMSO-d_6) δ (ppm): 8.78 – 8.65 (m, *J* = 4.44, 3H (In this case, the N-H part, there is in the same zone of the C-H of the ring), 7.73 (d, *J* = 4.44, 2H), 2.80 (d, *J* = 4.6 Hz, 3H). **^{13}C NMR** (101 MHz, D_2O) δ (ppm): 164.99 (C=O), 150.22 (CH x 2), 141.36 (C), 121.10 (CH x 2), 26.25 (CH_3). **IR** Symmetric stretching (ν_s), antisymmetric stretching (ν_{as}), symmetric bending (δ_s) and twisting (τ) (cm^{-1}): 3348-3304 (ν_s N-H), 3000-2852 (ν_s C-H), 1644 (ν_s C=O), 1543 - 1494 (ν_s C=N, ν_s C=C), 1407 (δ_s N-H), 1311 (δ_s C-H), 1065 (ν_{as} C=N), 838 (τ C-H). **UV-Vis** (H_2O) λ_{max}/nm (ε/$M^{-1}cm^{-1}$) = 266 (2706), 232 (4032), 221 (4535), 213 (5750). **HRMS** (DCI/CH_4): *m/z* calcd. for [($C_7H_8N_2O$) + H^+] 137.0715, found: 137.0712. **Elemental Anal.** calcd. for $C_7H_8N_2O{\cdot}0.15H_2O$: C, 60.55; H, 6.03; N, 20.17. Found: C, 60.95; H, 6.13; N, 19.73. **TLC Retention Factor** (MeOH/DCM 10%) = 0.41. M.p. = 113 ºC.

*N-methylnicotinamide (**17**)*

From nicotinohydroxamic acid (0.10 g, 0.734 mmol), NH_2CH_3 40% in water (0.228 g, 7.35 mmol) and $K_3[Fe(CN)_6]$ (0.604 g, 1.84 mmol). **Yield** = 68 % (0.067 g), white solid. **^{1}H NMR**

(400 MHz, DMSO-d_6) δ (ppm): 8.98 (d, *J* = 2.3 Hz, 1H), 8.69 (dd, *J* = 4.9, 1.6 Hz, 1H), 8.62 (s, 1H), 8.16 (dt, *J* = 8.0, 2.0 Hz, 1H), 7.49 (dd, *J* = 8.0, 4.8 Hz, 1H), 2.80 (d, *J* = 4.6 Hz, 3H). **^{13}C NMR** (101 MHz, D_2O) δ (ppm): 165.18 (C=O), 151.73 (CH), 148.25 (CH), 134.80 (CH), 129.96 (C), 123.47 (CH), 26.20 (CH_3). **IR** Symmetric stretching (ν_s), antisymmetric stretching (ν_{as}), symmetric bending (δ_s) and twisting (τ) (cm^{-1}): 3331 (ν_s N-H), 3091 - 2854 (ν_s C-H), 1644 (ν_s C=O), 1549 - 1484 (ν_s C=N, ν_s C=C), 1412 (δ_s N-H), 1315 (δ_s C-H), 1029 (ν_{as} C=N), 829 (τ C-H). **UV-Vis** (H_2O) λ_{max}/nm ($\varepsilon/M^{-1}cm^{-1}$) = 263 (3286), 212 (6723). **HRMS** (DCI/CH_4): *m/z* calcd. for [($C_7H_8N_2O$) + H^+]: 137.0670, found: 137.0706. **Elemental Anal.** calcd. for $C_7H_8N_2O{\cdot}0.2H_2O$: C, 60.16; H, 6.06; N, 20.04. Found: C, 60.07; H, 5.87; N, 19.67. **TLC Retention Factor** (MeOH/DCM 10%) = 0.47. M.p = 108 ºC.

*N-methylpyrazinamide (**18**)*

From pyrazinohydroxamic acid (0.10 g, 0.729 mmol) NH_2CH_3 40% in water (0.226 g, 7.29 mmol) and $K_3[Fe(CN)_6]$ (0.600 g, 1.82 mmol). **Yield** = 69% (0.068 g), white solid. **^{1}H NMR** (400 MHz, DMSO-d_6) δ (ppm): 9.17 (d, *J* = 1.4 Hz, 1H), 8.89 (s, 1H), 8.85 (d, *J* = 2.5 Hz, 1H), 8.71 (dd, *J* = 2.4, 1.6 Hz, 1H), 2.83 (d, *J* = 4.8 Hz, 3H). **^{13}C NMR** (101 MHz, D_2O) δ (ppm): 163.29 (C=O), 147.37 (CH), 144.87 (C), 143.35 (CH), 143.32 (CH), 25.98 (CH_3). **IR** Symmetric stretching (ν_s), antisymmetric stretching (ν_{as}), symmetric bending (δ_s) and twisting (δ) (cm^{-1}): 3358 (ν_s N-H), 2929 (ν_s C-H), 1669 (ν_s C=O), 1583 - 1542 (ν_s C=N, ν_s C=C), 1404 (δ_s N-H), 1294 (δ_s C-H), 1054 - 1024 (ν_{as} C=N), 868 (τ C-H). **UV-Vis** (H_2O) λ_{max}/nm ($\varepsilon/M^{-1}cm^{-1}$) = 310 (657), 270 (7045), 209 (8544). **HRMS** (DCI/CH_4): *m/z* calcd. for [($C_6H_7N_3O$) + H^+]: 138.0667, found: 137.0662. **TLC Retention Factor** (MeOH/DCM 10%) = 0.58. M.p = 110 ºC.

General protocol for the synthesis of sodium isonicotinoate, nicotinoate and pyrazinoate molecules

To a mixture of the suitable carboxylic acid (1 eq.) in water (8 mL) was added a solution of NaOH (0.85 eq.) in water (2 mL). The solution was stirred at room temperature for 30 min. The solvent was removed by evaporation under reduced pressure at 50 ºC. The solid obtained was characterized.

*Sodium Isonicotinoate (**7b**)*

From isonicotinic acid (0.12 g, 0.975 mmol) and NaOH (0.033 g, 0.817 mmol). **Yield** = 99.0% (0.140 g), white solid. **^{1}H NMR** (400 MHz, D_2O) δ (ppm): 8.64 (d, *J* = 2H), 7.78 (d, *J*

= 2H). **^{13}C NMR** (101 MHz, D_2O) δ (ppm): 173.28 (C=O), 148.42 (CH x 2), 147.47 (C), 124.19 (CH x 2), 49.50 (reference: CH_3OD). **IR** Symmetric stretching (ν_s), Antisymmetric stretching (ν_{as}), Symmetric bending (δ_s) and Twisting (τ) (cm^{-1}): 1576 (ν_s C=O), 1528 - 1408 (ν_s C=N, C=C), 1300 (δ_s C-H), 1012 (ν_{as} C=N), 760 (τ C-H). **UV-Vis** (H_2O) λ_{max}/nm ($\varepsilon/M^{-1}cm^{-1}$) = 268 (2343), 211 (6575). **Elemental Anal.** calcd. for $NaC_6H_4O_2 \cdot 0.1H_2O$: C, 49.06; H, 2.88; N, 9.54. Found: C, 49.10; H, 2.52; N, 9.45. Retention Factor (MeOH/DCM 50%) = 0.6.

*Sodium Nicotinoate (**8b**)*

From nicotinic acid (0.12 g, 0.975 mmol) and NaOH (0.033 g, 0.817 mmol). **Yield** = 99.5 % (0.14 g), white solid. **^{1}H NMR** (300 MHz, D_2O) δ (ppm): 8.95 (dd, *J* = 2.2, 0.9, 1H), 8.62 (dd, *J* = 5.1, 1.7, 1H), 8.34 (ddd, *J* = 8.0, 2.2, 1.7, 1H), 7.59 (ddd, *J* = 8.0, 5.1, 0.9, 1H). **^{13}C NMR** (101 MHz, D_2O) δ (ppm): 172.98 (C=O), 149.74 (CH), 148.51 (CH), 139.65 (CH), 133.54 (C), 125.04 (CH), 49.50 (reference: CH_3OD). **IR** Symmetric stretching (ν_s), Antisymmetric stretching (ν_{as}), Symmetric bending (δ_s) and Twisting (τ) (cm^{-1}): 1610 (ν_s C=O), 1562 - 1403 (ν_s C=N, ν_s C=C), 1322 (δ_s C-H), 1029 (ν_{as} C=N), 752 (τ C-H). **UV-Vis** (H_2O) λ_{max}/nm ($\varepsilon/M^{-1}cm^{-1}$) = 272 (2137), 265 (2819), 260 (2549), 212 (7350). **Elemental Anal.** calcd. for $NaC_6H_4O_2 \cdot 0.4H_2O$: C, 47.32; H, 3.18; N, 9.20. Found: C, 47.35; H, 2.96; N, 9.48. **TLC Retention Factor** (MeOH/DCM 50%) = 0.6.

*Sodium pyrazinoate (**9b**)*

From pyrazine-2-carboxylic acid (0.12 g, 0.970 mmol) and NaOH (0.033 g, 0.817 mmol). **Yield** = 87.5 % (0.124 g), white solid. **^{1}H NMR** (400 MHz, D_2O) δ (ppm): 9.09 (d, *J* = 1.1 Hz, 1H), 8.70 (m, 2H). **^{13}C NMR** (101 MHz, D_2O) δ (ppm): 170.87 (C=O), 148.54 (C), 146.46 (CH), 145.13 (CH), 144.79 (CH), 49.50 (reference: CH_3OD). **IR** Symmetric stretching (ν_s), Antisymmetric stretching (ν_{as}), Symmetric bending (δ_s) and Twisting (τ) (cm^{-1}) (cm^{-1}): 1620 (ν_s C=O), 1572 - 1428 (ν_s C=N, ν_s C=C), 1384 (δ_s C-H), 1012 (ν_{as} C=N), 844 (τ C-H). **UV-Vis** (H_2O) λ_{max}/nm ($\varepsilon/M^{-1}cm^{-1}$) = 313 (639.4), 271 (7074), 204 (7345). **Elemental Anal.** calcd. for $NaC_6H_4O_2$: C, 41.11; H, 2.07; N, 19.18. Found: C, 41.33; H, 1.65; N, 19.06. **TLC Retention Factor** (MeOH/DCM 50%) = 0.5.

Figure S1 - ^{1}H NMR spectra of a) sodium isonicotinoate, b) sodium nicotinoate acid, c) sodium pyrazinoate.

a)

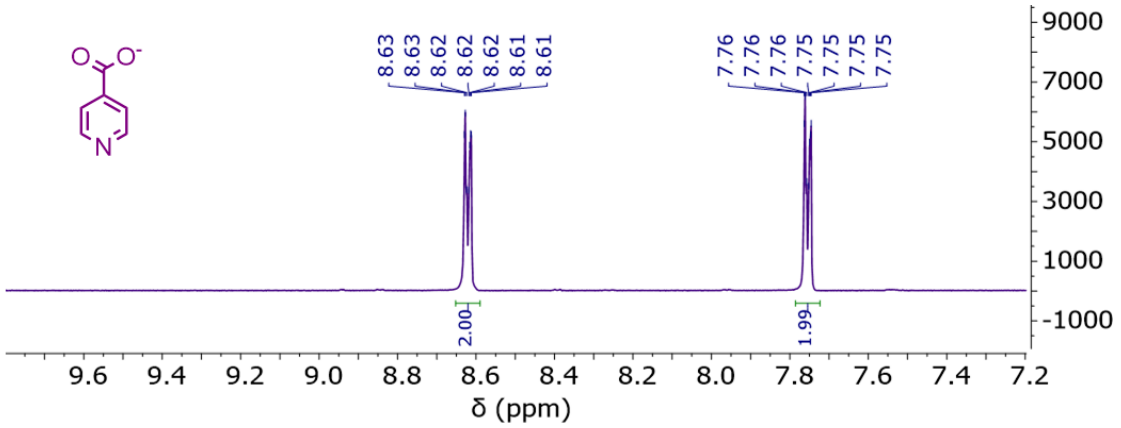

b)

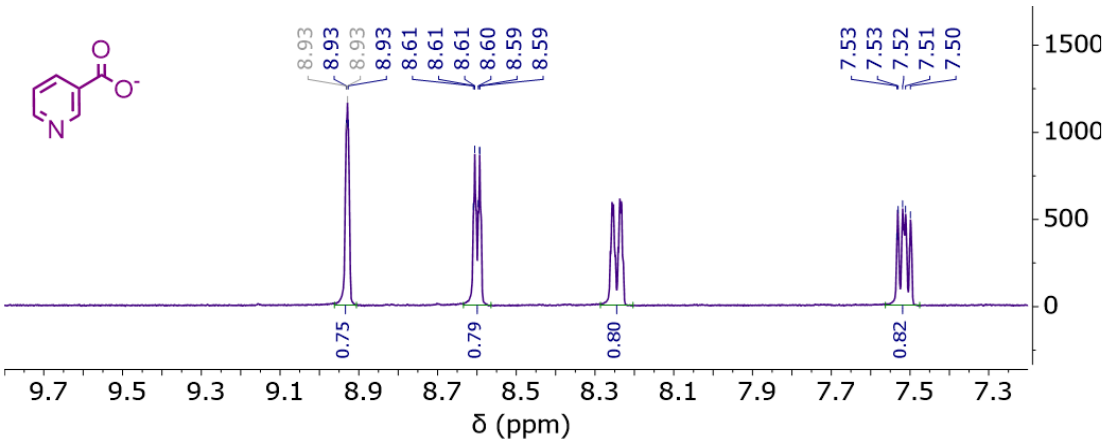

c)

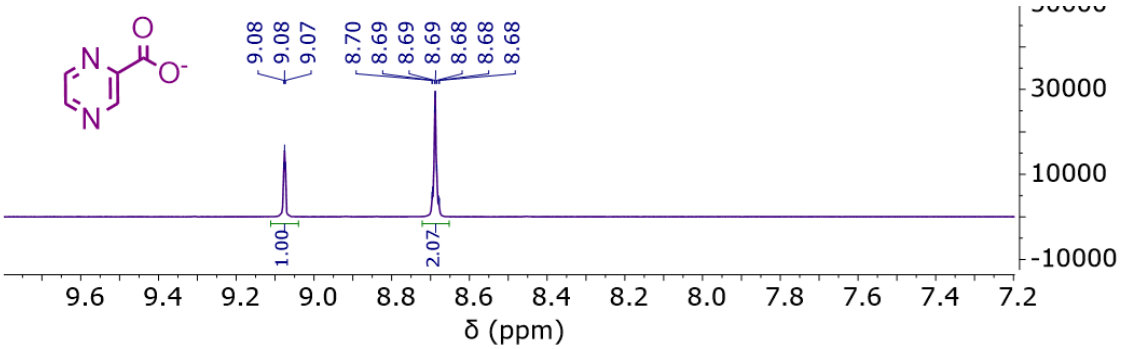

Reference: Elaborated by the author.

Figure S2 - Mass spectra of a) isonicotionohydroxamic acid, b) nicotinohydroxamic acid and c) pyrazinohydroxamic acid.

a)

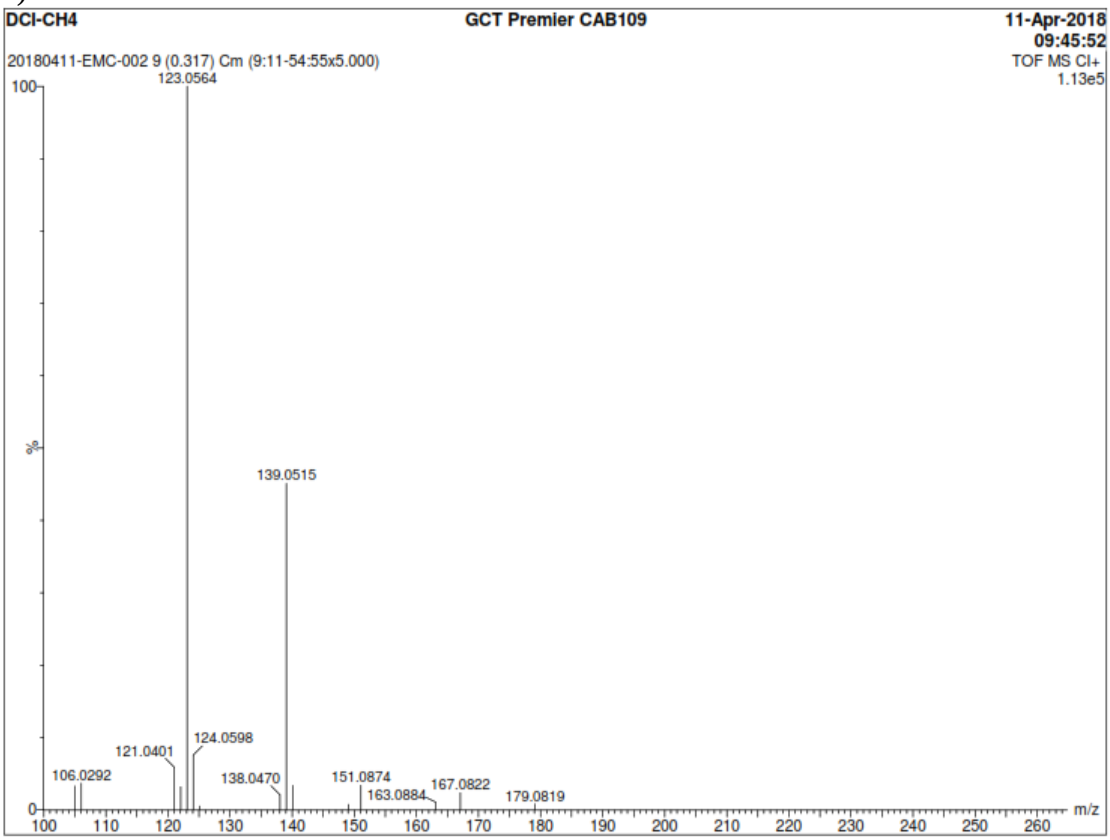

b)

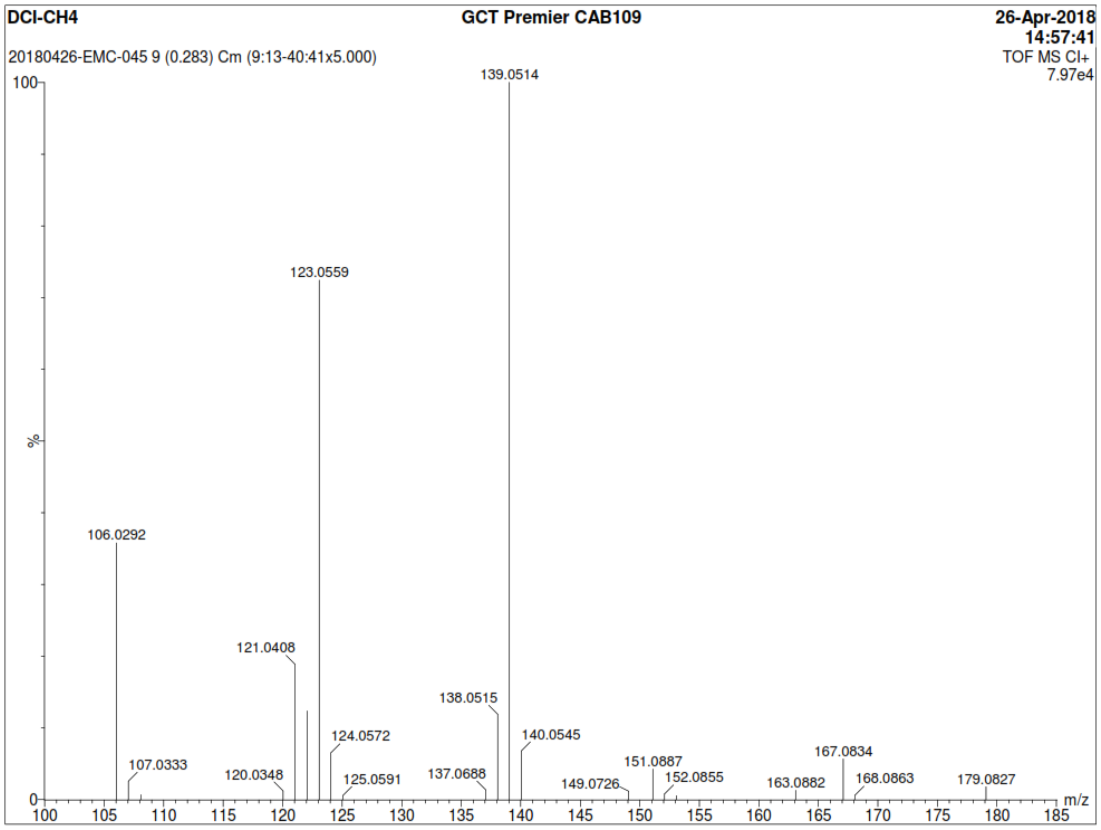

c)

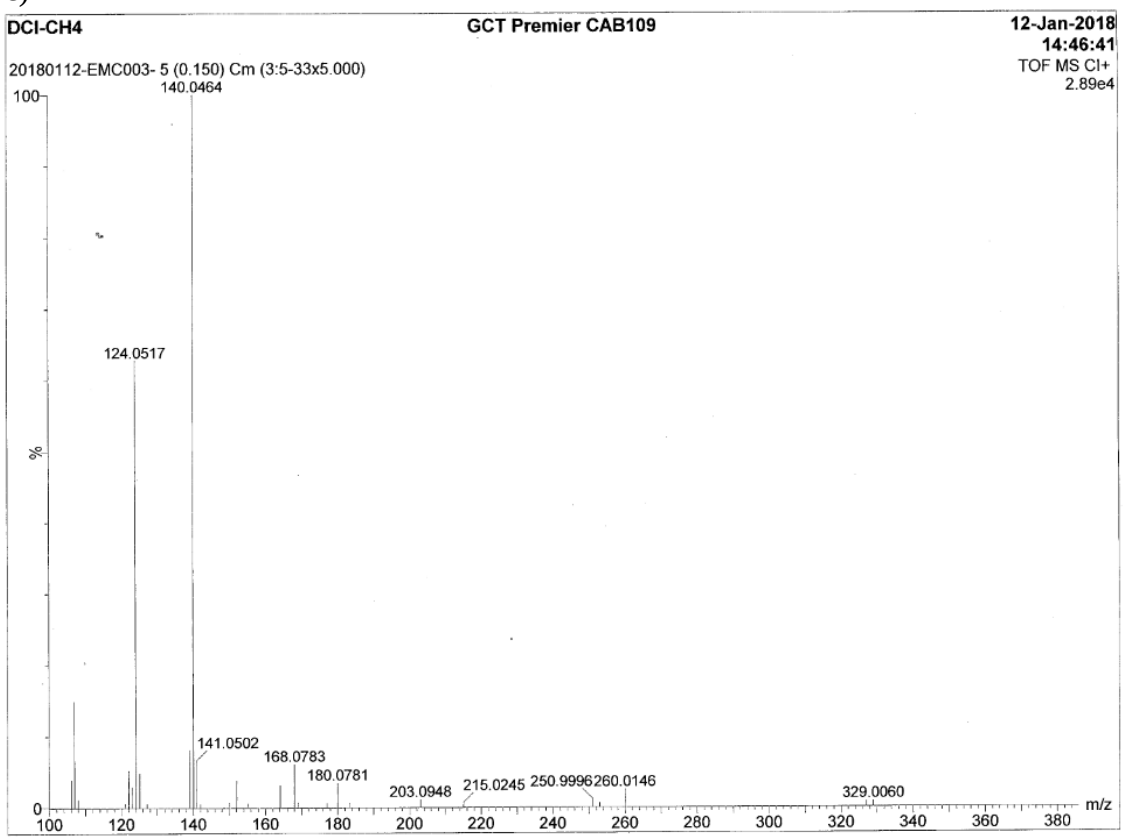

Reference: Elaborated by the author.

Figure S3 - Reactions of cPTIO with NO• or HNO, and EPR patterns of the products.

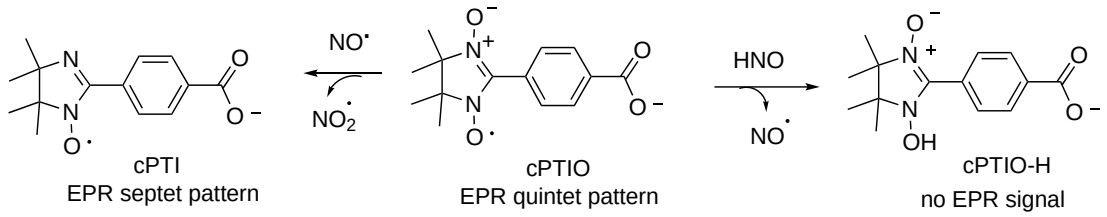

Reference: Elaborated by the author.

Figure S4a - EPR spectra of the controls: a) cPTIO (200 µM), b) cPTIO (200 µM) and $[Fe(CN)_6]^{3-}$ (15 mM), c) cPTIO (200 µM) and $[Fe(CN)_6]^{4-}$ (15mM), d) cPTIO (200 µM) and isonicotinohydroxamic acid (5 mM), e) cPTIO (200 µM) and nicotinohydroxamic acid (5 mM), and f) cPTIO (200 µM) and pyrazinohydroxamic acid (5 mM) 5.5 hours in phosphate buffer 40 mM, pH 7.4 at room temperature.

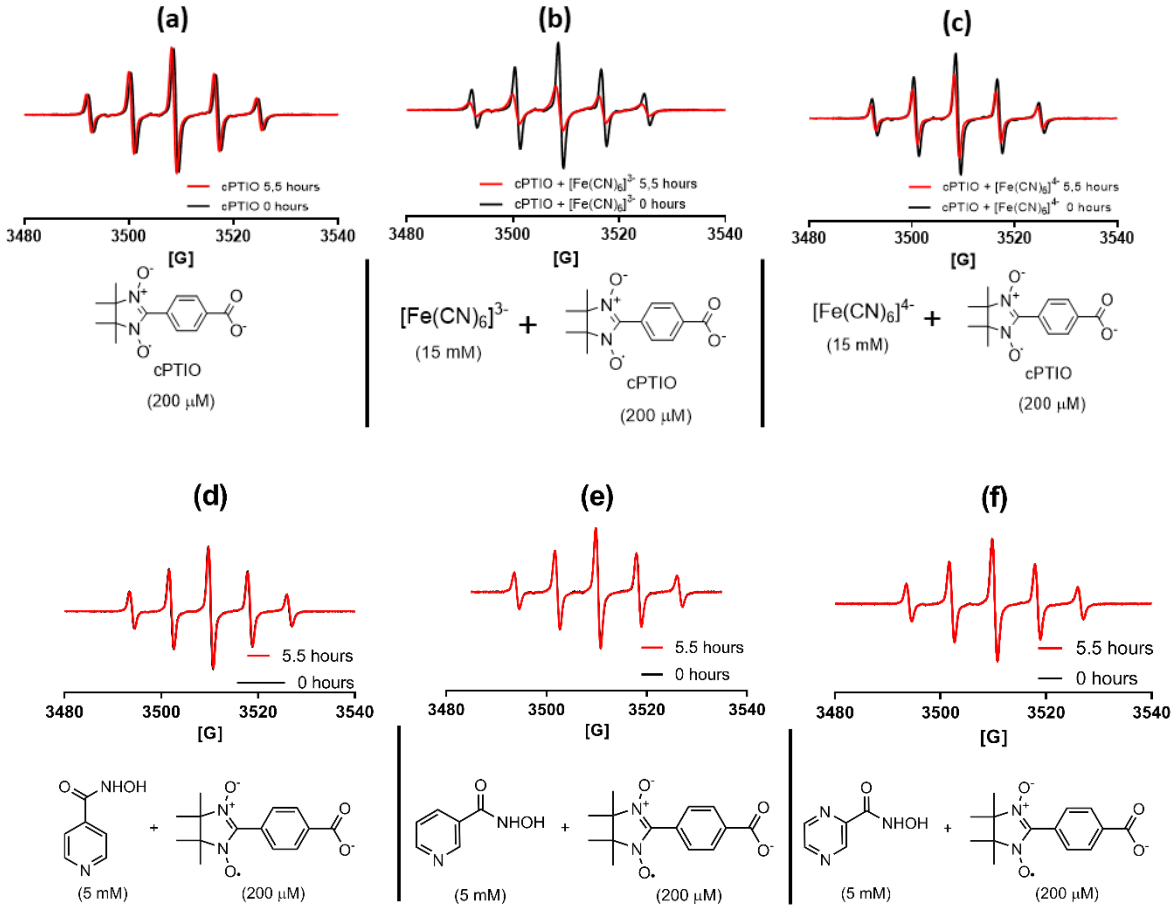

Reference: Elaborated by the author.

Figure S4b - EPR signal intensity of the reaction of isonicotinohydroxamic acid, nicotinohydroxamic acid and pyrazinohydroxamic acid (5 mM) with $[Fe(CN)_6]^{3-}$ (15 mM) in the presence of cPTIO (200 µM) at 0 and 5.5 h in phosphate buffer 40 mM (pH 7.4) and at room temperature.

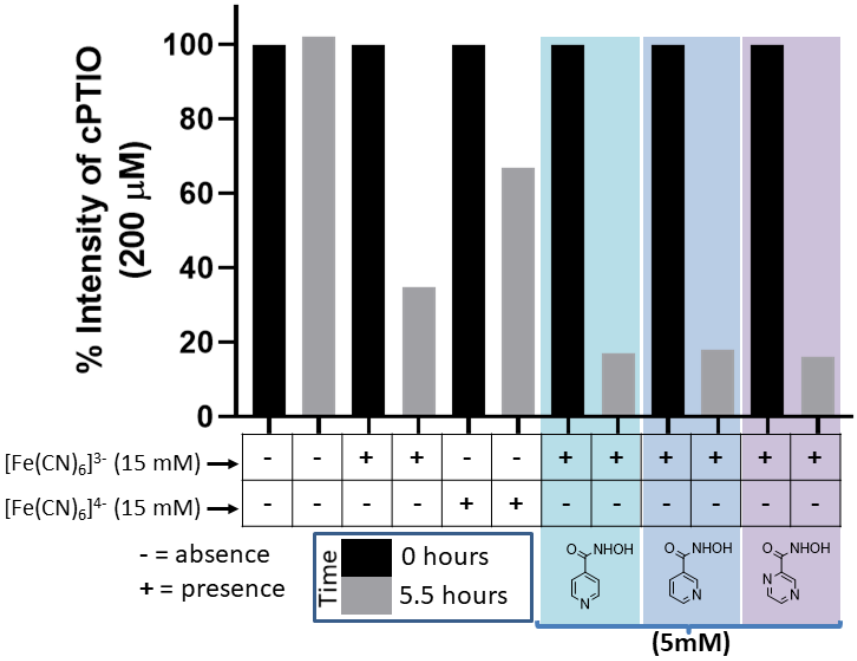

Reference: Elaborated by the author.

Figure S5 - UV-Vis absorption monitoring at 0-24 h of the evolution of a mixture of cPTIO (150 µM) and $K_3[Fe^{III}(CN)_6]$ (15 mM) in 40 mM phosphate buffer (pH 7.4) at room temperature.

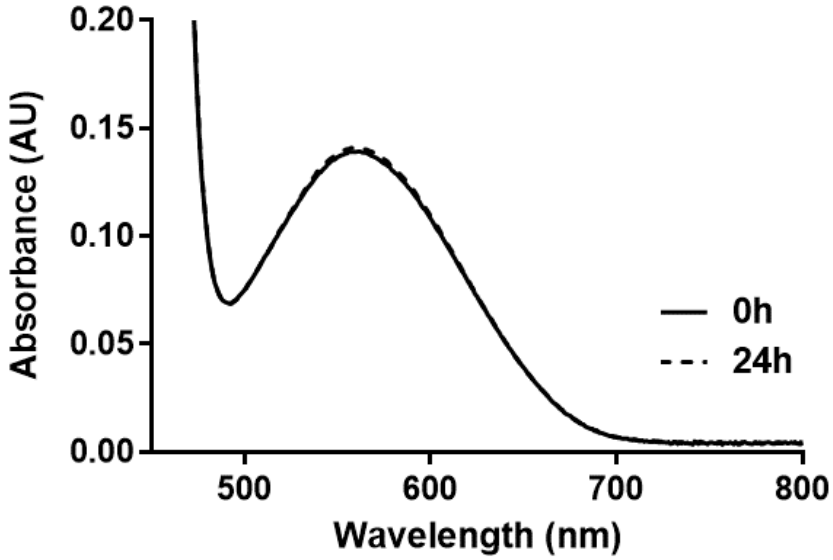

Reference: Elaborated by the author.

4.5 Unpublished results associated with the article

The oxidative reaction of the hydroxamic acids synthesized in this work was also studied in the presence of PBN (*N*-tert-butyl-α-phenylnitrone) spin trap, aiming at the detection of the aroyl radical as a potential intermediate. Furthermore, the Diels-Alder reaction was also investigated as a strategy to demonstrate the possible formation of a nitroso intermediate during oxidation of the isonicotino-hydroxamic acid ligand.

An attempt to synthesize a new pentacyanoferrate(II) complex based on the hybridization of isoniazid (INH) and pyrazinamide was also made. The results obtained from these experiments are presented and discussed briefly below.

4.5.1 Experimental section

Attempts to detect the aroyl radical

The experiments were monitored by EPR technique. All samples used were prepared in 40 mM phosphate buffer pH 7.4, at 0 °C, by mixing appropriate amounts of studied compound and PBN dissolved in phosphate buffer solution. The reactions were initiated by the addition of the oxidant (H_2O_2 or $[Mn(H_2P_2O_7)_3]^{3-}$). The first spectrum was recorded ca. 2 min after initiating the reaction. In the control experiments were used solutions containing INH (1 mL at 5 mM) or IQG607 (1 mL at 5 mM), the oxidizing agent (1 mL at 2.5 mM of $[Mn(H_2P_2O_7)_3]^{3-}$ for the INH oxidation, and 1 mL at 5 mM or 15 mM of the H_2O_2 for the IQG607 oxidation), and PBN (1 mL at 20 mM).

Attempt to trap the acyl nitroso intermediate via Diels-Alder reaction

The oxidative activation reaction of the isonicotino-hydroxamic acid ligand, in the presence of cyclohexa-1,3-diene, was performed using a THF:H_2O (2:1, 6 mL) solution containing the isonicotino-hydroxamic acid ligand (0.05 g, 36.2 mmol) and cyclohexa-1,3-diene (48.9 μL, 54.3 mmol, 97%). $K_3[Fe(CN)_6]\cdot 3H_2O$ (0.333 g, 90.5 mmol) was added in the previous solution and the mixture was stirred for 96 h at room temperature.[339] The organic phase was extracted with ethyl acetate (3 x 6 mL), combined, dried over $MgSO_4$ (anhydrous) and concentrated under vacuum. The crude was purified by flash chromatography (eluent: dichloromethane/methanol: 100/0 to 95/5).

4.5.2 Synthetic procedures

Oxidant agent $[Mn(H_2P_2O_7)_3]^{3-}$

The $[Mn(H_2P_2O_7)_3]^{3-}$ was prepared following the literature procedure with some adaptations.[340] Pyrophosphoric acid (1.75 mL, 5 M) was added dropwise in a pyrophosphate sodium solution (25 mL, 200 mM). The pH was measured at 4.4. Then, $Mn^{III}(OAc)_3{\cdot}2H_2O$ (0.027 g, 0.1 mmol) was added in the latter solution. The mixture was stirred overnight (16 h). After the time reaction, the concentration of the product $[Mn(H_2P_2O_7)_3]^{3-}$ was determined based on literature data: ε 6200 $M^{-1}cm^{-1}$ at 260 nm or 104 $M^{-1}cm^{-1}$ at 480 nm, the valor obtained for this synthesis was 3.7 mM. The final product is stable for several months at 4 ºC.

Ligand N'-(pyridine-4-carbonyl) pyrazine-2-carbohydrazide

A suspension of pyrazinoic acid (0.104 g, 0.838 mmol) in thionyl chloride (1.2 mL, 16.6 mmol) was refluxed at 75 ºC for 2.5 h. The color of solution changed from white to strong violet color. The excess of the thionyl chloride was then removed under vacuum. The crude was resuspended in dichloromethane (2 mL) and cooled to 0 ºC. INH (0.114 g, 0.838 mmol) and triethylamine (0.28 mL, 1.68 mmol) was added in the pyrazinoic acid solution. The reaction was stirred overnight (16 h) at r.t, and the residue was concentrated under vacuum (Scheme 23). The crude was purified by flash chromatography (eluent: dichloromethane/methanol: 100/0 to 94/6). The white solid was washed several times (4x) with dichloromethane.

Scheme 23 - Synthesis of *N'*-(pyridine-4-carbonyl) pyrazine-2-carbohydrazide.

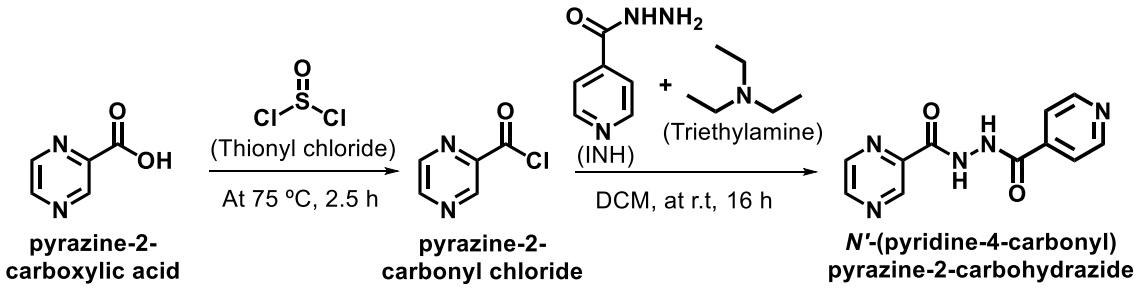

Reference: Elaborated by the author.

Yield = 39% (0.080 g), white solid. **^{1}H NMR** (400 MHz, DMSO-d_6) δ (ppm): 10.98 (s, 1H), 10.93 (s, 1H), 9.22 (d, *J* = 1.4 Hz, 1H), 8.95 (d, *J* = 2.5 Hz, 1H), 8.81 (m, 3H), 7.83 (d, *J* = 4.0 Hz, 2H). **^{13}C NMR** (101 MHz, DMSO-d_6) δ (ppm): 164.45 (C), 162.76 (C), 150.95 (CH x 2), 148.59 (CH), 144.52 (C), 144.23 (CH), 144.14 (CH), 139.85 (C), 121.79 (CH x 2). **IR**

Symmetric stretching (ν_s), Antisymmetric stretching (ν_{as}), Symmetric bending (δ_s) and Twisting (τ) (cm^{-1}): 3304-3244 (ν_s N-H), 1708-1660 (ν_s C=O), 1546-1468 (ν_s C=N, ν_s C=C), 1402 (δ_s N-H), 1282 (δ_s C-H), 1024-994 (ν_{as} C=N), 850 (τ C-H). **UV-Vis** (H_2O) λ_{max}/nm ($\varepsilon/M^{-1}cm^{-1}$) = 214 (15930), 274, (12480), 324 (914), 379 (188). **MS** (DCI/NH_3): m/z calcd. for $C_{11}H_9N_5O_2$: 243.2, found: 244.0 $(M + H)^+$. **Elemental Anal.** calcd. For $C_{11}H_9N_5O_2$: C, 54.32; H, 3.73; N, 28.79. Found: C, 53.92; H, 3.34; N, 28.44. **TLC Retention Factor** (MeOH/DCM 10%) = 0.41. **M.p**. = 215 °C.

Complex $Na_6[Fe_2(CN)_{10}$(N'-(pyridine-4-carbonyl) pyrazine-2-carbohydrazide)]

To a solution of $Na_3[Fe^{II}(CN)_5(NH_3)]\cdot 3H_2O$ (0.100 g, 0.31 mmol, 2 equiv.) in degassed water (2 mL), it was slowly added a solution of the ligand *N'*-(pyridine-4-carbonyl) pyrazine-2-carbohydrazide (0.038 g, 0.155 mmol, 1 equiv.) in degassed water (1 mL). The mixture was stirred at room temperature, under argon atmosphere and protected from light for 3 h. Then 100 mL of a cold solution of ethanol containing an excess of sodium iodide (30 equiv.) was added dropwise. The resulting suspension was kept overnight (16 h) at -20 °C before the precipitate was filtered, washed with cold ethanol, and dried in a vacuum desiccator.

4.5.3 Results and discussion

Attempts to detect aroyl radical

In order to check whether an aroyl radical is formed as intermediate during the hydroxamic acids oxidation, reactions using $[Mn(H_2P_2O_7)_3]^{3-}$ or H_2O_2 as oxidizing agents and PBN (*N*-tert-butyl-α-phenylnitrone), a well-known trap for carbon-centered radicals,[37,338] in phosphate buffer (40 mM, pH 7.4) were performed.

The INH and IQG607 were used as positive controls. Oxidation of INH by $[Mn(H_2P_2O_7)_3]^{3-}$ in the presence of PBN led to the formation of an EPR signal mainly consisting of a six-line spectrum with hyperfine splitting constants of a_N = 15.5 - 15.8 G and a_H = 3.2 - 3.6 G for a g-value of 2.006 attributed to the trapping, by PBN, of the isonicotinoyl radical (Figure 34A). Oxidation of IQG607 by H_2O_2 resulted in a six-line spectrum with hyperfine splitting constants of a_N = 15.5 - 15.6 G and a_H = 4.5 - 4.6 G for a g-value of 2.006, ascribed to the acyl radical of the IQG607 trapped by PBN, (Figure 34B), as described by Sousa and his collaborators.[37,338]

Figure 34 - EPR signals for PBN-spin trap experiments controls. A. Mixture of INH (5 mM), $[Mn(H_2P_2O_7)_3]^{3-}$ (2.5 mM), and PBN (20 mM) in phosphate buffer (40 mM, pH 7.4). B. Mixture of IQG607 (5 mM), H_2O_2 (5 mM) and PBN (20 mM) in phosphate buffer (40 mM, pH 7.4).

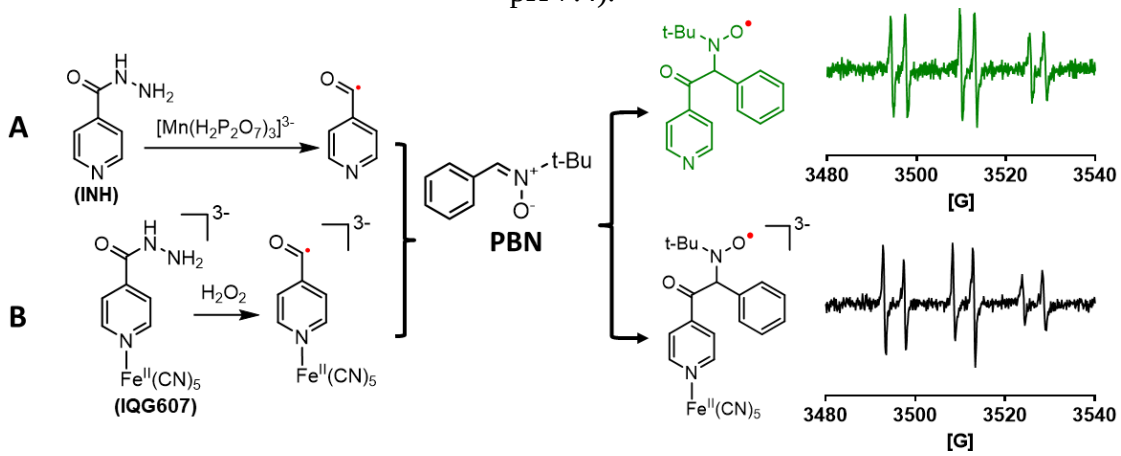

Reference: Elaborated by the author.

After the control experiments, the next step was then to study the chemical activation of isonicotino-, nicotino-, and pyrazino-hydroxamic acids free ligands and complexed with $Fe^{II}(CN)_5$ moiety in the presence of $[Mn(H_2P_2O_7)_3]^{3-}$ and PBN, in phosphate buffer (40 mM, pH 7.4). The resulting EPR spectra did not show any detectable signal (Figure 35A). In order to study the influence of the coordination to the pentacyanoferrate(II) moiety in the process of the oxidative activation, the same experiment was performed using the isonicotino-, nicotino-, and pyrazino-hydroxamic acids Fe^{II} complexes (Figure 35B), no signal was detectable, as well.

Figure 35 - EPR signals for PBN-spin trap experiments. A. Mixture of ligand (5 mM), $[Mn(H_2P_2O_7)_3]^{3-}$ (2.5 mM) and PBN (20 mM) in phosphate buffer (40 mM, pH 7.4). B. Mixture of complex (5 mM), $[Mn(H_2P_2O_7)_3]^{3-}$ (2.5 mM) and PBN (20 mM) in phosphate buffer (40 mM, pH 7.4). The vertical scale was kept identical for all spectra.

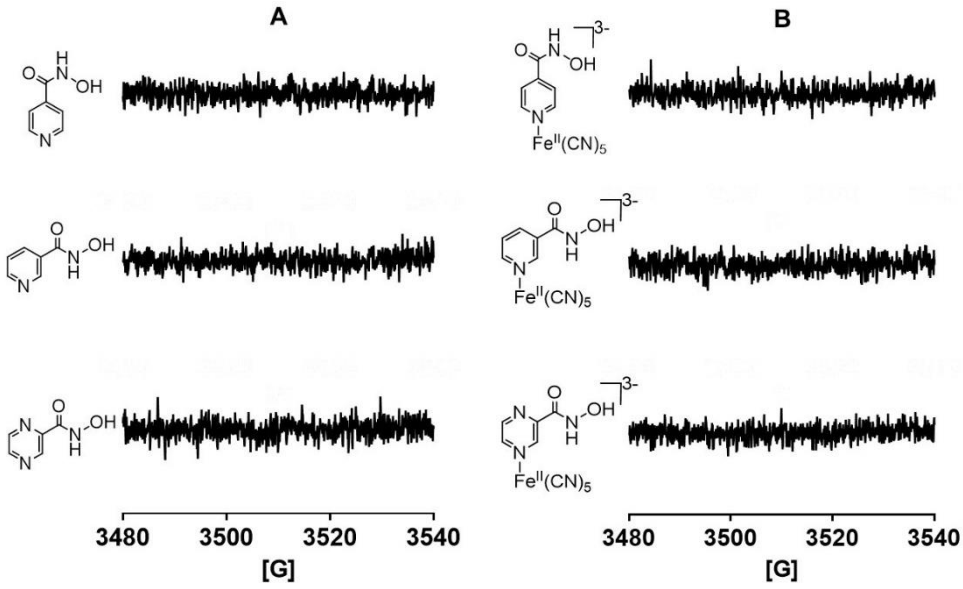

Reference: Elaborated by the author.

Then, similarly to the previous tests, the chemical activation of the isonicotino- and pyrazino-hydroxamic acid complexes was mediated by H_2O_2 and monitored by EPR in the presence of PBN, in phosphate buffer (40 mM, pH 7.4). Under these conditions, using two different proportions of complex:H_2O_2 (1:1 and 1:3), no signal was observed for the both complexes (Figure 36). In view of these results, experiments with the nicotino-hydroxamic acid pentacyanoferrate complex were not carried out. Altogether these results indicate that the aroyl radical is not an intermediate of the oxidation mechanism of the hydroxamic acid derivatives studied, corroborating the mechanistic proposition of this chapter.

Figure 36 - EPR signals for PBN-spin trap experiments. A. Mixture of isonicotino hydroxamic acid complex (5 mM), H_2O_2 (5 (black) or 15 (green) mM) and PBN (20 mM) in phosphate buffer (40 mM, pH 7.4). B. Mixture of pyrazino hydroxamic acid complex (5 mM), H_2O_2 (5 (black) or 15 (green) mM) and PBN (20 mM) in phosphate buffer (40 mM, pH 7.4). The vertical scale was kept identical for all spectra.

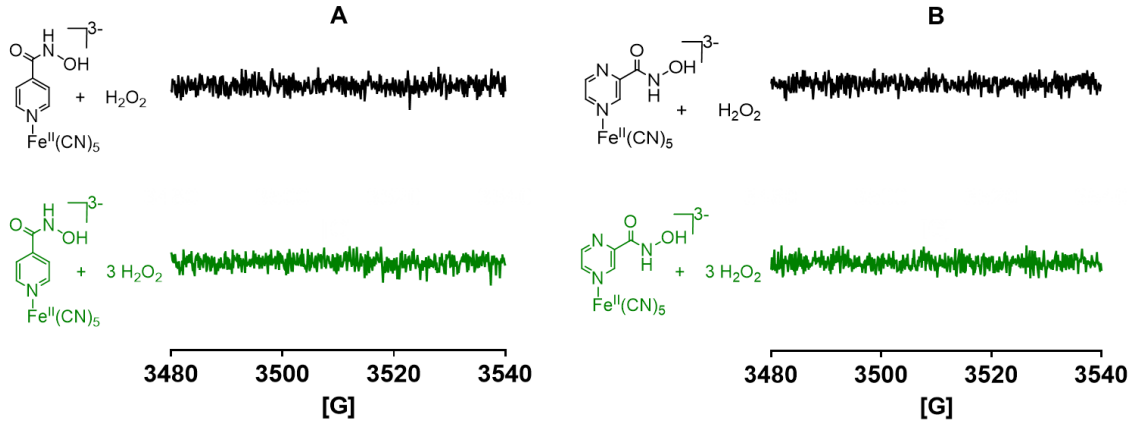

Reference: Elaborated by the author.

Attempts to trap the potential acyl nitroso intermediate by Diels-Alder reaction

As mentioned in article 2 (section 5.3), nitroso compound is one of the main intermediates proposed for hydroxamic acids oxidation. The Diels-Alder reactions, in organic solvent media, have been used as an approach for the detection of nitroso intermediate.[339] In this work, we tried to use this strategy in THF aqueous conditions (THF:H_2O (2:1)). For this, the oxidation of the hydroxamic acid by $[Fe(CN)_6]^{3-}$ (oxidizing agent) was performed in the presence of cyclohexa-1,3-diene, aiming at production of the (2-oxa-3-azabicyclo[2.2.2]oct-5-en-3-yl)(pyridin-4-yl)methanone, which could be an evidence for the nitroso intermediate formation (Scheme 24).

Scheme 24 - Detection of the isonicotino nitroso intermediate by Diels-Alder reaction.

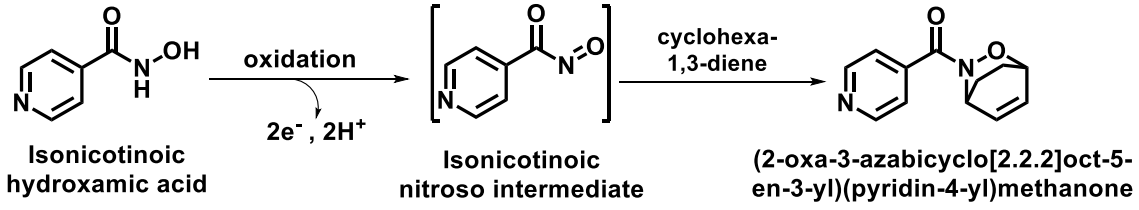

Reference: Elaborated by the author.

Nevertheless, the product of the reaction between the potential intermediate acyl nitroso and cyclohexa-1,3-diene was not observed. The ^{1}H NMR analysis of the crude, obtained at the end of the reaction, showed a higher percentage of the starting ligand and a small fraction of several other peaks non identifiable.

Complex $Na_6[Fe_2(CN)_{10}$(N'-(pyridine-4-carbonyl) pyrazine-2-carbohydrazide)]

Bearing in mind the idea of synthesizing new hybrid-type antituberculosis pro-drugs capable of exhibiting both isoniazid- (through isonicotinoyl radical potential formation) and pyrazinamide-like actions (through pyrazinoic acid potential formation), the synthesis of the binuclear complex $Na_6[Fe^{II}_2(CN)_{10}$(*N'*-(pyridine-4-carbonyl) pyrazine-2-carbohydrazide)] was investigated.

First, the ligand was prepared from a mixture of pyrazinoic acid and thionyl chloride (20 equiv.) at reflux (75 ºC), followed by, after solvent evaporation, addition of isoniazid and triethylamine in dichloromethane. More details are presented in the experimental part. The attempt to obtain the corresponding pentacyanoferrate complex was produced by reacting the ligand *N'*-(pyridine-4-carbonyl) pyrazine-2-carbohydrazide with the precursor $Na_3[Fe^{II}(CN)_5(NH_3)]$, following procedures already described for similar compounds.[37] Nevertheless, the desired compound was not obtained. By the ^{1}H-NMR technique, we observed that the product obtained corresponds to a mixture of pyridine-4-carboxylate and pyrazine-2-carboxylate compounds coordinated to $Fe(CN)_5$ moiety ($[Fe^{II}(CN)_5$(pyridine-4-carboxylate)$]^{4-}$ in D_2O, δ (ppm): 9.03 (d, *J* = 5.9, 2H), 7.46 (d, *J* = 5.9, 2H), and $[Fe^{II}(CN)_5$(pyrazine-2-carboxylate)$]^{4-}$ in D_2O, δ (ppm): 9.54 (s, 1H), 9.16 (d, *J* = 3.3 Hz, 1H), 8.28 (dd, *J* = 2.9, 1.5 Hz, 1H)), suggesting that the binuclear compound is very unstable and is rapidly oxidized and cleavage.

4.6 Conclusion

The oxidative activation of the hydroxamic acid compounds in the presence of PBN, did not show evidences for the aroyl radical formation, corroborating the activation mechanism proposed in this chapter *i.e.* passing through the *N,O*-di(di)azinoylhydroxylamine intermediate. The reaction of isonicotino-hydroxamic acid ligand, $[Fe(CN)_6]^{3-}$ and cyclohexa-1,3-diene in THF aqueous conditions did not lead to the Diels Alder adduct. Two explanations are possible: i) the nitroso compound is probably not the intermediate of oxidative reaction of hydroxamic acids or ii) the Diels Alder reaction does not work well under these THF-aqueous

conditions. Finally, the experimental results linked to synthesis of $Na_6[Fe_2(CN)_{10}$(*N*'-(pyridine-4-carbonyl) pyrazine-2-carbohydrazide)] showed that the desired product was not obtained. On the other hand, a mixture of the pentacyanoferrate(II) complexes, coordinated with the pyridine-4-carboxylate and pyrazine-2-carboxylate ligands were produced. The formation of such products may be related to the instability of the binuclear complex formed, which after undergoing oxidative reaction could form the acid compounds as mentioned.

4.7 Chapter 3 - New pro-drugs study of FeII hydroxamic acids complexes based: a new approach in antihypertensive and antituberculosis treatments

4.7.1 Article 3: Journal of Biological Inorganic Chemistry, 2020, 25, 887-901 - Résumé de l'article en français

Pentacyanoferrate(II) complex of pyridine-4- and pyrazine-2-hydroxamic acid as source of HNO: investigation of anti-tubercular and vasodilation activities

Edinilton Muniz Carvalho, Tercio de Freitas Paulo, Alix Sournia Saquet, Bruno Lopes Abbadi, Fernanda Souza Macchi, Cristiano Valim Bizarro, Rafael de Morais Campos, Talles Luann Abrantes Ferreira, Nilberto Robson Falcão do Nascimento, Luiz Gonzaga França Lopes, Remi Chauvin, Eduardo Henrique Silva Sousa, Vania Bernardes-Génisson.

*Journal of Biological Inorganic Chemistry, **2020**, 25, 887-901.*

La tuberculose (TB), maladie due à l'infection par *Mycobacterium tuberculosis* (*Mtb*), reste aujourd'hui un problème majeur de santé publique mondial causant plus d'un million de décès par an.[172] Bien que la guérison de la tuberculose puisse être obtenue par un régime thérapeutique impliquant les médicaments de première ligne (isoniazide (INH), la rifampicine, l'éthambutol et le pyrazinamide (PYZ)) (Figure 37), ce traitement de première intention devient inefficace face à des souches de *Mtb* résistantes à des multiples médicaments. Le PYZ est un promédicament qui est activé par la pyrazinamidase (PncA), une enzyme du *Mtb*.[341] Cette activation passe par la conversion du PYZ en l'acide carboxylique correspondant (acide pyrazinoïque), ce dernier reconnu comme étant l'agent toxique pour *Mtb*. Cependant, l'émergence de cas de souches résistantes à ce médicament a également limité son utilisation.[187]

Figure 37 - Structure des promédicaments antituberculeux rifampicine, isoniazide (INH), pyrazinamide (PZY), éthambutol et délamanide.

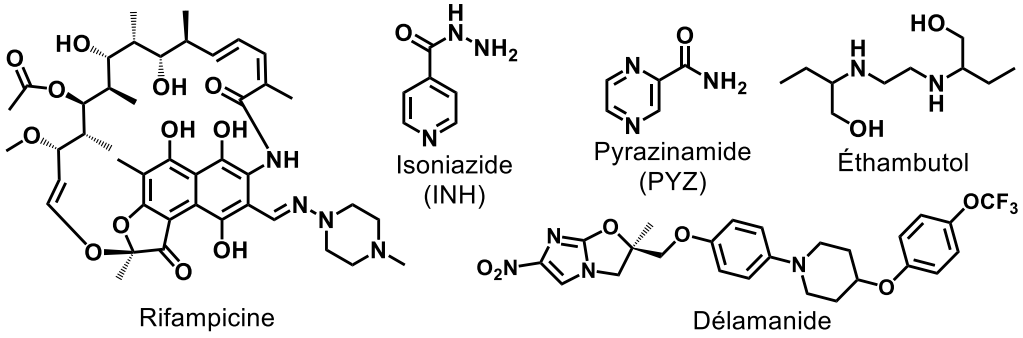

Référence : Élaboré par l'auteur.

Afin de surmonter les problèmes de résistances bactériennes dans le traitement de la TB, quelques nouveaux médicaments ont été développés. L'un de ces nouveaux médicaments est le délamanide (Figure 37), utilisé en troisième intention et approuvé pour le traitement de la tuberculose résistante.[342] Fort intéressant, il y a peu de cas de résistance rapportés pour ce médicament et son action est dirigée contre des souches de *Mtb* dormantes et réplicantes.[343] Le délamanide est en fait un promédicament nécessitant d'une étape d'activation enzymatique pour générer son métabolite actif, le HNO (nitroxyle). Une possible action émanant de NO• (oxyde nitrique) ne peut à ce jour être complètement exclue.[187]

Outre la tuberculose, les maladies cardiovasculaires représentent également un défi dans le domaine de la santé et la situation d'urgence appelle au développement de nouveaux agents thérapeutiques, y compris ceux capables de libérer NO• et HNO. Dans la lignée des médicaments donneurs de NO•, nous pouvons mettre en évidence le nitroprussiate de sodium (SNP) comme le seul donneur de NO•, à base de métal approuvé cliniquement pour les procédures cardiovasculaires d'urgence à l'hôpital.[24] En revanche, il n'existe actuellement aucun agent donneur de HNO cliniquement disponible.

Les acides hydroxamiques ont été classiquement signalés comme des espèces libérant des NO•/HNO après une réaction d'oxydation.[119] Dans cette même ligne d'activation oxydative, il a été décrit récemment dans la littérature, comme déjà cité précédemment, un système biomimétique, alternatif capable d'activer le promédicament antituberculeux INH tout en se franchissant de l'activation enzymatique par KatG à l'intérieur du *Mtb*. Ce système est basé sur la réactivité redox d'un complexe de Fe^{II} de l'INH ($[Fe^{II}(CN)_5(INH)]^{3-}$) qui en présence d'agents oxydants tels que H_2O_2,[37,344] génère le radical isonicotinoyle, espèce réactive de l'INH. L'activité antituberculeuse (*in vitro* MIC_{Mtb} ~ 3,5 μM),[38] la stabilité chimique et l'absence de toxicité (indice de sélectivité SI> 4000, DL50> 2000 mg/kg)[41] du complexe $[Fe^{II}(CN)_5(INH)]^{3-}$, nous a motivé à étendre cette approche d'activation aux acides

(di)azine hydroxamiques qui vont en fait servir de plateforme pour le développement de nouveaux complexes de fer capables de libérer HNO.

Cet article présente la synthèse et la caractérisation de deux complexes de pentacyanoferrate(II) avec l'acide hydroxamique pyrazinique (**3**) (analogue du PYZ) et l'acide hydroxamique isonicotinique (**6**) (analogue de l'INH) (Figure 38). Ces complexes ont été capables, par l'action d'un agent oxydant (H_2O_2), de générer du HNO et l'acide carboxylique correspondant : l'acide pyrazinique et isonicotinique, respectivement. Les oxydations du complexe **3** et **6** par H_2O_2 ont été suivies par RPE (à l'aide du piège sélectif cPTIO), UV-Vis et RMN ^{1}H, ceci dans le but d'étudier le mécanisme de la réaction d'oxydation.

Figure 38 - Complexes de type pentacyanoferrate(II) synthétisés.

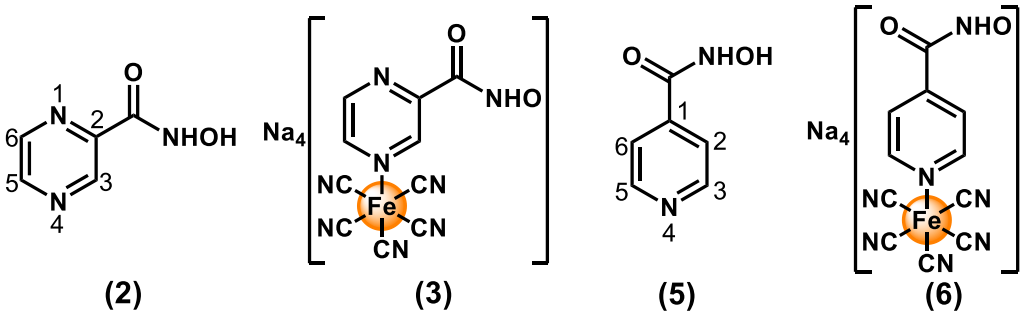

Référence : Élaboré par l'auteur.

Dans un premier temps, les ligands **2** et **5** ont été synthétisés à partir du pyrazine-2-carboxylate de méthyle et de l'isonicotinate de méthyle, respectivement, avec un excès d'hydroxylamine dans du méthanol. Après obtention des ligands, les complexes **3** et **6** ont été préparés en faisant réagir les acides hydroxamiques correspondants avec le complexe précurseur $Na_3[Fe^{II}(CN)_5(NH_3)]$ en milieu aqueux. Puis, les complexes ont été caractérisés par des techniques spectroscopiques telles que RMN (^{1}H, ^{13}C et ^{15}N), infrarouge (IR), Raman et UV-Vis, analyse élémentaire et électrochimique (voltamétrie cyclique).

Les spectres RMN ^{1}H des composés **3** et **6** montrent que les protons aromatiques des positions vicinales au fragment *N*-Fe(CN)$_5^{3-}$ (pour **3** : H3 s, 9,46 et H5 d, 9,18 ppm, pour **6** : H3 et H5 d, 9,05 ppm) sont déplacés vers un champ faible par rapport au ligand libre **2** (H3 *s*, 9,11 et H5 *d*, 8,80 ppm) et **5** (H3 e H5 d, 8,70 ppm) respectivement (Figure 38). En revanche, les protons aromatiques distaux H6 de **3** et H6 et H2 de **6**, sont déplacés vers un champ haut (pour **3** : 8,27 ppm ; pour **6** : 7,39 ppm) par rapport aux protons correspondants des ligands libre **2** (8,68 ppm) et **5** (7,67 ppm). Ce comportement a également été observé pour les noyaux ^{13}CH aromatiques correspondants lors de l'analyse par RMN ^{13}C. De plus, les

résultats de la corrélation HMQC ^{1}H-^{15}N de **3** ont montré sans ambigüité que la coordination de **2** se produit sélectivement en position N4 du cycle pyrazine. Les signaux $^{15}N1$ et $^{15}N4$ de **2** à 319,30 et 323,36 ppm sont respectivement décalés vers un champ haut à 308,56 et 301,11 ppm, respectivement dans le cas du complexe. Le déplacement le plus prononcé subi par N4 suggère fortement que la coordination de l'entité $Fe(CN)_5$ se produit à ce niveau. Les spectres d'infrarouges (IR) et Raman de **3** et **6,** à l'état solide, ont montré des bandes dans la région de 2050–2100 cm^{-1} caractéristiques des fréquences ν (C≡N) des systèmes Fe-C≡N.[338] Les comparaisons des spectres expérimentaux et théoriques (DFT) d'IR et Raman ont montré que les structures de **3** et **6** sont en accord avec celles représentées dans la Figure 38, c'est-à-dire avec l'espèce tétraanionique du complexe. Par ailleurs, les données de l'analyse élémentaire soutiennent aussi les formes tétraanioniques pour les composés **3** et **6**. Considérant que la valeur de pKa de **3** et **6** est voisine de 8,5 (déterminée par une méthode titrimétrique utilisant 0,025 M HCl), la forme tétraanonique des complexes est tout à fait cohérente, puisque la préparation de ces espèces a été faite en milieu basique (pH >> 9).

Les données de voltamétrie cyclique obtenues pour **2**, **3**, **5**, et **6** dans le tampon phosphate (0,1 M, pH 7,4) permettent de montrer que les ligands libres subissent deux processus d'oxydation (pour le composé **2** : 0,68 et 1,12 V *vs* NHE, pour le composé **5** : 0,767 et 1,207 V *vs* NHE), tandis que les complexes, sont sujets à un processus réversible d'oxydation et de réduction, attribué à la paire redox $Fe^{II/III}$, et à un processus d'oxydation, relatif à l'oxydation du ligand coordonné (pour le complexe **3** : i) paire redox $Fe^{II/III}$ = intervalle 0,50-0,90 V *vs* NHE, ii) oxydation de la partie organique du ligand coordonné = 1,091 V *vs* NHE ; pour le complexe **6** : i) paire redox $Fe^{II/III}$ = intervalle 0,40-0,70 V *vs* NHE, ii) oxydation de la partie organique du ligand coordonné = 1,099 V *vs* NHE). Il convient de noter que l'oxydation de la partie organique des ligands coordonnés peut être initiée par un processus intramoléculaire impliquant le centre Fe^{III}, bien qu'une réaction intermoléculaire ne puisse être strictement exclue.

Enfin, les spectres électroniques des complexes **3** et **6** en solution aqueuse (pH = 6,8), ont montré trois bandes principales avec des absorptions maximales à 216, 270 et 486 nm, pour le composé **3** et à 233, 266 et 439 nm pour le composé **6**. En général, les deux premières bandes sont attribuées à des transitions de type transfert de charge ligand-ligand (TCLL), tandis que la dernière est indiquée comme étant une transition de type transfert de charge métal-ligand (TCML). Les calculs TD-DFT ont validé le caractère de ces transitions.

Après l'obtention du composé **3**, celui-ci a été soumis à plusieurs expériences afin d'évaluer et de valider une éventuelle activation chimique médiée par H_2O_2. Les métabolites

actifs potentiellement formés au cours de cette oxydation ont également été étudiés. L'ensemble de l'étude a également été réalisée avec le composé **6** à des fins de comparaison.

La réaction d'oxydation du composé **3** suivie par spectroscopie de l'UV-Vis pendant 2 h, après l'ajout de H_2O_2, a montré que la bande avec un maximum d'absorption à 489 nm et caractéristique de la transition TCML entre le centre métallique Fe^{II} et le ligand **2** diminue progressivement. En effet, une fois que le centre métallique est oxydé en Fe^{III}, il n'y a plus d'électrons disponibles pour que cette transition TCML se produise, ce qui entraîne la disparition de cette bande. Cette expérience a indiqué que dans l'intervalle de temps étudié (2 h) l'agent H_2O_2 a agi efficacement dans l'oxydation du centre métallique de fer.

La réaction d'oxydation par H_2O_2 (2,5 équivalents) a également été suivie par spectroscopie de RMN ^{1}H. L'analyse spectral du milieu réactionnel après 52 h de réaction a révèle que **3** est presque totalement converti en acide pyrazinoique libre et que une toute petite fraction de l'acide pyrazinoique coordonné à $Fe(CN)_5$ en reste.

La réaction entre le complexe **3** (5 mM) et H_2O_2 (200 mM) a également été étudiée en présence de cPTIO par RPE. Au cours de la réaction, il a été observé que les signaux caractéristiques du cPTIO (quintuplet) diminuent, indiquant ainsi qu'une réaction potentielle entre cPTIO et le HNO généré *in situ* a eu lieu.[324] Puisque l'acide hydroxamique non complexé au fer est inerte à H_2O_2 (pas de libération de HNO) nous suggérons que l'oxydation des complexes par H_2O_2, conduisant à la libération de HNO, passe par un transfert intramoléculaire d'électrons du ligand acide hydroxamique vers le Fe^{III}, ce dernier issu de l'oxydation du Fe^{II} par l'H_2O_2. D'autre part, vu qu'aucun radical aroyle n'a pu être détecté par RPE au cours de la réaction, nous proposons en conséquence un mécanisme réactionnel passant par l'intermédiaire nitrosocarbonylé, via lequel la formation des métabolites finaux, HNO et l'acide pyrazinoique, pourrait être expliquée. Le complexe **6** a montré le même profil d'activation chimique médiée par H_2O_2, et a conduit aux mêmes types de métabolites finaux : HNO et l'acide isonicotinoique.

L'étude de l'activité inhibitrice de **3** et **6** ainsi que des ligands libres correspondants vis-à-vis de la croissance des souches H37Rv de *Mtb*, réalisée en collaboration avec Pr. Cristiano V. Bizarro et Pr. Luiz A. Basso où « Pontifícia Universidade Católica Do Rio Grande Do Sul (PUCRS), Porto Alegre, Brasil », a révélé qu'aucun des composés n'est actif (MIC > 10 μg/mL). Cependant, bien que ces complexes ne présentent pas d'activité anti-*Mtb* contre les souches non résistantes et en croissance active, l'activité putative de **3** et **6** contre les souches de *Mtb* intracellulaires (à l'intérieur des macrophages) ou encore contre *Mtb* dans un état de dormance, mérite d'être examinée.

La capacité de libération de NO•/HNO du composé **3** a également été évaluée par des tests de vasodilatation en collaboration avec l'équipe du Pr. Nilberto R. F. do Nascimento. Les ligands **2** et **5**, ainsi que le SNP et le complexe **6** ont également été testés à des fins de comparaison. Alors que les ligands libres **2** et **5** présentaient une valeur d'CE_{50} (concentration efficace médiane) significativement plus élevée pour l'activité de vasodilatation (19 μM) en comparaison à SNP (CE_{50} = 13 nM), le complexe **3** avait une valeur CE_{50} de 250 nM, étant ainsi 19 fois moins puissant que SNP. Le complexe **6** présente une CE_{50} inférieure (64 nM) à celle du composé **3** et est seulement cinq fois moins puissant que le SNP. De plus, les complexes **3** et **6** ont tous les deux montré une efficacité (effet de relaxation maximum) tout à fait comparable à celle du SNP.

En conclusion, les résultats obtenus dans ce chapitre indiquent le rôle clé de la partie métallique des complexes **3** et **6** dans la vasodilatation exercée par ces systèmes. Bien que les complexes **3** et **6** soient moins puissants que le SNP, cela peut être un avantage, car le SNP, libérant du NO• trop rapidement, peut provoquer d'importantes chutes de tension artérielle, nécessitant un contrôle minutieux par titrage. Sans parler encore du danger de la libération des ions cyanures par le SNP, que dans le cas des nouveaux complexes de type pentacyanoferrate(II) est assez réduit. Ces résultats montrent que ces complexes sont extrêmement prometteurs du point de vue cardiovasculaire et qu'ils méritent davantage d'études en vue d'une future application thérapeutique.

4.8 Article 3: Journal of Biological Inorganic Chemistry, 2020, 25, 887-901 - Printed

JBIC Journal of Biological Inorganic Chemistry
https://doi.org/10.1007/s00775-020-01805-z

ORIGINAL PAPER

Pentacyanoferrate(II) complex of pyridine-4- and pyrazine-2-hydroxamic acid as source of HNO: investigation of anti-tubercular and vasodilation activities

Edinilton Muniz Carvalho[1,2,3] · Tercio de Freitas Paulo[1,2,3] · Alix Sournia Saquet[1] · Bruno Lopes Abbadi[4,5] · Fernanda Souza Macchi[4,5] · Cristiano Valim Bizarro[4,5] · Rafael de Morais Campos[6] · Talles Luann Abrantes Ferreira[6] · Nilberto Robson Falcão do Nascimento[6] · Luiz Gonzaga França Lopes[3,5] · Remi Chauvin[1,2] · Eduardo Henrique Silva Sousa[3,5] · Vania Bernardes-Génisson[1,2]

Received: 4 May 2020 / Accepted: 5 July 2020

Abstract

A pharmacophore design approach, based on the coordination chemistry of an intimate molecular hybrid of active metabolites of pro-drugs, known to release active species upon enzymatic oxidative activation, is devised. This is exemplified by combining two anti-mycobacterial drugs: pyrazinamide (first line) and delamanid (third line) whose active metabolites are pyrazinoic acid (PyzCOOH) and likely nitroxyl (HNO (or NO^-)), respectively. Aiming to generate those active species, a hybrid compound was envisaged by coordination of pyrazine-2-hydroxamic acid (PyzCONHOH) with a $Na_3[Fe^{II}(CN)_5]$ moiety. The corresponding pentacyanoferrate(II) complex $Na_4[Fe^{II}(CN)_5(PyzCONHO^-)]$ was synthesized and characterized by several spectroscopic techniques, cyclic voltammetry, and DFT calculations. Chemical oxidation of this complex with H_2O_2 was shown to induce the release of the metabolite PyzCOOH, without the need of the *Mycobacterium tuberculosis* (*Mtb*) pyrazinamidase enzyme (PncA). Control experiments show that both H_2O_2- and N-coordinated pyrazine Fe^{II} species are required, ruling out a direct hydrolysis of the hydroxamic acid or an alternative oxidative route through chelation of a metal center by a hydroxamic group. The release of HNO was observed using EPR spectroscopy in the presence of a spin trapping agent. The devised iron metal complex of pyrazine-2-hydroxamic acid was found inactive against an actively growing/non-resistant *Mtb* strain; however, it showed a strong dose-dependent and reversible vasodilatory activity with mostly lesser toxic effects than the reference drug sodium nitroprussiate, unveiling thus a potential indication for acute or chronic cardiovascular pathology. This is a priori a further indirect evidence of HNO release from this metal complex, standing as a possible pharmacophore model for an alternative vasodilator drug.

Keywords Blood vessel vasodilation · Hybrid pro-drug activation · Metallodrug · Pyrazinamide · Sodium nitroprusside derivative · Tuberculosis

Introduction

Tuberculosis, a millennial disease due to the infection by *Mycobacterium tuberculosis* (*Mtb*), remains today a worldwide health problem causing more than 1 million deaths annually and being responsible for latent infections in about one third of the global population [1].

Although the cure of tuberculosis can be achieved by a therapeutic regimen involving four frontline drugs, isoniazid (INH), rifampicin, ethambutol and pyrazinamide (PYZ) (Scheme 1), without treatment, tuberculosis becomes lethal. Moreover, the first-line therapy is inefficient against multi

Electronic supplementary material The online version of this article (https://doi.org/10.1007/s00775-020-01805-z) contains supplementary material, which is available to authorized users.

✉ Eduardo Henrique Silva Sousa
eduardohss@dqoi.ufc.br

✉ Vania Bernardes-Génisson
vania.bernardes-genisson@lcc-toulouse.fr

Extended author information available on the last page of the article

Published online: 29 July 2020

and extensively drug-resistant *Mtb* strains, which are of increasing importance.

Second- and third-line drugs should thus be used against these virulent *Mtb* strains. However, these drugs display numerous toxic side effects, and even for them, resistant *Mtb* strains are emerging.

Recently, a novel antitubercular drug, delamanid [2] (Scheme 2), was approved as a third-line drug of the anti-tuberculosis therapy. This molecule has two particular interests: on the one hand, only a few cases of resistance have been yet reported, and, on the other, it acts upon both dormant and replicating *Mtb* strains [3, 4]. Delamanid, a nitro-dihydro-imidazole derivative, is reported as a pro-drug and thus requires an enzymatic activation step. The active metabolite is described as being nitroxyl, i. e. HNO (protonated one-electron reduced form of nitric oxide, NO·), resulting from a reductive decomposition of the nitroimidazole group by a mycobacterial nitroreductase enzyme (Ddn) [5, 6]. However, a possible action of the NO· radical cannot be entirely ruled out. On the other hand, no organic metabolite arisen from this bio-reductive activation step was until now identified as a bacterial growth inhibitor.

It is interesting to note that while HNO/NO· may exhibit anti-tuberculosis activities, it is also known to play a very important role on other biological processes as an anti-oxidant [7], anti-angiogenic [8], and also as a vasorelaxant

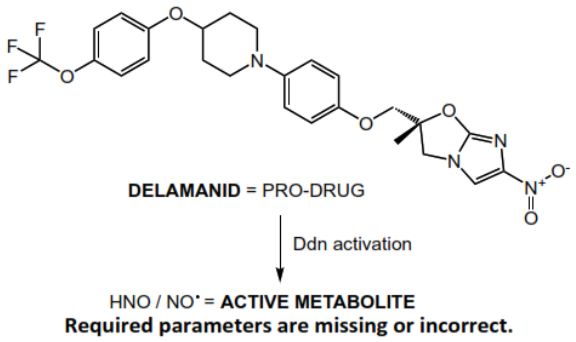

Scheme 2 Structure of the delamanid anti-tubercular pro-drug and its active metabolite(s)

agent [9]. Indeed, cardiovascular diseases are among the major causes of deaths around the world, for which there is an urgent need for new therapeutic agents, including HNO and nitric oxide (NO·) donors. Sodium nitroprusside, a nitrosylpentacyanoferrate(II) complex, is the only clinically approved metal-based nitric oxide donor, which has been used in cardiovascular emergency procedures for over 50 years. In contrast, there is no HNO donor agent clinically available so far. Together these examples show that HNO

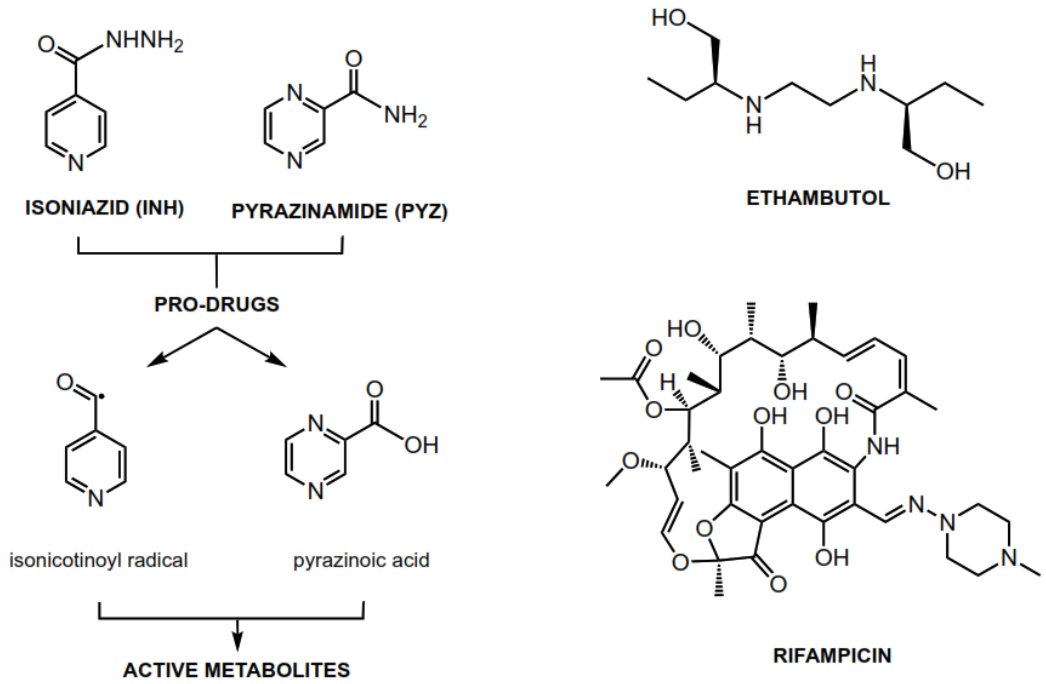

Scheme 1 First-line anti-tubercular (pro-)drugs and reactive species generated from the isoniazid and pyrazinamide pro-drugs.

donor molecules can be of great interest in the medical field as potential therapeutic agents.

Lately, some of the present authors have studied and developed a biomimetic system, as an alternative non enzyme-dependent way to activate the INH antituberculosis pro-drug (KatG = activation enzyme of INH), based on the redox reactivity of a metal complex of INH (called IQG607) in the presence of oxidizing agents such as H_2O_2 [10–12]. The anti-mycobacterial activity (in vitro $MIC_{Mtb} = 1.56$ µg/mL ~ 3.5 µM) [13], chemical stability, and absence of toxicity (selectivity index SI > 4000, $LD_{50} > 2000$ mg/kg) [14] of the $[Fe^{II}(CN)_5(INH)]^{3-}$ complex motivated us to extend this activation approach to heteroaryl hydroxamic acids used as ligands for the development of new HNO donor complexes. Thereby, to prepare HNO donors from $[Fe^{II}(CN)_5$(heteroaryl hydroxamic acid)] complexes with wide spectra of biological activities, including antituberculosis, the pyrazine-type nitrogen aryl ring was naturally first selected and used in this study. The pyrazine moiety is already present in the structure of a first-line antitubercular drug, pyrazinamide (PYZ, see Scheme 1). Pyrazinamide, like isoniazid and delamanid, is also a pro-drug and is activated by pyrazinamidase (PncA), an enzyme of *Mtb* [15, 16]. This reaction converts the pro-drug into the corresponding carboxylic acid (pyrazinoic acid = PyzCOOH) that is assigned to be the effective toxic agent for *Mtb* (Scheme 1). The sensitivity of *Mtb* to this drug is partly due to an inefficient efflux of PyzCOOH, that is found accumulated in the interior of the cell [17, 18].

Considering that the major route for PYZ resistances relies on point mutations on the PncA enzyme that is responsible for the conversion of PYZ into pyrazinoic acid [17–19], the synthesis of the $Na_3[Fe^{II}(CN)_5$(PyzCONHOH)] complex, could be judicious because the proposed complex can be considered as a hybrid source of the active metabolites of PYZ and delamanid that, under oxidative conditions, could generate, in an opportunistic way, two antitubercular agents, HNO and pyrazinoic acid. Both metabolites could be ideally released without the need of mycobacterial enzymes (overcoming resistance phenomena) and could act upon multiple targets simultaneously, reducing the chances of selection of resistant bacterial cells.

This paper mainly describes the synthesis, characterization, and chemical–biological studies of pyrazine-2-hydroxamic acid (**2**) and its pentacyanoferrate(II) complex **3** (Scheme 3). As proposed above, the ligand **2** is actually a functional hybrid of two different pharmacophores corresponding to the active metabolites of PYZ (PyzCOOH) and delamanid (HNO). After chemical activation of the prototype complex **3** (Fe(II) converted to Fe(III) upon oxidation), and independently of the functional state of the activating enzyme of *Mtb* (mutated or not), the released pharmacophores are expected to recognize different targets and act by different mechanisms, killing growing and, more particularly, non-growing *Mtb* strains (Scheme 3).

Isonicotinohydroxamic acid has also been synthesized in view of the fact that putative isonicotinic acid, formed after the activation step, can be considered as a bio-isostere of pyrazinoic acid.

Material and methods

Chemicals

Available reagents and solvents were purchased from commercial suppliers and used without further purification: methyl isonicotinate, methyl pyrazine-2-carboxylate (Alfa Aesar); hydroxylamine solution (NH_2OH, 50% in water) from Sigma-Aldrich, pyrazinoic acid, isonicotinic acid and potassium ferricyanide (III) ($K_3[Fe(CN)_6]\cdot 3H_2O$) from Sigma-Aldrich; isoniazid (INH) from ACROS

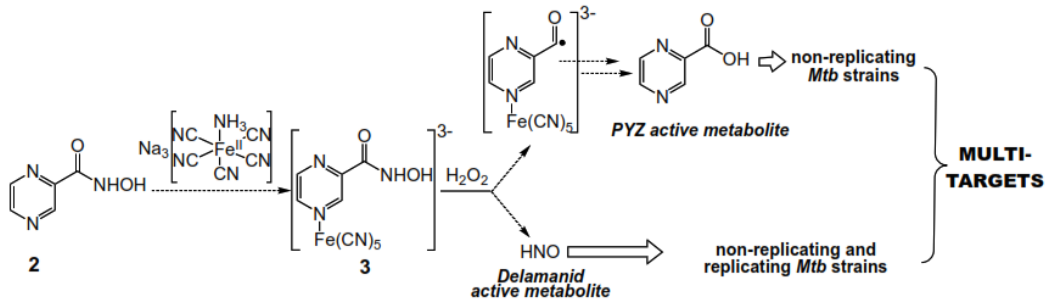

Scheme 3 Possible outcome route for oxidation of the $Na_3[Fe^{II}(CN)_5$(PyzCONHOH)] complex by H_2O_2

Organics; sodium dihydrogen phosphate (NaH_2PO_4), disodium hydrogen phosphate (Na_2HPO_4) and sodium trifluoroacetate ($NaC_2F_3O_2$) from PROLABO and Fluka; 2-(4-carboxyphenyl)-4,4,5,5-tetramethylimidazoline-1-oxyl-3-oxide potassium salt (c-PTIO) and *N-tert*-butyl-α-phenylnitrone (PBN), used as radical trapping agents, from Thermo Fisher Scientific and Alfa Aesar, respectively.

$Na_3[Fe^{II}(CN)_5(NH_3)]\cdot 3H_2O$ was prepared as previously described [20]. Methanol, ethanol, dichloromethane, and acetone were of chromatographic grade, and water used in the experiments was ultra-purified using a Milli-Q system (Millipore).

Instruments

^{1}H NMR spectra were recorded on a Bruker spectrometer at 300 and 400 MHz using D_2O and DMSO-*d*6 as solvents, with increasing chemical shifts at low field vs the tetramethylsilane ^{1}H nucleus reference derived from the deuterium lock signal of the solvent. ^{13}C NMR spectra were recorded on a Bruker spectrometer at 101 MHz using D_2O and DMSO-*d*6 as solvents, with increasing chemical shifts at low field vs the tetramethylsilane ^{13}C nucleus reference derived from the deuterium lock signal of the solvent. ^{15}N NMR spectra were recorded on a Bruker spectrometer at 50.7 MHz and external sample of CH_3NO_2 was used as the reference. Electrospray mass spectra (ESI) were obtained on a Perkin–Elmer SCIEX API 365 instrument high resolution and desorption chemical ionization (DCI) mass spectra were acquired on a Finnigan TQS 7000 spectrometer. Infrared spectra were obtained using a Perkin–Elmer Spectrum One spectrometer. UV–Vis spectra were recorded on a Perkin–Elmer UV/Vis/NIR Spectrometer—Lambda 950. Normal Raman (NR) spectra of the samples were acquired by means of an Xplora (Horiba) microspectrometer: the excitation radiation was the 785 nm line and the laser beam was focused on the sample by a × 50 long distance objective. Elemental analyses were obtained using a PERKIN ELMER 2400 series II instrument. Electrochemical measurements were performed using a BAS Epsilon E2 818 potentiostat/galvanostat system within a conventional three-electrode cell. Vitreous carbon, platinum, and calomel electrodes were used as working, auxiliary and reference electrodes, respectively. Voltammograms were recorded in phosphate buffer solution (PBS) 0.1 M, pH 7.4. Electron paramagnetic resonance (EPR, or electron spin resonance = ESR) spectra were recorded at room temperature (ca. 291 K) on a Bruker Elexsys-II E500 (X-Band) spectrometer using a modulation amplitude of 0.5 G, a microwave power of 5.15 mW, with an attenuation of 16 dB with repeated number of 2 scans. The samples were transferred into a capillary (Hirschmann, Duran, Ringcaps, 50 µL), which was then placed inside a larger quartz tube enabling the sample to be accurately positioned inside the resonator. All samples were prepared as 40 mM solutions in phosphate buffer pH 7.4, at 25 °C, by mixing suitable amounts of the studied compound and spin trap (cPTIO or PBN). The reactions were initiated by the addition of the H_2O_2 and the spectra immediately recorded.

Synthetic procedures

General procedure for hydroxamic synthesis

To a solution of methyl heteroaryl-carboxylate derivative (3.62 mmol) in methanol (10 mL) at room temperature and under stirring, 3.9 mL of hydroxylamine 50% (65.2 mmol) was slowly added. The solution was stirred for 72 h. The solvent was evaporated under vacuum and the solid was resuspended in dichloromethane, filtered, and thus washed from traces of pyrazine-2-carboxylate. Then, the solid was resuspended in water (4 mL) to remove traces of hydroxylamine: the pyrazine-2-hydroxamic acid being poorly soluble in water, the mixture was cooled down in an ice bath for 3 h to assist the product precipitation. Then, the solid was filtered, washed with cold acetone, and dried under vacuum.

Pyrazine-2-hydroxamic acid (2)

Yield = 85% (0.43 g), white solid. ^{1}H NMR (400 MHz, DMSO-d_6) δ (ppm): 11.62 (s, 1H), 9.28 (s, 1H), 9.12 (d, J = 1.5 Hz, 1H), 8.84 (d, J = 2.5 Hz, 1H), 8.68 (dd, J = 2.5, 1.5 Hz, 1H). ^{13}C NMR (101 MHz, DMSO-d_6) δ (ppm): 160.65 (C=O), 147.75 (CH), 145.52 (Cq), 143.85 (CH), 143.67 (CH). ^{15}N NMR (50.7 MHz, D_2O) δ (ppm): 319.30 (N_1), 323.36 (N_4). IR symmetric stretching (ν_s), anti-symmetric stretching (ν_{as}), symmetric bending (δ_s) and twisting (τ) (cm^{-1}): 3212 (ν_s O–H), 3061 (ν_s N–H), 2823 (ν_s C–H), 1662 (ν_s C=O), 1585 – 1524 ν C=N, ν_s C=C), 1417 (δ_s N–H), 1386 (δ_s C–H), 1023 (ν_{as} C=N), 916 (τ C–H). UV–Vis (H_2O) ν_{max}/nm (ν/M^{-1} cm^{-1}) = 211 (8169), 272 (7248), 312 (876). MS (DCI/CH_4) *m/z*: 140.04 [M + H$^+$], 124.05 [(M + H$^+$)-16]. HRMS (DCI/CH_4) *m/z*: for {($C_5H_5N_3O_2$) + H$^+$} calcd.: 140.0460 found: 140.0464. Elemental analysis calcd. for $C_5H_5N_3O_2$: C, 43.17; H, 3.62; N, 30.21. Found: C, 42.91; H, 3.51; N, 29.81. TLC (dichloromethane/methanol 90:10) R_f = 0.42. M.p. = 165 °C. Electrochemistry in 0.1 M phosphate buffer, pH 7.4, E_{pa} = 0.684 and 1.119 V vs NHE.

Pyridine-4-hydroxamic acid (5)

Yield = 98% (0.49 g), white solid. ^{1}H NMR (300 MHz, DMSO-d_6) δ (ppm): 11.50 (s, 1H), 9.32 (s, 1H), 8.70 (d, J = 6.1 Hz, 2H), 7.67 (d, J = 6.1 Hz, 2H). ^{13}C NMR (101 MHz, DMSO-d_6) δ (ppm): 162.48 (Cq), 150.68 (CH), 140.31 (Cq), 121.40 (CH). IR symmetric stretching (ν_s), anti-symmetric stretching (ν_{as}), symmetric bending (δ_s) and twisting (τ) (cm^{-1}) ν_{max} (cm^{-1}): 3324 (ν_s O–H), 3132 (ν_s N–H), 1640 (ν_s C=O), 1540–1520 (ν_s C=N, ν_s C=C), 1410 (δ_s N–H), 1316 (δ_s C–H), 1025 (ν_{as} C=N), 908 (τ C–H). UV–Vis (H_2O) λ_{max}/nm (ε/M^{-1} cm^{-1}) = 235 (3760), 260 (3710). HRMS (DCI/CH_4): for {($C_6H_6N_2O_2$) + H^+} calcd.: 139.0508 found: 139.0515. Elemental analysis calcd. for $C_6H_6N_2O_2$: C, 52.17; H, 4.38; N, 20.28. Found: C, 52.12; H, 4.21; N, 20.25. TLC (dichloromethane/methanol 90:10) R_f = 0.24. M.p = 154 °C. Electrochemistry in 0.1 M phosphate buffer, pH 7.4, E_{pa} = 0.767 and 1.207 V vs NHE.

General procedure for preparation of $Na_4[Fe^{II}(CN)_5$(HeteroarylCONHO$^-$)]compounds

To a solution of $Na_3[Fe^{II}(CN)_5(NH_3)]\cdot 3H_2O$ (0.150 g, 0.46 mmol, 1 equiv.) in water (3 mL), it was slowly added a solution of the ligand (pyrazine-2-hydroxamic acid, 0.077 g, 0.55 mmol, 1.2 equiv. or pyridine-4-hydroxamic acid, 0.076 g, 0.55 mmol, 1.2 equiv.) in water (2 mL). The mixture was stirred at room temperature, under argon atmosphere and protected from light for 3 h. Then 150 mL of a cold solution of ethanol containing an excess of sodium iodide (30 equiv.) was added dropwise. The resulting precipitate was kept overnight at −20 °C before it was collected by filtration, washed with cold ethanol, and dried in a vacuum desiccator. CAUTION: since these complexes are moderately light and oxygen sensitive, they must be stored in a vacuum desiccator protected from light to extend their lifetime.

$Na_4[Fe^{II}(CN)_5$(PyzCONHO$^-$)] ($Na_4$3) (PyzCONHO$^-$ = pyrazine-2-hydroxamate)

Yield = 87% (0.180 g), orange solid. ^{1}H NMR (400 MHz, D_2O) δ (ppm): 9.46 (s, 1H), 9.18 (d, J = 3.3 Hz, 1H), 8.27 (d, J = 3.2 Hz, 1H). ^{13}C NMR (101 MHz, D_2O) δ (ppm): 178.69 (CN_{eq}), 173.75 (CN_{ax}), 160.69 (C=O), 153.77 (CH), 150.66 (CH), 145.50 (Cq), 142.33 (CH). ^{15}N NMR (50.7 MHz, D_2O) δ (ppm): 301.10 (N_4), 308.56 (N_1). IR symmetric stretching (ν_s), antisymmetric stretching (ν_{as}), symmetric bending (δ_s), antisymmetric bending (δ_{as}) and wagging (π) (cm^{-1}): 3418 (ν_s N–H), 3452–3250 (ν_s C–H), 2053 (ν_s C≡N), 1609 (ν_s C=O), 1577 (ν_s C=N, C=C), 1391—1173 (δ_s C–H), 1033 (τ C–H). 908 (δ_{as} C–H), 854 and 753 (π C–H), 652 (ν_s C=N). UV–Vis (H_2O) λ_{max}/nm (ε/M^{-1} cm^{-1}) = 216 (18,820), 270 (6228), 486 (3638). Elemental analysis calcd. for $C_{10}H_4FeN_8O_2Na_4\cdot 3H_2O$: C, 25.55; H, 2.14; N, 23.84. Found: C, 25.93; H, 2.16; N, 23.94. Electrochemistry in phosphate buffer (0.1 M, pH 7.4): E_{pa} = 0.722 and 1.091 V vs NHE.

$Na_4[Fe^{II}(CN)_5$(PyCONHO$^-$)] ($Na_4$6) (PyCONHO$^-$ = pyridine-4-hydroxamate)

Yield = 79% (0.173 g), yellow solid. ^{1}H NMR (400 MHz, D_2O) δ (ppm): 9.05 (d, J = 4.96, 2H), 7.39 (d, J = 4.76, 2H). ^{13}C NMR (101 MHz, D_2O) δ (ppm): 180.64 (CN_{eq}), 176.39 (CN_{ax}), 164.02 (Cq), 157.34 (CH), 141.63 (Cq), 120.52 (CH). IR symmetric stretching (ν_s), antisymmetric stretching (ν_{as}), symmetric bending (δ_s), antisymmetric bending (δ_{as}), wagging (π), rocking (ρ) and twisting (τ) (cm^{-1}): 3483 (ν_s N–H), 3382–3047 (ν_s C–H), 2052 (ν_s C≡N), 1647 (ν_s C=O), 1546 (ν_s C=N, C=C), 1492—1414 (δ_s C–H), 1313 (π C–H), 1227 (τ C–H), 1165 (ν_s C–C). 908 (δ_{as} C–H), 846 (π C–H), 698 (π N–H). UV–vis (H_2O) λ_{max}/nm (ε/M^{-1} cm^{-1}) = 233 (14,400), 266 (5123), 439 (4052). Elemental analysis calcd. for $C_{11}H_5FeN_7O_2Na_4\cdot 3.5H_2O$: C, 27.64; H, 2.53; N, 20.51. Found: C, 27.66; H, 2.21; N, 20.76. Electrochemistry in 0.1 M phosphate buffer (pH 7.4): E_{pa} = 0.551 and 1.099 V vs NHE.

Computational details

All calculations were carried out using the density functional theory (DFT) with the B3LYP [21–23] functional as implemented in the Gaussian 09 program package, Revision D.01 (Gaussian Inc., Wallingford, CT) [24]. The 6-311++G(d,p) basis set was used for non-metal atoms, while the LANL2DZ relativistic effective core potential basis set was used for Fe atoms. Vibrational frequency analyses were carried out to confirm convergence to a minimum energy geometry by the absence of imaginary frequencies. A scaling factor of 0.9679 for the calculated harmonic vibrational wavenumbers considering the 6-311++G(d,p) basis set and the B3LYP functional. The vertical excitation energies were determined by the time-dependent density functional theory protocol (TD-DFT) using the B3LYP functional and mixed basis sets mentioned above. The polarizable continuum model (PCM) [25] was used in the case of vertical excitation energies to take into account the solvent effect, where the dielectric constant of water was considered. The FTIR, UV–Vis spectra were extracted from output files, while Raman spectra were calculated with the GaussSum 3.0 program [26]. This program was used to calculate the Raman intensity considering an exciting radiation of 785 nm.

Antimycobacterial activity

In vitro activity of the compounds **2**, **3**, **5** and **6** was evaluated against the *Mycobacterium tuberculosis* H37Rv ATCC 27294 reference strain (American Type Culture Collection, Rockville, Md.), by performing minimum inhibitory concentration assays (MIC), as described elsewhere [27]. This strain was grown up to mid-log phase (OD_{600} 0.8–1.0) in Middlebrook 7H9 broth (Difco™), supplemented with 10% ADC (albumin, dextrose and catalase—BD BBL™) and 0.05% Tween 80 (Sigma-Aldrich), with agitation (100 rpm), at 37 °C. Following that, a mycobacterial suspension was prepared using sterile glass beads (4 mm), which was aliquoted and stored at -80 °C until use. Compounds were first solubilized in ultrapure water (4 mg/mL) and diluted in 7H9 broth (200 µg/mL). Serial twofold dilutions (100 µL) of each compound were performed directly in 96-well plates in 7H9 broth, giving a concentration range of 100–0.2 µg/mL. An aliquot of mycobacterial suspension was thawed and diluted in 7H9 broth to a theoretical OD of 0.006, which was added to each well (100 µL). Compound and culture-free wells were used as positive and negative growth controls, respectively. Isoniazid (INH, ACROS Organics) was used as an anti-TB drug reference. Plates were sealed with Parafilm M® and incubated inside plastic bags in a bacteriological incubator (37 °C, 5% CO_2) for 7 days, before the addition of 60 µL of 0.01% (w/v) resazurin (Sigma-Aldrich) solution to each well. Minimum inhibitory concentration (MIC) was considered as the lowest compound concentration that prevented a color conversion from blue (no growth) to pink (growth). MIC values reported for each compound were the most frequently occurring value observed among three independent assays. INH was used as a positive control of MIC assays.

Vasodilation assay

Rats were sacrificed by overdose of sodium thiopental and the thoracic aorta was carefully removed and cut into rings of about 5 mm in length. The aortic rings were mounted in a 5 mL organ bath containing Krebs–Henseleit medium with the following composition: 120 mM NaCl, 4.7 mM KCl, 1.8 mM $CaCl_2$, 1.43 mM $MgCl_2$, 25.0 mM $NaHCO_3$, 1.17 mM KH_2PO_4, glucose and maintained at 37 °C. The rings were attached to a force transducer (TRI202P, Panlab, Barcelona, Spain) coupled to a Powerlab data acquisition systema (ADInstruments, Sydney, Australia) and data were recorded and analyzed using the Labchart 7.0 software. After equilibration, the rings were pre-contracted with 1 µM phenylephrine (PE), and once a stable plateau was achieved, cumulative concentration–response curves were constructed using the ligand **2** and **5** and the metal complexes **3** and **6** in a concentration range from 0.1 nM to 100 µM. Sodium nitroprusside (SNP, $Na_2[Fe(CN)_5(NO)]$) was used as positive control. This assay was performed using seven independent measurements prepared with different animals for statistical analysis. All procedures were performed according to the ethics committee of State University of Ceará number 2897836/15.

Systemic hemodynamics

Male WistarKyoto (WKY) or spontaneously hypertesive rats (SHR) (250–300 g) were anesthetized with sodium pentobarbital (50 mg/kg) and a polyethylene catheter (PE 240) was inserted into the trachea to help with spontaneous breathing. The left femoral artery was isolated and canulated with a polyethylene catheter (PE 10) and this catheter was coupled to a pressure transducer (MLT844, ADInstruments, Sydney, Australia) for continuous recording of blood pressure by means of a data acquisition system (Powerlab, ADInstruments) and a Labchart 7.0 software. The right carotid artery was canulated with a microtip pressure–volume catheter (SPR-869, Millar Instruments; Houston, TX) and this catheter was inserted into the left ventricle for continuous measurement of cardiac parameters such as cardiac output.

Results and discussion

Synthesis

The ligand moiety, pyrazine-2-hydroxamic acid (**2**) (PyzCONHOH) [28, 29], of the targeted hybrid complex **3**, was directly prepared from methyl pyrazinoate (**1**) in NH_2OH solution with 85% yield (Scheme 4) and fully characterized. Then, the coordination of **2** with $Na_3[Fe(CN)_5NH_3]$ was carried out in aqueous medium to afford Na_4**3** in 87% yield (Scheme 4). This compound was analyzed by $^1H/^{13}C/^{15}N$ NMR, IR, UV–Vis and Raman spectroscopy, along with cyclic voltammetry, elemental analysis and DFT calculations. Attempts to obtain crystals of the complex Na_4**3** for X-ray diffraction analysis were unsuccessful. Additionally, procedures to exchange the sodium cations by other more crystallogenic/solubilizing cations (e.g. PPN^+, NEt_4^+) also failed. (Protocol a: to a solution of salt (PPN^+ or NEt_4^+) in ethyl acetate, the iron complex was added. The mixture was stirred overnight in the shadow. The solution was filtered to remove the unsolubilized complex. The filtered solution was rotoevaporated and the crude product was characterized by ^{1}H-NMR. Protocol b: an aqueous solution containing the iron complex was added to a solution of salt cation (PPN^+ or NEt_4^+) in ethyl acetate. This mixture was stirred overnight in the shadow. Then the organic and aqueous phases were separated. The organic phase was rotoevaporated and the solid obtained was characterized by ^{1}H-NMR. No signal corresponding

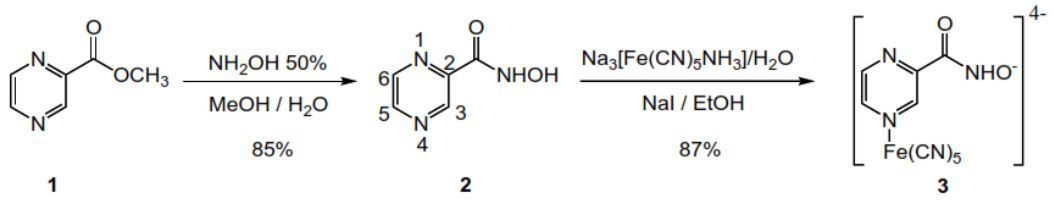

Scheme 4 Synthesis of the pentacyanoferrate(II) complex of pyrazine-2-hydroxamate from methyl pyrazine-2-carboxylate

to the complex framework was observed, just signals of the cation PPN^+ or NEt_4^+. The aqueous solution was also analyzed by ^{1}H-NMR; however, no characteristic signal of these salts was identified).

The pentacyanoferrate(II) complexes of pyridine-4-hydroxamic acid (PyCONHOH) and sodium pyrazine-2-carboxylate (PyzCOONa) were both synthesized for the purpose of comparison and for control experiments, respectively. Treatment of methyl isonicotinate **4** with hydroxylamine originated the corresponding hydroxamic acid **5** [30], which was converted to the metal complex Na_4**6,** using the same protocol employed for the preparation of **3** (Scheme 5). Likewise, deprotonation of pyrazinoic acid **7** led to sodium pyrazinoate **8**, which was then coordinated to the $Fe^{II}(CN)_5$ moiety with 64% yield in the complex **9** (see Supporting Information).

In all cases, the coordination to the diamagnetic Fe(II) center was shown to take place only at the less hindered N atom of the heteroaromatic ring as evidenced by spectroscopic analysis (see Sect. 3.2).

Characterizations

NMR spectroscopy

The ^{1}H NMR spectrum of **3** shows the aromatic protons in the vicinal positions from the *N*-$Fe(CN)_5^{3-}$ fragment (H3 *s*, 9.46 and H5 *d*, 9.18 ppm) are both shifted to low field as compared to those of the free protonated ligand **2** (PyzCONHOH: *s*, 9.11 and *d*, 8.80 ppm). On the other hand, the distal aromatic proton H6 of **3** is shifted up-field (8.27 ppm) with respect to the corresponding proton in the protonated free ligand **2** (8.68 ppm). The same trend was observed in the ^{13}C NMR spectra for the corresponding aromatic ^{13}CH nuclei. The 2D ^{1}H-^{15}N HMQC NMR spectrum of **3** unambiguously shows that coordination of **2** occurs selectively at the N-4 position of the pyrazine ring (Figure S1). As observed for the $[Fe(CN)_5(INH)]^{3-}$ complex, [31] the ^{15}N1 and ^{15}N4 signals of **2** at 319.30 and 323.36 ppm are, respectively, both shifted up-field to 308.56 and 301.11 ppm, for the complex. The more pronounced shifting undergone by N4 indicates

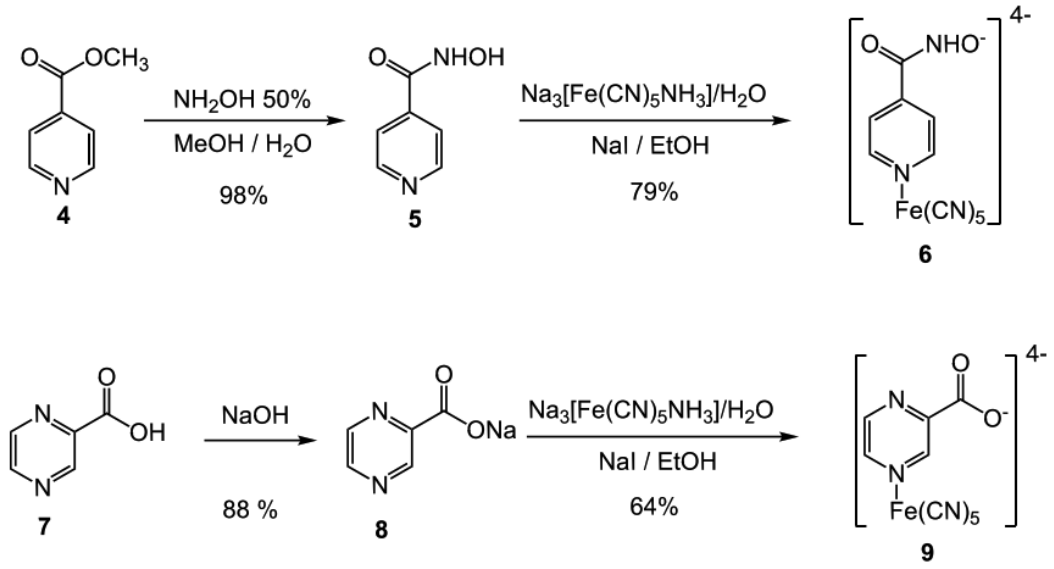

Scheme 5 Synthesis of pentacyanoferrate(II) complexes of pyridine-4-hydroxamic acid and sodium pyrazine-2-carboxylate

that the coordination of $Fe(CN)_5$ moiety occurs at this center. The high resolution of the NMR spectra of **3**, without signal broadening vs the spectra of **2**, provides a strong evidence that the iron atom of **3** is indeed in a low-spin + 2 oxidation state (Figure S1).

The cyanide ligands of **3** are revealed by two ^{13}C NMR signals at 178.7 and 173.8 ppm, characteristic of *sp* ^{13}CN nuclei in equatorial and axial positions vs the Fe–N axis. These results are consistent with those previously obtained for the pyrazine hydrazide complex $Na_3[Fe(CN)_5(PyzCONHNH_2)]$ [32].

Vibrational spectroscopy

The cyanide ligands were also characterized by infrared (IR) and Raman spectroscopy, where two bands in the range 2050–2100 cm^{-1} are assigned to the FeC≡N stretching frequencies ν(C≡N) [33]. The most relevant infrared and Raman vibration modes and wavenumbers can be found in the Supporting information (Table S1).

Unexpectedly, the experimental normal Raman spectrum of **3** in the solid state (Fig. 1) was indeed much more compatible with the corresponding DFT-simulated spectrum, than with the DFT-simulated spectrum of the O-protonated form (**3**H^+, Scheme 4). The O-deprotonated form of the ligand **2** in the tetraanionic complex **3** was also supported by elemental analysis (see experimental section). IR data reveal that the C=O band at 1662 cm^{-1} in the protonated free ligand **2** is shifted to *ca*. 1580 cm^{-1} in the complex **3**, in agreement with the anionic hydroxamate form of **2** in **3** (Scheme 4). The formation of **3** is a consequence of the basic medium (pH >> 9) used for the preparation of this complex.

The pK_a value of **3** in water solution, determined by a titrimetric method using 0.025 M HCl, is indeed as low as 8.5.

Cyclic voltammetry

Cyclic voltammograms of the ligand **2** and complex **3** in a phosphate buffer solution (0.1 M, pH 7.4) were recorded using a glassy carbon working electrode (Figure S2). For the free ligand **2**, two oxidative waves are observed at 0.68 V and 1.12 V vs NHE as irreversible electrochemical processes. In the cyclic voltammogram of the complex **3**H^+ (Figure S2 red line), the oxidation wave is observed in the potential range of 0.50–0.90 V vs NHE. This wave can be attributed to two processes corresponding to the local oxidation of the $Fe^{II} -> Fe^{III}$ and coordinated ligand. Additionally, a second irreversible electrochemical process is observed at 1.091 V vs NHE and assigned to the second ligand oxidation. The oxidation of the organic moiety likely initiates via an intramolecular process involving the formation of a Fe(III) center, although an intermolecular reaction cannot be strictly ruled out. Furthermore, there are kinetic evidences of an intramolecular electron transfer during the chemical oxidation of the $[Fe(CN)_5(INH)]^{3-}$ complex (IQG607), a process which might be similar in the chemical oxidation of **3**H^+ [10a]. In the cathodic scanning, only one wave at 0.54 V vs NHE is observed and attributed to the $Fe^{III} -> Fe^{II}$ reduction process.

UV–Vis absorption spectroscopy

The electronic spectra of the protonated free ligand **2** and complex **3**H^+ were recorded in slightly acidic aqueous

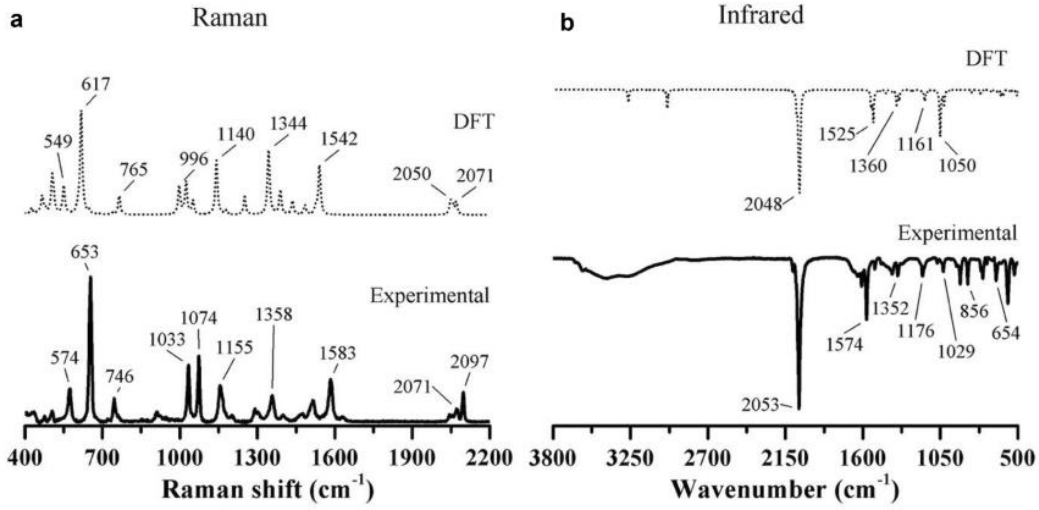

Fig. 1 Experimental normal Raman (**a**) and IR (**b**) spectra of the complex **3** under tetraanionic form, $Na_4[Fe(CN)_5L]$, L = $PyzCONHO^-$ (plain line), in the solid state, and DFT-simulated spectra for $[Fe(CN)_5L]^{4-}$ (dotted line)

solution (pH = 6.8). The free ligand **2** exhibits two main bands at 211 and 272 nm, and a shoulder at 312 nm, while the complex $\mathbf{3H}^+$ exhibits three main electronic transitions with absorption maxima at 216, 270, and 486 nm (Figure S3). The two first ones are consistent with bands relative to the ligand moiety, while the last band is characteristic of a metal-to-ligand charge transfer transition (MLCT). This type of transition occurs from an electron-rich Fe center to π-accepting ligands, which is in agreement with the + 2 oxidation state of the iron center. TD-DFT calculations further validate the character of these transitions (see Supporting information, Table S2 and Figure S4).

Chemical oxidation of the Fe(II) complex under physiological pH conditions and characterization of drug metabolites active against *Mtb*

As argued earlier, the complex $Na_4\mathbf{3}$ has been devised as a precursor of the anti-*Mtb* metabolites of pyrazinamide and delamanid, i.e. pyrazinoic acid (PyzCOOH) and nitroxyl (HNO/NO·), respectively. The search for evidences of the formation of the later organic and inorganic products upon chemical oxidation with H_2O_2 is addressed below:

Formation of PyzCOOH upon oxidation of 3

Chemical oxidation of **3** or its protonated form $\mathbf{3H}^+$ by action of H_2O_2 in a phosphate buffer solution (40 mM, pH = 7.4) can be considered as a mimic of the biological activation of PYZ by the pyrazinamidase (PncA) enzyme, which is often found mutated in PYZ-resistant *Mtb* strains. In these conditions, oxidation of **3** under its major hydroxamic acid form $\mathbf{3H}^+$ and the release of $PyzCOO^-$, without assistance of PncA, was thus investigated by UV–vis and ^{1}H NMR spectroscopy.

Before addition of H_2O_2, the trianionic complex $\mathbf{3H}^+$ (buffer solution of **3** at pH = 7.4) showed an absorption band with a maximum at 489 nm, characteristic of the MLCT transition as previously discussed. This band disappeared almost completely within 2 h (Fig. 2, red line) after addition of H_2O_2, indicating modification of the metal moiety. This result supports the hypothesis that this complex is activated by H_2O_2 via $Fe^{II} -> Fe^{III}$ oxidation (Fig. 2).

^{1}H NMR analysis of **3** in deuterated buffer solution and in the presence of 2.5 equivalents of H_2O_2, after 52 h, revealed that the signals relative to the aromatic protons of the trianionic complex $\mathbf{3H}^+$ had completely disappeared, while new signals corresponding to free pyrazine carboxylate (**8**) were observed. This was evidenced by a perfect matching of the new aromatic ^{1}H NMR signals (Fig. 3, spectrum C) with those of an authentic sample of sodium pyrazinoate (**8**) (Fig. 3, spectrum E). Remarkably, after oxidative activation, the organic metabolite **8** was found to be spontaneously released from the metal center, while only very little ligand remains coordinated to the $Fe^{II}(CN)_5^{3-}$ unit (Fig. 3, spectrum C and D)

It is worth noting that the free hydroxamic acid **2** in the presence of H_2O_2 is unable to produce pyrazinoic acid even after 52 h. In addition, in the presence of $Na_3[Fe^{III}(CN)_6]$ (2.5 equiv.), the hydroxamic group of **2** is only very slowly

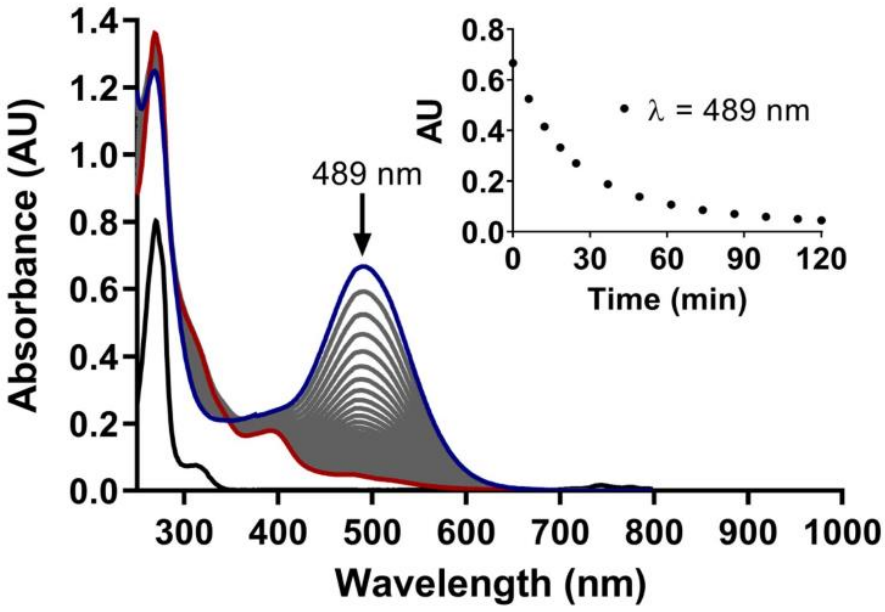

Fig. 2 UV–Vis monitoring of the reaction of **3** under the protonated main form $\mathbf{3H}^+$ (171 µM) with H_2O_2 (427.5 µM) in phosphate buffer solution, 40 mM, pH 7.4, 22 °C. Reaction at $t = 0$ min, before addition of H_2O_2, (blue line), and after 2 h (red line). The black curve corresponds to a solution of sodium 2-pyrazinoate (110 µM). Inset shows the kinetic curve based on changes at 489 nm

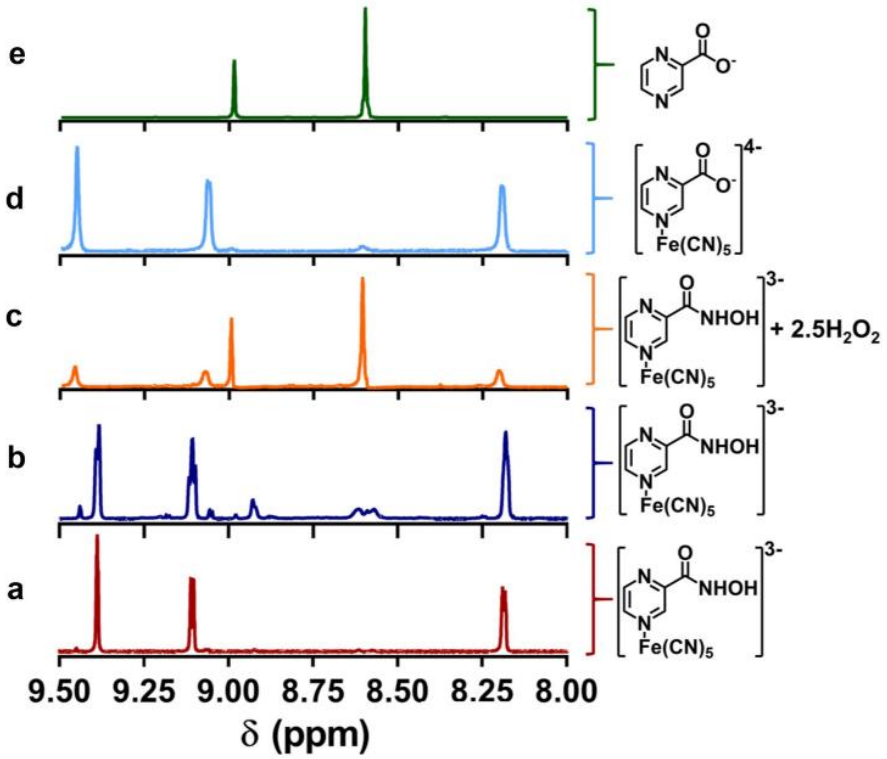

Fig. 3. ^{1}H-NMR spectra at 400 MHz: of the complex **3** under its protonated form $\mathbf{3H^+}$ (20 mM) at 0 h (**a**) and at 52 h (**b**) without addition of H_2O_2, at 52 h after reaction of $\mathbf{3H^+}$ with H_2O_2 (50 mM) (**c**), and of authentic samples of the complex **9** (20 mM) (**d**) and pyrazinoate salt (**8**) (20 mM) (**e**). Solutions in 40 mM phosphate buffer, pH 7.4, at 25 °C

and partially oxidized, and converted to the corresponding carboxylic acid PyzCOOH (even after 64 h), after hydrolysis of the putative dimer *N,O*-dipyrazinoylhydroxylamine (PyzC(O)NHOC(O)Pyz) formed as intermediate [34]. The latter intermediate has never been observed for the ligand of **3** in oxidative conditions. All together, these results show that both H_2O_2 and the N-coordinated Fe^{II} unit are needed for oxidative activation of the hydroxamic moiety, ruling out a random mechanism passing through a direct hydrolysis of the hydroxamic acid function ($PyzCONHOH + H_2O \rightarrow PyzCOOH + NH_2OH$) or an alternative activation route where the hydroxamic acid group would coordinate metal ions occasionally present in buffer solutions.

Formation of HNO/NO upon oxidation of 3

The inorganic metabolite of delamanid, i.e. the weak acid nitroxyl (HNO) or radical nitric oxide (NO), was targeted. Discrimination between these possible products was envisaged by EPR spectroscopy in the presence of the 2-(4-carboxyphenyl)-4,4,5,5-tetramethylimidazoline-1-oxyl-3-oxide potassium salt (cPTIO). This compound is a water-soluble nitronyl-nitroxide known to be readily reduced by NO, of which it is a specific scavenging agent, to give the corresponding cPTI nitroxide and the NO_2 radical (Scheme S1). This species (cPTI) presents characteristic EPR signatures different from the quintuplet signal of cPTIO (a septet for cPTI) [34]. cPTIO also reacts with HNO, by which it is reduced to the EPR-silent nitronyl-hydroxylamine, while releasing the NO radical (Scheme S1) [35, 36].

The first control of cPTIO with the free hydroxamic acid **2** or complex **3** showed that the EPR signal of cPTIO was not altered, even after 15 min (Fig. 4b, d). The same stability of cPTIO was observed in the presence of H_2O_2 and with the mixture of $FeCl_2 + H_2O_2$, a Fenton-reaction system generating hydroxyl radicals (Fig. 4c, e). Moreover, EPR monitoring did not show any evidence of reaction of cPTIO with $Na_3[Fe^{III}(CN)_6]$ (Fig. 4f). However, a net decrease of the cPTIO EPR signal was observed upon treatment of the Fe^{II} complex **3** with H_2O_2, indicating neutralization of the nitroxide radical, which would be a priori due to the release of HNO (Fig. 4a).

Our previous studies on the activation of $Na_3[Fe(CN)_5(INH)]$ (IQG607) complex in the presence of H_2O_2 gave evidences (by EPR spectroscopy) for the formation of the isonicotinoyl radical as an intermediate towards isonicotinoic acid [31, 37]. On this basis, it was decided to check whether the hydroxamate complex **3** or its acidic form $\mathbf{3H^+}$ could also generate pyrazinoic acid via a transient radical intermediate what could be an indirect evidence for the formation of $NO^{\cdot}$. By employing the same methodology used before for the investigation of the INH

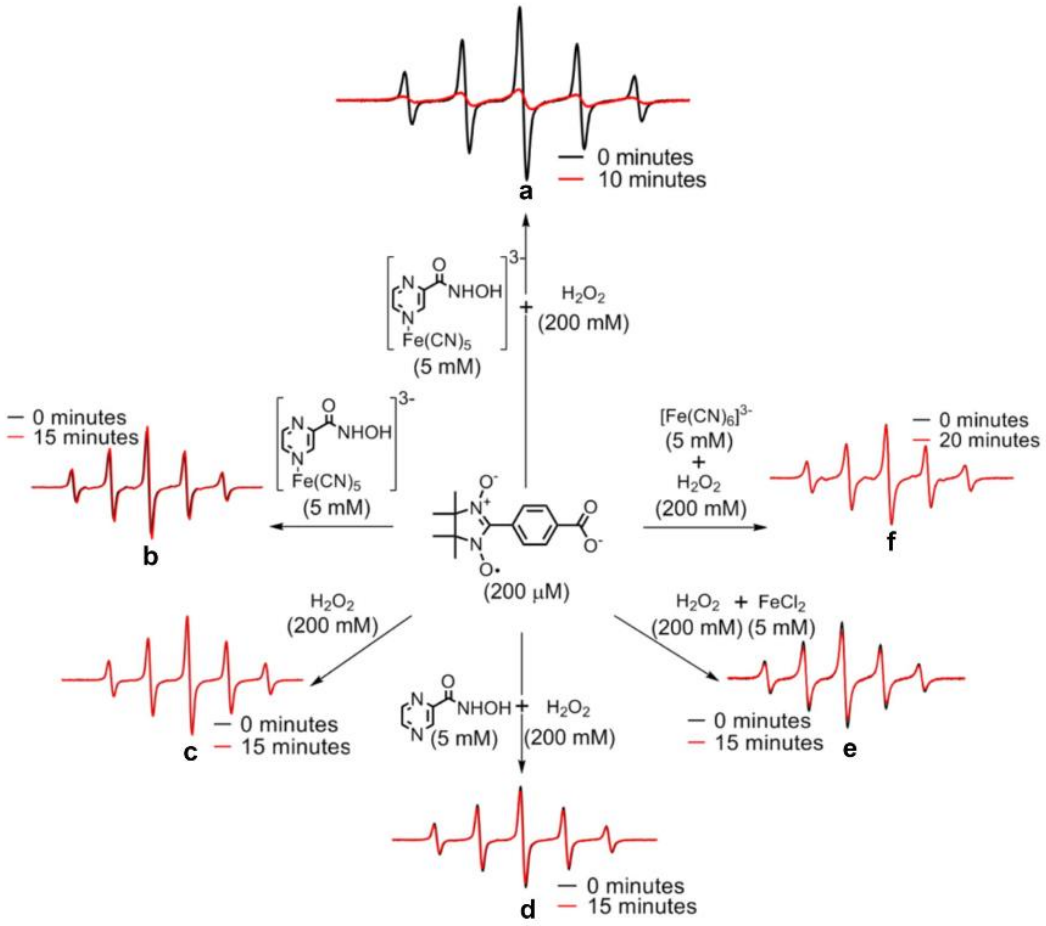

Fig. 4 **a** EPR signal of the cPTIO radical in the presence of the complex **3** under its protonated form $\mathbf{3H^+}$ and H_2O_2 (t_0 = black line and t_{10min} = red line) in phosphate buffer solution, 40 mM, pH 7.4. **b** Control of the stability of the cPTIO EPR signal in the presence of $Na_3Fe(CN)_5$-PyzCONHOH] (t_0 = black line and t_{15min} = red line). **c** Control of the stability of the cPTIO EPR signal in the presence of H_2O_2 (t_0 = black line and t_{15min} = red line). **d** Control of the stability of the cPTIO EPR signal in the presence of the ligand PyzCONHOH and H_2O_2 (t_0 = black line and t_{20min} = red line). **e** Control of the stability of the cPTIO EPR signal in Fenton reaction conditions [$FeCl_2$ (5 mM) and H_2O_2 (200 mM)] (t_0 = black line and t_{15min} = red line). **f** Control of the stability of the cPTIO EPR signal in the presence of $[Fe(CN)_6]^{3-}$ and H_2O_2 (t_0 = black line and t_{20min} = red line)

complex, EPR spectra were recorded using *N-tert*-butyl-α-phenylnitrone (PBN) as the spin trapping agent (Scheme S1B). In contrast to the parent iron complexes of isoniazid and of pyrazinoic acid hydrazide [30], $Na_3[Fe(CN)_5(INH)]$ and $Na_3[Fe(CN)_5(PyzCONHNH_2)]$, respectively, no radical could be trapped upon treatment of the pyrazine and even of the pyridine hydroxamic acid complexes (**3** and **6**, respectively), with H_2O_2 (Schemes 4 and 5).

To explain the latter results, two hypotheses can be proposed. In the case of the hydroxamic acid complexes, possibly formed HNO along with the aroyl radical (by analogy with the INH complex, Scheme 3) might quench the latter thus shortening its half-life time and preventing its detection by EPR. However, the process $HNO + ArC^{\bullet}=O \rightarrow NO^{\bullet} + PyzCHO$, would yield an aldehyde, which was not evidenced by ^1H NMR spectroscopy. Moreover, the benzile-like product of the radical coupling process $2\ ArCO^{\bullet} \rightarrow ArC(O)–C(O)Ar$ also failed to be isolated and even detected.

Another possibility is thus that, in the hydroxamic series, the carboxylic acid does not arise from an aroyl radical, but from another intermediate instead. This intermediate could be the undissociated aroyl-nitroso compound, generated upon an oxidation step, which could undergo a rapid heterolytic cleavage by the surrounding water molecules (Scheme 6), releasing HNO without any radical species, as previously suggested to occur from other hydroxamic acids [38, 39].

Inhibitory activity against *Mtb*

The antimycobacterial activity of the ligand **2** and complex **3** was investigated against the *Mtb* H37Rv reference strain, using INH as positive reference compound. The ligand **5** and the complex **6** were also introduced in these biological assays for comparison purposes. In this anti-mycobacterial assay, resazurin dye was employed to measure the lowest concentration of the tested compounds that could prevent any color change, which indicates a disruption of the growth. Those values were reported as MIC (minimum inhibitory concentration), which, for compounds **2** and **3**, **5** and **6** were, respectively, 100 and > 100 µg/mL, and for INH was 0.39 µg/mL. These results indicate that even at considerably high concentrations, there is no measurable inhibition of *Mtb* growth under these experimental conditions. However, putative activity against of *Mtb* strains within activated macrophage, or even in the non-replicating *Mtb* state, deserves further investigations.

Vasodilatory and antihypertensive activity

Aiming to test the hypothesis that metal complex **3** or $\mathbf{3H}^+$ can release HNO/NO, vasodilation assays were performed. Again, the ligand **2** and **5** and the complex **6** were also tested for comparison. The NO species is indeed known to induce vasodilation of blood vessels, and NO carrier molecules, such as sodium nitroprusside (SNP, $Na_2[Fe^{II}(CN)_5(NO)]$), have an important therapeutic effect for hypertensive crises [40]. At the same time, HNO, the reduced and protonated form of NO·, has also been reported to exhibit vasodilation activity, and shares many similar biological features of NO· [38, 39]. The structural analogy of the complexes **3** and **6** with SNP was thus a natural argument for such investigations, along with our further experimental evidences for HNO production (Fig. 4). Indeed, an assay carried out side-by-side with SNP and complexes **3** and **6** showed an interesting profile of vasodilation. While the free ligands **2** and **5** exhibited an expressively higher EC_{50} value for vasodilation activity at 19 µM, the metal complex **3** had an EC_{50} value of 250 nM only, a remarkable enhancement of 76-fold. Additionally, EC_{50} values for the complex **3** is 19-fold higher than SNP as measured side-by-side ($EC_{50} = 13$ nM). The complex **6** exhibits lower EC_{50} (64 nM) than **3** and SNP is only a fivefold more potent than **6**. The beneficial role of the iron complex moiety for vasodilation properties can be promptly noted by comparing the EC_{50} values of **2** and **3** and also **5** and **6** (Fig. 5). The concentration–response curve for the vasodilation experiments showed that the complex **3** as compared to SNP has the same efficacy and similar potency, which is a priori promising for the design of an alternative drug. Although SNP has several indications in cardiology such as heart failure, angina, after cardiac surgeries, hypertensive crisis, hypertensive encephalopathy, cardiogenic pulmonary oedema, it also has several contraindications and limitations such as liver toxicity, reflex tachycardia, and electrocardiographic alterations.

Although the water-soluble complexes **3** and **6**, able to release HNO/NO, are less potent than SNP, this can be an advantage because SNP, releasing NO rapidly, can cause major drops in blood pressure, thus requiring a careful control through titration.

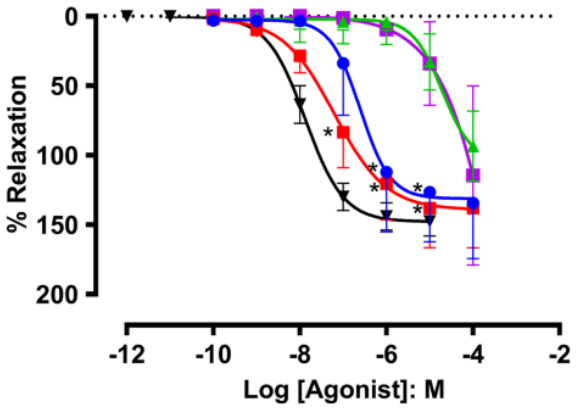

Fig. 5 Relaxation effects on aortic rings pre-contracted with 0.1 µM phenylephrine: $[Fe(CN)_5(\text{pyrazine-2-hydroxamic acid})]^{3-}$ (**3**) (blue), $Fe(CN)_5(\text{pyridine-4-hydroxamic acid})]^{3-}$ (**6**) (red), pyrazine-2-hydroxamic acid (**2**) (green), isonicotinoic hydroxamic acid (**5**) (purple) and SNP (black). *$p < 0.05$ vs. pyrazine-2-hydroxamic acid and isonicotinoic hydroxamic acid. The IC_{50} and respective 95% confidence interval were calculated only for **3** (250 nM, 91–690 nM) and **6** (64 nM, 25–160 nM)

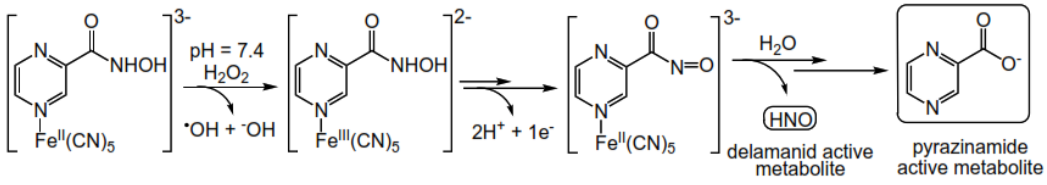

Scheme 6 Proposed outcome of the chemical oxidation of complex **3** under its trianionic form $\mathbf{3H}^+$ with H_2O_2

The complexes **3** and **6** can be all the more interesting since their efficacy (maximum relaxation effect) is quite similar to that of SNP. We should also point out that, in contrast to SNP, whose release of NO also promotes cyanide dissociation, the process is greatly reduced for new pentacyanoferrate complexes. Actually, a quick comparison of the lethal dose of SNP and the pentacyanoferrate(II)-INH complex (IQG607) illustrates this topic (mouse orally administered with SNP and IQG607 LD50 = 61 mg/kg and 2970 mg/kg, respectively), where SNP is over 48-fold more lethal [14, 41]. It is also noteworthy that those values correspond to oral dosages, but considering that pentacyanoferrate(II) complexes are particularly instable in acidic conditions—occurring in the rats' stomach— leading to decomposition and cyanide release—the real activity level might be even higher with other administration routes.

All these results indicate that the complex **3** or **6** might be a suitable model for designing alternative anti-hypertensive drugs. Modulation of the electronic effects on the metal center and changes on the aromatic hydroxamic ligand moiety might lead to more efficient tuning of their properties to achieve adjustable HNO/NO release. For instance, the compound **6**, which exhibited the lower EC_{50} (64 nM), was demonstrated to decrease blood pressure more efficiently in hypertensive rats (SHR) than its normotensive matched controls (Fig. 6). The doses of 1, 5, and 10 mg/kg promoted a drop in blood pressure equivalent to 45.6 ± 1.9%, 62.1 ± 2.5% and 65.1 ± 3.1% in SHR rats and 30.8 ± 2.3, 50.9 ± 4.2 and 53.3 ± 3.3 in normotensive rats, respectively. This compound did also increase cardiac output significantly, probably secondary to a decreased afterload and increased coronary flow.

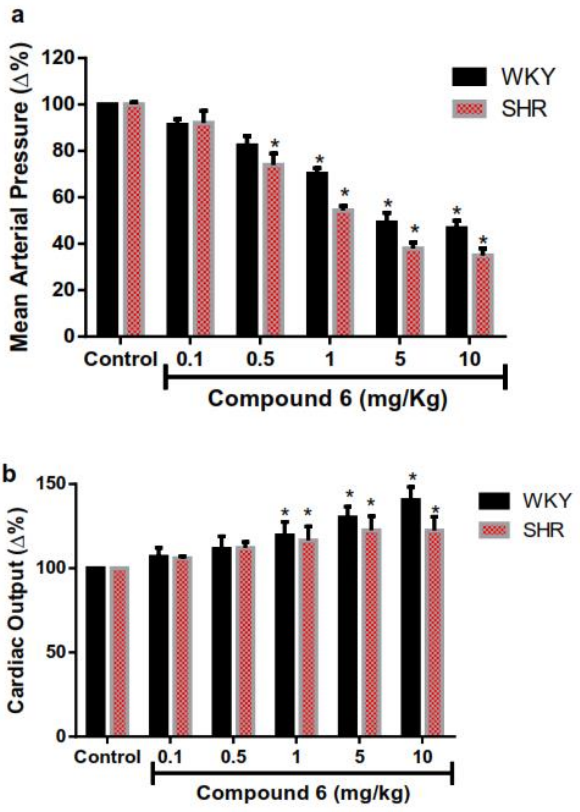

Fig. 6 Antihypertensive (**a**) and increased cardiac output (b) induced by compound **6** in normotensive (WKY) rats or spontaneously hypertensive rats (SHR). *$p < 0.05$ vs. control (administration of the vehicle)

Conclusion

The proposed strategy for metal-mediated oxidative activation of hybrid prodrugs, has been investigated for the anti-*Mtb* metabolites of pyrazinamide and delamanid in the hydroxamic hybrid series. The results unveil biological prospects of Fe(II) coordination complexes in pharmacophore design, while spanning a bridge between far-related medicinal challenges, from anti-bacterial to vasodilation effects. The complex **3** in the presence of H_2O_2 gave direct and indirect evidences for the release of pyrazinoic acid and HNO, respective active metabolites of pyrazinamide and delamanid. Although this complex did not exhibit anti-*Mtb* activity on actively growing non-resistant strains, further investigations may be warranted employing either/both single-condition whole-cell models (e.g., fatty acid carbon sources, hypoxia, low pH, biofilm, and carbon starvation) or/and multistress condition whole-cell models that try to recapitulate nonreplicating persistent bacilli, upon which pyrazinamide is active. Furthermore, promising advances have been established for antihypertensive therapy, where the hydroxamic complexes **3** and **6** have been shown to be globally as active as the SNP drug, with a more regular action and significantly lower toxicity. Additionally, comparison of vasodilation properties of **3** and **6** with those of **2** and **5** respectively, clearly show that the pentacyanoferrate moiety plays a beneficial role in the efficiency of the release of HNO from hydroxamic acids. Investigation of the expected longer duration of vasodilatory action of **3** and **6** will be performed in due course by systematic pharmacodynamic (PD) studies.

Acknowledgements The authors would also like to acknowledge financial support given by CNPq/FAPERGS/CAPES/BNDES to the National Institute of Science and Technology on Tuberculosis (INCT-TB), Brazil [grant numbers: 421703-2017-2/17-1265-8/14.2.0914.1; LGFLopes: CNPq 303355/2018-2; EHSS: CNPq 308383/2018-4, Universal 403866/2016-2) and COFECUB Project n° Ph-C 883/17. This study was financed in part by the Coordenação de Aperfeiçoamento de Pessoal de Nível Superior—Brasil (CAPES)—Finance Code 001.

Additionally, we are also in debt with Iury A. Paz, Renata Oliveira Santiago and Ariana Gomes da Silva for their assistance on the preliminary biological studies.

Compliance with ethical standards

Conflict of interest The authors declare have no conflict of interest.

Ethical approval All procedures were performed according to the ethics committee of State University of Ceará number 2897836/15.

References

1. Health World Organization annual report https://www.who.int/tb/publications/global_report/en/ Accessed 30 April 2020.
2. Ryan NJ, Lo JH (2014) Delamanid: first global approval. Drugs 74:1041–1045
3. Rustomjee R, Zumla A (2015) Delamanid expanded access novel treatment of drug resistant tuberculosis. Infect Drug Resist 8:359–366
4. Matsumoto M, Hashizume H, Tomishige T, Kawasaki M, Tsubouchi H, Sasaki H, Shimokawa Y, Komatsu M (2006) OPC-67683, a nitro-dihydro-imidazooxazole derivative with promising action against tuberculosis in vitro and in mice. PloS Med 3:e466
5. Singh R, Manjunatha U, Boshoff HIM, Ha YH et al (2008) PA-824 Kills Nonreplicating Mycobacterium tuberculosis by Intracellular NO Release. Science 322:1392–1395
6. Laborde J, Deraeve C, Bernardes-Génisson V (2017) Update of antitubercular prodrugs from a molecular perspective: mechanism of action, bioactivation pathways and associated resistance. ChemMedChem 12:1657–1676
7. Lopez BE, Shinnyashiki M, Han TH, Fukuto JM (2007) Antioxidant actions of nitroxyl (HNO). Free Radical Biol Med 42:482–491
8. Norris AJ, Sartippour MR, Lu M, Park T, Rao JY, Jackson MI, Fukuto JM, Brooks MN (2008) Nitroxyl inhibits breast tumor growth and angiogenesis. Int J Cancer 122:1905–1910
9. Nelli S, McIntosh L, Martin W (2001) Role of copper ions and cytochrome P450 in the vasodilator actions of the nytroxyl anion generator, Angeli's salt, on rat aorta. Eur J Pharmacol 412:281–289
10. Sousa EHS, Basso LA, Santos DS, Diógenes ICN, Longhinotti E, Lopes LGF, Moreira IS (2012) Isoniazid metal complex reactivity and insights for a novel anti-tuberculosis drug design. J Biol Inorg Chem 17:275–283
11. Basso LA, Schneider CZ, Santos AJAB, Santos AA Jr, Campos MM, Souto AA, Santos DS (2010) An inorganic complex that inhibits mycobacterium tuberculosis enoyl reductase as a prototype of a new class of chemotherapeutic agents to treat tuberculosis. J Braz Chem Soc 21:1384–1389
12. Sousa EHS, Pontes DL, Diogènes ICN, Lopes LGF, Oliveira JS, Basso LA, Santos DS, Moreira IS (2005) Electron transfer kinetics and mechanistic study of the thionicotinamide coordinated to the pentacyanoferrate(III)/(II) complexes: a model system for the in vitro activation of thioamides anti-tuberculosis drugs. J Inorg Biochem 99:368–375
13. Abbadi BL, Villela AD, Rodrigues-Junior VS, Subtil FT, Dalberto PF, Pinheiro APS, Santos DS, Machado P, Basso LA, Bizarro CV (2018) Revisiting activation of and mechanism of resistance to compound IQG-607 in *Mycobacterium tuberculosis*. Antimicrob Agents Chemother 62:e2222–e2317
14. Abbadi BL, Rodrigues-Junior VS, Dadda AS, Pissinate K, Villela AD, Campos MM, Lopes LGF, Bizarro CV, Machado P, Sousa EHS, Basso LA (2018) Is IQG-607 a potential metallodrug or metallopro-drug with a defined molecular target in Mycobacterium tuberculosis? Front Microbiol 9:880
15. Zhang Y, Mitchison D (2003) The curious characteristics of pyrazinamide: a review. Int J Tuberc Lung Dis 7:6–21
16. Vandal OH, Nathan CF, Ehrt S (2009) Acid resistance in *Mycobacterium tuberculosis*. J Bacteriol 191:4714–4721
17. Zhang Y, Mitchison D, Shi W, Zhang W (**2014**) Mechanisms of pyrazinamide action and resistance. Microbiol. Spectr. 2: MGM2-0023-2013
18. Njire M, Tan Y, Mugweru J, Wang C, Guo J, Yew W, Tan S, Zhang T (2016) Pyrazinamide resistance in *Mycobacterium tuberculosis*: review and update. Adv Med Sci 61:63–71
19. Stehr M, Elamin AA, Singh M (2015) Pyrazinamide: the importance of uncovering the mechanisms of action in mycobacteria. Expert Rev Anti Infect Ther 13:593–603
20. Pires BM, Jannuzzi SAV, Formiga ALB, Bonacin JA (2014) Prussian blue films produced by pentacyanidoferrate(II) and their application as active electrochemical layers. Eur J Inorg Chem 2014:5812–5819
21. Becke AD (1993) Density-functional thermochemistry. III. The role of exact exchange. J Chem Phys 98:5648–5652
22. Lee C, Yang W, Parr RG (1988) Development of the Colle-Salvetti correlation-energy formula into a functional of the electron density. Phys Rev B 37:785–789
23. Stephens PJ, Devlin FJ, Chabalowski CF, Frisch MJ (1994) Ab Initio calculation of vibrational absorption and circular dichroism spectra using density functional force fields. J Phys Chem 98:11623–11627
24. Frisch MJ, Trucks GW, Schlegel HB, Scuseria GE, Robb MA, Cheeseman JR, Scalmani G, Barone V, Mennucci B, Petersson GA, Nakatsuji H, Caricato M, Li X, Hratchian HP, Izmaylov AF, Bloino J, Zheng G, Sonnenberg JL, Hada M, Ehara M, Toyota K, Fukuda R, Hasegawa J, Ishida M, Nakajima T, Honda Y, Kitao O, Nakai H, Vreven T, Montgomery JA Jr, Peralta JE, Ogliaro F, Bearpark M, Heyd JJ, Brothers E, Kudin KN, Staroverov VN, Kobayashi R, Normand J, Raghavachari K, Rendell A, Burant JC, Iyengar SS, Tomasi J, Cossi M, Rega N, Millam JM, Klene M, Knox JE, Cross JB, Bakken V, Adamo C, Jaramillo J, Gomperts R, Stratmann RE, Yazyev O, Austin AJ, Cammi R, Pomelli C, Ochterski JW, Martin RL, Morokuma K, Zakrzewski VG, Voth GA, Salvador P, Dannenberg JJ, Dapprich S, Daniels AD, Farkas O, Foresman JB, Ortiz JV, Cioslowski J, Fox DJ (2013) Gaussian 09, Revision D.01. Gaussian Inc, Wallingford
25. Tomasi J, Mennucci B, Cammi R (2005) Quantum mechanical continuum solvation models. Chem Rev 105:2999–3093
26. O'Boyle NM, Tenderholt AL, Langner KM (2008) Cclib: a library for package-independent computational chemistry algorithms. J Comput Chem 29:839–845
27. Giacobbo BC, Pissinate K, Rodrigues-Junior V, Villela AD, Grams ES, Abbadi BL, Subtil FT, Sperotto N, Trindade RV, Back DF, Campos MM, Basso LA, Machado P, Santos DS (2017) New insights into the SAR and drug combination synergy of 2-(quinolin-4-yloxy)acetamides against *Mycobacterium tuberculosis*. Eur J Med Chem 126:491–501
28. Kushner S, Dalalian H, Sanjurjo JL, Bach FL Jr, Safir SR, Smith VK Jr, Williams JH (1952) Experimental chemotherapy of tuberculosis. II. The Synthesis of pyrazinamides and related compounds. J Am Chem Soc 74:3617–3621
29. Zhang YY, Gao W-X, Lin Y-J, Mi L-W, Jin G-X (2017) Syntheses, structures, and solution studies of multicomponent macrocycles and cages based on versatile ligands. Chem Eur J 23:11133–11140
30. Hackley BE Jr, Plafinger R, Stolberg M, Wagner-Jauregg T (1955) Accelaration of the hydrolysis of organic fluoro-phosphates and

fluorophosphonates with hydroxamic acids. J Am Chem Soc 77:3651–3653
31. Laborde J, Deraeve C, Vieira FGM, Sournia-Saquet A, Rechignat L, Villela AD, Abbadi BL, Macchi FS, Pissinate K, Lopes LGF, Sousa EHS, Pratviel G, Bernardes-Génisson V (2018) Synthesis and mechanistic investigation of iron(II) complexes of isoniazid and derivatives as a redox-mediated activation strategy for anti-tuberculosis therapy. J Inorg Biochem 179:71–81
32. Grandjean F, Samain L, Long GJ (2016) Characterization and utilization of Prussian blue and its pigments. Dalton Trans 45:18018–18044
33. Carvalho EM, Rechignat L, Sousa EHS, Lopes LGF, Chauvin R, Bernardes-Génisson V (2020) Mechanistic insights into the in vitro metal-promoted oxidation of (di)azine hydroxamic acids: evidence of HNO release and N, O-di(di)azinoyl hydroxylamine intermediate. New J Chem 44:11965–11973
34. Samuni U, Samuni Y, Goldstein S (2010) On the distinction between nitroxyl and nitric oxide using nitronyl nitroxides. J Am Chem Soc 132:8428–8432
35. Bobko AA, Ivanov A, Khramtsov VV (2013) Discriminative EPR detection of NO and HNO by encapsulated nitronyl nitroxides. Free Radic Res 47:74–81
36. Bobko AA, Khramtsov VV (2015) Redox properties of the nitronyl nitroxide antioxidants studied via their reactions with nitroxyl and ferrocyanide. Free Radic Res 49:919–926
37. Sousa EHS, Vieira FGM, Butler JS, Basso LA, Santiago DS, Santiago DS, Diógenes ICN, Lopes LGF, Sadler PJ (2014) $[Fe(CN)_5(isoniazid)]^{3-}$: an iron isoniazid complex with redox behavior implicated in tuberculosis therapy. J Inorg Biochem 140:236–244
38. Maimon E, Lemer A, Samuni A, Goldstein S (2018) Direct observation of acyl nitroso compounds in aqueous solution and the kinetics of their reactions with amines, thiols, and hydroxamic acids. J Phys Chem A 122:7006–7013
39. Maimon E, Lemer A, Samuni A, Goldstein S (2018) Nitrogen dioxide reaction with nitroxide radical derived from hydroxamic acids: the intermediacy of acyl nitroso and nitroxyl (HNO). J Phys Chem A 122:3747–3753
40. Silva Filho PM, Paz IA, Nascimento NRF, Santos CF, Araújo VR, Aquino CP, Ribeiro TS, Vasconcelos IF, Lopes LGF, Sousa EHS, Longhinotti E (2019) Incorporation of nitroprusside on silica nanoparticles—a strategy for safer use of this no donor in therapy. Mol Pharm. 16:2912–2921
41. RTECS—Register of toxic effects of chemical substances. https://www.cdc.gov/niosh/docs/97-119/default.html. Accessed 30 Apr 2020

Affiliations

Edinilton Muniz Carvalho[1,2,3] · Tercio de Freitas Paulo[1,2,3] · Alix Sournia Saquet[1] · Bruno Lopes Abbadi[4,5] · Fernanda Souza Macchi[4,5] · Cristiano Valim Bizarro[4,5] · Rafael de Morais Campos[6] · Talles Luann Abrantes Ferreira[6] · Nilberto Robson Falcão do Nascimento[6] · Luiz Gonzaga França Lopes[3,5] · Remi Chauvin[1,2] · Eduardo Henrique Silva Sousa[3,5] · Vania Bernardes-Génisson[1,2]

1 CNRS, Laboratoire de Chimie de Coordination, LCC, UPR 8241, 205 Route de Narbonne, BP 44099, 31077 Cedex 4 Toulouse, France

2 Université de Toulouse, Université Paul Sabatier, UPS, 118 Route de Narbonne, 31062 Cedex 9, Toulouse, France

3 Grupo de Bioinorgânica, Departamento de Química Orgânica E Inorgânica, Universidade Federal Do Ceará, Campus Pici, Fortaleza, CE 60455-760, Brazil

4 Centro de Pesquisas Em Biologia Molecular E Funcional (CPBMF), Pontifícia Universidade Católica Do Rio Grande Do Sul (PUCRS), Porto Alegre, Brazil

5 Instituto Nacional de Ciência E Tecnologia Em Tuberculose (INCT-TB), Porto Alegre, Brazil

6 Laboratório de Farmacologia Cardiovascular E Renal, Universidade Estadual Do Ceará, Campus do Itaperi, Fortaleza, CEP 60714-903, Brazil

4.9 Supporting information

4.9.1 Synthetic procedures

*Sodium pyrazine-2-carboxylate (**8**)*

To a suspension of pyrazinoic acid (0.12 g, 0.970 mmol) in water (8 mL) was added a solution of NaOH (0.033 g, 0.817 mmol) in water (2 mL). The final solution was stirred at room temperature for 30 min. The solvent was removed under vaccum at 50 °C. The solid was collected and recrystallized (solubilized in water (1mL) then addition of ethanol (50 mL)). The mixture was stirred for 30 min then the solid was collected and washed with ice-cold ethanol.

Yield = 87.5% (0.124 g), white solid. **^{1}H NMR** (400 MHz, D_2O) δ (ppm): 9.02 (s, 1H), 8.63-8.61 (s, 2H). **^{13}C NMR** (101 MHz, D_2O) δ (ppm): 170.37 (C=O), 148.04 (Cq), 145.96 (CH), 144.63 (CH), 144.29 (CH). **IR** symmetric stretching (ν_s), antisymmetric stretching (ν_{as}), symmetric bending (δ_s) and twisting (τ) (cm^{-1}): 1612 - 1572 (ν_s C=O), 1420 - 1380 (ν_s C=N, ν_s C=C), 1308 (δ_s C-H), 1156 - 1020 (ν_{as} C=N), 852 (τ C-H). **UV-Vis** (H_2O) λ_{max}/nm ($\varepsilon/M^{-1}cm^{-1}$) = 211 (6575), 268 (2343).

*$Na_4[Fe^{II}(CN)_5$(pyrazine-2-carboxylate)] (**9**)*

To a solution of $Na_3[Fe^{II}(CN)_5(NH_3)]\cdot 3H_2O$ (0.100 g, 0.307 mmol, 1 eq.) in water (3 mL) was slowly added a solution of the ligand sodium pyrazine-2-carboxylate (0.054 g, 0.368 mmol) in water (2 mL). The mixture was stirred at room temperature, under argon atmosphere and protected from light for 3 h. Then a cold solution of ethanol (150 mL) containing an excess of sodium iodide (30 eq.) was added dropwise. The resulting precipitate was stand overnight at -20 ºC before to be collected by filtration, washed with cold ethanol and dried in a vacuum desiccator. CAUTION: since these complexes are light- and oxygen-sensitive, they must be stored in a vacuum desiccator in the dark.

Yield = 64% (0.064 g), red solid. **^{1}H NMR** (400 MHz, D_2O) δ (ppm): 9.54 (s, 1H), 9.16 (d, J = 3.3 Hz, 1H), 8.28 (dd, J = 2.9, 1.5 Hz, 1H). **^{13}C NMR** (101 MHz, D_2O) δ (ppm): 178.81 (CN_{eq}), 173.95 (CN_{ax}), 171.02 (C=O), 154.05 (CH), 153.17 (CH), 147,09 (Cq), 142.44 (CH). **IR** symmetric stretching (ν_s), antisymmetric stretching (ν_{as}), symmetric bending (δ_s), antisymmetric bending (δ_{as}) and wagging (π) (cm^{-1}): 3532 - 3268 (ν_s C-H), 2052 (ν_s C≡N), 1638 (ν_s C=O), 1578 - 1470 (ν_s C=C, ν_s C=N), 1410 - 1169 (δ_s C-H), 1032 (τ C-H). 864 (δ_{as}

C-H), 792 and 743 (π C-H), 653 (ν_s C=N). **UV-Vis** (H_2O) λ_{max}/nm ($\varepsilon/M^{-1}cm^{-1}$) = 203 (22700), 268 (6228), 478 nm (3638). **Electrochemistry** in 0,1M Phosphate buffer pH 7.4: $E_{1/2}$ 0.581 V/NHE.

4.9.2 Tables and Figures

Table S1 - Selected **e**xperimental and calculated wavenumber values obtained from IR and NR spectra of solid complexes **3**, and **6**, and their corresponding vibrational assignments.

Complex	**λ_{EXP} /nm**	**λ_{DFT} /nm**	***Osc. Strength (f)***	**Key transition**	**Character**
3		496	0.0955	HOMO-1 →LUMO	MLCT
	360	385	0.0113	HOMO-1 →LUMO+1	MLCT
	270	273	0.0147	HOMO-6→LUMO	IL+LLCT
	216	218	0.0504	HOMO-17→LUMO	IL+LLCT
6	439	493	0.1334	HOMO-1→LUMO	MLCT
	266	284	0.0243	HOMO-3→LUMO	MLCT+LLCT
	233	240	0.0640	HOMO-12→LUMO	IL+LLCT

Reference: Elaborated by the author.

Table S2. Selected electronic transitions for complex **3** and **6**.

Wavenumber (cm^{-1})								vibrational assignment
Compound								
3		**6**		**3**		**6**		
Infrared				**Raman**				
Exp.	DFT	Exp.	DFT	Exp.	DFT	Exp.	DFT	
			508	503	507			β(FeC≡N)
571		572	587	574	549	575	508	$\beta(NH)_{OP}$
654	617	697	663	653	617			Ring
749	745			746	745			Ring
856	828	849	828			701	722	$\beta(CH)_{OP}$
				1033	996	1023	975	Ring
		1035	1034	1074	1023	1066		Ring+*ν*(NO)
		1169	1135	1155	1140			β(CH)
1029	1050							Ring
1176	1161						1135	Ring
				1292	1344	1227	1191	ν(C–NH)+β(CH)
1352	1360	1316	1339	1358	1388	1314	1338	β(NH)+β(CH)
1574	1525	1415	1485					β(CH)+*ν*(C=O)+β(NH)
	1539	1652	1560	1583	1542			*ν*(CC)ring+*ν*(C=O)+β(NH)
						1610	1560	*ν*(CC)ring
2053	2048	2047	2046	2071	2050	2070	2047	*ν*(C≡N)
2094	2057	2093	2065	2097	2071	2093	2065	*ν*(C≡N)

Op = out-of-plane

Reference: Elaborated by the author.

Figure S1 - (A) and (B) ^{1}H NMR spectra of **2** and **3**, respectively, in D_2O, 400 MHz. (C) and (D) ^{13}C NMR spectra of **2** and **3**, respectively, in D_2O, 101 MHz (^{13}C reference = MeOD). (E) and (F) 2D ^{1}H-^{15}N HMQC NMR spectrum of **2** and **3**, respectively, in D_2O, 50.7 MHz.

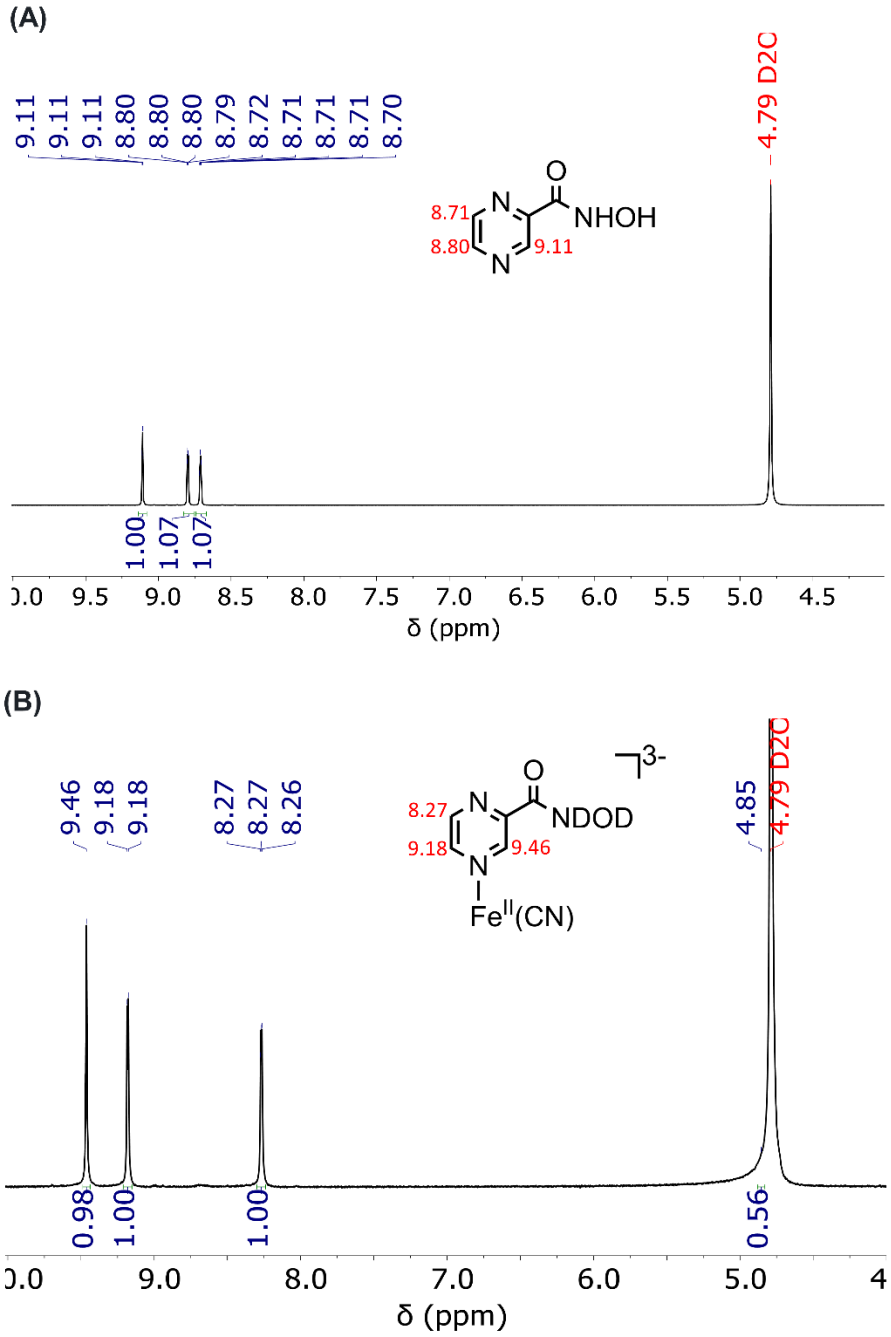

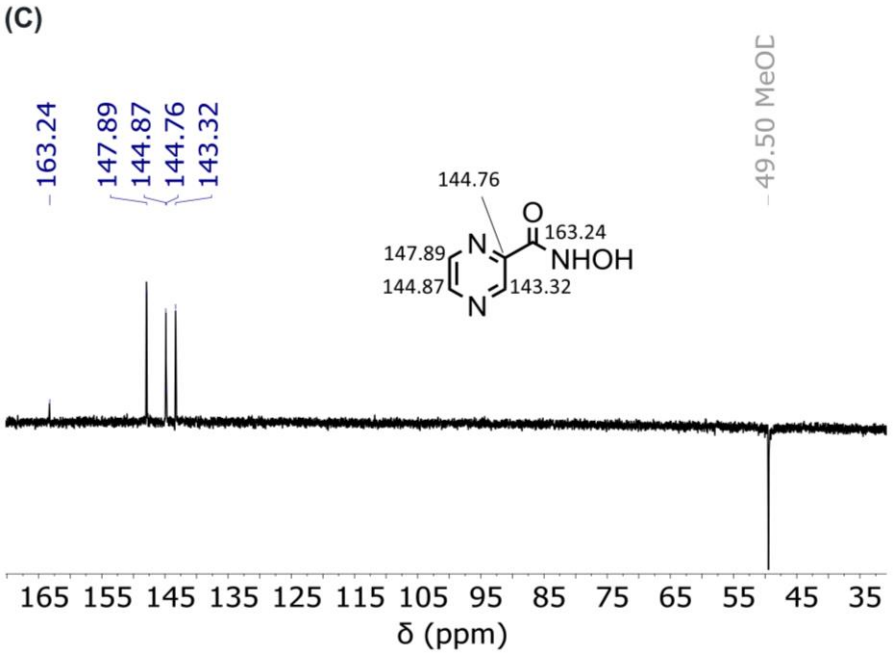
(C)
163.24
147.89
144.87
144.76
143.32
49.50 MeOD
144.76
O
163.24
NHOH
147.89
144.87
143.32
N
N
165 155 145 135 125 115 105 95 85 75 65 55 45 35
δ (ppm)

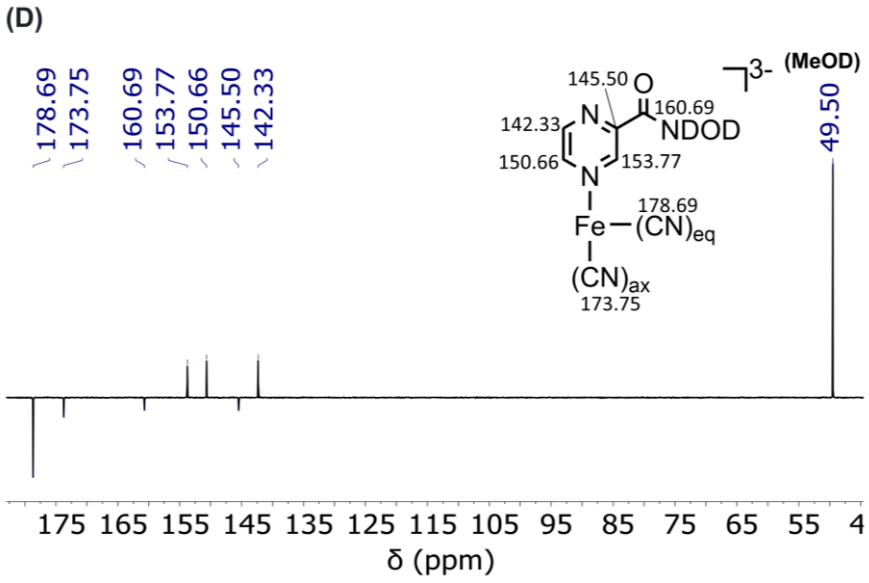
(D)
178.69
173.75
160.69
153.77
150.66
145.50
142.33
49.50
(MeOD)
3-
145.50
O
160.69
NDOD
142.33
150.66
153.77
N
178.69
Fe
(CN)eq
(CN)ax
173.75
175 165 155 145 135 125 115 105 95 85 75 65 55 4
δ (ppm)

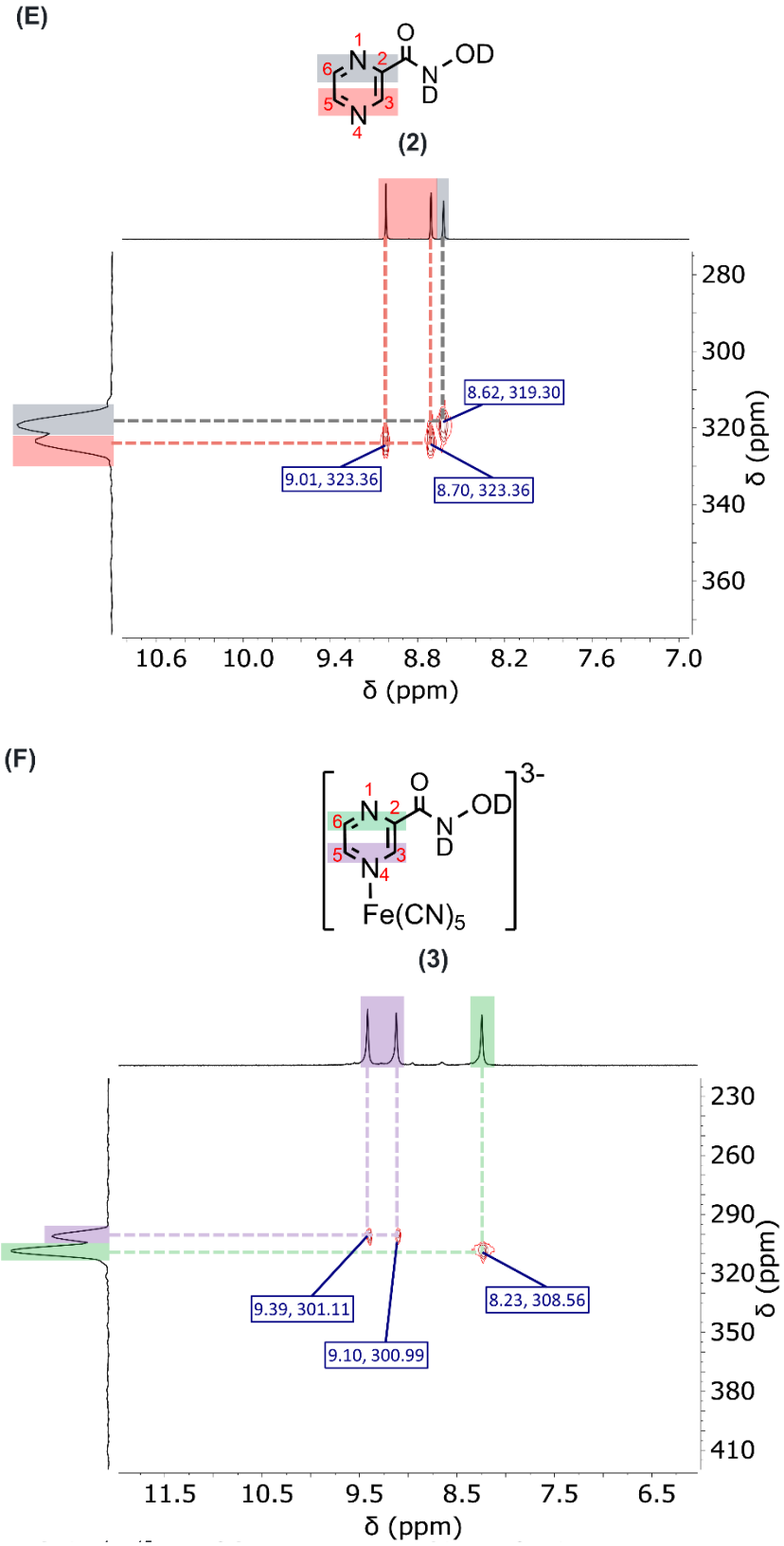

Reference: Elaborated by the author.

Figure S2 - Cyclic voltammograms of glassy carbon electrode in solution of compound $[Fe^{II}(CN)_5(PyzCONHO)]^{3-}$ (A) and $[Fe^{II}(CN)_5(PyCONHO)]^{3-}$ (B), using vitreous carbon electrode as work, platinum electrode as auxiliary electrode and saturated calomel electrode (SCE) as reference, in phosphate buffer 0.1M pH 7.4 as electrolyte. Scan speed of 200 mV s^{-1}. Potential values were plotted from SCE to NHE for comparative purposes. Ligands in blue and complex in red.

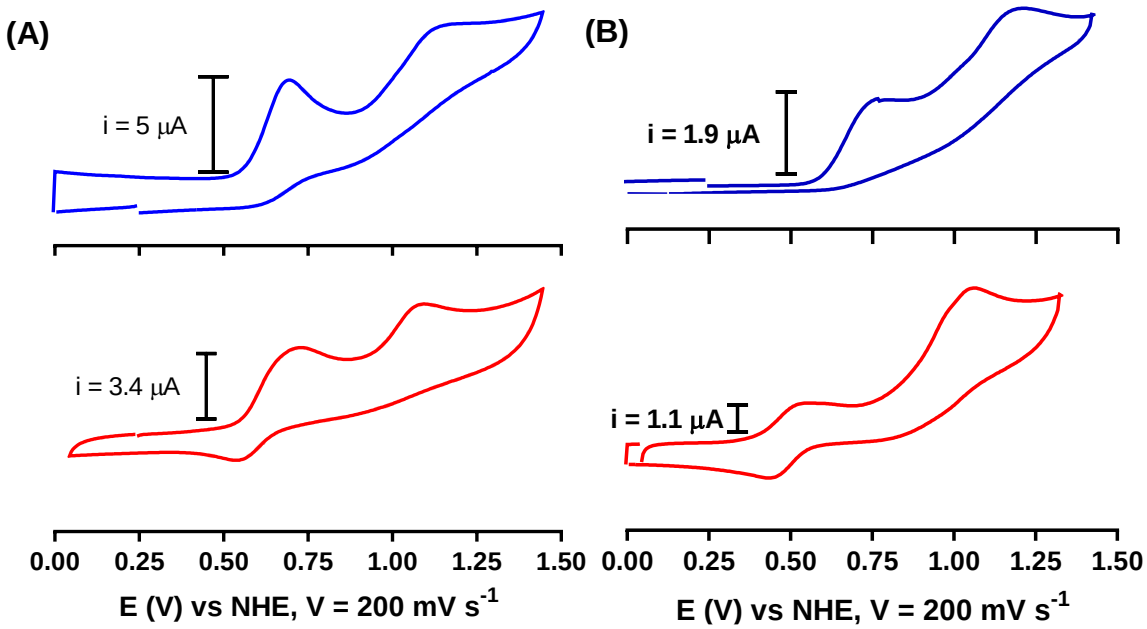

Reference: Elaborated by the author.

Figure S3 - UV-Visible absorption spectra of the free ligand **2** (103 µM, blue) and complex **3** (45 µM, red) in water solution, at pH = 6.8.

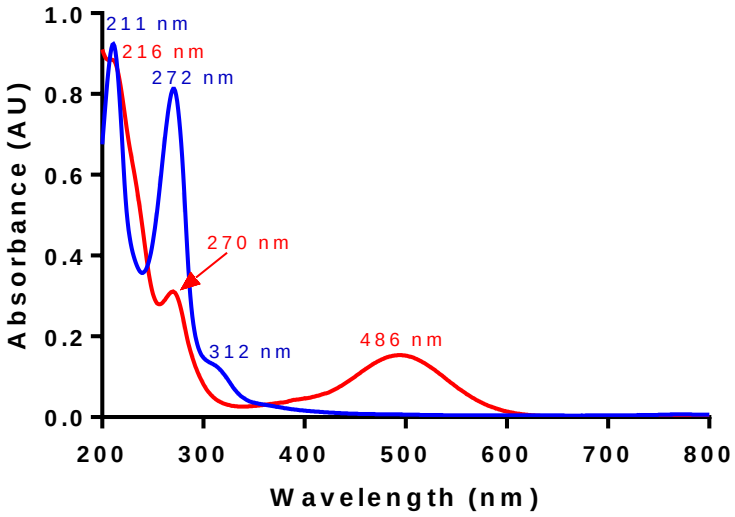

Reference: Elaborated by the author.

Figure S4 - Calculated UV-Visible absorption spectra and calculated singlet−singlet transition energies of the complexes **3** (a) and **6** (b) taking account in a water solvent field.

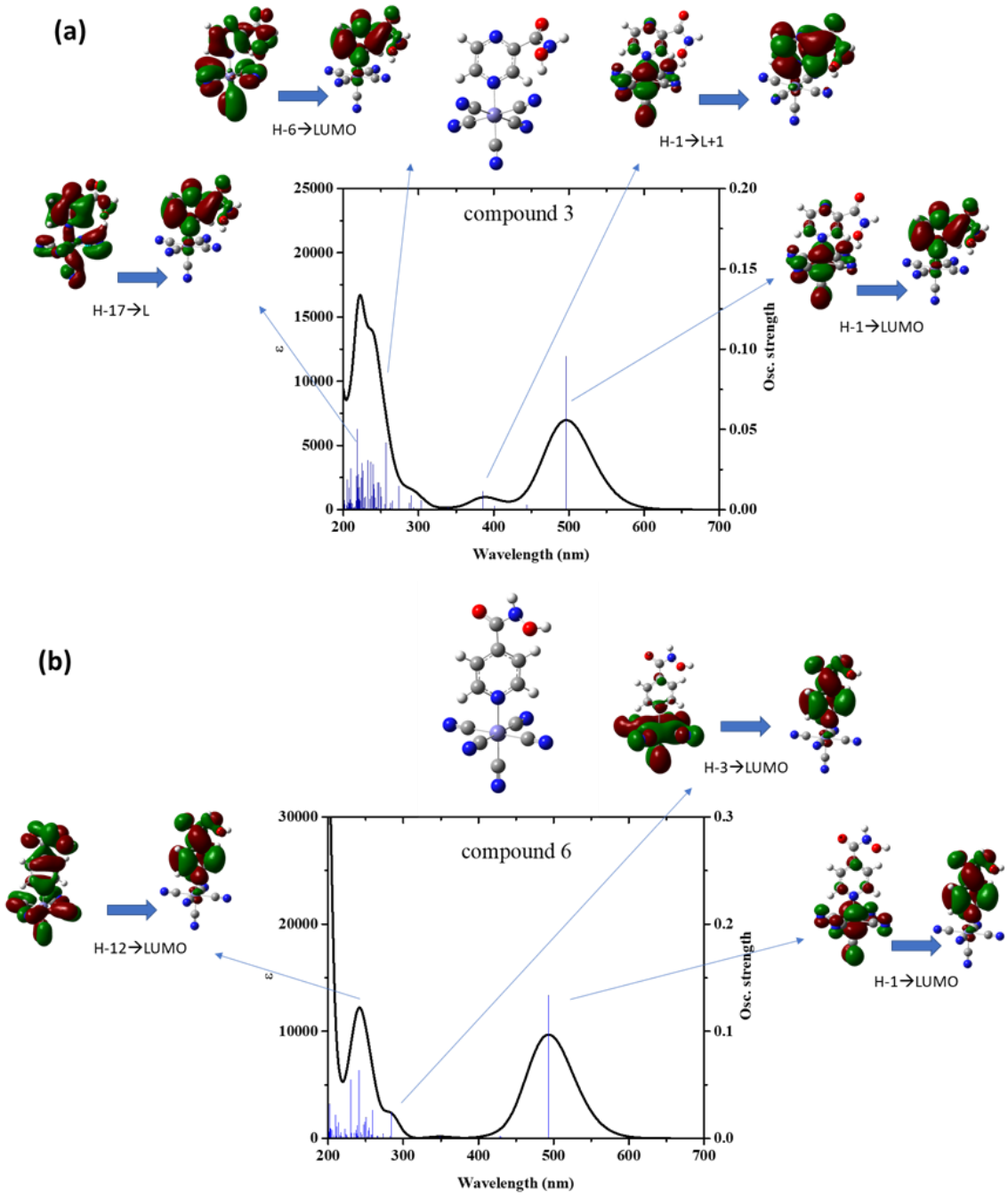

Reference: Elaborated by the author.

Scheme S1 - (A) Reactions of cPTIO with HNO and NO• and (B) Trapping reaction of the isonicotinoyl radical by PBN.

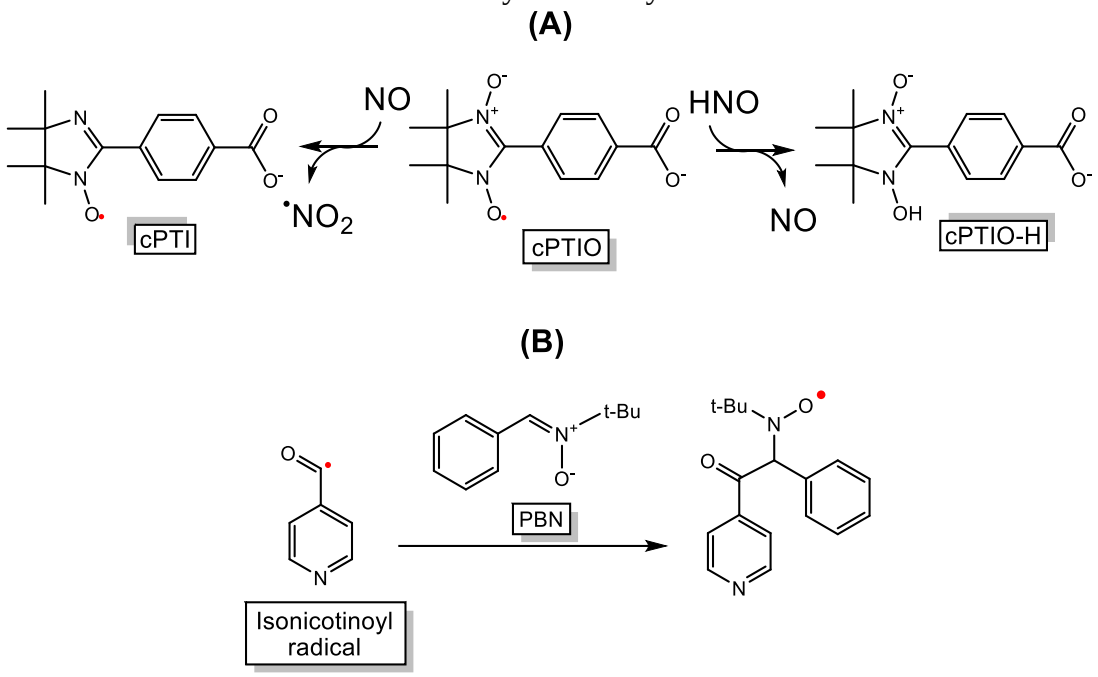

Reference: Elaborated by the author.

4.10 Unpublished results associated with the article

This study allowed the development of the compound $Na_4[Fe^{II}(CN)_5$(pyridine-3-hydroxamic acid)] (**13**), as well as its characterization and the study of its oxidative activation as done for complexes **3** and **6**. Despite not being included in the previous article, this complex presented chemical and biological results similar to compounds **3** and **6**. The results regarding this complex are presented and discussed briefly below.

4.10.1 Synthetic procedures

*Pyridine-3-hydroxamic acid (**10**)*

The synthesis of pyridine-3-hydroxamic acid followed the same protocol mentioned in the article for the preparation of hydroxamic acids ligands.

Yield = 82 % (0.40 g), white solid. **^{1}H NMR** (300 MHz, DMSO-d_6) δ (ppm): 11.39 (s, 1H), 9.21 (s, 1H), 8.90 (dd, J = 2.3, 0.9 Hz, 1H), 8.70 (dd, J = 4.8, 1.7 Hz, 1H), 8.10 (ddd, J = 7.9, 2.3, 1.7 Hz, 1H). **^{13}C NMR** (101 MHz, DMSO-d_6) δ (ppm): 163.04 (C=O), 152.30 (CH), 148.34 (CH), 135.13 (CH), 128.95 (Cq), 124.02 (CH). **IR** symmetric stretching (ν_s), antisymmetric stretching (ν_{as}), symmetric bending (δ_s) and twisting (τ) (cm^{-1}): 3197 (ν_s N-H), 3100 (ν_s O-H), 1643 (ν_s C=O), 1588 – 1499 (ν_s C=N, ν_s C=C), 1300 (δ_s C-H), 1192 - 1024 (ν_{as}

C=N), 808 (τ C-H). **UV-Vis** (H_2O) λ_{max}/nm ($\varepsilon/M^{-1}cm^{-1}$) = 208 (7459), 261 (3544). **HRMS** (DCI/CH_4): for {($C_5H_5N_3O_2$) + H^+} calcd.: 139.0508 found: 139.0514. **Anal. Calcd.** for $C_6H_6N_2O_2$: C, 52.17; H, 4.38; N, 20.28. Found: C, 52.09; H, 3.96; N, 20.12. **Retention Factor** (methanol/dichloromethane 10%) = 0.31. **M.T** = 164 °C **Electrochemistry** (0,1 M Phosphate buffer pH 7.4) E_{pa} = 0.641, 0.963 and 1.104 V *vs* NHE.

*Pyridine-4-carboxylate (**11**) and pyridine-3-carboxylate (**12**) sodium salt*

The synthesis protocol of pyridine-4-carboxylate (**11**) and pyridine-3-carboxylate (**12**) sodium salt was the same employed for the sodium pyrazine-3-carboxylate (described in the supplementary material of the article).

*Pyridine-4-carboxylate sodium salt (**11**)*

Yield = 99.0 % (0.140 g), white solid. **^{1}H NMR** (400 MHz, D_2O) δ (ppm): 8.66 (d, *J* = 4.8, 1H), 7.85 (d, *J* = 4.9, 1H). **^{13}C NMR** (101 MHz, D_2O) δ (ppm): 173.28 (C=O), 148.42 (CH), 147.47 (Cq), 124.19 (CH), 49.50 (MeOD). **IR** symmetric stretching (ν_s), antisymmetric stretching (ν_{as}), symmetric bending (δ_s) and twisting (τ) (cm^{-1}): 1588 (C=O), 1540 - 1396 (ν_s C=N, ν_s C=C), 1300 (δ_s C-H), 1216 - 1024 (ν_{as} C=N), 844 (τ C-H). **UV-Vis** (H_2O) λ_{max}/nm ($\varepsilon/M^{-1}cm^{-1}$) = 211 (6575), 268 (2343). **Anal. Calcd.** for $NaC_6H_4O_2 \cdot 0.1H_2O$: C, 49.06; H, 2.88; N, 9.54. Found: C, 49.10; H, 2.52; N, 9.45.

*Pyridine-3-carboxylate sodium salt (**12**)*

Yield = 99 % (0.14 g), white solid. **^{1}H NMR** (300 MHz, D_2O) δ (ppm): 8.95 (dd, *J* = 2.2, 0.9 Hz, 1H), 8.61 (dd, *J* = 5.0, 1.7 Hz, 1H), 8.25 (ddd, *J* = 7.9, 2.2, 1.7 Hz, 1H), 7.52 (ddd, *J* = 7.9, 5.0, 0.9 Hz, 1H). **^{13}C NMR** (101 MHz, D_2O) δ (ppm): 172.98 (C=O), 149.74 (CH), 148.51 (CH), 139.65 (CH), 133.54 (Cq), 125.04 (CH). **IR** symmetric stretching (ν_s), antisymmetric stretching (ν_{as}), symmetric bending (δ_s) and twisting (τ) (cm^{-1}): 1616 (ν_s C=O), 1557 - 1403 (ν_s C=N, ν_s C=C), 1301 (δ_s C-H), 1200 - 1029 (ν_{as} C=N), 837 (τ C-H). **UV-Vis** (H_2O) λ_{max}/nm ($\varepsilon/M^{-1}cm^{-1}$) = 212 (7350), 260 (2549), 265 (2819), 272 (2137). **Anal. Calcd.** for $NaC_6H_4O_2$: C, 49.67; H, 2.78; N, 9.65. Found: C, 49.47; H, 2.07; N, 9.53.

Pentacyanoferrate(II) complexes

The synthesis protocol of $Na_4[Fe^{II}(CN)_5$(pyridine-3-hydroxamic acid)] (**13**), $Na_4[Fe^{II}(CN)_5$(pyridine-4-carboxylate)] (**14**), and $Na_4[Fe^{II}(CN)_5$(pyridine-3-carboxylate)] (**15**) was the same employed for the complex **3** (see article).

*$Na_4[Fe^{II}(CN)_5$(pyridine-3-hydroxamic acid)] **(13)***

Yield = 92 % (0.202 g), yellow solid. **^{1}H NMR** (400 MHz, D_2O) δ (ppm): 9.19 (d, *J* = 2.0 Hz, 1H), 9.08 (dd, *J* = 5.7, 1.4 Hz, 1H), 7.95 (dt, *J* = 7.9, 1.8 Hz, 1H), 7.30 (dd, *J* = 7.9, 5.6 Hz, 1H). **^{13}C NMR** (101 MHz, D_2O) δ (ppm): 180.64 (CN_{eq}), 175.84 (CN_{ax}), 165.30 (Cq), 159.35 (CH), 154.67 (CH), 135.10 (CH), 128.83 (Cq), 123.91 (CH). **IR** symmetric stretching (ν_s), symmetric bending (δ_s), antisymmetric bending (δ_{as}) and twisting (τ) (cm^{-1}): 3452 (ν_s N-H), 3312 - 3102 (ν_s O-H), 2056 (ν_s C≡N), 1638 - 1572 (ν_s C=C, ν_s C=N, ν_s C=O), 1319 (δ_s C-H), 1022 (τ C-H), 912 (δ_{as} C-H). **UV-Vis** (H_2O) λ_{max}/nm ($\varepsilon/M^{-1}cm^{-1}$) = 215 (18870), 261 (5254), 394 (2608). **Anal. Calcd.** for $C_{11}H_5FeN_7O_2Na_4 \cdot 3.6H_2O$: C, 27.53; H, 2.56; N, 20.43. Found: C, 27.23; H, 2.92; N, 20.17. **Electrochemistry** in 0,1 M Phosphate buffer pH 7.4: E_{pa} = 0.623 and 0.891 V *vs* NHE, E_{pc} = 0.818 and 0.447 V *vs* NHE.

*$Na_4[Fe^{II}(CN)_5$(pyridine-4-carboxylate)] **(14)***

Yield = 42 % (0.042 g), yellow solid. **^{1}H NMR** (400 MHz, D_2O) δ (ppm): 9.03 (d, *J* = 5.9, 2H), 7.46 (d, *J* = 5.9, 2H). **^{13}C NMR** (101 MHz, D_2O) δ (ppm): 180.71 (CN_{eq}), 176.45 (CN_{ax}), 170.66 (Cq), 157.50 (CH), 143.89 (Cq), 122.42 (CH), 49.50 (MeOD). **IR** symmetric stretching (ν_s), symmetric bending (δ_s), antisymmetric bending (δ_{as}) and twisting (τ) (cm^{-1}): 2044 (ν_s C≡N), 1636 – 1540 (ν_s C=C, ν_s C=N, ν_s C=O), 1384 (δ_s C-H), 1036 (τ C-H), 928 (δ_{as} C-H). **UV-Vis** (H_2O) λ_{max}/nm ($\varepsilon/M^{-1}cm^{-1}$) = 262 (2509), 416 (1934). **Anal. Calcd.** for $C_{11}H_4FeN_6O_2Na_4 \cdot 4.2H_2O$: C, 27.78; H, 2.63; N, 17.67. Found: C, 27.38; H, 2.24; N, 17.35. **Electrochemistry** in 0,1M Phosphate buffer pH 7.4: $E_{1/2}$ = 0.478 V/NHE.

*$Na_4[Fe^{II}(CN)_5$((pyridine-3-carboxylate)] **(15)***

Yield = 60 % (0.060 g), yellow solid. **^{1}H NMR** (400 MHz, D_2O) δ (ppm): 9.35 (s, 1H), 9.02 (d, *J* = 5.5, 1H), 8.05 (d, *J* = 7.8, 1H), 7.25 (dd, *J* = 7.9, 5.6, 1H). **^{13}C NMR** (101 MHz, D_2O) δ (ppm): 180.88 (CN_{eq}), 176.60 (CN_{ax}), 173.40 (Cq), 158.64 (CH), 157.58 (CH), 136.62 (CH), 132.05 (Cq), 123.45 (CH), 49.50 (MeOD). **IR** symmetric stretching (ν_s), symmetric bending (δ_s), wagging (π) and twisting (τ) (cm^{-1}): 2044 (ν_s C≡N), 1612 – 1564 (ν_s C=C, ν_s C=N, ν_s C=O), 1396 (δ_s C-H), 1192 (τ C-H), 856 (π C–H). **UV-Vis** (H_2O) λ_{max}/nm ($\varepsilon/M^{-1}cm^{-1}$) = 214 (21630), 261 (5872), 382 (2911). **Anal. Calcd.** for $C_{11}H_4FeN_6O_2Na_4 \cdot 2H_2O \cdot 0.3NaI$: C, 27.47; H, 1.68; N, 17.47. Found: C, 27.44; H, 1.65; N, 17.37. **Electrochemistry** in 0,1 M Phosphate buffer pH 7.4: $E_{1/2}$ = 0.468 V *vs* NHE.

4.10.2 Results and discussion

i. Characterizations

As with complexes **3** and **6**, the characterization results also indicated that compound **13** was successfully obtained. The data were very similar to that reported for **3**, so that only the spectra and tables relevant to the characterization of the complex **13** are illustrated below.

NMR spectroscopy

Figure 39 - (A) and (B) ^{1}H NMR spectra of **10** and **13**, respectively, in D_2O, 400 MHz.

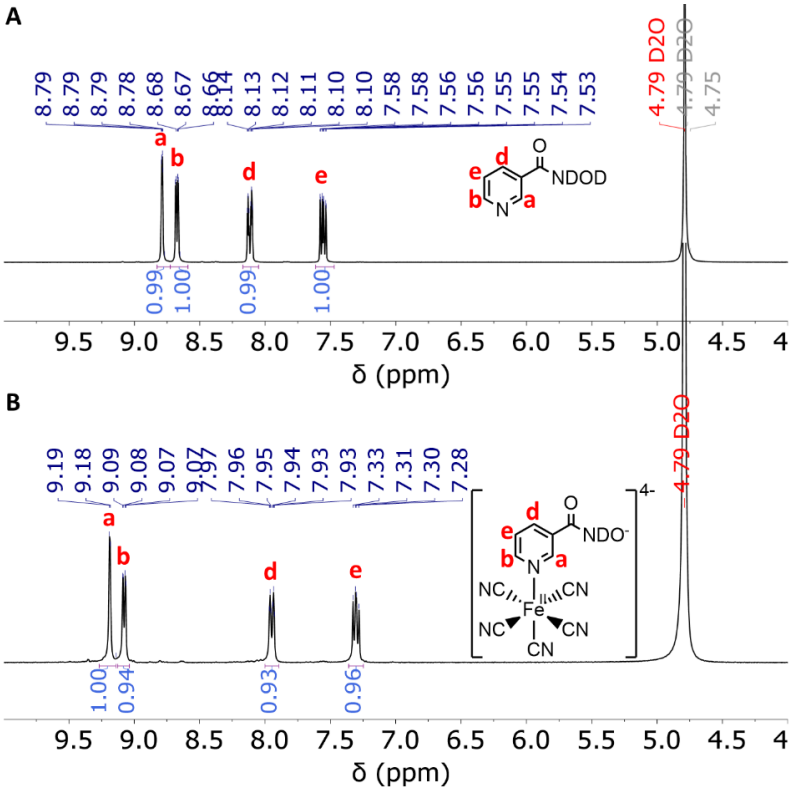

Reference: Elaborated by the author.

Figure 40 - (A) and (B) ^{1}H NMR spectra of **11** and **14**, respectively, in D_2O, 400 MHz.

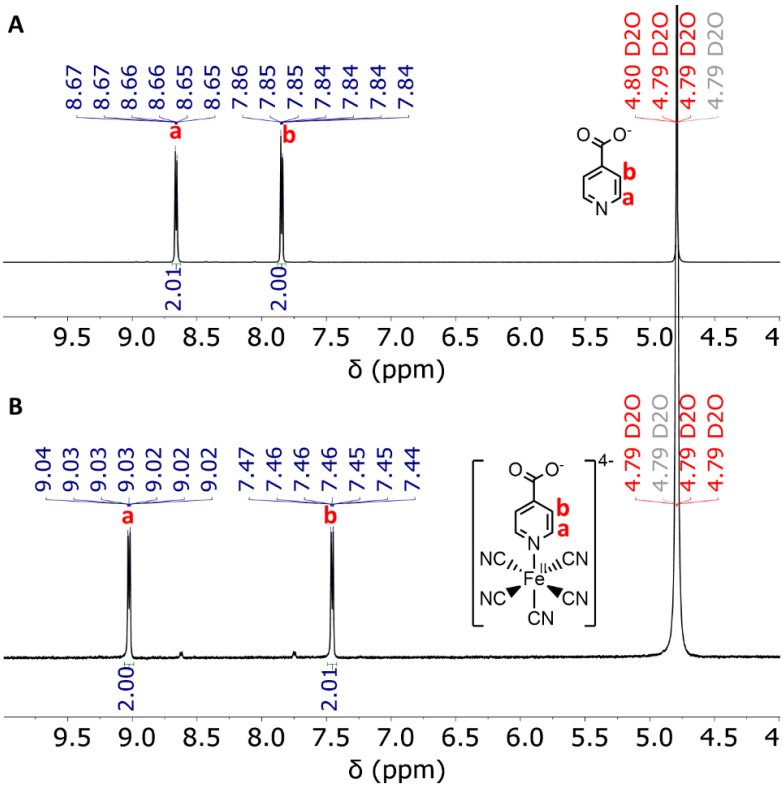

Reference: Elaborated by the author.

Figure 41 - (A) and (B) ^{1}H NMR spectra of **12** and **15**, respectively, in D_2O, 400 MHz.

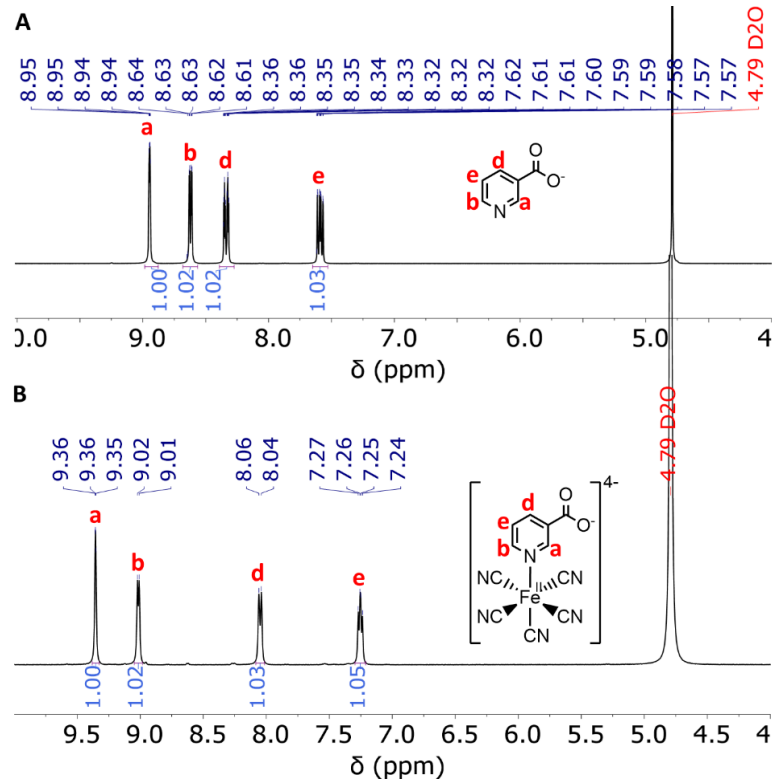

Reference: Elaborated by the author.

Figure 42 - (A), (B) and (C) ^{13}C NMR spectra of **13**, **14** and **15**, respectively, in D_2O, 101 MHz (^{13}C reference = MeOD).

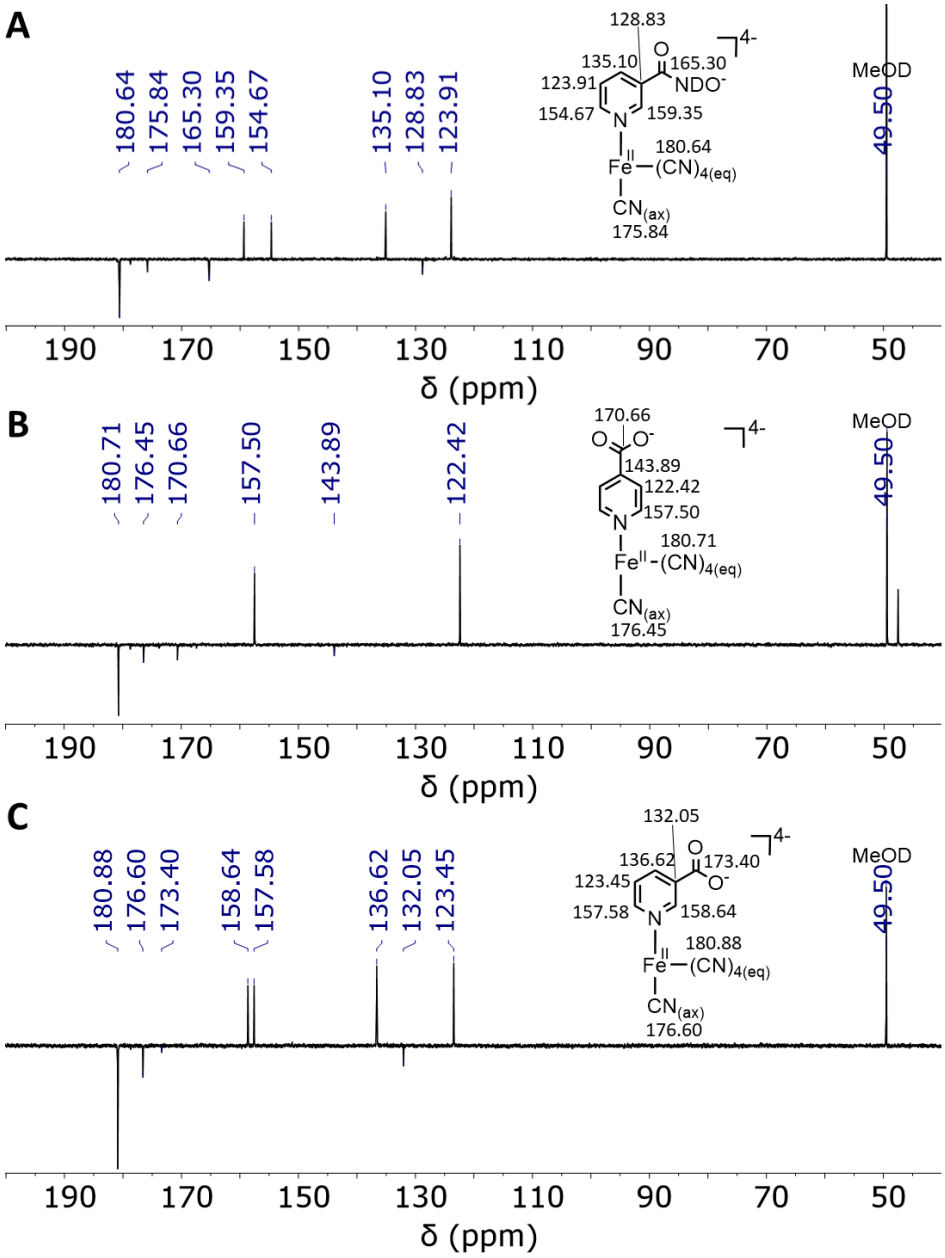

Reference: Elaborated by the author.

Vibrational spectroscopy

Table 1 - Selected experimental and calculated wavenumber values obtained from IR and NR spectra of solid complex **13**, and their corresponding vibrational assignments.

Wavenumber (cm^{-1})				Vibrational Assignment
Infrared		Raman		
Exp.	DFT	Exp.	DFT	
		497	471	β(FeC≡N)
571	524	577	548	$\beta(NH)_{op}$
692	689	647	629	Ring
912		714	746	$\beta(CH)_{op}$
		914		Ring
		1036	1011	Ring + ν(NO)
		1204	1238	β(CH)
1022	1042			Ring
1176	1148			Ring
		1327	1347	ν(C–NH) + β(CH)
1319	1348	1337	1375	β(NH) + β(CH)
1638	1537	1599	1573	ν(CC)ring + ν(C=O) + β(NH)
		1577	1557	ν(CC)ring
2056	2055	2094	2069	ν(C≡N)
2100	2086	2084	2060	ν(C≡N)

Op = out-of-plane / ν = symmetric stretching / β = symmetric bending.

Reference: Elaborated by the author.

Figure 43 - Experimental NR (A) and IR (B) spectra of the complex **13** under tetraanionic form, $Na_4[Fe(CN)_5L]$, L = $NicCONHO^-$ (black line), in the solid state, and DFT-simulated spectra for $[Fe(CN)_5L]^{4-}$ (gray line).

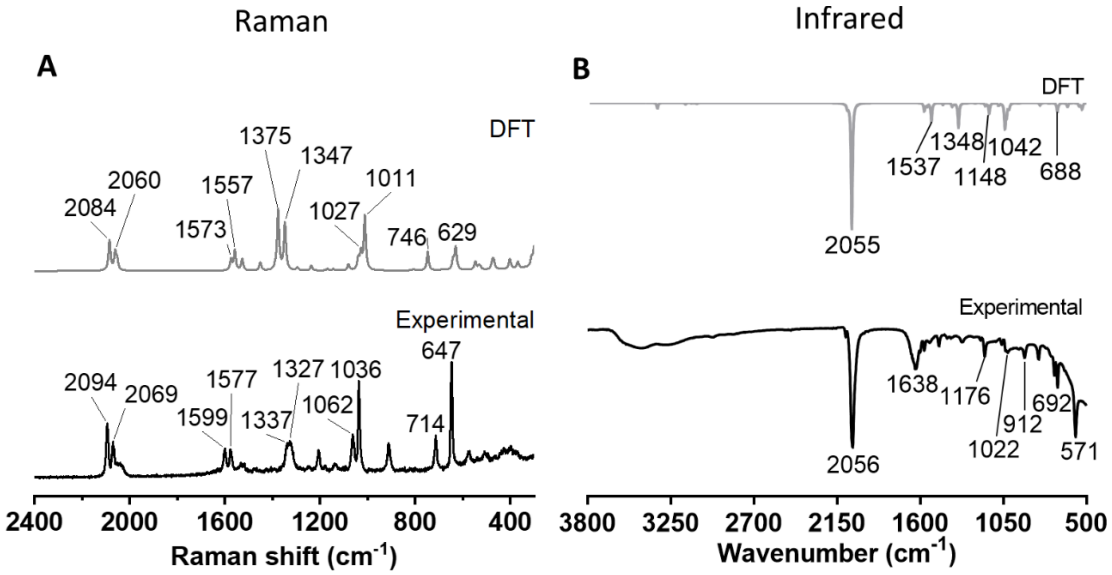

Reference: Elaborated by the author.

Cyclic voltammetry

Figure 44 - Cyclic voltammograms of glassy carbon electrode in solution of **10** (blue) and **13** (red), using vitreous carbon electrode as work, platinum electrode as auxiliary electrode and saturated calomel electrode (SCE) as reference, in phosphate buffer 0.1 M pH 7.4 as electrolyte. Scan speed of 200 mV s^{-1}. Potential values were plotted from SCE to NHE for comparative purposes.

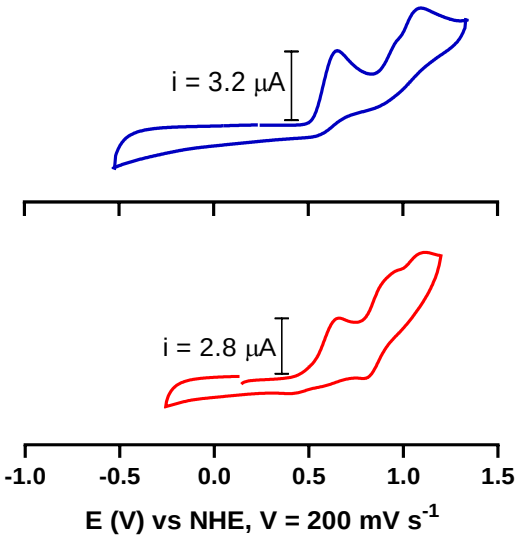

Reference: Elaborated by the author.

UV–Vis absorption spectroscopy

Figure 45 - UV-Visible absorption spectra of the (A) ligand **5** (217 μM, blue) and complex **6**H^+ (50 μM, red), and (B) ligand **10** (105 μM, blue) and complex **13**H^+ (47 μM, red), in water solution, at pH = 6.8.

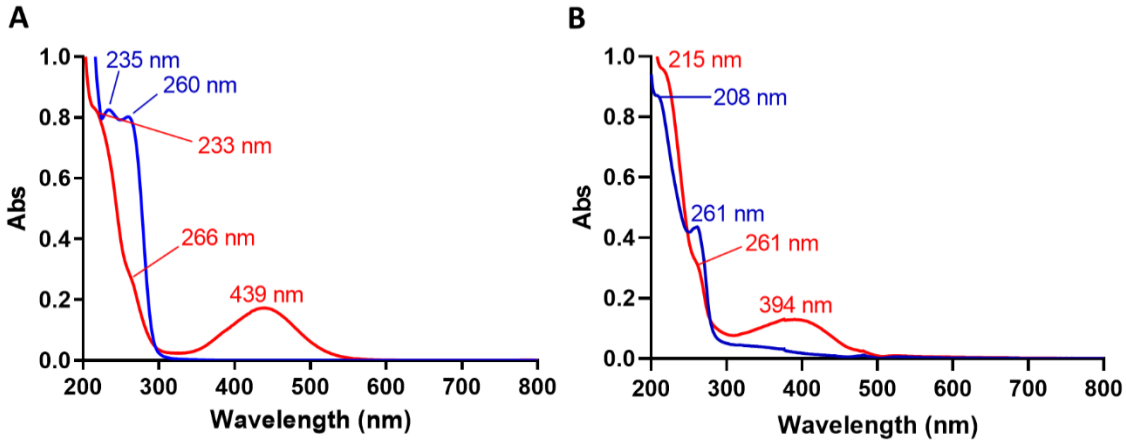

Reference: Elaborated by the author.

Table 2 - Selected electronic transitions for complex **13**H^+.

λ_{exp} (nm)	λ_{DFT} (nm)	Osc. Strength (f)	Key transition	Character
394	437	0.0289	HOMO-1→LUMO	MLCT
	375	0.0290	HOMO-1→LUMO+1	MLCT
261	247	0.0227	HOMO-6→LUMO	LLCT
215	239	0.0547	HOMO-4→LUMO+1	LLCT
	223	0.0594	HOMO-7→LUMO+1	LLCT

LLCT = ligand-to-ligand charge transfer/ MLCT = metal-to-ligand charge transfer.

Reference: Elaborated by the author.

Figure 46 - Calculated UV-Visible absorption spectra and calculated singlet−singlet transition energies of the complex **13**H^+ taking account in a water solvent field.

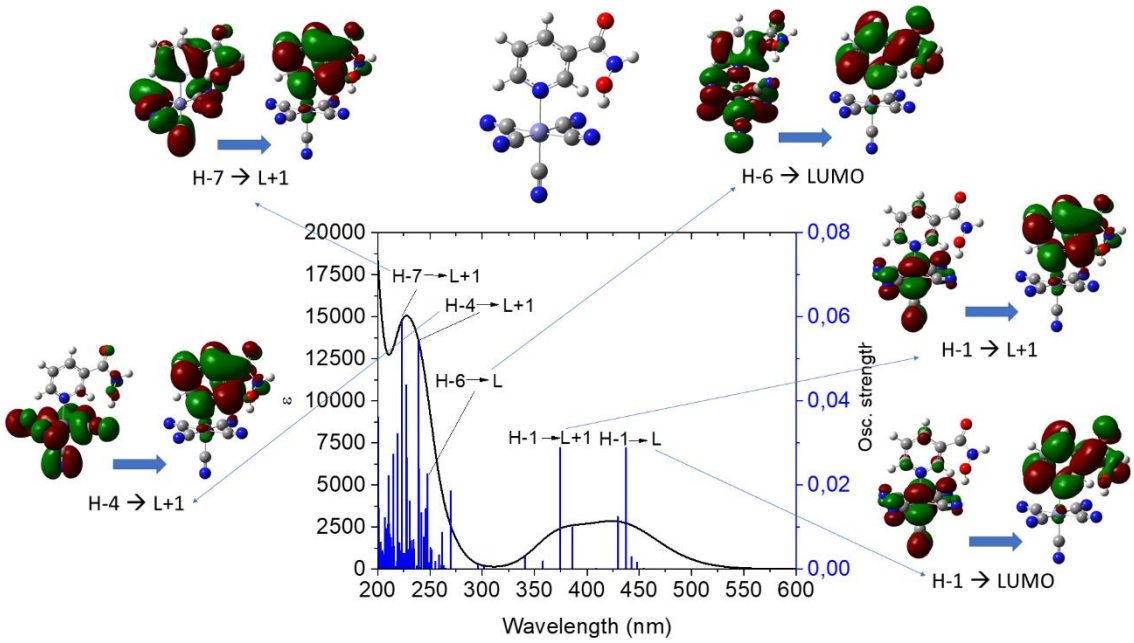

Reference: Elaborated by the author.

4.10.3 Chemical oxidation of the Fe^{II} complex under physiological pH conditions

The chemical oxidation studies of complexes **6** and **13** via UV-Vis, ^{1}H-NMR, and EPR (formation of NO$^{\bullet}$/HNO), also presented experimental behavior similar to the compound **3**. The results obtained are reported below.

Figure 47 - UV–Vis monitoring of the reaction of **6**H^+ (A) and **13**H^+ (B) (171 µM for both complexes) with H_2O_2 (427.5 µM) in phosphate buffer solution, 40 mM, pH 7.4, 22 ºC. Reaction at $t = 0$ min, before addition of H_2O_2, (blue line), and after 2 h (red line). Inset shows the kinetic curve based on changes at 431 nm to the **6**H^+, and 396 nm to the **13**H^+.

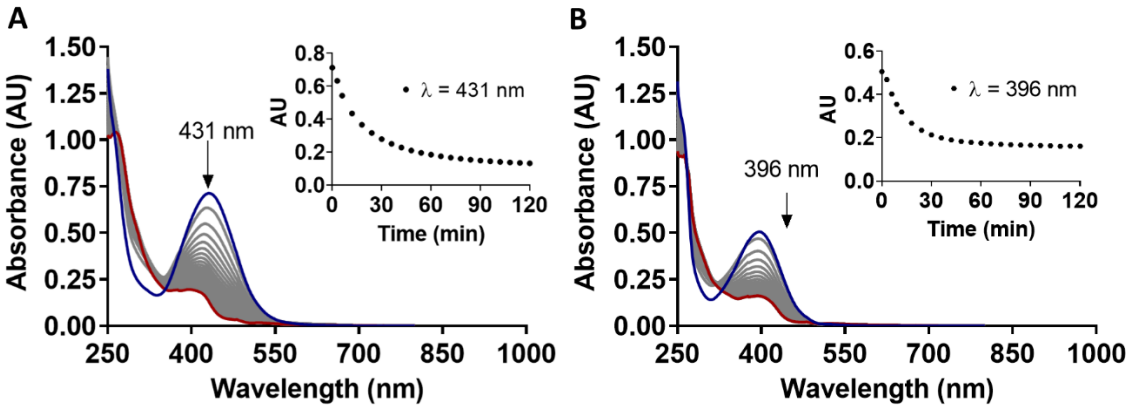

Reference: Elaborated by the author.

Figure 48 - ^{1}H-NMR spectra at 400 MHz: of the complex **6**H^+ (20 mM) at 0 h (A) and at 52 h (B) without addition of H_2O_2, at 52 h after reaction of **6**H^+ with H_2O_2 (50 mM) (C), and **14** complex (20 mM) (D) and isonicotinic carboxylate (**11**) (20 mM) (E). Solutions in 40 mM phosphate buffer, pH 7.4, at 25 ºC.

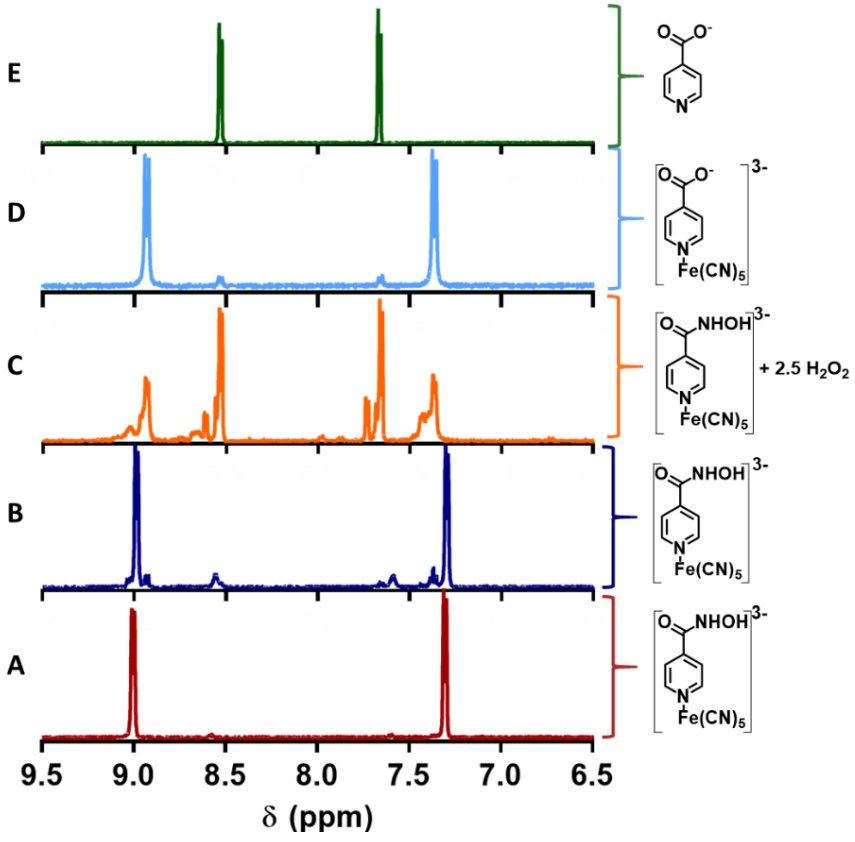

Reference: Elaborated by the author.

Figure 49 - ^{1}H-NMR spectra at 400 MHz: of the complex **13**H^{+} (20 mM) at 0 h (A) and at 52 h (B) without addition of H_2O_2, at 52 h after reaction of **13**H^{+} with H_2O_2 (50 mM) (C), and **15** complex (20 mM) (D) and nicotinic carboxylate (**12**) (20 mM) (E). Solutions in 40 mM phosphate buffer, pH 7.4, at 25 ºC.

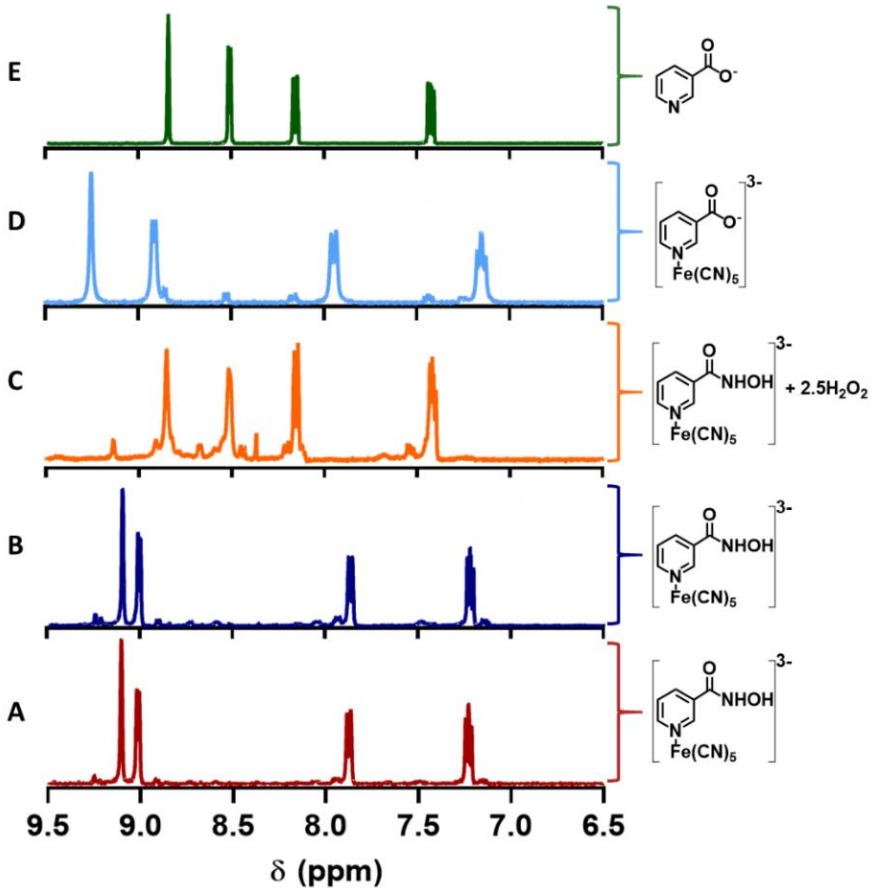

Reference: Elaborated by the author.

Figure 50 - EPR signal of the cPTIO radical in the presence of H_2O_2 and the complexes (**6**H^+ (A) and **13**H^+ (D)) (t_0 = black line and t_{10min} = red line). Control of the stability of the cPTIO EPR signal in the presence of **6**H^+ (B) and **13**H^+ (C) (t_0 = black line and t_{15min} = red line). Control of the stability of the cPTIO EPR signal in the presence of free ligands (**5** (C) and **10** (F)) and H_2O_2 (t_0 = black line and t_{15min} = red line). All spectra were recorded in phosphate buffer solution, 40 mM, pH 7.4.

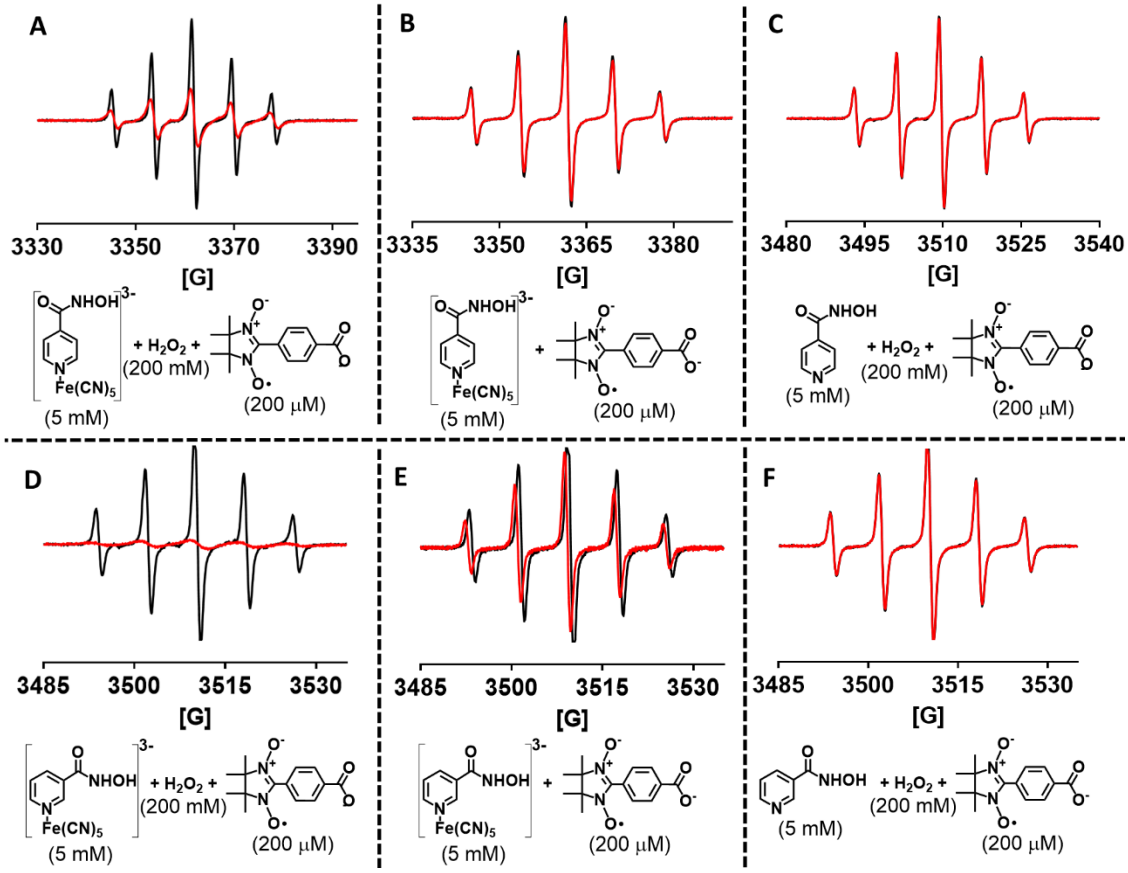

Reference: Elaborated by the author.

4.10.4 Anti-Mtb and vasodilation activities

Complex **13**, as well as its ligand **10**, did not show anti-*Mtb* activity against H37Rv strains, with MIC values > 100 μg/mL as compounds **2**, **3**, **5** and **6**. However, a vasodilating activity was also observed for **13** (Figure 51). The hydroxamic acid complex **13** showed a promising vasodilator profile with EC_{50} = 106 nM, whereas ligand **10** showed a benefic action only in high concentration with EC_{50} = 43 μM. This remarkable difference supports the key role of metal center, which enhanced ca. 406-fold the activity. This metal complex exhibited a more moderate action compared to SNP (EC_{50} = 13 nM), showing an EC_{50} value 8-fold higher than SNP. In addition, the concentration-response curve of the

vasodilation experiment shows that **13** have lower efficacy than the SNP and the other complexes **3** and **6**.

Figure 51 - Relaxation effects on aortic rings pre-contracted with 0.1 µM phenylephrine: **10** (red), **13** (blue), and SNP (black). The EC_{50} and respective 95% confidence interval were calculated only for **13** (106 nM, 62-181 nM).

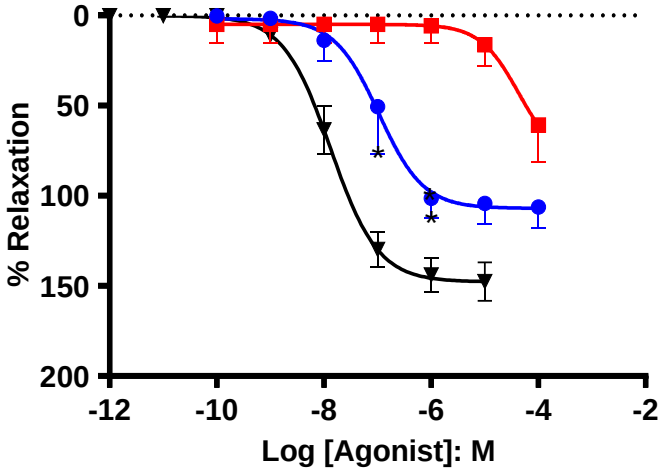

Reference: Elaborated by the author.

4.10.5 Cytotoxicity

The cytotoxicity of the complexes (**3**, **6** and **13**) and their respective free ligands (**2**, **5** and **10**), was tested by Mrs Sandra Bourgeade-Delmas in Pharmadev laboratory (IRD-UPS, Toulouse), whose the director is Pr. Nicolas Fabre, using macrophage cells (J774A.1) in accord with the references.[345-347] The CC_{50} values (concentration equal to 50% of the cytotoxicity effect) obtained for the six compounds were generally higher than 60 µM, being significantly less toxic (1200 -fold) than the doxorubicin control (CC_{50} = 0.05 µM) (Table 3), a chemotherapeutic used in the treatment against solid tumors of several cancers.[348] These high CC_{50} values are indicative of a low cytotoxic activity by the hydroxamic acid derivatives studied.

Table 3 - CC_{50} values to cytotoxic of complexes **3**, **6**, and **13**, and ligands **2**, **5**, and **10**, measured using macrophage (J774A.1) cells.

Compound	**CC_{50} (µM)**
2	285.10 (± 2,22)
3	> 106.37
5	59.80 (± 1,26)
6	68.26 (± 2,57)
10	133.79 (± 0,65)
13	> 104.60
Doxorubicin	0.05 (± 0,01)

Reference: Elaborated by the author.

4.10.6 Antiparasitic activity (leishmaniasis and malaria)

In an opportunistic way, the anti-leishmania and anti-malaria action of the complexes (**3**, **6**, and **13**) and the corresponding free ligands (**2**, **5**, and **10**) were also evaluated in collaboration with Pharmadev laboratory (IRD-UPS) in accord with the references.[345-347] The set of hydroxamic acids derivatives (ligands and complexes) tested showed high IC_{50} values (> 60 µM) for leishmaniasis, being approximately 860 -fold less active than the control amphotericin B (IC_{50} = 0.07 µM) (Table 4), a second-line antileishmanial drug.[349] These results showed that compounds **2-13** have no promising action against this type of disease. In contrast, anti-malaria tests exhibited more promising results, particularly to the free ligands **2**, **5** and **10**, which presented IC_{50} values of 21.57, 2.53, and 3.98 µM, respectively, being relatively better than their respective Fe^{II} complexes (Table 4) and in the case of **5**, it is only 14 less active than the antimalarial drug chloroquine (IC_{50} = 0.18 µM).[350] Interestingly, the presence of the [-$Fe(CN)_5$] moiety was not responsible for beneficial effects, suggesting that biological action is not due to HNO as metabolite.

Table 4 - Antileishmanial and antimalarial activity from the compounds **2**, **3**, **5**, **6**, **10**, and **13**.

Compound	Anti-leishmania	Anti-malaria
	IC_{50} (µM)*	**IC_{50} (µM)***
2	117.03	21.57
3	82.33	38.29
5	85.43	2.53
6	61.57	4.81
10	121.70	3.98
13	66.25	5.23
Amphotericin B	0.07	-
Chloroquine	-	0.18

*Concentrations referring to a single measure.

Reference: Elaborated by the author.

4.11 Conclusion

The complex **13** has exhibited the same chemical and biological behave as the complexes **3** and **6**. Although **13** also had no action against *Mtb* strains, it has proven to be an interesting vasodilating agent, which stimulates future studies. In addition, none of the complexes has shown high cytotoxicity in trials with macrophages, indicating that such compounds may be safe for further *in vivo* studies. The anti-leishmaniasis tests do not encourage us to use such systems for this purpose. Anti-malaria studies have shown that ligands **5** and **10** have a significant action against malaria, however the introduction of the metal center has not been responsible for improving antimalarial action and therefore HNO may not be a toxic metabolite for *Plasmodium falciparum.*

5 GENERAL CONCLUSION AND PERSPECTIVES

Metal complexes have proven to be quite versatile tools in the development of new therapeutic approaches. As part of this thesis, the association of metal system with ligands acting as $NO^{\bullet}$ or HNO donors emerged as a promising alternative in cardiovascular and anticancer drug research.

The first chapter focused on the reactivity of the *trans*-[Fe(cyclam)(NO)Cl]Cl_2 complex. Although this complex was known to release $NO^{\bullet}$ upon light stimulus, in this work we demonstrated that it also exhibits a high potential as direct $NO^{\bullet}$ and HNO donor in physiological conditions. This property is associated with the antihypertensive and antiangiogenic activities observed for this complex. In this way, the results of antiangiogenic activity through the inhibition of HIF-1α suggest this nitrosyl metal complex as a strong candidate in anticancer drug design. Moreover, the vasodilation studies show that the *trans*-[Fe(cyclam)(NO)Cl]Cl_2 complex allows a milder control of the blood pressure (IC_{50} = 910 nM) than the classical metal pro-drug SNP (IC_{50} = 24 nM), the latter being currently used in cases of hypertensive crisis. This can be considered as an advantage, the general use of the more potent vasodilator SNP being indeed limited by its abrupt capacity in inducing vasodilatation. In addition, the absence of cyanide ions in the coordination sphere of the Fe^{II} center, which, if released, can be very toxic for patients treated by SNP, supports the potential use of the present complex in future pre-clinical studies.

The second part of the thesis has concerned the study of (di)azine hydroxamic acid derivatives, with emphasis on the ability of these molecules to release HNO after oxidative activation. A study of the oxidation of isonicotino-, nicotino-, and pyrazino-hydroxamic acids by $K_3[Fe^{III}(CN)_6]$ in aqueous conditions, revealed that a *N*,*O*-di(di)azinoylhydroxylamine intermediate was formed and no nitrosocarbonyl intermediate could be detected (Figure 52). These results contrast with the frequently reported hypothesis that a nitrosocarbonyl intermediate is responsible for the release of HNO by oxidation of hydroxamic acids. By performing the same oxidative treatment in the presence of NH_2CH_3, we put forwards that the *N*,*O*-di(di)azinoylhydroxylamine intermediate has an electrophilic character similar to that of a putative nitrosocarbonyl intermediate. In addition, the corresponding (di)azine carboxylic acids are the final products, thus resulting from the oxidation of hydroxamic acids, not from their hydrolysis.

Figure 52 - Mechanistic hypotheses for HNO release by oxidation of aryl hydroxamic acids.

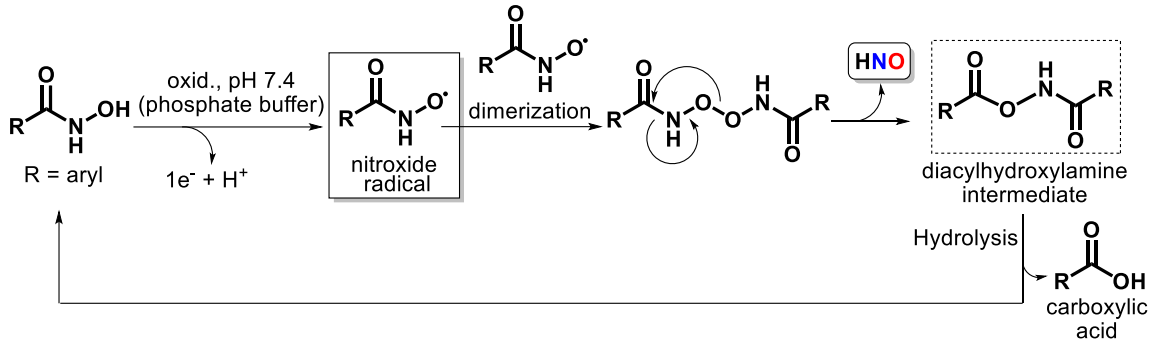

Reference: Elaborated by the author.

The third chapter concerns the development of new iron-metal complexes derived from the molecules discussed above serving as ligands: the basic idea is the design of a hybrid metallic pro-drug through the association of precursors of the active metabolites of isoniazid (isonicotinoyl radical) or pyrazinamide (pyrazinoic acid) and delamanid (HNO). While *in vitro* treatment (at pH 7.4, 37 ºC) of the complexes **3**, **6**, and **13** (Figure 53) by the endogenous oxidizing agent H_2O_2 did not lead to any aroyl radical species, it was shown to trigger the formation of HNO and carboxylic acid derivatives, thus validating the concept of pyrazinamide-delamanid hybrid complex. These complexes failed to inhibit the growth of non-resistant *Mtb* strains. However, knowing that pyrazinamide is active upon non-replicating bacilli and not upon growing strains, it should be relevant to test these compounds towards this more appropriate model. On the other hand, a promising vasodilating action was found for the three complexes studied, with emphasis on the complex **6** (EC_{50} = 64 nM), which is only 5-fold less potent than the SNP drug (EC_{50} = 13 nM). As shown for the *trans*-[Fe(cyclam)(NO)Cl]Cl_2 complex, hydroxamic acid complexes exhibit a moderate action as compared to SNP, and may thus provide a valuable advance in the design of new antihypertensive agents, since the rapid release of NO$^{\bullet}$ from SNP can cause hazardous sudden drops in blood pressure. Moreover, while the complexes **3** and **6** showed efficacy similar to that of SNP, **13** was found slightly less effective. These results stimulated the consideration of complex **6** in studies of antihypertensive action in rats. Increasing the doses of complex **6** (1, 5, and 10 mg/kg) promoted a decrease in blood pressure more efficiently on hypertensive rats (by 45, 62, and 65%, respectively) than on normotensive rats (31, 51 and 53%, respectively). Comparison of the vasodilation curves of the "free ligands" with those of their complexes clearly show that the pentacyanoferrate(II) moiety plays a crucial role in the activation of hydroxamic acids leading to HNO release.

Figure 53 - Structure of the pyrazino- (**3**), isonicotino- (**6**) and nicotino- (**13**) hydroxamic acids pentacyanoferrate(II) complexes.

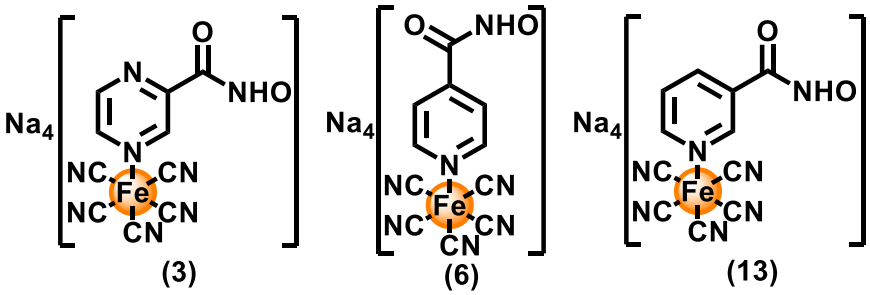

Reference: Elaborated by the author.

In summary, this work unveils significant systems and proposals in the area of bioinorganic chemistry. The results reported in this thesis confirm the possible use of metallo-compounds as an alternative strategy in the development of new therapeutic drugs, with special emphasis on the release of NO• and HNO. As a perspectives, further studies on the vasodilation effect of hydroxamic acid complexes may focus on mechanistic issues, e.g., using inhibitors of the soluble guanylyl cyclase (e.g., ODQ = 1*H*-[1,2,4]oxadiazolo[4,3-a]quinoxalin-1-one) and NOS (e.g., L-NAME = "L-N^G-nitro arginine methyl ester"), which are extremely important enzymes involved in the NO•-mediated vasodilation mechanism. These studies deserve to be undertaken to bring more information about the vasorelaxant activity of the Fe^{II} complexes **3**, **6** and **13**.

Conclusion générale et perspectives

Les complexes métalliques se sont avérés être des outils polyvalents dans le développement de nouvelles approches thérapeutiques. Dans le cadre de cette thèse, l'association d'un système métallique à une molécule donneuse de NO• ou HNO, de type acide hydroxamique jouant le rôle de ligand est apparue comme une alternative prometteuse dans la recherche de médicaments cardiovasculaires et anticancéreux.

Le premier chapitre a porté sur l'étude de la réactivité du complexe *trans*-[Fe(cyclam)(NO)Cl]Cl_2. Bien que la bibliographie indique que ce complexe libère NO• par action d'un stimulus lumineux, ce travail de thèse a permis de montrer que ce complexe présente un fort potentiel pour le relargage direct de NO• ou HNO dans des conditions physiologiques (à pH 7,4, à 37 ºC). Cette propriété permet d'expliquer les activités antihypertensives et antiangiogènes ce complexe, mises en évidence au cours de cette thèse.

Par ailleurs, les résultats de l'activité antiangiogène par inhibition de HIF-1α suggèrent que ce complexe de nitrosyle est un candidat pertinent pour être étudié comme agent anticancéreux. En outre, les études de vasodilatation ont montré que le complexe *trans*-[Fe(cyclam)(NO)Cl]Cl_2 permet un contrôle plus doux de la pressions artérielle (IC_{50} = 910 nM) que la pro-drogue métallique classiquement utilisée en cas de crise d'hypertension, le SNP (IC_{50} = 24 nM). Ceci peut être considéré comme un avantage, l'utilisation du SNP, puissant vasodilatateur, étant limitée par sa capacité "abrupte" à induire la vasodilatation. De plus, l'absence d'ion cyanure dans la sphère de coordination du centre Fe^{II}, potentiellement toxique pour le patient dans le cas du SNP, est un argument de poids pour envisager ce complexe dans de futures études précliniques.

La deuxième partie de la thèse a porté sur l'étude d'acides (di)azine hydroxamiques, en mettant l'accent sur leur capacité à libérer HNO après une activation oxydante. Une étude de l'oxydation des acides hydroxamiques isonicotinique, nicotinique et pyrazinique par $K_3[Fe^{III}(CN)_6]$ en milieu aqueux, a révélé non seulement la libération de HNO, mais aussi la formation d'intermédiaires de type *N,O*-di(di)azinoylhydroxylamine, aucun dérivé nitrosocarbonylé n'ayant été détecté (Figure 54). Ces résultats sont en contradiction avec l'hypothèse fréquemment rapportée que l'intermédiaire nitrosocarbonylé est le précurseur de HNO par oxydation des acides hydroxamiques. Par le même traitement oxydant, mais en présence de NH_2CH_3, nous avons pu mettre en avant que l'intermédiaire *N,O*-di(di)azinoylhydroxylamine présente aussi un caractère électrophile, similaire à celui de l'intermédiaire nitrosocarbonylé virtuel. En outre, les acides carboxyliques correspondants ont été identifiés comme les produits finaux, résultant donc de l'oxydation des acides hydroxamiques (et non de leur hydrolyse).

Figure 54 - Hypothèses mécanistiques pour la libération de HNO par oxydation d'acides aryl hydroxamiques.

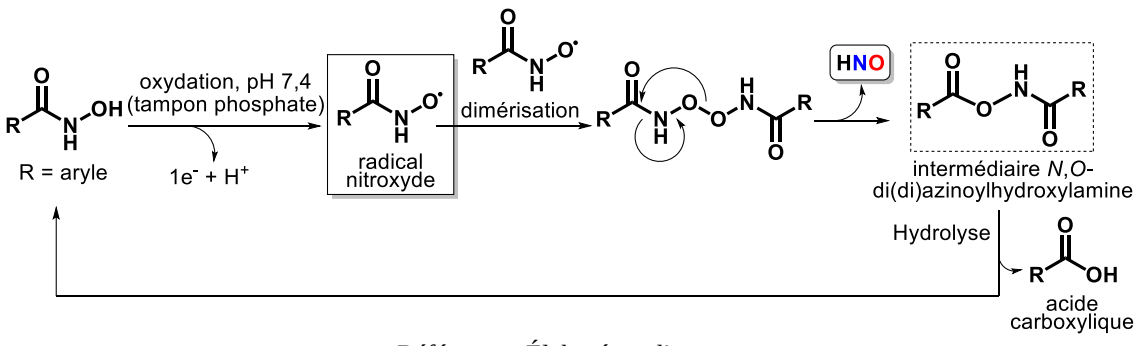

Référence : Élaboré par l'auteur.

Le troisième chapitre concerne le développement de complexes métalliques à ligands acides hydroxamiques, présentés précédemment à l'état libre : l'objectif ultime est la conception d'une pro-drogue hybride métallique issue de l'association, sur un centre métallique Fe^{II}, de précurseurs des métabolites actif de l'isoniazide (radical isonicotinoyle) ou du pyrazinamide (acide pyrazinoique) et du délamanide (HNO). Tandis que le traitement *in vitro* (à pH 7,4 à 37 ºC) des complexes **3**, **6** et **13** (Figure 55) par l'agent oxydant endogène H_2O_2, n'a pas conduit à de quelconque radicaux aroyle, il a en revanche été démontré induire la formation de HNO et de l'acide carboxylique, validant ainsi le concept de complexe hybride pyrazinamide-délamanide. Ces composés n'ont pas été observé inhiber la croissance de souches actives de *Mtb* non-résistantes. Toutefois, sachant que le pyrazinamide est actif sur les bacilles latents et non sur des souches en croissance, il serait pertinent à l'avenir de tester ces complexes sur un modèle plus approprié. D'autre part, des activités vasodilatatrices prometteuses ont été trouvées pour les trois complexes, en particulier pour le complexe **6** (EC_{50} = 64 nM), seulement 5 fois moins puissant que le SNP (EC_{50} = 13 nM). Comme dans le cas du complexe *trans*-[Fe(cyclam)(NO)Cl]Cl_2, l'activité modérée des complexes d'acides hydroxamiques, en comparaison du SNP, peut être considérée comme une avancée dans la conception de nouveaux agents antihypertenseurs, la libération trop rapide de NO˙ par le SNP pouvant provoquer de dangereuses baisses brutales de la pression artérielle. Les complexes **3** et **6** ont montré une efficacité similaire à celle du SNP, tandis que celle du complexe **13** était moindre. Ces résultats ont encouragé l'utilisation du complexe **6** dans des études de l'action antihypertensive chez les rats. L'augmentation des doses du complexe **6** (1, 5, et 10 mg/kg) a été observée favoriser une diminution de la pression artérielle, et ceci plus efficacement chez les rats hypertendus (de 45, 62, et 65%, respectivement) que chez les rats normotenseurs (de 31, 51 and 53%, respectivement). La comparaison des courbes de vasodilatation des complexes et des "ligands libres" montre clairement que le centre pentacyanoferrate(II) joue un rôle crucial dans l'activation des acides hydroxamiques conduisant à la libération de HNO.

Figure 55 - Structure des complexes pentacyanoferrate(II) des acides hydroxamiques pyrazinique (**3**), isonicotinique (**6**) et nicotinique (**13**).

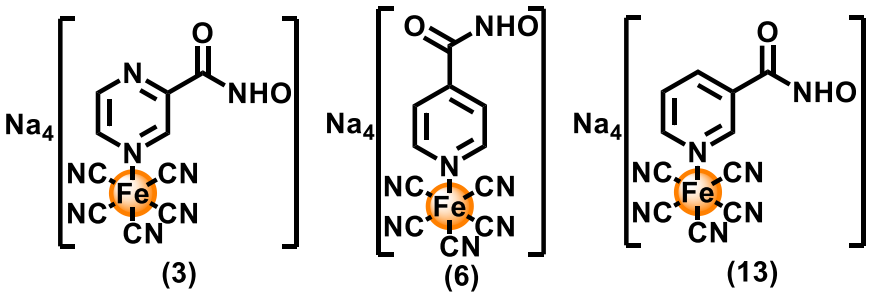

Référence : Élaboré par l'auteur.

En résumé, ce travail a mis au jour de nouveaux systèmes métallo-organiques capables de libérer HNO dans des conditions physiologiques, ainsi que des propositions plus générales dans le domaine de la chimie bio-inorganique. Les résultats rapportés dans cette thèse confirment le potentiel de tels complexes comme nouveaux agents thérapeutiques, en particulier comme agents cardiovasculaires. En perspectives, l'étude des propriétés vasodilatatrices des complexes d'acide hydroxamique mérite d'être complétée du point de vue mécanistique, en utilisant, par exemple, des inhibiteurs de la guanylyl cyclase soluble (par exemple le ODQ = 1*H*- [1,2,4] oxadiazolo [4,3-a] quinoxalin-1-one) et de la NOS (par exemple le L-NAME = L-NG-nitro arginine méthylester), qui sont des enzymes jouant un rôle clé dans le mécanisme de vasodilatation induite par NO•. Ces études sont méritent d'être entreprises en vue d' obtenir des informations complémentaires sur l'activité vasorelaxante des complexes **3**, **6** et **13**.

BIBLIOGRAPHY

1 MJOS, K. D.; ORVIG, C. Metallodrugs in medicinal inorganic chemistry. **Chemical Reviews**, v. 114, n. 8, p. 4540-4563, 2014.

2 LLOYD, N. C.; MORGAN, H. W.; NICHOLSON, B. K.; RONIMUS, R. S. The composition of Ehrlich's salvarsan: resolution of a century-old debate. **Angewandte Chemie International Edition**, v. 44, n. 6, p. 941-944, 2005.

3 SUTTON, B. M. Gold compounds for rheumatoid arthritis. **Gold Bulletin**, v. 19, n. 1, p. 15-16, 1986.

4 PRICKER, S. P. Medical uses of gold compounds: past, present and future. **Gold Bulletin**, v. 29, n. 2, p. 53-60, 1996.

5 ARNESANO, F.; NATILE, G. Mechanistic insight into the cellular uptake and processing of cisplatin 30 years after its approval by FDA. **Coordination Chemistry Reviews**, v. 253, n. 15-16, p. 2070-2081, 2009.

6 ROSENBERG, B.; VANCAMP, L.; TROSKO, J. E.; MANSOUR, V. H. Platinum compounds: a new class of potent antitumour agents. **Nature**, v. 222, n. 5191, p. 385-386, 1969.

7 ROMERO-CANELON, I.; SADLER, P. J. Next-generation metal anticancer complexes: multitargeting via redox modulation. **Inorganic Chemistry**, v. 52, n. 21, p. 12276-12291, 2013.

8 HAAS, K. L.; FRANZ, K. J. Application of metal coordination chemistry to explore and manipulate cell biology. **Chemical Reviews**, v. 109, n. 10, p. 4921-4960, 2009.

9 THOMPSON, K. H.; ORVIG, C. Boon and bane of metal ions in medicine. **Science**, v. 300, n. 5621, p. 936-939, 2003.

10 REICHERT, D. E.; LEWIS, J. S.; ANDERSON, C. J. Metal complexes as diagnostic tools. **Coordination Chemistry Reviews**, v. 184, n. 1, p. 3-66, 1999.

11 MARKWALTER, C. F.; KANTOR, A. G.; MOORE, C. P.; RICHARDSON, K. A.; WRIGHT, D. W. Inorganic Complexes and Metal-Based Nanomaterials for Infectious Disease Diagnostics. **Chemical Reviews**, v. 119, n. 2, p. 1456-1518, 2019.

12 DASARI, S.; TCHOUNWOU, P. B. Cisplatin in cancer therapy: molecular mechanisms of action. **European Journal of Pharmacology**, v. 740, p. 364-378, 2014.

13 DILRUBA, S.; KALAYDA, G. V. Platinum-based drugs: past, present and future. **Cancer Chemother Pharmacol**, v. 77, n. 6, p. 1103-1124, 2016.

14 ZHONG, Y.; JIA, C.; ZHANG, X.; LIAO, X.; YANG, B.; CONG, Y.; PU, S.; GAO, C. Targeting drug delivery system for platinum(IV)-Based antitumor complexes. **European Journal of Medicinal Chemistry**, v. 194, p. 112229, 2020.

15 XU, X.; WANG, H.; LI, H.; HU, X.; ZHANG, Y.; GUAN, X.; TOY, P. H.; SUN, H. S-Dimethylarsino-glutathione (Darinaparsin®) targets histone H3.3, leading to TRAIL-induced apoptosis in leukemia cells. **Chemical Communications**, v. 55, n. 87, p. 13120-13123, 2019.

16 KAIMING, C.; SHENG, Y.; ZHENG, S.; YUAN, S.; HUANG, G.; LIU, Y. Arsenic trioxide preferentially binds to the ring finger protein PML: understanding target selection of the drug. **Metallomics**, v. 10, n. 11, p. 1564-1569, 2018.

17 BARRY, N. P.; SADLER, P. J. Exploration of the medical periodic table: towards new targets. **Chemical Communications**, v. 49, n. 45, p. 5106-5131, 2013.

18 THOTA, S.; RODRIGUES, D. A.; CRANS, D. C.; BARREIRO, E. J. Ru(II) Compounds: Next-Generation Anticancer Metallotherapeutics?. **Journal of Medicinal Chemistry**, v. 61, n. 14, p. 5805-5821, 2018.

19 IMBERTI, C.; ZHANG, P.; HUANG, H.; SADLER, P. J. New Designs for Phototherapeutic Transition Metal Complexes. **Angewandte Chemie International Edition**, v. 59, n. 1, p. 61-73, 2020.

20 CHITAMBAR, C. R. Gallium-containing anticancer compounds. **Future Medicinal Chemistry**, v. 4, n. 10, p. 1257-1272, 2012.

21 NIH U.S. National Library of Medicine. **ClinicalTrials.gov**, 2020. Available in: https://clinicaltrials.gov/ct2/show/NCT00050687?term=maltolate&draw=2&rank=2. Accessed in: 21 july 2020, 12:15.

22 KUBISTA, B.; SCHOEFL, T.; MAYR, L.; VAN SCHOONHOVEN, S.; HEFFETER, P.; WINDHAGER, R.; KEPPLER, B. K.; BERGER, W. Distinct activity of the bone-targeted gallium compound KP46 against osteosarcoma cells - synergism with autophagy inhibition. **Journal of Experimental & Clinical Cancer Research**, v. 36, n. 1, p. 1-13, 2017.

23 BALDARI, S.; DI ROCCO, G.; TOIETTA, G. Current Biomedical Use of Copper Chelation Therapy. **International Journal of Molecular Sciences**, v. 21, n. 3, p. 1-20, 2020.

24 HOTTINGER, D. G.; BEEBE, D. S.; KOZHIMANNIL, T.; PRIELIPP, R. C.; BELANI, K. G. Sodium nitroprusside in 2014: A clinical concepts review. **Journal of Anaesthesiology Clinical Pharmacology**, v. 30, n. 4, p. 462-471, 2014.

25 PAGE, I. H.; CORCORAN, A. C.; DUSTAN, H. P.; KOPPANYI, T. Cardiovascular actions of sodium nitroprusside in animals and hypertensive patients. **Circulation**, v. 11, n. 2, p. 188-198, 1955.

26 HSIAO, H. Y.; CHUNG, C. W.; SANTOS, J. H.; VILLAFLORES, O. B.; LU, T. T. Fe in biosynthesis, translocation, and signal transduction of NO: toward bioinorganic engineering of dinitrosyl iron complexes into NO-delivery scaffolds for tissue engineering. **Dalton Transactions**, v. 48, n. 26, p. 9431-9453, 2019.

27 BONETTA, R. Potential Therapeutic Applications of MnSODs and SOD-Mimetics. **Chemistry**, v. 24, n. 20, p. 5032-5041, 2018.

28 ADENIJI, A. A.; KNOLL, K. E.; LOOTS, D. T. Potential anti-TB investigational compounds and drugs with repurposing potential in TB therapy: a conspectus. **Applied Microbiology and Biotechnology**, v. 104, n. 13, p. 5633-5662, 2020.

29 GUNATILLEKE, S. S.; BARRIOS, A. M. Tuning the Au(I)-mediated inhibition of cathepsin B through ligand substitutions. **Journal of Inorganic Biochemistry**, v. 102, n. 3, p. 555-563, 2008.

30 MCCARRON, P.; MCCANN, M.; DEVEREUX, M.; KAVANAGH, K.; SKERRY, C.; KARAKOUSIS, P. C.; AOR, A. C.; MELLO, T. P.; SANTOS, A. L. S.; CAMPOS, D. L.; PAVAN, F. R. Unprecedented in Vitro Antitubercular Activitiy of Manganese(II) Complexes Containing 1,10-Phenanthroline and Dicarboxylate Ligands: Increased Activity, Superior Selectivity, and Lower Toxicity in Comparison to Their Copper(II) Analogs. **Frontiers in Microbiology**, v. 9, p. 1-10, 2018.

31 LOPES, L. G. F.; CARVALHO, E. M.; SOUSA, E. H. S. A bioinorganic chemistry perspective on the roles of metals as drugs and targets against Mycobacterium tuberculosis - a journey of opportunities. **Dalton Transactions**, v. 49, p. 15988-16003, 2020.

32 STRINGER, T.; SELDON, R.; LIU, N.; WARNER, D. F.; TAM, C.; CHENG, L. W.; LAND, K. M.; SMITH, P. J.; CHIBALE, K.; SMITH, G. S. Antimicrobial activity of organometallic isonicotinyl and pyrazinyl ferrocenyl-derived complexes. **Dalton Transactions**, v. 46, n. 30, p. 9875-9885, 2017.

33 PLUTÍN, A. M.; ALVAREZ, A.; MOCELO, R.; RAMOS, R.; CASTELLANO, E. E.; SILVA, M. M.; COLINA-VEGAS, L.; PAVAN, F. R.; BATISTA, A. A. Anti-Mycobacterium tuberculosis activity of platinum(II)/N,N-disubstituted-N′-acyl thiourea complexes. **Inorganic Chemistry Communications**, v. 63, p. 74-80, 2016.

34 AHMED, M.; ROONEY, D.; MCCANN, M.; DEVEREUX, M.; TWAMLEY, B.; GALDINO, A. C. M.; SANGENITO, L. S.; SOUZA, L. O. P.; LOURENÇO, M. C.; GOMES, K.; SANTOS, A. L. S. Synthesis and antimicrobial activity of a phenanthroline-isoniazid hybrid ligand and its Ag^{+} and Mn^{2+} complexes. **Biometals**, v. 32, n. 4, p. 671-682, 2019.

35 OLIVEIRA, C. G.; MAIA, P. I. S.; SOUZA, P. C.; PAVAN, F. R.; LEITE, C. Q.; VIANA, R. B.; BATISTA, A. A.; NASCIMENTO, O. R.; DEFLON, V. M. Manganese(II) complexes with thiosemicarbazones as potential anti-*Mycobacterium tuberculosis* agents. **Journal of Inorganic Biochemistry**, v. 132, p. 21-29, 2014.

36 AGUIAR, I.; TAVARES, A.; ROVEDA JR., A. C.; SILVA, A. C. H.; MARINO, L. B.; LOPES, E. O.; PAVAN, F. R.; LOPES, L. G. F.; FRANCO, D. W. Antitubercular activity of Ru (II) isoniazid complexes. **European Journal of Pharmaceutical Sciences**, v. 70, p. 45-54, 2015.

37 SOUSA, E. H. S.; VIEIRA, F. G. M.; BUTLER, J. S.; BASSO, L. A.; SANTIAGO, D. S.; DIÓGENES, I. C. N.; LOPES, L. G. F.; SADLER, P. J. $[Fe(CN)_5(isoniazid)]^{3-}$: an iron isoniazid complex with redox behavior implicated in tuberculosis therapy. **Journal of Inorganic Biochemistry**, v. 140, p. 236-244, 2014.

38 ABBADI, B. L.; VILLELA, A. D.; RODRIGUES-JUNIOR, V. S.; SUBTIL, F. T.; DALBERTO, P. F.; PINHEIRO, A. P. S.; SANTOS, D. S.; MACHADO, P.; BASSO, L. A.; BIZARRO, C. V. Revisiting Activation of and Mechanism of Resistance to Compound IQG-607 in *Mycobacterium tuberculosis***. Antimicrob Agents Chemother**, v. 62, n. 2, p. 1-5, 2018.

39 RODRIGUES-JUNIOR, V. S.; VILLELA, A. D.; ABBADI, B. L.; SPEROTTO, N. D. M.; PISSINATE, K.; PICADA, J. N.; SILVA, J. B.; BIZARRO, C. V.; MACHADO, P.; BASSO, L. A. Nonclinical evaluation of IQG-607, an anti-tuberculosis candidate with potential use in combination drug therapy. **Regulatory Toxicology and Pharmacology**, v. 111, p. 104553, 2020.

40 RODRIGUES-JUNIOR, V. S.; CINTRA, L.; MACHADO, P.; DADDA, A.; BASSO, L. A.; MAFRA, A.; CAMPOS, A. H.; CAMPOS, M. M.; SANTOS, D. S. Toxicological profile of IQG-607 after single and repeated oral administration in minipigs: An essential step towards phase I clinical trial. **Regulatory Toxicology and Pharmacology**, v. 90, p. 78-86, 2017.

41 ABBADI, B. L.; RODRIGUES-JUNIOR, V. D. S.; DADDA, A. D. S.; PISSINATE, K.; VILLELA, A. D.; CAMPOS, M. M.; LOPES, L. G. F.; BIZARRO, C. V.; MACHADO, P.; SOUSA, E. H. S.; BASSO, L. A. Is IQG-607 a Potential Metallodrug or Metallopro-Drug With a Defined Molecular Target in *Mycobacterium tuberculosis*?. **Fronters in Microbiology**, v. 9, p. 1-21, 2018.

42 RODRIGUES-JUNIOR, V. S.; MACHADO, P.; CALIXTO, J. B.; SIQUEIRA, J. M.; ANDRADE, E. L.; BENTO, A. F.; CAMPOS, M. M.; BASSO, L. A.; SANTOS, D. S. Preclinical safety evaluation of IQG-607 in rats: Acute and repeated dose toxicity studies. **Regulatory Toxicology and Pharmacology**, v. 86, p. 11-17, 2017.

43 DADDA, A. D. S.; RODRIGUES-JUNIOR, V. S.; CARRENO, F.; PETERSEN, G. O.; PINTO, A. F. M.; DALBERTO, P. F.; SPEROTTO, N. D. M.; PISSINATE, K.; BIZARRO, C. V.; MACHADO, P.; CAMPOS, M. M.; COSTA, T. D.; SANTOS, D. S.; BASSO, L. A. Preclinical pharmacokinetic profiling of IQG-607, a potential oral metallodrug to treat tuberculosis. **European Journal of Pharmaceutical Sciences**, v. 111, p. 393-398, 2018.

44 R. M. J. PALMER; FERRIGE, A. G.; MONCADA, S. Nitric oxide release accounts for the biological activity of endothelium-derived relaxing factor**. Nature**, v. 327, p. 524–526, 1987.

45 FOLLMANN, M.; GRIEBENOW, N.; HAHN, M. G.; HARTUNG, I.; MAIS, F. J.; MITTENDORF, J.; SCHAFER, M.; SCHIROK, H.; STASCH, J. P.; STOLL, F.; STRAUB, A. The chemistry and biology of soluble guanylate cyclase stimulators and activators. **Angewandte Chemie International Edition**, v. 52, n. 36, p. 9442-9462, 2013.

46 KNOWLES, R. G.; MONCADA, S. Nitric oxide synthases in mammals. **Biochemical Journal**, v. 298, p. 249-258, 1994.

47 FORSTERMANN, U.; SESSA, W. C. Nitric oxide synthases: regulation and function. **European Heart Journal**, v. 33, n. 7, p. 829–837, 2012.

48 ZHOU, L.; ZHU, D. Y. Neuronal nitric oxide synthase: structure, subcellular localization, regulation, and clinical implications. **Nitric Oxide**, v. 20, n. 4, p. 223-230, 2009.

49 TAYLOR, B. S.; GELLER, D. A. Molecular regulation of the human inducible nitric oxide synthase (iNOS) gene. **Shock**, v. 13, n. 6, p. 413-424, 2000.

50 RAMAN, C. S.; LI, H.; MARTASEK, P.; KRAL, V.; MASTERS, B. S.; POULOS, T. L. Crystal structure of constitutive endothelial nitric oxide synthase: a paradigm for pterin function involving a novel metal center . **Cell**, v. 95, n. 7, p. 939-950, 1998.

51 DAFF, S. NO synthase: Structures and mechanisms. **Nitric Oxide**, v. 23, n. 1, p. 1-11, 2010.

52 RITCHIE, R. H.; DRUMMOND, G. R.; SOBEY, C. G.; DE SILVA, T. M.; KEMP-HARPER, B. K. The opposing roles of NO and oxidative stress in cardiovascular disease. **Pharmacological Research**, v. 116, p. 57-69, 2017.

53 HORST, B. G.; MARLETTA, M. A. Physiological activation and deactivation of soluble guanylate cyclase. **Nitric Oxide**, v. 77, p. 65-74, 2018.

54 KANG, Y.; LIU, R.; WU, J. X.; CHEN, L. Structural insights into the mechanism of human soluble guanylate cyclase. **Nature**, v. 574, n. 7777, p. 206-210, 2019.

55 SCHERMULY, R. T.; STASCH, J. P.; PULLAMSETTI, S. S.; MIDDENDORFF, R.; MULLER, D.; SCHLUTER, K. D.; DINGENDORF, A.; HACKEMACK, S.; KOLOSIONEK, E.; KAULEN, C.; DUMITRASCU, R.; WEISSMANN, N.; MITTENDORF, J.; KLEPETKO, W.; SEEGER, W.; GHOFRANI, H. A.; GRIMMINGER, F. Expression and function of soluble guanylate cyclase in pulmonary arterial hypertension. **European Respiratory Journal**, v. 32, n. 4, p. 881-891, 2008.

56 KOMSUOGLU-CELIKYURT, I.; GOCMEZ, S. S.; MUTLU, O.; GACAR, N.; ARICIOGLU, F.; UTKAN, T. Evidence for the involvement of neuronal nitric oxide synthase and soluble guanylate cyclase on cognitive functions in rats. **Life Sciences**, v. 89, n. 23-24, p. 905-910, 2011.

57 WANG, Y.; KRAMER, S.; LOOF, T.; MARTINI, S.; KRON, S.; KAWACHI, H.; SHIMIZU, F.; NEUMAYER, H. H.; PETERS, H. Stimulation of soluble guanylate cyclase slows progression in anti-thy1-induced chronic glomerulosclerosis. **Kidney International**, v. 68, n. 1, p. 47-61, 2005.

58 BALTRONS, M. A.; AGULLÓ, L.; GARCÍA, A. Dexamethasone Up-Regulates a Constitutive Nitric Oxide Synthase in Cerebellar Astrocytes but Not in Granule Cells in Culture. **Journal of Neurochemistry**, v. 64, n. 1, p. 447-450, 1995.

59 MÜLSCH, A.; BÖHME, E.; BUSSE, R. Stimulation of soluble guanylate cyclase by endothelium-derived relaxing factor from cultured endothelial cells. **European Journal of Pharmacology**, v. 135, n. 2, p. 247-250, 1987.

60 MIRANDA, K. M. The chemistry of nitroxyl (HNO) and implications in biology. **Coordination Chemistry Reviews**, v. 249, n. 3-4, p. 433-455, 2005.

61 PAGLIARO, P.; MANCARDI, D.; RASTALDO, R.; PENNA, C.; GATTULLO, D.; MIRANDA, K. M.; FEELISCH, M.; WINK, D. A.; KASS, D. A.; PAOLOCCI, N. Nitroxyl affords thiol-sensitive myocardial protective effects akin to early preconditioning. **Free Radical Biology and Medicine**, v. 34, n. 1, p. 33-43, 2003.

62 KATORI, T.; DONZELLI, S.; TOCCHETTI, C. G.; MIRANDA, K. M.; CORMACI, G.; THOMAS, D. D.; KETNER, E. A.; LEE, M. J.; MANCARDI, D.; WINK, D. A.; KASS, D. A.; PAOLOCCI, N. Peroxynitrite and myocardial contractility: *in vivo* versus *in vitro* effects. **Free Radical Biology and Medicine**, v. 41, n. 10, p. 1606-1618, 2006.

63 SHOEMAN, D. W.; SHIROTA, F. N.; DEMASTER, E. G.; NAGASAWA, H. T. Reaction of nitroxyl, an aldehyde dehydrogenase inhibitor, with N-acetyl-L-cysteine. **Alcohol**, v. 20, n. 1, p. 55-59, 2000.

64 AUGUSTYNIAK, A.; SKOLIMOWSKI, J.; BLASZCZYK, A. Cytotoxicity of nitroxyl (HNO/NO^-) against normal and cancer human cells. **Chemico-Biological Interactions**, v. 206, n. 2, p. 262-271, 2013.

65 NORRIS, A. J.; SARTIPPOUR, M. R.; LU, M.; PARK, T.; RAO, J. Y.; JACKSON, M. I.; FUKUTO, J. M.; BROOKS, M. N. Nitroxyl inhibits breast tumor growth and angiogenesis. **International Journal of Cancer**, v. 122, n. 8, p. 1905-1910, 2008.

66 FUKUTO, J. M.; DUTTON, A. S.; HOUK, K. N. The chemistry and biology of nitroxyl (HNO): a chemically unique species with novel and important biological activity. **Chembiochem**, v. 6, n. 4, p. 612-619, 2005.

67 PAOLOCCI, N.; JACKSON, M. I.; LOPEZ, B. E.; MIRANDA, K.; TOCCHETTI, C. G.; WINK, D. A.; HOBBS, A. J.; FUKUTO, J. M. The pharmacology of nitroxyl (HNO) and its therapeutic potential: not just the Janus face of NO. **Pharmacology & Therapeutics**, v. 113, n. 2, p. 442-458, 2007.

68 PAGLIARO, P.; GATTULLO, D.; PENNA, C. Nitroglycerine and sodium trioxodinitrate: from the discovery to the preconditioning effect. **Journal of Cardiovascular Medicine**, v. 14, n. 10, p. 698-704, 2013.

69 PAOLOCCI, N.; WINK, D. A. The shy Angeli and his elusive creature: the HNO route to vasodilation. **American Journal of Physiology Heart and Circulatory Physiology**, v. 296, n. 5, p. H1217-H1220, 2009.

70 EBERHARDT, M.; DUX, M.; NAMER, B.; MILJKOVIC, J.; CORDASIC, N.; WILL, C.; KICHKO, T. I.; ROCHE, J.; FISCHER, M.; SUAREZ, S. A.; BIKIEL, D.; DORSCH, K.; LEFFLER, A.; BABES, A.; LAMPERT, A.; LENNERZ, J. K.; JACOBI, J.; MARTI, M. A.; DOCTOROVICH, F.; HOGESTATT, E. D.; ZYGMUNT, P. M.; IVANOVIC-BURMAZOVIC, I.; MESSLINGER, K.; REEH, P.; FILIPOVIC, M. R. H_2S and NO cooperatively regulate vascular tone by activating a neuroendocrine HNO-TRPA1-CGRP signalling pathway. **Nature Communications**, v. 5, p. 1-17, 2014.

71 CORTESE-KROTT, M. M.; KUHNLE, G. G.; DYSON, A.; FERNANDEZ, B. O.; GRMAN, M.; DUMOND, J. F.; BARROW, M. P.; MCLEOD, G.; NAKAGAWA, H.; ONDRIAS, K.; NAGY, P.; KING, S. B.; SAAVEDRA, J. E.; KEEFER, L. K.; SINGER, M.; KELM, M.; BUTLER, A. R.; FEELISCH, M. Key bioactive reaction products of the NO/H_2S interaction are S/N-hybrid species, polysulfides, and nitroxyl. **Proceedings of The National Academy of Sciences of The USA**, v. 112, n. 34, p. E4651-E4660, 2015.

72 LI, H.; YAO, Q.; XU, F.; XU, N.; MA, X.; FAN, J.; LONG, S.; DU, J.; WANG, J.; PENG, X. Recognition of Exogenous and Endogenous Nitroxyl in Living Cells via a Two-Photon Fluorescent Probe. **Analytical Chemistry**, v. 90, n. 7, p. 4641-4648, 2018.

73 DONZELLI, S.; GOETZ, M.; SCHMIDT, K.; WOLTERS, M.; STATHOPOULOU, K.; DIERING, S.; PRYSYAZHNA, O.; POLAT, V.; SCOTCHER, J.; DEES, C.; SUBRAMANIAN, H.; BUTT, E.; KAMYNINA, A.; SCHOBESBERGER, S.; KING, S. B.; NIKOLAEV, V. O.; WIT, C.; LEICHERT, L. I.; FEIL, R.; EATON, P.; CUELLO, F. Oxidant sensor in the cGMP-binding pocket of PKGIalpha regulates nitroxyl-mediated kinase activity. **Scientific Reports**, v. 7, n. 1, p. 1-14, 2017.

74 ALVAREZ, L.; SUAREZ, S. A.; GONZALEZ, P. J.; BRONDINO, C. D.; DOCTOROVICH, F.; MARTI, M. A. The Underlying Mechanism of HNO Production by the Myoglobin-Mediated Oxidation of Hydroxylamine. **Inorganic Chemistry**, v. 59, n. 12, p. 7939-7952, 2020.

75 SHAFIROVICH, V.; LYMAR, S. V. Nitroxyl and its anion in aqueous solutions: spin states, protic equilibria, and reactivities toward oxygen and nitric oxide. **Proceedings of The National Academy of Sciences of The USA**, v. 99, n. 11, p. 7340-7345, 2002.

76 SMULIK, R.; DEBSKI, D.; ZIELONKA, J.; MICHALOWSKI, B.; ADAMUS, J.; MARCINEK, A.; KALYANARAMAN, B.; SIKORA, A. Nitroxyl (HNO) reacts with molecular oxygen and forms peroxynitrite at physiological pH Biological implications. **Journal of Biological Chemmistry**, v. 289, n. 51, p. 35570-35581, 2014.

77 PAOLOCCI, N.; KECELI, G.; WINK, D. A.; KASS, D. A. From Heaven to Heart: Nitroxyl (HNO) in the Cardiovascular System and Beyond. *In:* DOCTOROVICH, F.; J., FARMER P.; A., MARTI M. **The Chemistry and Biology of Nitroxyl (HNO)**, Elsevier, 1 ed., 2017, p. 353-387.

78 ADAK, S.; WANG, Q.; STUEHR, D. J. Arginine conversion to nitroxide by tetrahydrobiopterin-free neuronal nitric-oxide synthase. Implications for mechanism. **Journal of Biological Chemistry**, v. 275, n. 43, p. 33554-33561, 2000.

79 OKADA, D. Tetrahydrobiopterin-dependent stabilization of neuronal nitric oxide synthase dimer reduces susceptibility to phosphorylation by protein kinase C in vitro. **FEBS Letters**, v. 434, n. 3, p. 261-264, 1998.

80 MOENS, A. L.; KASS, D. A. Tetrahydrobiopterin and cardiovascular disease. **Arteriosclerosis, Thrombosis, and Vascular Biology**, v. 26, n. 11, p. 2439-2444, 2006.

81 KAMADA, Y.; JENKINS, G. J.; LAU, M.; DUNBAR, A. Y.; LOWE, E. R.; OSAWA, Y. Tetrahydrobiopterin depletion and ubiquitylation of neuronal nitric oxide synthase. **Molecular Brain Research**, v. 142, n. 1, p. 19-27, 2005.

82 ABU-SOUD, H. M.; GACHHUI, R.; RAUSHEL, F. M.; STUEHR, D. J. The ferrous-dioxy complex of neuronal nitric oxide synthase. Divergent effects of L-arginine and tetrahydrobiopterin on its stability. **Journal of Biological Chemistry**, v. 272, n. 28, p. 17349-17353, 1997.

83 HYLAND, K.; HEALES, S. J. R. Chapter C7 - The hph-1 Mouse. *In:* LeDoux, M. **Animal Models of Movement Disorders**, Elsevier, 1 ed., 2005, p. 293-297.

84 WANG, Z.-Q.; WEI, C.-C.; SANTOLINI, J.; PANDA, K.; WANG, Q.; STUEHR, D. J. A Tryptophan that Modulates Tetrahydrobiopterin-Dependent Electron Transfer in Nitric Oxide Synthase Regulates Enzyme Catalysis by Additional Mechanisms. **Biochemistry**, v. 44, p. 4676-4690, 2005.

85 PUFAHL, R. A.; WISHNOK, J. S.; MARLETTA, M. A. Hydrogen Peroxide-Supported Oxidation of NG-Hydroxy-L-Arginine by Nitric Oxide Synthase. **Biochemistry**, v. 34, n. 6, p. 1930-1941, 1995

86 STOYANOVSKY, D. A.; TYURINA, Y. Y.; TYURIN, V. A.; ANAND, D.; MANDAVIA, D. N.; GIUS, D.; IVANOVA, J.; PITT, B.; BILLIAR, T. R.; KAGAN, V. E. Thioredoxin and lipoic acid catalyze the denitrosation of low molecular weight and protein S-nitrosothiols. **Journal of the American Chemical Society**, v. 127, n. 45, p. 15815-15823, 2005.

87 WEDMANN, R.; ZAHL, A.; SHUBINA, T. E.; DURR, M.; HEINEMANN, F. W.; BUGENHAGEN, B. E.; BURGER, P.; IVANOVIC-BURMAZOVIC, I.; FILIPOVIC, M. R. Does perthionitrite ($SSNO^-$) account for sustained bioactivity of NO? A (bio)chemical characterization. **Inorganic Chemistry**, v. 54, n. 19, p. 9367-9380, 2015.

88 LIOCHEV, S. I.; FRIDOVICH, I. Copper,zinc superoxide dismutase as a univalent NO(-) oxidoreductase and as a dichlorofluorescin peroxidase. **Journal of Biological Chemistry**, v. 276, n. 38, p. 35253-35257, 2001.

89 NIKETIĆ, V.; STOJANOVIĆ, S.; NIKOLIĆ, A.; SPASIĆ, M.; MICHELSON, A. M. Exposure of Mn and FeSODs, but not Cu/ZnSOD, to NO leads to nitrosonium and nitroxyl ions generation which cause enzyme modification and inactivation: an in vitro study. **Free Radical Biology and Medicine**, v. 27, n. 9-10, p. 992-996, 1999.

90 SALEEM, M.; OHSHIMA, H. Xanthine oxidase converts nitric oxide to nitroxyl that inactivates the enzyme. **Biochemical and Biophysical Research Communications**, v. 315, n. 2, p. 455-462, 2004.

91 MIAO, Z.; KING, S. B. Recent advances in the chemical biology of nitroxyl (HNO) detection and generation. **Nitric Oxide**, v. 57, p. 1-14, 2016.

92 FILIPOVIC, M. R.; MILJKOVIC, J.; NAUSER, T.; ROYZEN, M.; KLOS, K.; SHUBINA, T.; KOPPENOL, W. H.; LIPPARD, S. J.; IVANOVIC-BURMAZOVIC, I. Chemical characterization of the smallest S-nitrosothiol, HSNO; cellular cross-talk of H_2S and *S*-nitrosothiols. **Journal of the American Chemical Society**, v. 134, n. 29, p. 12016-12027, 2012.

93 VOS, O. Role of endogenous thiols in protection. **Advances in Space Research**, v. 12, n. 2-3, p. 201-207, 1992.

94 BISWAS, S.; CHIDA, A. S.; RAHMAN, I. Redox modifications of protein-thiols: emerging roles in cell signaling. **Biochemical Pharmacology**, v. 71, n. 5, p. 551-564, 2006.

95 TIAN, M.; GUO, F.; SUN, Y.; ZHANG, W.; MIAO, F.; LIU, Y.; SONG, G.; HO, C. L.; YU, X.; SUN, J. Z.; WONG, W. Y. A fluorescent probe for intracellular cysteine overcoming the interference by glutathione. **Organic & Biomolecular Chemistry**, v. 12, n. 32, p. 6128-6133, 2014.

96 MANSOOR, M. A.; SVARDAL, A. M.; UELAND, P. M. Determination of the *in vivo* redox status of cysteine, cysteinylglycine, homocysteine, and glutathione in human plasma. **Analytical Biochemistry**, v. 200, n. 2, p. 218-229, 1992.

97 UELAND, P. M.; REFSUM, H.; STABLER, S. P.; MALINOW, M. R.; ANDERSSON, A.; ALLEN, R. H. Total homocysteine in plasma or serum: methods and clinical applications. **Clinical Chemistry**, v. 39, n. 9, p. 1764-1779, 1993.

98 ZHANG, C.; BIGGS, T. D.; DEVARIE-BAEZ, N. O.; SHUANG, S.; DONG, C.; XIAN, M. S-Nitrosothiols: chemistry and reactions. **Chemical Communications**, v. 53, n. 82, p. 11266-11277, 2017.

99 KEVIL, C. G.; PATEL, R. P. S-Nitrosothiol biology and therapeutic potential in metabolic disease. **Current opinion in investigational drugs**, v. 11, n. 10, p. 1127-1134, 2010.

100 ASTUTI, R. I.; NASUNO, R.; TAKAGI, H. Nitric Oxide Signalling in Yeast. **Advances in Microbial Physiology**, v. 72, p. 29-63, 2018.

101 KIM, W.; STAMLER, J. S.; LIPTON, S. A. [27] - Redox Congeners of Nitric Oxide, N-Methyl-d-Aspartate Receptors, and Intracellular Calcium Ion. **Methods in Neurosciences**, v. 31, p. 309-318, 1996.

102 HARDELAND, R.; BACKHAUS, C.; FADAVI, A. Reactions of the NO redox forms NO^+, $^{\bullet}NO$ and HNO (protonated NO^-) with the melatonin metabolite N^1-acetyl-5-methoxykynuramine. **Journal of Pineal Research**, v. 43, n. 4, p. 382-388, 2007.

103 POOLE, L. B. The basics of thiols and cysteines in redox biology and chemistry. **Free Radical Biology and Medicine**, v. 80, p. 148-157, 2015.

104 GRAMINSKI, G. F.; KUBO, Y.; ARMSTRONG, R. N. Spectroscopic and kinetic evidence for the thiolate anion of glutathione at the active site of glutathione S-transferase. **Biochemistry**, v. 28, n. 8, p. 3562-3568, 1989.

105 AWOONOR-WILLIAMS, E.; ROWLEY, C. N. Evaluation of Methods for the Calculation of the pKa of Cysteine Residues in Proteins. **Journal of Chemical Theory and Computation**, v. 12, n. 9, p. 4662-4673, 2016.

106 PIRIE, N. W.; PINHEY, K. G. Titration Curve of Glutathione. **The Journal of Biological Chemistry**, v. 84, p. 321−333, 1929.

107 GLUSHCHENKO, A. V.; JACOBSEN, D. W. Molecular targeting of proteins by L-homocysteine: mechanistic implications for vascular disease. **Antioxidants and Redox Signaling**, v. 9, n. 11, p. 1883-1898, 2007.

108 DORO, F. G.; PEPE, I. M.; GALEMBECK, S. E.; CARLOS, R. M.; ROCHA, Z. N.; BERTOTTI, M.; TFOUNI, E. Reactivity, photolability, and computational studies of the ruthenium nitrosyl complex with a substituted cyclam *fac*-$[Ru(NO)Cl_2(k^3N^4,N^8,N^{11}$(1-carboxypropyl)cyclam)]$Cl{\cdot}H_2O$. **Dalton Transactions**, v. 40, n. 24, p. 6420-6432, 2011.

109 HOSHINO, M.; MAEDA, M.; KONISHI, R.; SEKI, H.; FORD, P. C. Studies on the Reaction Mechanism for Reductive Nitrosylation of Ferrihemoproteins in Buffer Solutions. **Journal of the American Chemical Society**, v. 118, n. 24, p. 5702-5707, 1996.

110 SHARPE, M. A.; COOPER, C. E. Reactions of nitric oxide with mitochondrial cytochrome c: a novel mechanism for the formation of nitroxyl anion and peroxynitrite. **Biochemical Journal**, v. 332, p. 9-19, 1998.

111 SILKSTONE, R. S.; MASON, M. G.; NICHOLLS, P.; COOPER, C. E. Nitrogen dioxide oxidizes mitochondrial cytochrome c. **Free Radical Biology and Medicine**, v. 52, n. 1, p. 80-87, 2012.

112 DONZELLI, S.; ESPEY, M. G.; FLORES-SANTANA, W.; SWITZER, C. H.; YEH, G. C.; HUANG, J.; STUEHR, D. J.; KING, S. B.; MIRANDA, K. M.; WINK, D. A.

Generation of nitroxyl by heme protein-mediated peroxidation of hydroxylamine but not N-hydroxy-L-arginine. **Free Radical Biology and Medicine**, v. 45, n. 5, p. 578-584, 2008.

113 SCHMIDT, H. H.; HOFMANN, H.; SCHINDLER, U.; SHUTENKO, Z. S.; CUNNINGHAM, D. D.; FEELISCH, M. No NO from NO synthase. **Proceedings of The National Academy of Sciences of The USA**, v. 93, n. 25, p. 14492-14497, 1996.

114 LOUTERS, L. L.; SCRIPTURE, J. P.; KUIPERS, D. P.; GUNNINK, S. M.; KUIPER, B. D.; ALABI, O. D. Hydroxylamine acutely activates glucose uptake in L929 fibroblast cells. **Biochimie**, v. 95, n. 4, p. 787-792, 2013.

115 GROSS, P. Biologic activity of hydroxylamine: a review. **CRC Critical Reviews in Toxicology**, v. 14, n. 1, p. 87-99, 1985.

116 ARNELLE, D. R.; STAMLER, J. S. NO^+, $NO^\bullet$, and NO^- donation by S-nitrosothiols: implications for regulation of physiological functions by S-nitrosylation and acceleration of disulfide formation. **Archives of Biochemistry and Biophysics**, v. 318, n. 2, p. 279-285, 1995.

117 GOUGH, D. R.; COTTER, T. G. Hydrogen peroxide: a Jekyll and Hyde signalling molecule. **Cell Death & Disease**, v. 2, p. 1-8, 2011.

118 KIM, D.; KIM, G.; NAM, S. J.; YIN, J.; YOON, J. Visualization of endogenous and exogenous hydrogen peroxide using a lysosome-targetable fluorescent probe. **Scientific Reports**, v. 5, n. 8488, p. 1-6, 2015.

119 GOLDSTEIN, S.; SAMUNI, A. Oxidation Mechanism of Hydroxamic Acids Forming HNO and NO: Implications for Biological Activity. **Advances in Inorganic Chemistry NOx Related Chemistry**, v. 67, p. 315-333, 2015.

120 MARTI, M. A.; ÁLVAREZ, L.; SUAREZ, S. A.; DOCTOROVICH, F. Is Azanone Endogenously Produced in Mammals?. DOCTOROVICH, F.; J., FARMER P.; A., MARTI M. **The Chemistry and Biology of Nitroxyl (HNO)**, Elsevier, 1 ed., 2017, p. 337-351.

121 PORSHNEVA, K.; PAPIERNIK, D.; PSURSKI, M.; NOWAK, M.; MATKOWSKI, R.; EKIERT, M.; MILCZAREK, M.; BANACH, J.; JAROSZ, J.; WIETRZYK, J. Combination Therapy with DETA/NO and Clopidogrel Inhibits Metastasis in Murine Mammary Gland Cancer Models via Improved Vasoprotection. **Molecular Pharmaceutics**, v. 15, n. 11, p. 5277-5290, 2018.

122 MANICAM, C.; GINTER, N.; LI, H.; XIA, N.; GOLOBORODKO, E.; ZADEH, J. K.; MUSAYEVA, A.; PFEIFFER, N.; GERICKE, A. Compensatory Vasodilator Mechanisms in the Ophthalmic Artery of Endothelial Nitric Oxide Synthase Gene Knockout Mice. **Scientific Reports**, v. 7, n. 7111, p. 1-12, 2017.

123 CRUZ, J. P.; ARREBOLA, M. M.; GUERRERO, A.; CUESTA, F. S. Influence of nitric oxide on the in vitro antiaggregant effect of ticlopidine. **Vascular Pharmacology**, v. 38, n. 3, p. 183-186, 2002.

124 World Health Organization. **Cancer**, 2020. Available in: https://www.who.int/health-topics/cancer#tab=tab_1. Accessed in: 27 september 2020, 15:45.

125 FULDA, S. Evasion of apoptosis as a cellular stress response in cancer. **International Journal of Cell Biology**, v. 2010, p. 1-6, 2010.

126 RAJABI, M.; MOUSA, S. A. The Role of Angiogenesis in Cancer Treatment. **Biomedicines**, v. 5, n. 2, p. 34, 2017.

127 LUGANO, R.; RAMACHANDRAN, M.; DIMBERG, A. Tumor angiogenesis: causes, consequences, challenges and opportunities. **Cellular and Molecular Life Sciences**, v. 77, n. 9, p. 1745-1770, 2020.

128 FARES, J.; FARES, M. Y.; KHACHFE, H. H.; SALHAB, H. A.; FARES, Y. Molecular principles of metastasis: a hallmark of cancer revisited. **Signal Transduction and Targeted Therapy**, v. 5, n. 28, p. 1-17, 2020.

129 BRAY, F.; FERLAY, J.; SOERJOMATARAM, I.; SIEGEL, R. L.; TORRE, L. A.; JEMAL, A. Global cancer statistics 2018: GLOBOCAN estimates of incidence and mortality worldwide for 36 cancers in 185 countries. **CA: A Cancer Journal for Clinicians**, v. 68, n. 6, p. 394-424, 2018.

130 KIM, H. C.; OH, S. M. Noncommunicable diseases: current status of major modifiable risk factors in Korea. **Journal of Preventive Medicine and Public Health**, v. 46, n. 4, p. 165-172, 2013.

131 TULCHINSKY, T. H.; VARAVIKOVA, E. A. Non-Communicable Diseases and Conditions. THEODORE H. T.; ELENA A. V. **The New Public Health**, Elsevier, 3rd ed., 2014, p. 237-309.

132 GALLAGHER, M. P.; KELLY, P. J.; JARDINE, M.; PERKOVIC, V.; CASS, A.; CRAIG, J. C.; ERIS, J.; WEBSTER, A. C. Long-term cancer risk of immunosuppressive regimens after kidney transplantation. **Journal of the American Society of Nephrology**, v. 21, n. 5, p. 852-858, 2010.

133 VERSMISSEN, J.; LENNEP, J. R.; SIJBRANDS, E. J. G. Clinical Aspects of Transgenerational Epigenetics. TRYGVE T. **Transgenerational Epigenetics**, Elsevier, 1 ed., 2014, p. 357-367.

134 TANNOCK, I. F. Conventional cancer therapy: promise broken or promise delayed?. **The Lancet**, v. 351, p. SII9-SII16, 1998.

135 VELCHETI, V.; SCHALPER, K. Basic Overview of Current Immunotherapy Approaches in Cancer. American Society of Clinical Oncology Educational Book, v. 35, p. 298-308, 2016.

136 YANG, Y. Cancer immunotherapy: harnessing the immune system to battle cancer. **Journal of Clinical Investigation**, v. 125, n. 9, p. 3335-3337, 2015.

137 ABRAHAM, J.; STAFFURTH, J. Hormonal therapy for cancer. **Medicine**, v. 48, n. 2, p. 103-107, 2020.

138 BIDRAM, E.; ESMAEILI, Y.; RANJI-BURACHALOO, H.; AL-ZAUBAI, N.; ZARRABI, A.; STEWART, A.; DUNSTAN, D. E. A concise review on cancer treatment methods and delivery systems. **Journal of Drug Delivery Science and Technology**, v. 54, p. 101350, 2019.

139 TSIMBERIDOU, A. M. Targeted therapy in cancer. **Cancer Chemotherapy and Pharmacology**, v. 76, n. 6, p. 1113-1132, 2015.

140 XU, M. M.; PU, Y.; ZHANG, Y.; FU, Y. X. The Role of Adaptive Immunity in the Efficacy of Targeted Cancer Therapies. **Trends in Immunology**, v. 37, n. 2, p. 141-153, 2016.

141 SAVA, G. P.; ALI, S. Developing themes in targeted therapies for hormone receptor positive breast cancer. **Current Opinion in Endocrine and Metabolic Research**, v. 15, p. 15-23, 2020.

142 REED, J. C. Apoptosis-targeted therapies for cancer. **Cancer Cell**, v. 3, n. 1, p. 17-22, 2003.

143 ZHANG, Q.; CHEN, G.; LIU, X.; QIAN, Q. Monoclonal antibodies as therapeutic agents in oncology and antibody gene therapy. **Cell Res**, v. 17, n. 2, p. 89-99, 2007.

144 MOKHTARI, R. B.; HOMAYOUNI, T. S.; BALUCH, N.; MORGATSKAYA, E.; KUMAR, S.; DAS, B.; YEGER, H. Combination therapy in combating cancer. **Oncotarget**, v. 8, n. 23, p. 38022-38043, 2017.

145 GAMPENRIEDER, S. P.; WESTPHAL, T.; GREIL, R. Antiangiogenic therapy in breast cancer. **Memo**, v. 10, n. 4, p. 194-201, 2017.

146 HUANG, Z.; FU, J.; ZHANG, Y. Nitric Oxide Donor-Based Cancer Therapy: Advances and Prospects. **Journal of Medicinal Chemistry**, v. 60, n. 18, p. 7617-7635, 2017.

147 THOMAS, D. D.; RIDNOUR, L. A.; ISENBERG, J. S.; FLORES-SANTANA, W.; SWITZER, C. H.; DONZELLI, S.; HUSSAIN, P.; VECOLI, C.; PAOLOCCI, N.; AMBS, S.; COLTON, C. A.; HARRIS, C. C.; ROBERTS, D. D.; WINK, D. A. The chemical biology of nitric oxide: implications in cellular signaling. **Free Radical Biology and Medicine**, v. 45, n. 1, p. 18-31, 2008.

148 SECORD, A. A.; SIAMAKPOUR-REIHANI, S. Chapter 5 - Angiogenesis. *In*: BIRRER, M. J.; CEPPI, L. **Translational Advances in Gynecologic Cancers**, Elsevier, 1 ed., 2017, p. 79-109.

149 GASPAR, J. M.; VELLOSO, L. A. Hypoxia Inducible Factor as a Central Regulator of Metabolism - Implications for the Development of Obesity. **Frontiers Neuroscience**, v. 12, n. 813, p. 1-12, 2018.

150 METZEN, E.; ZHOU, J.; JELKMANN, W.; FANDREY, J.; BRUNE, B. Nitric oxide impairs normoxic degradation of HIF-1alpha by inhibition of prolyl hydroxylases. **Molecular Biology of the Cell**, v. 14, n. 8, p. 3470-3481, 2003.

151 SWITZER, C. H.; FLORES-SANTANA, W.; MANCARDI, D.; DONZELLI, S.; BASUDHAR, D.; RIDNOUR, L. A.; MIRANDA, K. M.; FUKUTO, J. M.; PAOLOCCI, N.; WINK, D. A. The emergence of nitroxyl (HNO) as a pharmacological agent. **Biochimica et Biophysica Acta (BBA) - Bioenergetics**, v. 1787, n. 7, p. 835-840, 2009.

152 SOUSA, E. H. S.; RIDNOUR, L. A.; FLORÊNCIO S. GOUVEIA, J.; SILVA, C. D. S.; WINK, D. A.; LOPES, L. G. F.; SADLER, P. J. Thiol-Activated HNO Release from a Ruthenium Antiangiogenesis Complex and HIF-1alpha Inhibition for Cancer Therapy. **ACS Chemical Biology**, v. 11, n. 7, p. 2057-2065, 2016.

153 World Health Organization. **Cardiovascular diseases**, 2020. Available in: https://www.who.int/health-topics/cardiovascular-diseases/#tab=tab_1. Accessed in: 22 july 2020, 16:30.

154 World Health Organization. **Global Atlason cardiovascular disease prevention and control**, 2020. Available in: https://www.who.int/cardiovascular_diseases/publications/atlas_cvd/en/. Accessed in: 27 september 2020, 16:50.

155 CHARLTON, M.; THOMPSON, J. P. Drugs acting on the heart: antihypertensive drugs. **Anaesthesia & Intensive Care Medicine**, v. 16, n. 5, p. 227-231, 2015.

156 ROTH, G. A.; JOHNSON, C.; ABAJOBIR, A.; ABD-ALLAH, F.; ABERA, S. F.; ABYU, G.; AHMED, M.; AKSUT, B.; ALAM, T.; ALAM, K.; ALLA, F.; ALVIS-GUZMAN, N.; AMROCK, S.; ANSARI, H.; ARNLOV, J.; ASAYESH, H.; ATEY, T. M.; AVILA-BURGOS, L.; AWASTHI, A.; BANERJEE, A.; BARAC, A.; BARNIGHAUSEN, T.; BARREGARD, L.; BEDI, N.; BELAY KETEMA, E.; BENNETT, D.; BERHE, G.; BHUTTA, Z.; BITEW, S.; CARAPETIS, J.; CARRERO, J. J.; MALTA, D. C.; CASTANEDA-ORJUELA, C. A.; CASTILLO-RIVAS, J.; CATALA-LOPEZ, F.; CHOI, J. Y.; CHRISTENSEN, H.; CIRILLO, M.; COOPER, L., JR.; CRIQUI, M.; CUNDIFF, D.; DAMASCENO, A.; DANDONA, L.; DANDONA, R.; DAVLETOV, K.; DHARMARATNE, S.; DORAIRAJ, P.; DUBEY, M.; EHRENKRANZ, R.; EL SAYED ZAKI, M.; FARAON, E. J. A.; ESTEGHAMATI, A.; FARID, T.; FARVID, M.; FEIGIN, V.; DING, E. L.; FOWKES, G.; GEBREHIWOT, T.; GILLUM, R.; GOLD, A.; GONA, P.; GUPTA, R.; HABTEWOLD, T. D.; HAFEZI-NEJAD, N.; HAILU, T.; HAILU, G. B.; HANKEY, G.; HASSEN, H. Y.; ABATE, K. H.; HAVMOELLER, R.; HAY, S. I.; HORINO, M.; HOTEZ, P. J.; JACOBSEN, K.; JAMES, S.; JAVANBAKHT, M.; JEEMON, P.; JOHN, D.; JONAS, J.; KALKONDE, Y.; KARIMKHANI, C.; KASAEIAN, A.; KHADER, Y.; KHAN, A.; KHANG, Y. H.; KHERA, S.; KHOJA, A. T.; KHUBCHANDANI, J.; KIM, D.; KOLTE, D.; KOSEN, S.; KROHN, K. J.; KUMAR, G. A.; KWAN, G. F.; LAL, D. K.; LARSSON, A.; LINN, S.; LOPEZ, A.; LOTUFO, P. A.; EL RAZEK, H. M. A.; MALEKZADEH, R.; MAZIDI, M.; MEIER, T.; MELES, K. G.; MENSAH, G.; MERETOJA, A.; MEZGEBE, H.; MILLER, T.; MIRRAKHIMOV, E.;

MOHAMMED, S.; MORAN, A. E.; MUSA, K. I.; NARULA, J.; NEAL, B.; NGALESONI, F.; NGUYEN, G.; OBERMEYER, C. M.; OWOLABI, M.; PATTON, G.; PEDRO, J.; QATO, D.; QORBANI, M.; RAHIMI, K.; RAI, R. K.; RAWAF, S.; RIBEIRO, A.; SAFIRI, S.; SALOMON, J. A.; SANTOS, I.; SANTRIC MILICEVIC, M.; SARTORIUS, B.; SCHUTTE, A.; SEPANLOU, S.; SHAIKH, M. A.; SHIN, M. J.; SHISHEHBOR, M.; SHORE, H.; SILVA, D. A. S.; SOBNGWI, E.; STRANGES, S.; SWAMINATHAN, S.; TABARES-SEISDEDOS, R.; TADELE ATNAFU, N.; TESFAY, F.; THAKUR, J. S.; THRIFT, A.; TOPOR-MADRY, R.; TRUELSEN, T.; TYROVOLAS, S.; UKWAJA, K. N.; UTHMAN, O.; VASANKARI, T.; VLASSOV, V.; VOLLSET, S. E.; WAKAYO, T.; WATKINS, D.; WEINTRAUB, R.; WERDECKER, A.; WESTERMAN, R.; WIYSONGE, C. S.; WOLFE, C.; WORKICHO, A.; XU, G.; YANO, Y.; YIP, P.; YONEMOTO, N.; YOUNIS, M.; YU, C.; VOS, T.; NAGHAVI, M.; MURRAY, C. Global, Regional, and National Burden of Cardiovascular Diseases for 10 Causes, 1990 to 2015. Journal of the American College of Cardiology, v. 70, n. 1, p. 1-25, 2017.

157 GANATRA, S.; DANI, S. S.; SHAH, S.; ASNANI, A.; NEILAN, T. G.; LENIHAN, D.; KY, B.; BARAC, A.; HAYEK, S. S.; LEJA, M.; HERRMANN, J.; THAVENDIRANATHAN, P.; FRADLEY, M.; BANG, V.; SHREYDER, K.; PARIKH, R.; PATEL, R.; SINGH, A.; BRAR, S.; GUHA, A.; GUPTA, D.; MASCARI, P.; PATTEN, R. D.; VENESY, D. M.; NOHRIA, A.; RESNIC, F. S. Management of Cardiovascular Disease During Coronavirus Disease (COVID-19) Pandemic. **Trends in Cardiovascular Medicine**, v. 30, n. 6, p. 315-325, 2020.

158 MAI, F.; DEL PINTO, R.; FERRI, C. COVID-19 and Cardiovascular Diseases. **Journal of Cardiology**, v. 76, n 5, p. 453-458, 2020.

159 PRANATA, R.; HUANG, I.; LIM, M. A.; WAHJOEPRAMONO, E. J.; JULY, J. Impact of cerebrovascular and cardiovascular diseases on mortality and severity of COVID-19-systematic review, meta-analysis, and meta-regression. **Journal of Stroke and Cerebrovascular Diseases**, v. 29, n. 8, p. 104949, 2020.

160 LI, G.; HU, R.; GU, X. A close-up on COVID-19 and cardiovascular diseases. **Nutrition, Metabolism and Cardiovascular Diseases**, v. 30, n. 7, p. 1057-1060, 2020.

161 World Health Organization. **Prevention of Cardiovascular Disease - Guidelines for assessment and management of cardiovascular risk**, 2020. Available in: https://www.who.int/cardiovascular_diseases/guidelines/Full%20text.pdf. Accessed in: 27 september 2020, 18:23.

162 PAPAKONSTANTINOU, N. A.; BAIKOUSSIS, N. G.; DEDEILIAS, P.; ARGIRIOU, M.; CHARITOS, C. Cardiac surgery or interventional cardiology? Why not both? Let's go hybrid. **Journal of Cardiology**, v 69, n. 1, p. 46-56, 2017.

163 FRAGASSO, G.; MARGONATO, A.; SPOLADORE, R.; LOPASCHUK, G. D. Metabolic effects of cardiovascular drugs. **Trends Cardiovasc Trends in Cardiovascular Medicine**, v. 29, n. 3, p. 176-187, 2019.

164 ZHANG, K.; ZHAO, Y.; FENT, K. Cardiovascular drugs and lipid regulating agents in surface waters at global scale: Occurrence, ecotoxicity and risk assessment. **Science of The Total Environment**, v. 729, p. 138770, 2020.

165 LAURENT, S. Antihypertensive drugs. **Pharmacological Research**, v. 124, p. 116-125, 2017.

166 ZSOTÉR, T. T. Vasodilators. **Canadian Medical Association Journal**, v. 129, p. 424-428, 1983.

167 DERBYSHIRE, E. R.; MARLETTA, M. A. Structure and regulation of soluble guanylate cyclase. **Annual Review of Biochemistry**, v. 81, p. 533-559, 2012.

168 ZHU, G.; GRONEBERG, D.; SIKKA, G.; HORI, D.; RANEK, M. J.; NAKAMURA, T.; TAKIMOTO, E.; PAOLOCCI, N.; BERKOWITZ, D. E.; FRIEBE, A.; KASS, D. A. Soluble guanylate cyclase is required for systemic vasodilation but not positive inotropy induced by nitroxyl in the mouse. **Hypertension**, v. 65, n. 2, p. 385-392, 2015.

169 SUN, H. J.; WU, Z. Y.; CAO, L.; ZHU, M. Y.; NIE, X. W.; HUANG, D. J.; SUN, M. T.; BIAN, J. S. Role of nitroxyl (HNO) in cardiovascular system: From biochemistry to pharmacology. **Pharmacological Research**, v. 159, p. 104961, 2020.

170 SOUSA, E. H. S.; CAREPO, M. S. P.; MOURA, J. J. G. Nitrate-nitrite fate and oxygen sensing in dormant Mycobacterium tuberculosis: A bioinorganic approach highlighting the importance of transition metals. **Coordination Chemistry Reviews**, v. 423, p. 213476, 2020.

171 World Health Organization. **Global tuberculosis report 2019**, 2019. Available in: https://www.who.int/tb/publications/global_report/en/. Accessed in: 27 september 2020, 19:00.

172 HOUBEN, R. M.; DODD, P. J. The Global Burden of Latent Tuberculosis Infection: A Re-estimation Using Mathematical Modelling. **PLoS Medicine**, v. 13, n. e1002152, p.1-13, 2016.

173 CHURCHYARD, G.; KIM, P.; SHAH, N. S.; RUSTOMJEE, R.; GANDHI, N.; MATHEMA, B.; DOWDY, D.; KASMAR, A.; CARDENAS, V. What We Know About Tuberculosis Transmission: An Overview. **Journal of Infectious Diseases**, v. 216, p. S629-S635, 2017.

174 CREVEL, R.; OTTENHOFF, T. H. M.; MEER, J. W. M. Innate immunity to Mycobacterium tuberculosis. **Clinical Microbiology Reviews**, v. 15, n. 2, p. 294-309, 2002.

175 LABORDE, J. **Pro-drogues antituberculeuses : Approches pour lutter contre les résistances et compréhension des mécanismes oxydatifs d'activation**. 2016. Thesis (PhD in Organic Chemistry) - ED SDM, Chimie-Biologie-Santé - CO 042, Université Paul Sabatier -Toulouse III, 2006.

176 RUSSELL, D. G.; BARRY 3rd, C. E.; FLYNN, J. L. Tuberculosis: what we don't know can, and does, hurt us. **Science**, v. 328, n. 5980, p. 852-856, 2010.

177 KAUFMANN, S. H. EFIS lecture. Immune response to tuberculosis: How to control the most successful pathogen on earth. **Immunology Letters**, v. 175, p. 50-57, 2016.

178 KOURBATOVA, E. V.; LEONARD, M. K., JR.; ROMERO, J.; KRAFT, C.; DEL RIO, C.; BLUMBERG, H. M. Risk factors for mortality among patients with extrapulmonary tuberculosis at an academic inner-city hospital in the US. **European Journal of Epidemiology**, v. 21, n. 9, p. 715-721, 2006.

179 VINCENT, A. T.; NYONGESA, S.; MORNEAU, I.; REED, M. B.; TOCHEVA, E. I.; VEYRIER, F. J. The Mycobacterial Cell Envelope: A Relict From the Past or the Result of Recent Evolution?. **Frontiers in Microbiology**, v. 9, n. 2341, p. 1-9, 2018.

180 GAO, L. Y.; LAVAL, F.; LAWSON, E. H.; GROGER, R. K.; WOODRUFF, A.; MORISAKI, J. H.; COX, J. S.; DAFFE, M.; BROWN, E. J. Requirement for kasB in Mycobacterium mycolic acid biosynthesis, cell wall impermeability and intracellular survival: implications for therapy. **Molecular Microbiology**, v. 49, n. 6, p. 1547-1563, 2003.

181 PANG, Y.; ZHAO, A.; COHEN, C.; KANG, W.; LU, J.; WANG, G.; ZHAO, Y.; ZHENG, S. Current status of new tuberculosis vaccine in children. **Human Vaccines & Immunotherapeutics**, v. 12, n. 4, p. 960-970, 2016.

182 RABAHI, M. F.; SILVA JUNIOR, J.; FERREIRA, A. C. G.; TANNUS-SILVA, D. G. S.; CONDE, M. B. Tuberculosis treatment. **Jornal Brasileiro de Pneumologia**, v. 43, n. 6, p. 472-486, 2017.

183 PONTALI, E.; RAVIGLIONE, M. C.; MIGLIORI, G. B. Regimens to treat multidrug-resistant tuberculosis: past, present and future perspectives. **European Respiratory Review**, v. 28, n. 190035, p. 1-7, 2019.

184 BAHUGUNA, A.; RAWAT, D. S. An overview of new antitubercular drugs, drug candidates, and their targets. Medicinal Research Reviews, v. 40, n. 1, p. 263-292, 2020.

185 KEAM, S. J. Pretomanid: First Approval. **Drugs**, v. 79, n. 16, p. 1797-1803, 2019.

186 World Health Organization. **WHO consolidated guidelines on drug-resistant tuberculosis treatment**, 2019. Available in: https://www.who.int/tb/publications/2019/consolidated-guidelines-drug-resistant-TB-treatment/en/. Accessed in: 27 september, 20:12.

187 LABORDE, J.; DERAEVE, C.; BERNARDES-GENISSON, V. Update of Antitubercular Prodrugs from a Molecular Perspective: Mechanisms of Action, Bioactivation Pathways, and Associated Resistance. **ChemMedChem**, v. 12, n. 20, p. 1657-1676, 2017.

188 SINGH, R.; MANJUNATHA, U.; BOSHOFF, H. I.; HA, Y. H.; NIYOMRATTANAKIT, P.; LEDWIDGE, R.; DOWD, C. S.; LEE, I. Y.; KIM, P.; ZHANG, L.; KANG, S.; KELLER, T. H.; JIRICEK, J.; BARRY 3rd, C. E. PA-824 kills nonreplicating Mycobacterium tuberculosis by intracellular NO release. **Science**, v. 322, n. 5906, p. 1392-1395, 2008.

189 JAMAATI, H.; MORTAZ, E.; PAJOUHI, Z.; FOLKERTS, G.; MOVASSAGHI, M.; MOLOUDIZARGARI, M.; ADCOCK, I. M.; GARSSEN, J. Nitric Oxide in the Pathogenesis and Treatment of Tuberculosis. **Frontiers in Microbiology**, v. 8, n. 2008, p. 1-11, 2017.

190 GALIZIA, J.; ACOSTA, M. P.; URDANIZ, E.; MARTI, M. A.; PIURI, M. Evaluation of nitroxyl donors' effect on mycobacteria. **Tuberculosis**, v. 109, p. 35-40, 2018.

191 WEINBERGER, B.; LASKIN, D. L.; HECK, D. E.; LASKIN, J. D. The toxicology of inhaled nitric oxide. **Toxicological Sciences**, v. 59, n. 1, p. 5-16, 2001.

192 WANG, P. G.; XIAN, M.; TANG, X.; WU, X.; WEN, Z.; CAI, T.; JANCZUK, A. J. Nitric oxide donors: chemical activities and biological applications. **Chemical Reviews**, v. 102, n. 4, p. 1091-1134, 2002.

193 CSONT, T.; FERDINANDY, P. Cardioprotective effects of glyceryl trinitrate: beyond vascular nitrate tolerance. **Pharmacology & Therapeutics**, v. 105, n. 1, p. 57-68, 2005.

194 WANG, K.; SAMAI, K. Role of high-dose intravenous nitrates in hypertensive acute heart failure. **The American Journal of Emergency Medicine**, v. 38, n. 1, p. 132-137, 2020.

195 RALPH, D. J.; EARDLEY, I.; TAUBEL, J.; TERRILL, P.; HOLLAND, T. Efficacy and Safety of MED2005, a Topical Glyceryl Trinitrate Formulation, in the Treatment of Erectile Dysfunction: A Randomized Crossover Study. **Journal of Sexual Medicine**, v. 15, n. 2, p. 167-175, 2018.

196 MUNZEL, T.; STEVEN, S.; DAIBER, A. Organic nitrates: update on mechanisms underlying vasodilation, tolerance and endothelial dysfunction. **Vascular Pharmacology**, v. 63, n. 3, p. 105-113, 2014.

197 Reference Module in Biomedical Sciences. **Isosorbide Dinitrate**, 2018. Available in: https://www.sciencedirect.com/science/article/pii/B9780128012383967114. Accessed in: 27 september 2020, 23:01.

198 ZIAEIAN, B.; FONAROW, G. C.; HEIDENREICH, P. A. Clinical Effectiveness of Hydralazine-Isosorbide Dinitrate in African-American Patients With Heart Failure. **JACC Heart Fail**, v. 5, n. 9, p. 632-639, 2017.

199 TRAVESSA, A. M.; MENEZES FALCAO, L. Vasodilators in acute heart failure - evidence based on new studies. **European Journal of Internal Medicine**, v. 51, p. 1-10, 2018.

200 MÜLSCH, A.; BUSSE, R.; BASSENGE, E. Desensitization of guanylate cyclase in nitrate tolerance does not impair endothelium-dependent responses. **European Journal of Pharmacology**, v. 158, n. 3, p. 191-198, 1988.

201 LEO, C. H.; FERNANDO, D. T.; TRAN, L.; NG, H. H.; MARSHALL, S. A.; PARRY, L. J. Serelaxin Treatment Reduces Oxidative Stress and Increases Aldehyde Dehydrogenase-2 to Attenuate Nitrate Tolerance. **Frontiers in Pharmacology**, v. 8, n. 141, p. 1-11, 2017.

202 MÜNZEL, T.; SAYEGH, H.; FREEMAN, B. A.; TARPEY, M. M.; HARRISON, D. G. Evidence for enhanced vascular superoxide anion production in nitrate tolerance. A novel mechanism underlying tolerance and cross-tolerance. **Journal of Clinical Investigation**, p. 187–194, 1995.

203 DALAL, J.; YAO, L.; PARKER, J. O. Nitrate tolerance: influence of isosorbide dinitrate on the hemodynamic and antianginal effects of nitroglycerin. **Journal of the American College of Cardiology**, v. 2, n. 1, p. 115-120, 1983.

204 WAGNER, F; SIEFERT, F; TRENK D; E, J. Relationship between pharmacokinetics and hemodynamic tolerance to isosorbide-5-mononitrate. **European Journal of Clinical Pharmacology**, v. 38, p. S53-S59, 1990.

205 SEKIYA, M.; SATO, M.; FUNADA, J.; OHTANI, T.; AKUTSU, H.; WATANABE, K. Effects of the long-term administration of nicorandil on vascular endothelial function and the progression of arteriosclerosis. **Journal of Cardiovascular Pharmacology**, v. 46, n. 1, p. 63-67, 2005.

206 THADANI, U.; PRASAD, R.; HAMILTON, S. F.; VOYLES, W.; DOYLE, R.; KARPOW, S.; REDER, R.; TEAGUE, S. M. Usefulness of twice-daily isosorbide-5-mononitrate in preventing development of tolerance in angina pectoris. **The American Journal of Cardiology**, v. 60, n. 7, p. 477-482, 1987.

207 KINOSHITA, M.; SAKAI, K. Pharmacology and Therapeutic Effects of Nicorandil. **Cardiovascular Drugs and Therapy**, v. 4, n. 4, p. 1075-1088, 1990.

208 WANG, H.; WANG, L.; XIE, Z.; ZHOU, S.; LI, Y.; ZHOU, Y.; SUN, M. Nitric Oxide (NO) and NO Synthases (NOS)-Based Targeted Therapy for Colon Cancer. **Cancers (Basel)**, v. 12, n. 7, p. 1-25, 2020.

209 KUMAR, S.; SINGH, R. K.; BHARDWAJ, T. R. Therapeutic role of nitric oxide as emerging molecule. **Biomedicine & Pharmacotherapy**, v. 85, p. 182-201, 2017.

210 DAIBER, A.; MUNZEL, T. Organic Nitrate Therapy, Nitrate Tolerance, and Nitrate-Induced Endothelial Dysfunction: Emphasis on Redox Biology and Oxidative Stress. **Antioxidants & Redox Signaling**, v. 23, n. 11, p. 899-942, 2015.

211 WONG, P. S.; FUKUTO, J. M. Reaction of organic nitrate esters and S-nitrosothiols with reduced flavins: a possible mechanism of bioactivation. **Drug Metabolism and Disposition**, v. 27, n 4, p. 502-509, 1999.

212 YEATES, R A; LAUFEN, H.; LEITOLD, M. The reaction between organic nitrates and sulfhydryl compounds. A possible model system for the activation of organic nitrates. **Molecular Pharmacology**, v. 28, p. 555-559, 1985.

213 PAGE, N. A.; FUNG, H. L. Organic nitrate metabolism and action: toward a unifying hypothesis and the future-a dedication to Professor Leslie Z. Benet. **Journal of Pharmaceutical Sciences**, v. 102, n. 9, p. 3070-3081, 2013.

214 MAJUMDER, S.; SINHA, S.; SIAMWALA, J. H.; MULEY, A.; REDDY SEERAPU, H.; KOLLURU, G. K.; VEERIAH, V.; NAGARAJAN, S.; SRIDHARA, S. R.; PRIYA, M. K.; KUPPUSAMY, M.; SRINIVASAN, S.; KONIKKAT, S.; SOUNDARARAJAN, G.; VENKATARAMAN, S.; SARAN, U.; CHATTERJEE, S. A comparative study of NONOate based NO donors: spermine NONOate is the best suited NO donor for angiogenesis. **Nitric Oxide**, v. 36, p. 76-86, 2014.

215 MILLER, M. R.; MEGSON, I. L. Recent developments in nitric oxide donor drugs. **British Journal of Pharmacology**, v. 151, n. 3, p. 305-321, 2007.

216 MARAGOS, C. M.; MORLEY, D.; WINK, D. A.; DUNAMS, T. M.; SAAVEDRA, J. E.; HOFFMAN, A.; BOVE, A. A.; ISAAC, L.; HRABIE, J. A.; KEEFER, L. K. Complexes of ·NO with nucleophiles as agents for the controlled biological release of nitric oxide. Vasorelaxant effects. **Journal of Medicinal Chemistry**, v. 34, n. 11, p. 3242-3247, 1991.

217 HOMER, K.; WANSTALL, J. In vitro comparison of two NONOates (novel nitric oxide donors) on rat pulmonary arteries. **European Journal of Pharmacology**, v. 356, n. 1, p. 49-57, 1998.

218 GRESELE, P.; MOMI, S.; GUGLIELMINI, G. Nitric oxide-enhancing or -releasing agents as antithrombotic drugs. **Biochemical Pharmacology**, v. 166, p. 300-312, 2019.

219 DAVIES, K. M.; WINK, D. A.; SAAVEDRA, J. E.; KEEFER, L. K. Chemistry of the diazeniumdiolates. 2. Kinetics and mechanism of dissociation to nitric oxide in aqueous solution. **Journal of the American Chemical Society**, v. 123, n. 23, p. 5473-5481, 2001.

220 SHAIKH, N.; VALIEV, M.; LYMAR, S. V. Decomposition of amino diazeniumdiolates (NONOates): molecular mechanisms. **Journal of Inorganic Biochemistry**, v. 141, p. 28-35, 2014.

221 DUTTON, A. S.; FUKUTO, J. M.; HOUK, K. N. The mechanism of NO formation from the decomposition of dialkylamino diazeniumdiolates: density functional theory and CBS-QB3 predictions. **Inorganic Chemistry**, v. 43, n. 3, p. 1039-1045, 2004.

222 NANDURDIKAR, R. S.; MACIAG, A. E.; CAO, Z.; KEEFER, L. K.; SAAVEDRA, J. E. Diazeniumdiolated carbamates: a novel class of nitric oxide donors. **Bioorganic & Medicinal Chemistry**, v. 20, n. 6, p. 2025-2029, 2012.

223 ALIMORADI, H.; GREISH, K.; GAMBLE, A. B.; GILES, G. I. Controlled Delivery of Nitric Oxide for Cancer Therapy. **Pharmaceutical Nanotechnology**, v. 7, n. 4, p. 279-303, 2019.

224 KNOX, C. D.; KAM, P. J.; AZER, K.; WONG, P.; EDERVEEN, A. G.; SHEVELL, D.; MORABITO, C.; MEEHAN, A. G.; LIU, W.; REYNDERS, T.; DENEF, J. F.; MITSELOS, A.; JONATHAN, D.; GUTSTEIN, D. E.; MITRA, K.; SUN, S. Y.; LO, M. M.; CULLY, D.; ALI, A. Discovery and Clinical Evaluation of MK-8150, A Novel Nitric Oxide Donor With a Unique Mechanism of Nitric Oxide Release. **Journal of the American Heart Association**, v. 5, n. 9, p. 1-12, 2016.

225 OLIVEIRA, M. G. S-Nitrosothiols as Platforms for Topical Nitric Oxide Delivery. **Basic & Clinical Pharmacology & Toxicology**, v. 119, n. S3, p. 49-56, 2016.

226 BURG, A.; COHEN, H.; MEYERSTEIN, D. The reaction mechanism of nitrosothiols with copper(I). **Journal of Biological Inorganic Chemistry**, v. 5, n. 2, p. 213-217, 2000.

227 SWIFT, H. R.; WILLIAMS, D. L. H. Decomposition of S-nitrosothiols by mercury(II) and silver salts. **Journal of the Chemical Society, Perkin Transactions**, v. 2, n. 10, p. 1933-1935, 1997.

228 JOURD'HEUIL, D.; LAROUX, F. S.; MILES, A. M.; WINK, D. A.; GRISHAM, M. B. Effect of superoxide dismutase on the stability of S-nitrosothiols. **Archives of Biochemistry and Biophysics**, v. 361, n. 2, p. 323-330, 1999.

229 OLIVEIRA, M. G.; SHISHIDO, S. M.; SEABRA, A. B.; MORGON, N. H. Thermal Stability of PrimaryS-Nitrosothiols: Roles of Autocatalysis and Structural Effects on the Rate of Nitric Oxide Release. **The Journal of Physical Chemistry A**, v. 106, n. 38, p. 8963-8970, 2002.

230 SOUZA, G. F. P.; DENADAI, J. P.; PICHETH, G. F.; OLIVEIRA, M. G. Long-term decomposition of aqueous S-nitrosoglutathione and S-nitroso-N-acetylcysteine: Influence of concentration, temperature, pH and light. **Nitric Oxide**, v. 84, p. 30-37, 2019.

231 SINGH, R. J.; HOGG, N.; JOSEPH, J.; KALYANARAMAN, B. Photosensitized decomposition of S-nitrosothiols and 2-methyl-2-nitrosopropane Possible use for site-directed nitric oxide production. **FEBS Letters**, v. 360, n. 1, p. 47-51, 1995.

232 PARK, J. Y.; LEE, Y. N. Solubility and decomposition kinetics of nitrous acid in aqueous solution. **The Journal of Physical Chemistry**, v. 92, n. 22, p. 6294-6302, 1988.

233 GILES, N. M.; KUMARI, S.; GANG, B. P.; YUEN, C. W.; BILLAUD, E. M.; GILES, G. I. The molecular design of S-nitrosothiols as photodynamic agents for controlled nitric oxide release. **Chemical Biology and Drug Design**, v. 80, n. 3, p. 471-478, 2012.

234 KAPOSZTA, Z.; CLIFTON, A.; MOLLOY, J.; MARTIN, J. F.; MARKUS, H. S. S-nitrosoglutathione reduces asymptomatic embolization after carotid angioplasty. **Circulation**, v. 106, n. 24, p. 3057-3062, 2002.

235 ClinicalTrials.gov. **GSNOR Phenotyping/GSNO Challenge in Severe Asthma**, 2020. Available in: https://www.clinicaltrials.gov/ct2/show/NCT03926741?term=GSNO&draw=2&rank=1. Accessed in: 06 september 2020, 13:43.

236 POPOV, S. A.; SEMENOVA, M. D.; BAEV, D. S.; SOROKINA, I. V.; ZHUKOVA, N. A.; FROLOVA, T. S.; TOLSTIKOVA, T. G.; SHULTS, E. E.; TURKS, M. Lupane-type conjugates with aminoacids, 1,3,4- oxadiazole and 1,2,5-oxadiazole-2-oxide derivatives: Synthesis, anti-inflammatory activity and in silico evaluation of target affinity. **Steroids**, v. 150, p. 108443, 2019.

237 FERNANDES, G. F. S.; SOUZA, P. C.; MARINO, L. B.; CHEGAEV, K.; GUGLIELMO, S.; LAZZARATO, L.; FRUTTERO, R.; CHUNG, M. C.; PAVAN, F. R.; SANTOS, J. L. Synthesis and biological activity of furoxan derivatives against *Mycobacterium tuberculosis*. **European Journal of Medicinal Chemistry**, v. 123, p. 523-531, 2016.

238 MOTT, B. T.; CHENG, K. C.; GUHA, R.; KOMMER, V. P.; WILLIAMS, D. L.; VERMEIRE, J. J.; CAPPELLO, M.; MALONEY, D. J.; RAI, G.; JADHAV, A.; SIMEONOV, A.; INGLESE, J.; POSNER, G. H.; THOMAS, C. J. A furoxan-amodiaquine hybrid as a potential therapeutic for three parasitic diseases. **Medchemcomm**, v. 3, n. 12, p. 1505-1511, 2012.

239 DUTRA, L. A.; GUANAES, J. F. O.; JOHMANN, N.; LOPES PIRES, M. E.; CHIN, C. M.; MARCONDES, S.; DOS SANTOS, J. L. Synthesis, antiplatelet and antithrombotic activities of resveratrol derivatives with NO-donor properties. **Bioorganic & Medicinal Chemistry Letters**, v. 27, n. 11, p. 2450-2453, 2017.

240 HUANG, Y.; LIU, M.; MENG, L.; FENG, P.; GUO, Y.; YING, M.; ZHU, X.; CHEN, Y. Synthesis and antitumor evaluation of novel hybrids of phenylsulfonylfuroxan and epiandrosterone/dehydroepiandrosterone derivatives. **Steroids**, v. 101, p. 7-14, 2015.

241 CARVALHO, P. S.; MARÓSTICA, M.; GAMBERO, A.; JR., J. P. Synthesis and pharmacological characterization of a novel nitric oxide-releasing diclofenac derivative containing a benzofuroxan moiety. **European Journal of Medicinal Chemistry**, v. 45, n. 6, p. 2489-2493, 2010.

242 ZANG, Y.; LAI, F.; FU, J.; LI, C.; MA, J.; CHEN, C.; LIU, K.; ZHANG, T.; CHEN, X.; ZHANG, D. Novel nitric oxide-releasing derivatives of triptolide as antitumor and anti-inflammatory agents: Design, synthesis, biological evaluation, and nitric oxide release studies. **European Journal of Medicinal Chemistry**, v. 190, p. 112079, 2020.

243 CENA, C.; LOLLI, M. L.; LAZZARATO, L.; GUAITA, E.; MORINI, G.; CORUZZI, G.; MCELROY, S. P.; MEGSON, I. L.; FRUTTERO, R.; GASCO, A. Antiinflammatory, gastrosparing, and antiplatelet properties of new NO-donor esters of aspirin. **Journal of Medicinal Chemistry**, v. 46, n. 5, p. 747-754, 2003.

244 HORTON, A.; SCHIEFER, I. T. Pharmacokinetics and pharmacodynamics of nitric oxide mimetic agents. **Nitric Oxide**, v. 84, p. 69-78, 2019.

245 SORBA, G.; MEDANA, C.; FRUTTERO, R.; CENA, C.; DI STILO, A.; GALLI, U.; GASCO, A. Water soluble furoxan derivatives as NO prodrugs. **Journal of Medicinal Chemistry**, v. 40, n. 4, p. 463-469, 1997.

246 FEELISCH, M.; SCHÖNAFINGERI, K.; NOACK, H. Thiol-mediated generation of nitric oxide accounts for the vasodilator action of furoxans. **Biochemical Pharmacology**, v. 44, n. 6, p. 1149-1157, 1992.

247 SAKO, M.; ODA, S.; OHARA, S.; HIROTA, K.; MAKI, Y. Facile Synthesis and NO-Generating Property of 4H-[1,2,5]Oxadiazolo[3,4-d]pyrimidine-5,7-dione 1-Oxides. **Journal of Organic Chemistry**, v. 63, n. 20, p. 6947-6951, 1998.

248 SEYMOUR, C. P.; TOHDA, R.; TSUBAKI, M.; HAYASHI, M.; MATSUBARA, R. Photosensitization of Fluorofuroxans and Its Application to the Development of Visible Light-Triggered Nitric Oxide Donor. **The Journal of Organic Chemistry**, v. 82, n. 18, p. 9647-9654, 2017.

249 MATSUBARA, R.; TAKAZAWA, S.; ANDO, A.; HAYASHI, M.; TOHDA, R.; TSUBAKI, M. Study on the Photoinduced Nitric-Oxide-Releasing Ability of 4-Alkoxy Furoxans. **Asian Journal of Organic Chemistry**, v. 6, n. 5, p. 619-626, 2017.

250 BUSSE, R.; POHL, U.; MULSCH, A.; BASSENGE, E. Modulation of the vasodilator action of SIN-1 by the endothelium. **Journal of Cardiovascular Pharmacology**, v. 14 Suppl 11, p. S81-S85, 1989.

251 STENGELE, E.; RUF, G.; JÄHNCHEN, E.; TRENK, D.; LÖFFLER, K.; SCHULZ, W.; ROSKAMM, H. Short-term hemodynamic, anti-ischemic, and antianginal effects of pirsidomine, a now sydnonimine. **The American Journal of Cardiology**, v. 77, n. 11, p. 937-941, 1996.

252 SIEGFRIED, M. R.; ERHARDT, J.; RIDER, T.; MA, X. L.; LEFER, A. M. Cardioprotection and attenuation of endothelial dysfunction by organic nitric oxide donors in myocardial ischemia-reperfusion. **Journal of Pharmacology and Experimental Therapeutics**, v. 260, n. 2, p. 668-675, 1992.

253 VINATIER, V.; SOULERE, L.; HOFFMANN, P. Esterase-activated chromane-sydnonimine prodrug hybrids. **Nitric Oxide**, v. 15, n. 4, p. 363-369, 2006.

254 SHARMA, R.; JOUBERT, J.; MALAN, S. F. Recent Developments in Drug Design of NO-donor Hybrid Compounds. **Mini-Reviews in Medicinal Chemistry**, v. 18, n. 14, p. 1175-1198, 2018.

255 GRUNER, J. A.; MATHIASEN, J. R.; FLOOD, D. G.; GASIOR, M. Characterization of pharmacological and wake-promoting properties of the dopaminergic stimulant sydnocarb in rats. **Journal of Pharmacology and Experimental Therapeutics**, v. 337, n. 2, p. 380-390, 2011.

256 CAI, T. B.; LU, D.; TANG, X.; ZHANG, Y.; LANDERHOLM, M.; WANG, P. G. New glycosidase activated nitric oxide donors: glycose and 3-morphorlinosydnonimine conjugates. **The Journal of Organic Chemistry**, v. 70, n. 9, p. 3518-3524, 2005.

257 NORTCLIFFE, A.; BOTTING, N. P.; O'HAGAN, D. Novel amino acids: synthesis of furoxan and sydnonimine containing amino acids and peptides as potential nitric oxide releasing motifs. **Organic & Biomolecular Chemistry**, v. 11, n. 28, p. 4657-4671, 2013.

258 LAURSEN, B. E.; STANKEVICIUS, E.; PILEGAARD, H.; MULVANY, M.; SIMONSEN, U. Potential protective properties of a stable, slow-releasing nitric oxide donor, GEA 3175, in the lung. **Cardiovascular Drug Reviews**, v. 24, n. 3-4, p. 247-260, 2006.

259 FEELISCH, M.; OSTROWSKI, J.; NOACK, E. On the mechanism of NO release from Sydnonimines. **Journal of Cardiovascular Pharmacology**, v. 14, p. S13-S22, 1989.

260 SALMON, D. J.; TORRES DE HOLDING, C. L.; THOMAS, L.; PETERSON, K. V.; GOODMAN, G. P.; SAAVEDRA, J. E.; SRINIVASAN, A.; DAVIES, K. M.; KEEFER, L. K.; MIRANDA, K. M. HNO and NO release from a primary amine-based diazeniumdiolate as a function of pH. **Inorganic Chemistry**, v. 50, n. 8, p. 3262-3270, 2011.

261 ZARPELON, A. C.; SOUZA, G. R.; CUNHA, T. M.; SCHIVO, I. R.; MARCHESI, M.; CASAGRANDE, R.; PINGE-FILHO, P.; CUNHA, F. Q.; FERREIRA, S. H.; MIRANDA, K. M.; VERRI, W. A., JR. The nitroxyl donor, Angeli's salt, inhibits inflammatory hyperalgesia in rats. **Neuropharmacology**, v. 71, p. 1-9, 2013.

262 CHIN, K. Y.; MICHEL, L.; QIN, C. X.; CAO, N.; WOODMAN, O. L.; RITCHIE, R. H. The HNO donor Angeli's salt offers potential haemodynamic advantages over NO or dobutamine in ischaemia-reperfusion injury in the rat heart *ex vivo*. **Pharmacological Research**, v. 104, p. 165-175, 2016.

263 STOYANOVSKY, D. A.; SCHOR, N. F.; NYLANDER, K. D.; SALAMA, G. Effects of pH on the cytotoxicity of sodium trioxodinitrate (Angeli's salt). **Journal of Medicinal Chemistry**, v. 47, n. 1, p. 210-217, 2004.

264 ANDREI, D.; SALMON, D. J.; DONZELLI, S.; WAHAB, A.; KLOSE, J. R.; CITRO, M. L.; SAAVEDRA, J. E.; WINK, D. A.; MIRANDA, K. M.; KEEFER, L. K. Dual mechanisms of HNO generation by a nitroxyl prodrug of the diazeniumdiolate (NONOate) class. **Journal of the American Chemical Society**, v. 132, n. 46, p. 16526-16532, 2010.

265 HOLLAND, R. J.; PAULISCH, R.; CAO, Z.; KEEFER, L. K.; SAAVEDRA, J. E.; DONZELLI, S. Enzymatic generation of the NO/HNO-releasing IPA/NO anion at controlled rates in physiological media using β-galactosidase. **Nitric Oxide**, v. 35, n. 30, p. 131-136, 2013.

266 BHARADWAJ, G.; BENINI, P. G.; BASUDHAR, D.; RAMOS-COLON, C. N.; JOHNSON, G. M.; LARRIVA, M. M.; KEEFER, L. K.; ANDREI, D.; MIRANDA, K. M. Analysis of the HNO and NO donating properties of alicyclic amine diazeniumdiolates. **Nitric Oxide**, v. 42, p. 70-78, 2014.

267 AIZAWA, K.; NAKAGAWA, H.; MATSUO, K.; KAWAI, K.; IEDA, N.; SUZUKI, T.; MIYATA, N. Piloty's acid derivative with improved nitroxyl-releasing characteristics. **Bioorganic & Medicinal Chemistry Letters**, v. 23, n. 8, p. 2340-2343, 2013.

268 CLINE, M. R.; TU, C.; SILVERMAN, D. N.; TOSCANO, J. P. Detection of nitroxyl (HNO) by membrane inlet mass spectrometry. **Free Radical Biology and Medicine**, v. 50, n. 10, p. 1274-1279, 2011.

269 SIRSALMATH, K.; SUAREZ, S. A.; BIKIEL, D. E.; DOCTOROVICH, F. The pH of HNO donation is modulated by ring substituents in Piloty's acid derivatives: azanone donors at biological pH. **Journal of Inorganic Biochemistry**, v. 118, p. 134-139, 2013.

270 ARCARO, A.; LEMBO, G.; TOCCHETTI, C. G. Nitroxyl (HNO) for treatment of acute heart failure. **Current Heart Failure Reports**, v. 11, n. 3, p. 227-235, 2014.

271 KAWAGUCHI, M.; TANI, T.; HOMBU, R.; IEDA, N.; NAKAGAWA, H. Development and cellular application of visible-light-controllable HNO releasers based on caged Piloty's acid. **Chemical Communications**, v. 54, n. 73, p. 10371-10374, 2018.

272 GUTHRIE, D. A.; NOURIAN, S.; TAKAHASHI, C. G.; TOSCANO, J. P. Curtailing the hydroxylaminobarbituric acid-hydantoin rearrangement to favor HNO generation. **Journal of Organic Chemistry**, v. 80, n. 3, p. 1349-1356, 2015.

273 GUTHRIE, D. A.; KIM, N. Y.; SIEGLER, M. A.; MOORE, C. D.; TOSCANO, J. P. Development of N-substituted hydroxylamines as efficient nitroxyl (HNO) donors. **Journal of the American Chemical Society**, v. 134, n. 4, p. 1962-1965, 2012.

274 GUTHRIE, D. A.; HO, A.; TAKAHASHI, C. G.; COLLINS, A.; MORRIS, M.; TOSCANO, J. P. "Catch-and-release" of HNO with pyrazolones. **Journal of Organic Chemistry**, v. 80, n. 3, p. 1338-1348, 2015.

275 MOHAMED, H. A.; ABDEL-AZIZ, M.; ABUO-RAHMA GEL, D.; KING, S. B. New acyloxy nitroso compounds with improved water solubility and nitroxyl (HNO) release kinetics and inhibitors of platelet aggregation. **Bioorganic & Medicinal Chemistry**, v. 23, n. 17, p. 6069-6077, 2015.

276 SHA, X.; ISBELL, T. S.; PATEL, R. P.; DAY, C. S.; KING, S. B. Hydrolysis of acyloxy nitroso compounds yields nitroxyl (HNO). **Journal of the American Chemical Society**, v. 128, n. 30, p. 9687-9692, 2006.

277 ZENG, B. B.; HUANG, J.; WRIGHT, M. W.; KING, S. B. Nitroxyl (HNO) release from new functionalized *N*-hydroxyurea-derived acyl nitroso-9,10-dimethylanthracene

cycloadducts. **Bioorganic & Medicinal Chemistry Letters**, v. 14, n. 22, p. 5565-5568, 2004.

278 MAIMON, E.; SAMUNI, A.; GOLDSTEIN, S. Nitrogen Dioxide Reaction with Nitroxide Radical Derived from Hydroxamic Acids: The Intermediacy of Acyl Nitroso and Nitroxyl (HNO). **Journal of Physical Chemistry A**, v. 122, n. 15, p. 3747-3753, 2018.

279 MEMEO, M. G.; QUADRELLI, P. Generation and Trapping of Nitrosocarbonyl Intermediates. **Chemical Reviews**, v. 117, n. 3, p. 2108-2200, 2017.

280 MATSUO, K.; NAKAGAWA, H.; ADACHI, Y.; KAMEDA, E.; TSUMOTO, H.; SUZUKI, T.; MIYATA, N. Alternative photoinduced release of HNO or NO from an acyl nitroso compound, depending on environmental polarity. **Chemical Communications**, v. 46, n. 21, p. 3788-3790, 2010.

281 ADACHI, Y.; NAKAGAWA, H.; MATSUO, K.; SUZUKI, T.; MIYATA, N. Photoactivatable HNO-releasing compounds using the retro-Diels-Alder reaction. **Chemical Communications**, v. 41, p. 5149-5151, 2008.

282 GAO, W. D.; MURRAY, C. I.; TIAN, Y.; ZHONG, X.; DUMOND, J. F.; SHEN, X.; STANLEY, B. A.; FOSTER, D. B.; WINK, D. A.; KING, S. B.; VAN EYK, J. E.; PAOLOCCI, N. Nitroxyl-mediated disulfide bond formation between cardiac myofilament cysteines enhances contractile function. **Circulation Research**, v. 111, n. 8, p. 1002-1011, 2012.

283 DONZELLI, S.; FISCHER, G.; KING, B. S.; NIEMANN, C.; DUMOND, J. F.; HEEREN, J.; WIEBOLDT, H.; BALDUS, S.; GERLOFF, C.; ESCHENHAGEN, T.; CARRIER, L.; BOGER, R. H.; ESPEY, M. G. Pharmacological characterization of 1-nitrosocyclohexyl acetate, a long-acting nitroxyl donor that shows vasorelaxant and antiaggregatory effects. **American Society for Pharmacology and Experimental Therapeutics**, v. 344, n. 2, p. 339-347, 2013.

284 SHOMAN, M. E.; DUMOND, J. F.; ISBELL, T. S.; CRAWFORD, J. H.; BRANDON, A.; HONOVAR, J.; VITTURI, D. A.; WHITE, C. R.; PATEL, R. P.; KING, S. B. Acyloxy nitroso compounds as nitroxyl (HNO) donors: kinetics, reactions with thiols, and vasodilation properties. **Journal of Medicinal Chemistry**, v. 54, n. 4, p. 1059-1070, 2011.

285 CARVALHO, E. M.; RECHIGNAT, L.; SOUSA, E. H. S.; LOPES, L. G. F.; CHAUVIN, R.; BERNARDES-GÉNISSON, V. Mechanistic insights into the in vitro metal-promoted oxidation of (di)azine hydroxamic acids: evidence of HNO release and *N,O*-di(di)azinoyl hydroxylamine intermediate. **New Journal of Chemistry**, v. 44, p. 11965-11973, 2020.

286 ANH, D. T.; HAI, P. T.; HUONG, L. T.; PARK, E. J.; JUN, H. W.; KANG, J. S.; KWON, J. H.; DUNG, D. T. M.; ANH, V. T.; HUE, V. T. M.; HAN, S. B.; NAM, N. H. Exploration of certain 1,3-oxazole- and 1,3-thiazole-based hydroxamic acids as histone deacetylase inhibitors and antitumor agents. **Bioorganic Chemistry**, v. 101, p. 103988, 2020.

287 MONZYK, B.; CRUMBLISS, A. L. Mechanism of ligand substitution on high-spin iron(III) by hydroxamic acid chelators. Thermodynamic and kinetic studies on the formation and dissociation of a series of monohydroxamatoiron(III) complexes. **Journal of the American Chemical Society**, v. 101, n. 21, p. 6203-6213, 1979.

288 YU, X.; ZHANG, R.; YANG, S.; LIU, C.; HE, G.; WANG, H.; WANG, J. A novel decanedioic hydroxamic acid collector for the flotation separation of bastnäsite from calcite. **Minerals Engineering**, v. 151, p. 106306, 2020.

289 LI, Z.; YAMAMOTO, H. Hydroxamic acids in asymmetric synthesis. **Accounts of Chemical Research**, v. 46, n. 2, p. 506-518, 2013.

290 MARKS, P. A. Discovery and development of SAHA as an anticancer agent. **Oncogene**, v. 26, n. 9, p. 1351-1356, 2007.

291 HAILU, G. S.; ROBAA, D.; FORGIONE, M.; SIPPL, W.; ROTILI, D.; MAI, A. Lysine Deacetylase Inhibitors in Parasites: Past, Present, and Future Perspectives. **Journal of Medicinal Chemistry**, v. 60, n. 12, p. 4780-4804, 2017.

292 PARIS, M.; PORCELLONI, M.; BINASCHI, M.; FATTORI, D. Histone deacetylase inhibitors: from bench to clinic. **Journal of Medicinal Chemistry**, v. 51, n. 6, p. 1505-1529, 2008.

293 ALAM, M. A. Methods for Hydroxamic Acid Synthesis. **Current Organic Chemistry**, v. 23, n. 9, p. 978-993, 2019.

294 ZHANG, J. H.; MOTTAMAL, M.; JIN, H. S.; GUO, S.; GU, Y.; WANG, G.; ZHAO, L. M. Design, synthesis and evaluation of belinostat analogs as histone deacetylase inhibitors. **Future Medicinal Chemistry**, v. 11, n. 21, p. 2765-2778, 2019.

295 GUARDA, C. C.; SILVEIRA-MATTOS, P. S. M.; YAHOUEDEHOU, S.; SANTIAGO, R. P.; ALELUIA, M. M.; FIGUEIREDO, C. V. B.; FIUZA, L. M.; CARVALHO, S. P.; OLIVEIRA, R. M.; NASCIMENTO, V. M. L.; LUZ, N. F.; BORGES, V. M.; ANDRADE, B. B.; GONCALVES, M. S. Hydroxyurea alters circulating monocyte subsets and dampens its inflammatory potential in sickle cell anemia patients. **Scientific Reports**, v. 9, n. 14829, p. 1-11, 2019.

296 ATKINSON, R. N.; STOREY, B. M.; KING, S. B. Reactions of acyl nitroso compounds with amines: Production of nitroxyl (HNO) with the preparation of amides. **Tetrahedron Letters**, v. 37, n. 52, p. 9287-9290, 1996.

297 SAMUNI, Y.; WINK, D. A.; KRISHNA, M. C.; MITCHELL, J. B.; GOLDSTEIN, S. Suberoylanilide hydroxamic acid radiosensitizes tumor hypoxic cells in vitro through the oxidation of nitroxyl to nitric oxide. **Free Radical Biology and Medicine**, v. 73, p. 291-298, 2014.

298 KING, S. B. N-hydroxyurea and acyl nitroso compounds as nitroxyl (HNO) and nitric oxide (NO) donors. **Current Topics in Medicinal Chemistry**, n. 5, v. 7, p. 665-673, 2005.

299 ZHANG, P.; SADLER, P. J. Advances in the design of organometallic anticancer complexes. **Journal of Organometallic Chemistry**, v. 839, p. 5-14, 2017.

300 WALDRON, K. J.; RUTHERFORD, J. C.; FORD, D.; ROBINSON, N. J. Metalloproteins and metal sensing. **Nature**, v. 460, n. 7257, p. 823-830, 2009.

301 WINKLER, J. R.; GRAY, H. B. Electron flow through metalloproteins. **Chemical Reviews**, v. 114, n. 7, p. 3369-3380, 2014.

302 SILVA FILHO, P. M.; PAZ, I. A.; NASCIMENTO, N. R. F.; SANTOS, C. F.; ARAUJO, V. R.; AQUINO, C. P.; RIBEIRO, T. S.; VASCONCELOS, I. F.; LOPES, L. G. F.; SOUSA, E. H. S.; LONGHINOTTI, E. Incorporation of Nitroprusside on Silica Nanoparticles-A Strategy for Safer Use of This NO Donor in Therapy. **Molecular Pharmaceutics**, v. 16, n. 7, p. 2912-2921, 2019.

303 LIU, T.; ZHANG, M.; TERRY, M. H.; SCHROEDER, H.; WILSON, S. M.; POWER, G. G.; LI, Q.; TIPPLE, T. E.; BORCHARDT, D.; BLOOD, A. B. Hemodynamic Effects of Glutathione-Liganded Binuclear Dinitrosyl Iron Complex: Evidence for Nitroxyl Generation and Modulation by Plasma Albumin. **Molecular Pharmacology**, v. 93, n. 5, p. 427-437, 2018.

304 SOUSA, A. P.; FERNANDES, A. F.; PAZ, I. A.; NASCIMENTO, N. R. F.; ELLENA, J.; SOUSA, E. H. S.; LOPES, L. G. F.; HOLANDA, A. K. M. A Potential Visible-Light NO Releaser: Synthesis, Reactivity and Vasodilator Properties. **Journal of the Brazilian Chemical Society**, v. 28, p. 2117-2129, 2017.

305 SILVA, C. D. S.; PAZ, I. A.; ABREU, F. D.; SOUSA, A. P.; VERISSIMO, C. P.; NASCIMENTO, N. R. F.; PAULO, T. F.; ZAMPIERI, D.; EBERLIN, M. N.; GONDIM, A. C. S.; ANDRADE, L. C.; CARVALHO, I. M. M.; SOUSA, E. H. S.; LOPES, L. G. F. Thiocarbonyl-bound metallonitrosyl complexes with visible-light induced DNA cleavage and promising vasodilation activity. **Journal of Inorganic Biochemistry**, v. 182, p. 83-91, 2018.

306 COSTA, P. P. C.; CAMPOS, R.; CABRAL, P. H. B.; GOMES, V. M.; SANTOS, C. F.; WALLER, S. B.; DE SOUSA, E. H. S.; LOPES, L. G. F.; FONTELES, M. C.; NASCIMENTO, N. R. F. Antihypertensive potential of *cis*-$[Ru(bpy)_2(ImN)(NO)]^{3+}$, a ruthenium-based nitric oxide donor. **Research in Veterinary Science**, v. 130, p. 153-160, 2020.

307 EROY-REVELES, A. A.; LEUNG, Y.; BEAVERS, C. M.; OLMSTEAD, M. M.; MASCHARAK, P. K. Near-infrared light activated release of nitric oxide from designed photoactive manganese nitrosyls: strategy, design, and potential as NO donors. **Journal of the American Chemical Society**, v. 130, n. 13, p. 4447-4458, 2008.

308 OSTROWSKI, A. D.; FORD, P. C. Metal complexes as photochemical nitric oxide precursors: Potential applications in the treatment of tumors. **Dalton Transactions**, v. 48, p. 10660–10669, 2009.

309 LERCH, M. M.; HANSEN, M. J.; DAM, G. M.; SZYMANSKI, W.; FERINGA, B. L. Emerging Targets in Photopharmacology. **Angewandte Chemie International Edition**, v. 55, n. 37, p. 10978-10999, 2016.

310 HUANG, H.; BANERJEE, S.; QIU, K.; ZHANG, P.; BLACQUE, O.; MALCOMSON, T.; PATERSON, M. J.; CLARKSON, G. J.; STANIFORTH, M.; STAVROS, V. G.; GASSER, G.; CHAO, H.; SADLER, P. J. Targeted photoredox catalysis in cancer cells. **Nature Chemistry**, v. 11, n. 11, p. 1041-1048, 2019.

311 KARGES, J.; HEINEMANN, F.; JAKUBASZEK, M.; MASCHIETTO, F.; SUBECZ, C.; DOTOU, M.; VINCK, R.; BLACQUE, O.; THARAUD, M.; GOUD, B.; VINUELAS ZAHI NOS, E.; SPINGLER, B.; CIOFINI, I.; GASSER, G. Rationally Designed Long-Wavelength Absorbing Ru(II) Polypyridyl Complexes as Photosensitizers for Photodynamic Therapy. **Journal of the American Chemical Society**, v. 142, n. 14, p. 6578-6587, 2020.

312 KARGES, J.; YEMPALA, T.; THARAUD, M.; GIBSON, D.; GASSER, G. A Multi-action and Multi-target Ru^{II}-Pt^{IV} Conjugate Combining Cancer-Activated Chemotherapy and Photodynamic Therapy to Overcome Drug Resistant Cancers. **Angewandte Chemie International Edition**, v. 59, n. 18, p. 7069-7075, 2020.

313 SILVA, F. O. N.; ARAÚJO, S. X. B.; HOLANDA, A. K. M.; MEYER, E.; SALES, F. A. M.; DIÓGENES, I. C. N.; CARVALHO, I. M. M.; MOREIRA, Í. S.; LOPES, L. G. F. Synthesis, Characterization, and NO Release Study of the *cis*- and *trans*-$[Ru(bpy)_2(SO_3)(NO)]^+$ Complexes. **European Journal of Inorganic Chemistry**, v. 2006, n. 10, p. 2020-2026, 2006.

314 CÂNDIDO, M. C. L.; OLIVEIRA, A. M.; SILVA, F. O. N.; HOLANDA, A. K. M.; PEREIRA, W. G.; SOUSA, E. H. S.; CARNEIRO, Z. A.; SILVA, R. S.; LOPES, L. G. F. Photochemical and Electrochemical Study of the Release of Nitric Oxide from $[Ru(bpy)_2L(NO)](PF_6)^n$ Complexes (L = Imidazole, 1-Methylimidazole, Sulfite and Thiourea), Toward the Development of Therapeutic Photodynamic Agents. **Journal of the Brazilian Chemical Society**, v. 26, p. 1824-1830, 2015.

315 ROVEDA, A. C., JR.; SANTOS, W. G.; SOUZA, M. L.; ADELSON, C. N.; GONCALVES, F. S.; CASTELLANO, E. E.; GARINO, C.; FRANCO, D. W.; CARDOSO, D. R. Light-activated generation of nitric oxide (NO) and sulfite anion radicals ($SO_3^{\cdot-}$) from a ruthenium(II) nitrosylsulphito complex. **Dalton Transactions**, v. 48, n. 29, p. 10812-10823, 2019.

316 CHIANG, C. K.; CHU, K. T.; LIN, C. C.; XIE, S. R.; LIU, Y. C.; DEMESHKO, S.; LEE, G. H.; MEYER, F.; TSAI, M. L.; CHIANG, M. H.; LEE, C. M. Photoinduced NO and HNO Production from Mononuclear $\{FeNO\}^6$ Complex Bearing a Pendant Thiol. **Journal of the American Chemical Society**, v. 142, n. 19, p. 8649-8661, 2020.

317 WEISSLEDER, R.; NTZIACHRISTOS, V. Shedding light onto live molecular targets. **Nature Medicine**, v. 9, n. 1, p. 123-128, 2003.

318 LI, Y. H.; GUO, M.; SHI, S. W.; ZHANG, Q. L.; YANG, S. P.; LIU, J. G. A ruthenium-nitrosyl-functionalized nanoplatform for the targeting of liver cancer cells

and NIR-light-controlled delivery of nitric oxide combined with photothermal therapy. **Journal of Materials Chemistry B**, v. 5, n. 38, p. 7831-7838, 2017.

319 CARVALHO, E. M.; RIDNOUR, L. A.; GOUVEIA JR, F. S.; CABRAL, P. H. B.; NASCIMENTO, N. R. F.; WINK, D. A.; FRANCO, D. W.; MEDEIROS, M. J. C.; PONTES, D. L.; LONGHINOTTI, E.; PAULO, T. F.; BERNARDES-GENISSON, V.; CHAUVIN, R.; SOUSA, E. H. S.; LOPES, L. G. F. A divergent mode of activation of a nitrosyl iron complex with unusual antiangiogenic activity. **Journal of Inorganic Biochemistry**, v. 210, p. 111133, 2020.

320 CARVALHO, E. M.; PAULO, T. F.; SAQUET, A. S.; ABBADI, B. L.; MACCHI, F. S.; BIZARRO, C. V.; CAMPOS, R. M.; FERREIRA, T. L. A.; NASCIMENTO, N. R. F.; LOPES, L. G. F.; CHAUVIN, R.; SOUSA, E. H. S.; BERNARDES-GÉNISSON, V. Pentacyanoferrate(II) complex of pyridine-4- and pyrazine-2-hydroxamic acid as source of HNO: investigation of anti-tubercular and vasodilation activities. **Journal of Biological Inorganic Chemistry**, v. 25, n. 6, p. 887-901, 2020.

321 LEWANDOWSKA, H.; KALINOWSKA, M.; BRZOSKA, K.; WOJCIUK, K.; WOJCIUK, G.; KRUSZEWSKI, M. Nitrosyl iron complexes-synthesis, structure and biology. **Dalton Transactions**, v. 40, n. 33, p. 8273-8289, 2011.

322 REGLINSKI, J.; BUTLER, A. R.; GLIDEWELL, C. Metal-Nitrosyl complexes as a source of new vasodilators: Strategies derived from systematic chemistry and nitrosyl ligand reactivity. **Applied Organometallic Chemistry**, v. 8, n. 1, p. 25-31, 1994.

323 HOLANDA, A. K. M.; SILVA, F. O. N.; CARVALHO, I. M. M.; BATISTA, A. A.; ELLENA, J.; CASTELLANO, E. E.; MOREIRA, Í. S.; LOPES, L. G. F. Crystal structure, electrochemical and photochemical studies of the *trans*-[Fe(cyclam)(NO)Cl]Cl_2 complex (cyclam=1,4,8,11-tetraazacyclotetradecane). **Polyhedron**, v. 26, n. 16, p. 4653-4658, 2007.

324 SAMUNI, U.; SAMUNI, Y.; GOLDSTEIN, S. On the Distinction between Nitroxyl and Nitric Oxide Using Nitronyl Nitroxides. **Journal of the American Chemical Society**, v. 132, p. 8428-8432, 2010.

325 SOUZA, M. L.; ROVEDA JR., A. C.; PEREIRA, J. C. M.; FRANCO, D. W. New perspectives on the reactions of metal nitrosyls with thiolates as nucleophiles. **Coordination Chemistry Reviews**, v. 306, p. 615-627, 2016.

326 SILVA, F. O. N.; CANDIDO, M. C. L.; HOLANDA, A. K. M.; DIOGENES, I. C. N.; SOUSA, E. H. S.; LOPES, L. G. F. Mechanism and biological implications of the NO release of *cis*-$[Ru(bpy)_2L(NO)]^{n+}$ complexes: A key role of physiological thiols. **Journal of Inorganic Biochemistry**, v. 105, n. 5, p. 624-629, 2011.

327 RONCAROLI, F.; OLABE, J. A. The reactions of nitrosyl complexes with cysteine. **Inorganic Chemistry**, v. 44, n. 13, p. 4719-4727, 2005.

328 ZAPATA, A. L.; KUMAR, M. R.; PERVITSKY, D.; FARMER, P. J. A singular value decomposition approach for kinetic analysis of reactions of HNO with myoglobin. **Journal of Inorganic Biochemistry**, v. 118, p. 171-178, 2013.

329 SHARMA, V. S.; ISAACSON, R. A.; JOHN, M. E.; WATERMAN, M. R.; CHEVION, M. Reaction of Nitric Oxide with Heme Proteins: Studies on Metmyoglobin, Opossum Methemoglobin, and Microperoxidase. **Biochemistry**, v. 22, n. 16, p. 3897-3902, 1983.

330 YALE, H. L. The Hydroxamic Acids. **Chemical Reviews**, v. 33, n. 3, p. 209-256, 1943.

331 MURI, E. M.; NIETO, M. J.; SINDELAR, R. D.; WILLIAMSON, J. S. Hydroxamic acids as pharmacological agents. **Current Medicinal Chemistry**, v. 9, n. 17, p. 1631-1653, 2002.

332 SAMUNI, Y.; SAMUNI, U.; GOLDSTEIN, S. The mechanism underlying nitroxyl and nitric oxide formation from hydroxamic acids. **Biochimica et Biophysica Acta (BBA) - General Subjects**, v. 1820, n. 10, p. 1560-1566, 2012.

333 LOSSEN, H. Ueber die Oxalohydroxamsäure. **Annalen der Chemie und Pharmacie**, v. 150, n. 3, p. 314-322, 1869.

334 IRVINE, J. C.; RITCHIE, R. H.; FAVALORO, J. L.; ANDREWS, K. L.; WIDDOP, R. E.; KEMP-HARPER, B. K. Nitroxyl (HNO): the Cinderella of the nitric oxide story. **Trends in Pharmacological Sciences**, v. 29, n. 12, p. 601-608, 2008.

335 SHOMAN, M. E.; ALY, O. M. Nitroxyl (HNO): A Possible Strategy for Fighting Cancer. **Current Topies in Medicinal Chemistry**, v. 16, n. 22, p. 2464-2470, 2016.

336 DOCTOROVICH, F.; BIKIEL, D.; PELLEGRINO, J.; SUÁREZ, S. A.; LARSEN, A.; MARTÍ, M. A. Nitroxyl (azanone) trapping by metalloporphyrins. **Coordination Chemistry Reviews**, v. 255, n. 23-24, p. 2764-2784, 2011.

337 BARTBERGER, M. D.; FUKUTO, J. M.; HOUK, K. N. On the acidity and reactivity of HNO in aqueous solution and biological systems. **Proceedings of the National Academy of Sciences of the United States of America**, v. 98, n. 5, p. 2194-2198, 2001.

338 LABORDE, J.; DERAEVE, C.; VIEIRA, F. G. M.; SOURNIA-SAQUET, A.; RECHIGNAT, L.; VILLELA, A. D.; ABBADI, B. L.; MACCHI, F. S.; PISSINATE, K.; BIZARRO, C. V.; MACHADO, P.; BASSO, L. A.; PRATVIEL, G.; LOPES, L. G. F.; SOUSA, E. H. S.; BERNARDES-GENISSON, V. Synthesis and mechanistic investigation of iron(II) complexes of isoniazid and derivatives as a redox-mediated activation strategy for anti-tuberculosis therapy. **Journal of Inorganic Biochemistry**, v. 179, p. 71-81, 2018.

339 FRAZIER, C. P.; BUGARIN, A.; ENGELKING, J. R.; ALANIZ, J. R. Copper-Catalyzed Aerobic Oxidation of N-Substituted Hydroxylamines: Efficient and Practical Access to Nitroso Compounds. **Organic Letters**, v.14, n. 14, p. 3620-3623, 2012.

340 NGUYEN, M.; CLAPAROLS, C.; BERNADOU, J.; MEUNIER, B. A Fast and Efficient Metal-Mediated Oxidation of Isoniazid and Identification of Isoniazid-NAD(H) Adducts. **ChemBioChem**, v. 2, n. 12, p. 877-883, 2001.

341 VANDAL, O. H.; NATHAN, C. F.; EHRT, S. Acid resistance in *Mycobacterium tuberculosis*. **Journal of Bacteriology**, v. 191, n. 15, p. 4714-4721, 2009.

342 RYAN, N. J.; LO, J. H. Delamanid: first global approval. **Drugs**, v. 74, n. 9, p. 1041-1045, 2014.

343 MATSUMOTO, M.; HASHIZUME, H.; TOMISHIGE, T.; KAWASAKI, M.; TSUBOUCHI, H.; SASAKI, H.; SHIMOKAWA, Y.; KOMATSU, M. OPC-67683, a nitro-dihydro-imidazooxazole derivative with promising action against tuberculosis in vitro and in mice. **PLoS Medicine**, v. 3, n. e466, p. 2131-2144, 2006.

344 SOUSA, E. H.; BASSO, L. A.; SANTOS, D. S.; DIOGENES, I. C.; LONGHINOTTI, E.; LOPES, L. G.; MOREIRA IDE, S. Isoniazid metal complex reactivity and insights for a novel anti-tuberculosis drug design. **Journal of Biological Inorganic Chemistry**, v. 17, n. 2, p. 275-283, 2012.

345 THANGAMANI, S.; YOUNIS, W.; SELEEM, M. N. Repurposing Clinical Molecule Ebselen to Combat Drug Resistant Pathogens. **PLoS One**, v. 10, n. 7, p. 1-16, 2015.

346 MARZOCCO, S.; RUSSO, R.; BIANCO, G.; AUTORE, G.; SEVERINO, L. Pro-apoptotic effects of nivalenol and deoxynivalenol trichothecenes in J774A.1 murine macrophages. **Toxicology Letters**, v. 189, n. 1, p. 21-26, 2009.

347 CASTRO, I.; FABRE, N.; BOURGEADE-DELMAS, S.; SAFFON, N.; GANDINI, C.; SAUVAIN, M.; CASTILLO, D.; BOURDY, G.; JULLIAN, V. Structural Characterization and Anti-infective Activity of 9,10-Seco-29-norcycloartane Glycosides Isolated from the Flowers of the Peruvian Medicinal Plant *Cordia lutea*. **Journal of Natural Products**, v. 82, n. 12, p. 3233-3241, 2019.

348 SHEN, B. Y.; CHEN, C.; XU, Y. F.; SHEN, J. J.; GUO, H. M.; LI, H. F.; LI, X. N.; KANG, D.; SHAO, Y. H.; ZHU, Z. P.; YIN, X. X.; XIE, L.; WANG, G. J.; LIANG, Y. Is the combinational administration of doxorubicin and glutathione a reasonable proposal?. **Acta Pharmacologica Sinica**, v. 40, n. 5, p. 699-709, 2019.

349 MALLI, S.; POMEL, S.; DENNEMONT, I.; LOISEAU, P. M.; BOUCHEMAL, K. Combination of amphotericin B and chitosan platelets for the treatment of experimental cutaneous leishmaniasis: Histological and immunohistochemical examinations. **Journal of Drug Delivery Science and Technology**, v. 50, p. 34-41, 2019.

350 SLATER, A. F. G. Chloroquine: Mechanism of drug action and resistance in plasmodium falciparum. **Pharmacology & Therapeutics**, v. 57, n. 2-3, p. 203-235, 1993.

ATTACHMENT A – COTUTELA THESIS/ FINANCE AGENCY

Este trabalho consiste de uma tese em cotutela entre as instituições Universidade Federal do Ceará (UFC) e "Université Paul Sabatier – Toulouse III" (UPS-III) financiada pela Coordenação de Aperfeiçoamento de Pessoal de Nível Superior (CAPES, Brasil) e "Comité Français d´Evaluation de la Coopération Universitaire avec le Brésil" (COFECUB, França), Projeto n° Ph-C 883/17.

This work consists of a thesis in cotutela between the "Universidade Federal do Ceará" (UFC) and "Université Paul Sabatier – Toulouse III" (UPS-III) institutions funded by the "Coordenação de Aperfeiçoamento de Pessoal de Nível Superior" (CAPES, Brazil) and "Comité Français d'Evaluation de la Coopération Universitaire avec le Brésil" (COFECUB, France), Project n° Ph-C 883/17.